Uncoupling of Circadian and Other Maternal Cues in Decidualizing Endometrial Cells

Joanne Muter

A thesis submitted to the University of Warwick for the degree of Doctor of Philosophy.

Division of Translational and Systems Medicine

Warwick Medical School

University of Warwick

November 2015

Table of Contents

List of Figures

Chapter 4: PRIP-1 ACTS AS A MOLECULAR SWITCH PROMOTING HESC SURVIVAL VIA REGULATION OF THE AKT PATHWAY

List of Tables

Chapter 1: INTRODUCTION

Acknowledgments

A good relationship between student and supervisor is said to be the key to successfully completing a PhD. I am very grateful to have had the privilege of being supported by one of the best supervisors around, Professor Jan Brosens. He has been a mentor and friend. His commitment, patience and high standards have moulded me into a much better scientist than I would ever have been without him. I can't imagine a better supervisor.

I wish to take this opportunity to express my sincere appreciation for the Chancellor's scholarship award from Warwick University and the financial backing of the Biomedical Research Unit for the supplies and provisions required for this thesis. Special thanks to Professor Siobhan Quenby for her infectious enthusiasm and clinical dedication.

During the course of this work, my friendships with lab members have been vital. Without their kind help and guidance, always generously given, the completion of this thesis would have been endlessly more difficult, and certainly a lot less enjoyable. As such, I thank Dr Paul Brighton, Dr Emma Lucas, Dr Andy Blanks, Dr Flavio Barros, Scarlett Salter, Ruban Durairaj, Nanya Patel, Dr Maru Yojiro and Raffaella Lucciola.

An obvious gratitude is owed to friends and family. I would like to acknowledge the love, support and motivation I have been immeasurably fortunate to receive. My parents who showed me the value of hard work, dedication, and most of all kindness; my proofreading wonder of a sister, Jenny; my wonderful friends for providing homes away from home; and my 'tremendous' partner Rob for the purpose built desk I never used, the endless encouragement, and everything in between.

Finally, I want to thank the women who have donated their tissues samples to this project, to whom this thesis is dedicated.

Declaration

This thesis is submitted to the University of Warwick in support of my application for the degree of Doctor of Philosophy. It has been composed by myself and has not been submitted in any previous application for any degree.

The work presented (including data generated and data analysis) was carried out by the author except in the cases outlined below:

i) Collaboration with Dr Paul Brighton regarding data collection and analysis of m-3M3FBS-mediated Ca^{2+} signalling in decidualized HESCs

ii) Collaboration with Dr Yi-Wah Chan in the analysis of the RNA-Seq data set.

Parts of this thesis have been published by the author:

Muter, J., Lucas, E. S., Chan, Y.-W., Brighton, P. J., Moore, J. D., Lacey, L., Quenby, S., Lam, E. W. F. & Brosens, J. J. (2015) The clock protein period 2 synchronizes mitotic expansion and decidual transformation of human endometrial stromal cells. *The FASEB Journal*, 29 (4): 1603-1614.

Abstract

The differentiation of human endometrial stromal cells (HESCs) into specialised decidual cells prepares the endometrium for embryonic implantation. The biochemical and morphological transformation of these cells is highly temporally regulated in order to define a transient period of endometrial receptivity. Currently, the involvement of circadian machinery, and clock dependent pathways in this process are not fully understood. Firstly, analysis of circadian rhythms in HESCs revealed a consistent loss of oscillations in clock components upon decidualization. Down-regulation of *Period 2 (PER2)* expression, apparent in the early stages of differentiation, was shown to be sufficient to cause this aperiodicity. In turn, temporal suppression of *PER2* expression was achieved via reduced CLOCK binding to a non-canonical E-box enhancer in the *PER2* promoter. RNA sequencing analysis upon premature *PER2* knockdown revealed a disorganised decidual phenotype in which cell cycle and mitotic regulators were perturbed. As such, PER2 acts to uncouple the endometrium from circadian oscillations during decidualization.

Secondly, the gene *PRIP-1* was shown to be *PER2* dependent in undifferentiated HESCs. Endometrial expression of PRIP-1 was induced and maintained upon decidualization by the post-ovulatory rise in progesterone. Analysis of Ca^{2+} fluxes demonstrated the ability of PRIP-1 to act as a chelator of IP_3 signalling. Additionally, PRIP-1, via its regulation of the AKT pathway, is shown to be an anti-apoptotic regulator in decidual HESCs. Together, these results indicate PRIP-1 functions as a molecular switch in response to progesterone signalling. High *PRIP-1* levels during differentiation enable AKT and IP_3 mediated cell survival, whilst declining levels upon P4 withdrawal leads to decidual apoptosis.

In summary, I provide a novel paradigm whereby both PER2 and PRIP-1 act to uncouple the endometrium from various signalling inputs, enabling an autonomous decidual response. Asynchrony in these pathways can lead to a cascade of events resulting in an array of adverse pregnancy complications.

List of Abbreviations

8-br-cAMP	8-Bromoadenosine-3', 5'-cyclic monophosphate
AOR	Adjusted odds ratio
ART	Assisted reproductive technologies
ATP	Adenosine triphosphate
AVP	Arginine vasopressin
BMAL1	Brain and muscle Arnt-like protein
BMI	Body mass index
BRE	Brain and reproductive organ expressed
BRE-AS1	BRE-antisense 1
BSA	Bovine serum albumin
C	Catalytic subunit
Ca^{2+}	Calcium ion
cAMP	Cyclic adenosine monophosphate
CARM1	Co-activator associated arginine methyl transferase
cDNA	Complementary DNA
CEBP/β	CCAAT/ enhancer binding protein β
ChIP	Chromatin Immunoprecipitation
CK1δ/ε	Casein kinase δ/ε
CK2	Casein kinase 2
CLOCK	Circadian locomotor output cycles kaput
COX2	Cyclooxygenase 2
CPLA2	Cytosolic phospholipase A2
CRE	cAMP response element
CREB	cAMP response element binding protein
CREM	cAMP response element modulators
CRH	Corticotrophin releasing hormone
CRY	Cryptochrome
CSF	Cerebrospinal fluid
DCC	Dextran coated charcoal
DMEM	Dulbecco's modified eagles medium
DMSO	Dimethyl sulphoxide
dPRL	Decidual prolactin
DTT	Dithiothreitol
E2	Estradiol
ECM	Extracellular matrix
EDTA	Ethylenediaminetetraacetic acid
EPAC	Exchange nucleotide protein directly activated by cAMP
FACS	Fluorescence activated cell sorting
FISH	Fluorescence in situ hybridization
FIU	Fluorescence intensity units
FOXO1	Forkhead box transcription factor O
FSH	Follicle stimulating factor
GABA	γ-aminobutiric acid
GDP	Guanosine diphosphate
GEO	Gene expression omnibus

GnRH	Gonadotrophin releasing hormone
GRP	Gastrin releasing peptide
GSK3β	Glycogen synthase kinase 3β
GTP	Guanosine triphosphate
HB-EGF	Heparin binding EGF like growth factor
hCG	Human chorionic gonadotrophin
HESC	Human endometrial stromal cell
HGEx-Erdb	Human gene expression endometrial receptivity database
ICER	Inducible cAMP early repressor
IGFBP1	Insulin-like growth factor binding protein-1
IL	Interleukin
IVF	In vitro fertilisation
LH	Luteinizing hormone
LIF	Leukaemia inhibitory factor
MAPK	Mitogen activated protein kinase
mg	Milligram
µg	Microgram
miRNA	Micro RNA
MLC2	Myosin light chain 2
MMP	Matrix metalloproteinases
MPA	17a-medroxyprogesterone actetate
MSC	Mesenchymal stem cell
MUC-1	Mucin-1
N-CoR	Nuclear receptor co-repressor
NT	Non targeting
P4	Progesterone
PAI-1	Plasminogen activator inhibitor-1
pCAF	P300/CBP associated factor
PCR	Polymerase chain reaction
PDE4	Phosphodiesterase 4
PER	Period
PFA	Paraformaldehyde
PG	Prostaglandin
pg	Picogram
PGE2	Prostaglandin E2
PH	Plekstrin homology
PIAS	Protein inhibitor of activated STAT-1
PKA	Protein kinase A
PLC	Phospholipase C
PLCL1	Phospholipase C like-1
PLZF	Promyelocytic leukaemia zinc finger protein
PR	Progesterone receptor
PRE	Progesterone response element
PRIP-1	[Phospholipase C Related, but catalytically Inactive Protein-1
PRL	Prolactin
PROK1	Prokineticin 1
qRT-PCR	Quantitative real time PCR
R	Regulatory subunit

RHT	Retinohypothalamic tract
RIF	Recurrent implantation failure
RIPA	RadioImmuno precipitation assay
RNA	Ribonucleic acid
RORα	RAR-related orphan receptor α
RPL	Recurrent pregnancy loss
SCN	Suprachiasmatic nucleus
SDS	Sodium dodecylsulphate
siRNA	Small interfering RNA
SIRT	Sirtuin 1
SMRT	Silencing mediator of retinoid and thyroid receptor
STAT5	Signal transducer and activator of transcription 5
SUMO	Small ubiquitin-like modifier
TBS	Tris-buffered saline
TLR9	Toll-like receptor 9
TTP	Time to pregnancy
uNK	Uterine Natural Killer cells
VIP	Vasoactive intestinal peptide

Chapter 1

Introduction

1.1 The Human Endometrium

The endometrium is the inner mucosal layer of the mammalian uterus and functions as a lining for the womb, maintaining the patency of the uterine cavity. Its main role reproductively is to provide a nutritive local environment permissible for viable embryo implantation (Tabibzadeh, 1998). It is an astonishingly plastic tissue. Throughout the female adult reproductive life, ovarian steroid hormones control continuous cycles of proliferation, differentiation and degeneration. In the absence of an implanting embryo, the functional layer of the endometrium is shed, however within 2 weeks full restoration of the tissue is apparent (Knobil, 2013). The events underlying this phenomenon are highly complex and not fully understood. However they are known to include re-epithelialization, proliferation, angiogenesis, cell differentiation and extracellular matrix remodelling (Groothuis *et al.*, 2007). Once the functional layer of the endometrium has successfully been re-established, the cyclic actions of oestrogen and progesterone prime the endometrium into a receptive state once more.

1.2 Structure of the Endometrium

The lining of the human uterus is composed primarily of two main compartments: the stratum basalis, a basal layer which persists from cycle to cycle, and the stratum functionalis, a transitory and dynamic layer which is highly responsive to ovarian steroid hormones (Figure 1.1). The apical edge of the endometrium comprises of a single layer of prismatic epithelial cells which rest of top of a deeply cellular stromal layer containing a rich supply of blood vessels creating a vascular bed (Rogers, 1996). Blood supply to the endometrium originates from arteries within the myometrium, a smooth muscle layer consisting mainly of uterine myocytes. Although the main function of the myometrium is to provide uterine contractions, it also supports the endometrial stromal compartment both structurally and vascularly. Radial arteries within the myometrium split in the endometrium to form basal arteries which supply

the stratum basalis. Spiral arterioles extend towards the endometrial surface and supply the functional layer (Farrer-Brown *et al.*, 1970). These spiral arteries are distinctively coiled and are dynamic throughout the menstrual cycle. Additionally, tubular uterine glands are found in the functional layer of the endometrium and are lined by columnar epithelial cells. The glands secrete uterine histotroph, critical for survival and development of a conceptus (Gray *et al.*, 2001). As the glands form part of the functional endometrial layer, their structure is regulated throughout the menstrual cycle. The functional layer undergoes cyclical changes in proliferation, differentiation and eventual resolution via menstruation. However in the presence of an implanting embryo, the stratus functionalis persists and together with the myometrial junctional zone forms the maternal part of the placenta (Brosens *et al.*, 2002).

The permanent basal layer of the endometrium provides cells for generation of a new functional layer each month during a woman's reproductive years. The average woman from a developed country will have around 400 cycles resulting in menstruation in her lifetime. Surprisingly, it is only recently that several studies have identified progenitor or stem-like cells in the human endometrium which are thought to be the basis of this cyclic regeneration. (Chan *et al.*, 2004; Gargett & Masuda, 2010; Masuda *et al.*, 2010). The endometrium contains mesenchymal stem-like cells (MSCs), with initial studies identifying and isolating a population of stromal cells which demonstrated multipotentcy, immunoprivilege, clonogenicty and the capacity to reconstitute endometrium when xenotransplanted into mice (Gargett & Masuda, 2010; Miyazaki *et al.*, 2012; Wolff *et al.*, 2007). Several approaches have been employed to isolate endometrial stromal populations enriched in MSCs, summarized in Table 1.1. Recent evidence has suggested that as well as residing within the basal layer, stem-like cells may also be found in the functional layer - as demonstrated by their presence in menstrual blood (Patel *et al.*, 2008).

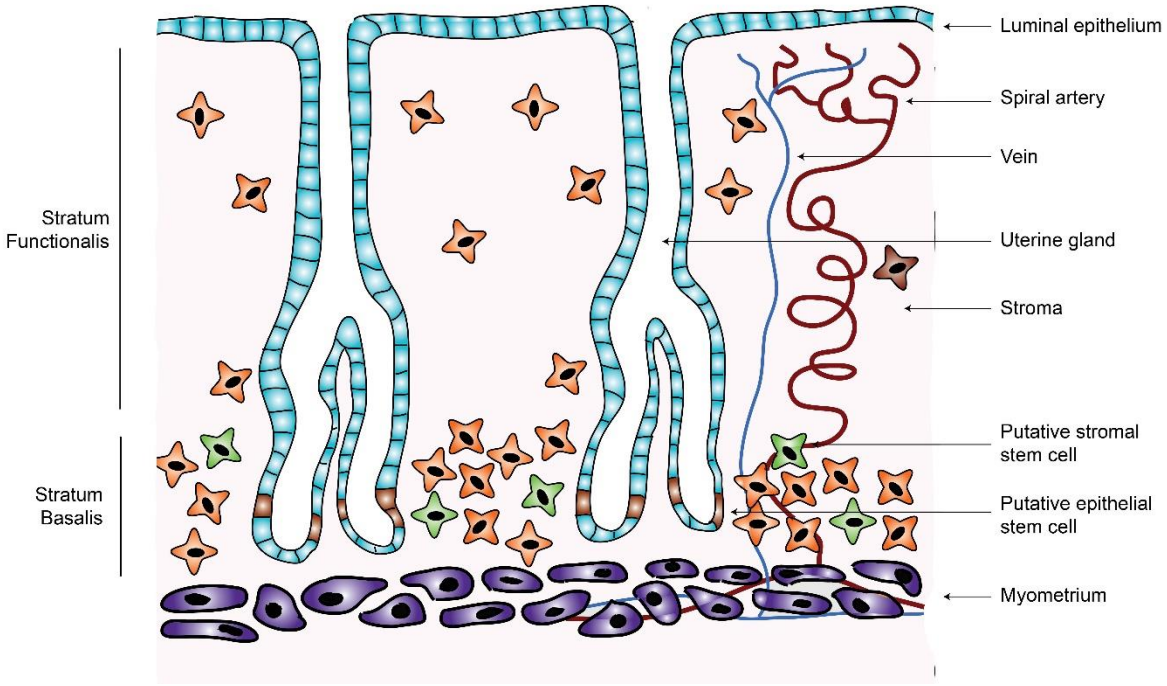

Figure 1.1: ***The human endometrium.***

The endometrium is divided into the superficial stratum functionalis and the persistent stratum basalis. The basal layer serves as an area of regeneration for the functional layer. Spiral arteries and uterine glands are illustrated.

Table 1.1: ***Isolation and characterisation of endometrial stem-like cells*****.**

Stem cell marker	***Property***	***Results***	***Reference***
Low Hoechst 33342 fluorescence	DNA stain	- 2% of total cells from human endometrium displayed side population phenotype by Hoeschst staining. - Side population cells differentiated in various endometrial cell types including glandular epithelium, stromal and endothelial cells. - Endometrial side population cells able to form mature blood vessels in mouse kidney.	(Masuda *et al.*, 2010)
CD146 and PDGF-Rβ	Perivascular markers	- FACS sorted into $CD146^{+}PDGF\text{-}R\beta^{+}$ and $CD146^{-}PDGF\text{-}r\beta^{-}$populations. - Positive cells accounted for 1.5% of sorted population. - Positive cells enriched for colony forming ability. - Differentiate into adipogenic, osteogenic, myogenic and chondrogenic lineages.	(Schwab et al., 2007)
W5C5	Monoclonal antibody	- W5C5 antibody selectively binds MSC enriched populations in endometrium and bone marrow. - $W5C5^{+}$ account for ≈ 5% of endometrial population depending on cell to cell contact and activation of Notch signalling pathways. - $W5C5^{+}$ cells are the dominant source of chemokines and cytokines upon stromal cell differentiation.	(Masuda *et al.*, 2012; Murakami *et al.*, 2014)
CD117 and CD34	Haematopoietic Stem cell markers	- Stem cell markers consistently expressed in the stroma of the basalis layer	(Cho *et al.*, 2004)

1.3 The Menstrual Cycle

In women of reproductive age, the endometrium undergoes cyclical changes in response to ovarian steroid hormones resulting in waves of proliferation, differentiation, inflammation, apoptosis and regeneration (Figure 1.2). Endometrial proliferation is induced by accumulating oestrogen production from granulosa cells within the ovarian follicle. During this proliferative phase (cycle days 5-13) epithelial and endothelial cells rapidly proliferate to reconstitute narrow uterine glands and lengthen the spiral arteries respectively (Brosens *et al.*, 2002; Gray *et al.*, 2001). Concurrently, endometrial stromal cells also proliferate as evidenced by numerous mitotic divisions. This proliferative phase results in an increase in endometrial thickness from 1-2mm after ovulation to 7-8mm by the time of ovulation (cycle day 14). Increasing serum oestrogen concentrations result in a surge of luteinising hormone (LH) which in turn stimulates progesterone production from the corpus luteum, signifying the secretory phase of the cycle. Post-ovulatory progesterone inhibits endometrial proliferation and induces a differentiation programme termed decidualization. The secretory phase is characterised by dramatic structural and functional changes in order to render the endometrium receptive to an implanting blastocyst. Uterine glands become increasingly coiled with widened lumens and produce a glycogen rich secretion. This is accompanied by increased blood flow to spiral arteries, which also become more coiled in nature. An influx of specialised uterine natural killer (uNK) cells is apparent during this secretory phase, which is concomitant with extensive remodelling of the extracellular matrix (ECM) and local oedema within the stromal compartment (Gellersen & Brosens, 2003; Gellersen & Brosens, 2014; Hanna *et al.*, 2006). Together, these modifications are required in order to provide a supporting environment for embryo implantation and development. Human chorionic gonadotrophin (hCG) secretion from the trophoblast sustains the corpus luteum and preserves progesterone production. However, in the absence of a

conceptus, the corpus luteum regresses and serum progesterone levels decline, triggering a cascade of events resulting in proteolytic breakdown.

Menstruation is a rare occurrence with only humans, elephant shrews, fruit bats and some old world primates capable of monthly endometrial shedding (Emera *et al.*, 2012). Furthermore, decidualization in the absence of an implanting embryo only occurs within menstruating species. Changes in serum concentrations of progesterone are known to cause both of these phenomena with increasing and decreasing levels resulting in decidualization and menstruation respectively (Figure 1.2). Thus, in mice, menstruation can be artificially induced if decidualization has been primed to occur prior to progesterone withdrawal (Xu *et al.*, 2007). Proteolytic breakdown of the endometrium is characterized by apoptosis and infiltration of inflammatory neutrophils and mast cells. Leukocyte populations within the endometrium account for up to 40% of the total cell population immediately before menstruation, release pro-inflammatory cytokines into the stromal compartment (Salamonsen *et al.*, 2002). Activation of matrix metalloproteinase (MMP) degrade the ECM, whilst local production of prostaglandin results in vasospasm of the spiral arterioles and ischemia, leading to sloughing of the superficial endometrium.

Debate is still ongoing regarding the evolutionary purpose of menstruation. One theory predicts that menstruation is a form of protection against excessive maternal investment in poor quality embryos (Teklenburg *et al.*, 2010a), whilst others argue that it is metabolically more efficient than maintaining a continual receptive state (Strassmann, 1996). The theory of preconditioning suggests that cyclic menstruation serves to condition uterine tissues to inflammatory and oxidative stressors associated with deep placentation (Brosens *et al.*, 2009). However, more pragmatically many view menstruation as serving no purpose other than to restart the endometrial cycle in the absence of pregnancy.

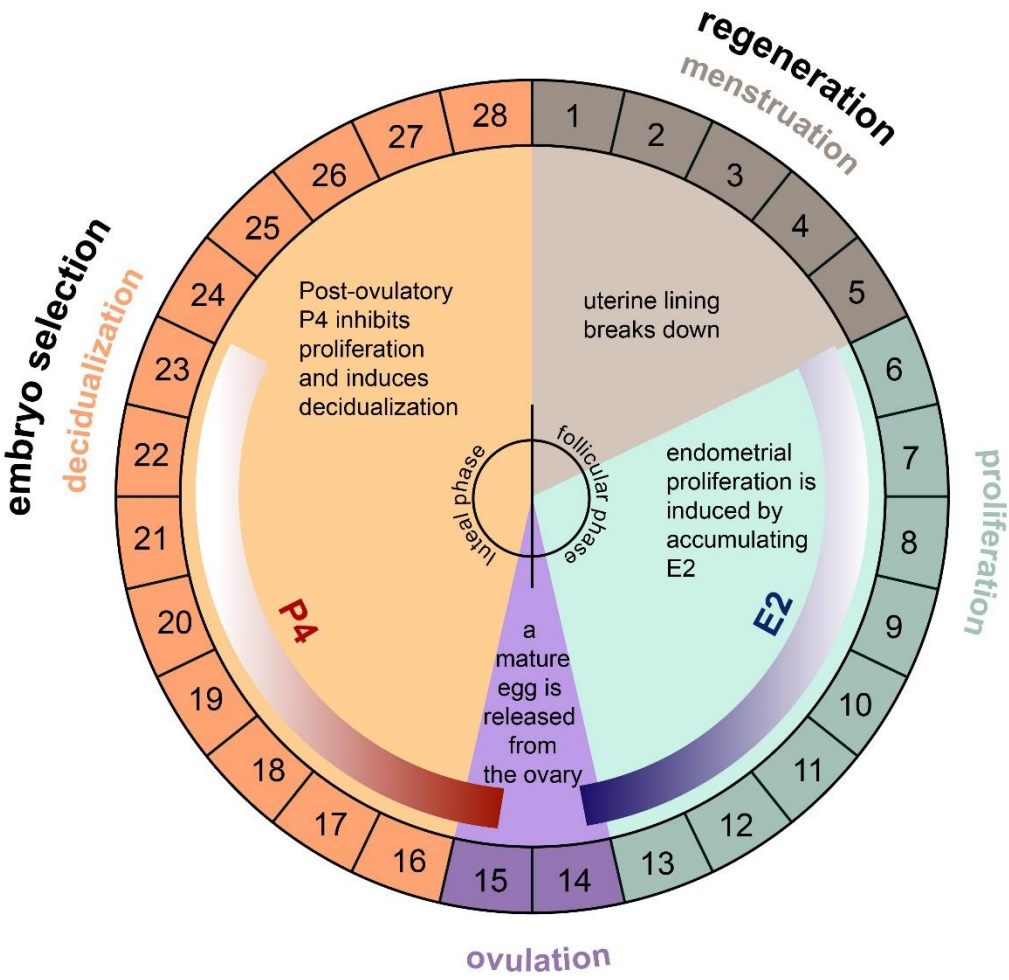

Figure 1.2*: The menstrual cycle.*

The menstrual cycle is governed by a series of cyclic change in levels of ovarian steroid hormones and can be divided into the follicular and luteal phases. Decidualization represents a period of endometrial selectivity in which embryo selection occurs. Menstruation signifies a period of endometrial shedding and subsequent regeneration from the stem cell niche.

1.4 Decidualization of the Endometrium

The first morphological signs of decidualization are apparent 10 days after the post-ovulatory rise in progesterone levels. These occur in the endometrial stromal cells surrounding the terminal spiral arteries and the underlying luminal epithelium. In their undifferentiated form, human endometrial stromal cells (HESCs) have an elongated spindle-shaped fibroblast appearance (Figure 1.3). Decidualization bestows a secretory and epithelioid phenotype on HESCs. Sub-cellularly this is characterised by the rounding of the nucleus, enlargement of the rough endoplasmic reticulum, and cytoplasmic accumulation of glycogen and lipid droplets. Additionally, numerous projections appear on the HESC surface which extend into the ECM or indent into adjacent cells. Decidualizing HESCs produce a wealth of ECM proteins including fibronectin, type IV collagen and heparin sulphate proteoglycan, which precipitate into a basement membrane-like material.

In concert, the cytoskeleton of HESCs is extensively modified. Increases in filamentous actin polymerisation, dephosphorylation of light chain of myosin 2 (MLC2), expression of desmin, vimentin and α-smooth muscle actin results in a more contractile myofibroblastic phenotype (Can *et al.*, 1995; Glasser & Julian, 1986; Ihnatovych *et al.*, 2007; Oliver *et al.*, 1999). Acquisition of this characteristic phenotype enables decidualizing stromal cells to actively migrate and surround the implanting embryo, as evidenced by time-lapse imaging studies of human blastocysts placed on a monolayer of decidualizing HESCs (Grewal *et al.*, 2010; Grewal *et al.*, 2008). The decidual process is critical for successful pregnancy in humans and other species with placentation as it bestows characteristics on the endometrium critical for placental formation, including the ability to regulate vascular and immune responses, withstand increased levels of reactive oxygen species, and establish maternal tolerance to foetal antigens. Accumulating evidence suggests that impaired

preparation of the endometrium may lead to a myriad of pregnancy complications, including miscarriage, pre-eclampsia, foetal growth restriction and preterm labour (Brosens & Gellersen, 2010).

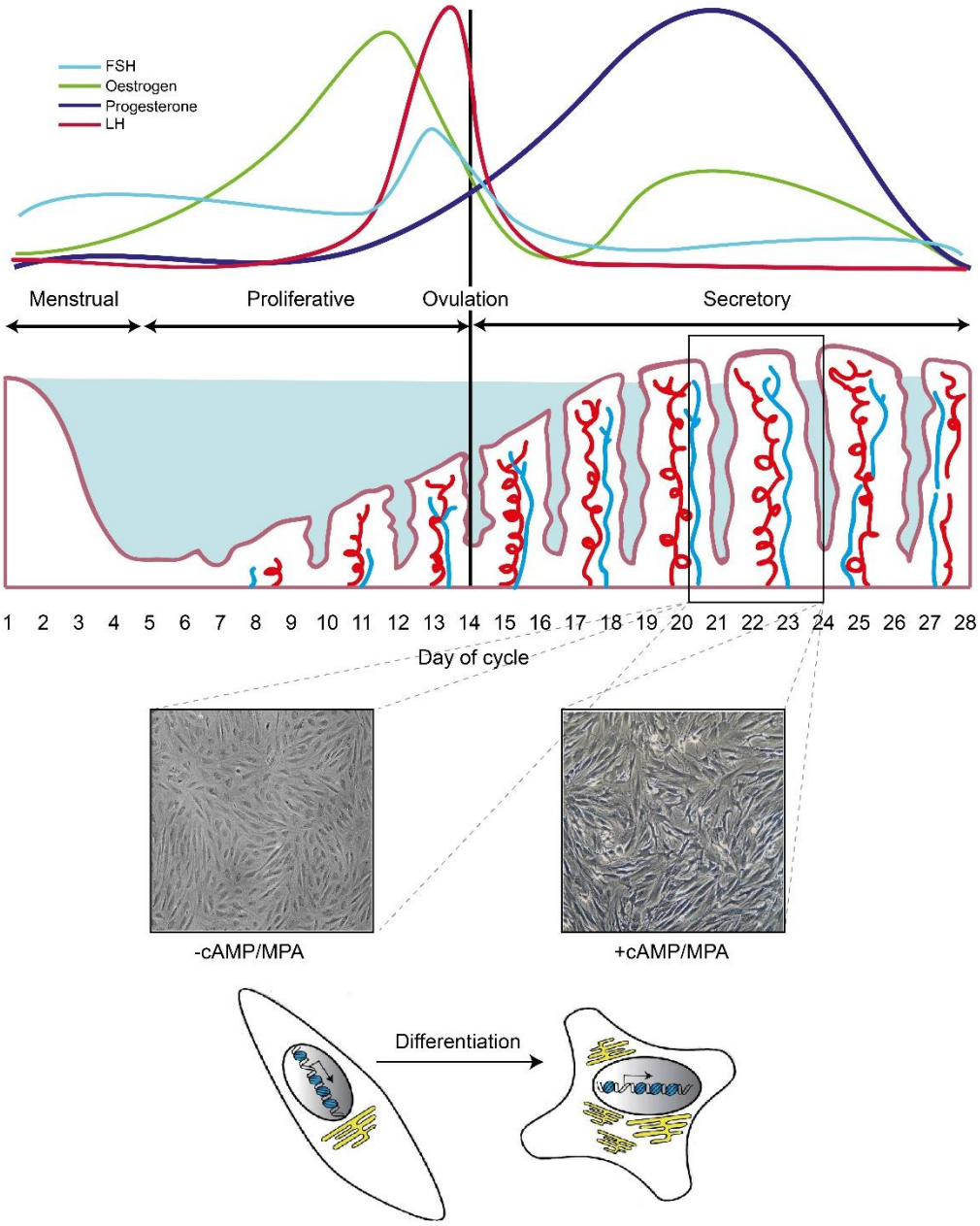

Figure 1.3*: Decidual transformation.*

Decidualization is initiated during the mid-secretory phase of the menstrual cycle by the post-ovulatory rise in progesterone. *In vitro* decidualization can be recapitulated by treatment of HESCs with a cell permeable cAMP analogue (8-br-cAMP) and a synthetic progestin MPA.

1.5 Decidualizing Signals

1.5.1 cAMP Signalling Pathway

The ubiquitous second messenger cyclic adenosine monophosphate (cAMP) is require for functional decidualization. It is produced upon binding of extracellular ligands to G_s protein-coupled receptors, resulting in activation of adenylyl cyclase which in turn generates cAMP from adenosine triphosphate (ATP). *In vivo* adenylyl cyclase activity, and thus cAMP levels, are higher during the secretory phase of the cycle (Tanaka *et al.*, 1993) in response to endocrine cues including relaxin, cortiocotrophin-releasing hormone (CRH), and prostaglandin E2 (PGE2) (Bartsch *et al.*, 2004; Milne *et al.*, 2001; Zoumakis *et al.*, 2000). Continued elevated cAMP levels are required for the induction of decidual marker genes. Inhibition of protein kinase A (PKA), a major downstream target of cAMP, inhibits this response (Yoshino *et al.*, 2003). Furthermore, inhibition of phosphodiesterase-4 (PDE4), a cAMP degrading enzyme, is sufficient to stimulate decidualization by increasing intracellular cAMP. As such, treatment with PDE4 inhibitors, such as Rolipram has therefore been suggested for application to the endometrium in subfertile women (Bartsch *et al.*, 2004; Bartscha & Ivell, 2004).

The holoenzyme PKA comprises of two regulatory (R) and two catalytic (C) subunits. Two cAMP molecules bind to each of the two R subunits. This causes a conformational change resulting in the release of the C subunits. The C subunits in turn phosphorylate numerous cytoplasmic and nuclear targets, propagating the extracellular signal. These targets include cAMP response element (CRE), CRE binding protein (CREB) and CRE modulator (CREM). Upon PKA signalling, CREB is activated and drives transcription of genes with CRE motifs in their promoters (Telgmann *et al.*, 1997). Additionally, CREM, due to alternative splicing and

alternative translation initiation, functions as both a transcriptional activator and transcriptional repressor of cAMP responsive genes (Gellersen *et al.*, 1997). Other targets include STAT5, CCAAT-enhancer binding protein (CEBP-β) and Forkhead box protein O1 (FOXO1), all of which are required for functional decidualization of HESCs (Gellersen & Brosens, 2014). EPAC (exchange protein directly activated by cAMP) isoforms EPAC1 and EPAC2 have also been shown to play a role in cAMP-dependent decidualization. Activated by cAMP, they act to exchange guanosine disphosphate (GDP) with guanosine triphosphate (GTP) on RAS proteins resulting in regulation of multiple processes including tissue remodelling and calcium homeostasis. Knockdown of either isoform halts differentiation of HESCs (Kusama *et al.*, 2013).

Contrary to other cell types, HESCs do not form a negative feedback loop resulting in reduction of cAMP levels. Instead they act to form a positive feed-forward mechanism, ensuring persistent elevated cAMP concentrations. This is achieved by shifting the ratio of R:C PKA subunits in favour of C. By selectively down-regulating the R subunits, kinase activity is sustained (Telgmann & Gellersen, 1998). Furthermore, inducible cAMP early repressor (ICER), which functions as a repressor of CRE-responsive gene promoters (including its own) is constituently elevated upon decidualization, thereby preventing the creating a negative feedback loop. As such, persistent PKA signalling, together with stimulatory CREM isoforms maintains cAMP dependent signalling in these cells (Gellersen *et al.*, 1997).

1.5.2 Progesterone Signalling Pathway

Although treatment of primary cultures with 8-br-cAMP is able to trigger the expression of the decidual markers prolactin (PRL) and insulin-like growth factor-binding protein 1 (IGFBP1) within hours, the decidual phenotype cannot be sustained

by cAMP signalling alone. The addition of a progestin to cultures acts to enhance and maintain the cAMP induced response and is required for a sustained decidual phenotype. Progesterone acts predominately by binding its nuclear receptors PR-A and PR-B, (the two isoforms are derived from differential promoter usage from a single gene), in order to activate or repress target genes (Kastner *et al.*, 1990). PR-A lacks the 164 N-terminal amino acids found in PR-B, however both isoforms display equivalent ligand and DNA-binding affinities (Li & O'Malley, 2003). PR-A acts primarily as a dominant inhibitor of PR-B and other nuclear receptors, whilst PR-B displays more transcriptional activation activity (Brosens *et al.*, 2004; Li & O'Malley, 2003). Double knockout of PR-A/PR-B renders the mouse uterus unable to mount a decidual response and thus implantation is impaired (Brosens *et al.*, 1999; Conneely *et al.*, 2001; Mote *et al.*, 2000).

The two isoforms are differentially spatiotemporally regulated during the menstrual cycle. PR-A is highly expressed in stromal cells throughout the cycle, however its expression in the epithelial compartment is high during the proliferative phase, although it drops post-ovulation. On the other hand, PR-B expression is found in both the stromal and epithelial compartments during the proliferative phase, however decidualization is associated with the rapid down regulation of PR-B, making PR-A the dominant isoform (Mangal *et al.*, 1997; Mote *et al.*, 2000; Mulac-Jericevic & Conneely, 2004). Regulation of PR-A and PR-B is essential as aberrations in the spatiotemporal ratio between the isoforms in the uterus has been linked to endometrial neoplasia (Arnett-Mansfield *et al.*, 2001). The dominance of PR-A is demonstrated by knockdown. In its absence, progesterone acts to induce epithelial proliferation, decidual transformation is absent, and as a result the mice are sterile (Conneely *et al.*, 2001). In addition to the regulation of PR isoforms, other mechanisms control the expression of PR. Promoter regulating RNAs have been shown to modulate the *PR* promoter by enhancing or diminishing gene expression

through binding noncoding transcripts overlapping target promoters (Chu *et al.*, 2012). Furthermore, several micro RNAs (miRNAs) have been shown to influence PR mRNA half-life (Lam *et al.*, 2012).

Structurally, the unliganded PR is a large multi-subunit complex containing various chaperone proteins, including heat shock proteins and immunophilins (Pratt & Toft, 1997), which are necessary for maintaining a 3D structure permissible for progesterone binding. Upon hormone binding, the receptor undergoes a conformational change resulting in phosphorylation, dissociation from chaperone proteins, receptor dimerization, binding to specific progesterone response elements (PREs) in target genes, and recruitment of transcription machinery. Steroid-receptor co-activators (SRCs) are required for these latter events, including histone acetyltransferases CBP, CBP associated factor (pCAF) and coactivator associated arginine methyltransferase 1 (CARM1), in order to modify the chromatin landscape for induction of transcription. Conversely, corepressors such as silencing mediator of retinoid and thyroid receptor (SMRT) and nuclear receptor corepressor (N-CoR) are required for transcriptional repression (Shibata *et al.*, 1996; Wagner *et al.*, 1998).

1.5.3 Convergence of cAMP and Progesterone Signalling

Importantly, although primary HESCs express all the components of the progesterone signalling pathway, very few genes are acutely responsive to treatment with progesterone alone. It is apparent that the convergence of the cAMP and progesterone pathways is required in order for full decidualization. This is achieved via multiple mechanisms including epigenetic remodelling, post-translational modifications and induction of decidua-specific transcription factors (Gellersen & Brosens, 2014). Functional decidualization requires an intracellular increase in cAMP levels in order to sensitize HESCs to progesterone signalling. Firstly, cAMP

analogues have been shown to enhance hormone dependent transcriptional activity of PR by possible disruption of protein:protein interactions between PR and corepressors such as NCoR and SMRT, and thus increasing interactions with coactivators including SRC-1 and CBP (Rowan & O'Malley, 2000; Wagner *et al.*, 1998). Activation of cAMP through PKA dependent and independent pathways also results in an increase of various transcription factors including CEBP/β, STAT5 and FOXO1, all of which are able to interact with PR (Christian *et al.*, 2002a; Richer *et al.*, 1998; Takano *et al.*, 2007). For example, FOXO1a augments the activity of the PRL decidua specific promoter (dPRL) in concert with CEBP/β through an incomplete PRE motif (Christian *et al.*, 2002b). Furthermore, STAT5 significantly enhances dPRL activity in the presence of cAMP and progestin (Mak *et al.*, 2002). Therefore, it is hypothesised that PR, along with multimeric complexes of cAMP induced factors, allows activation of a decidua specific gene network (Figure 1.4). Moreover, regulation of these transcription factors, including PR, are modulated by various posttranslational modifications including ubiquitination, acetylation and sumolylation. For example, cAMP attenuates ligand-dependent sumoylation of PR via protein inhibitors of activated STAT (PIAS) activity (Jones *et al.*, 2006). As such, complete activation of decidua specific gene networks is absolutely reliant upon the conjunction and cooperation of multiple signalling pathways.

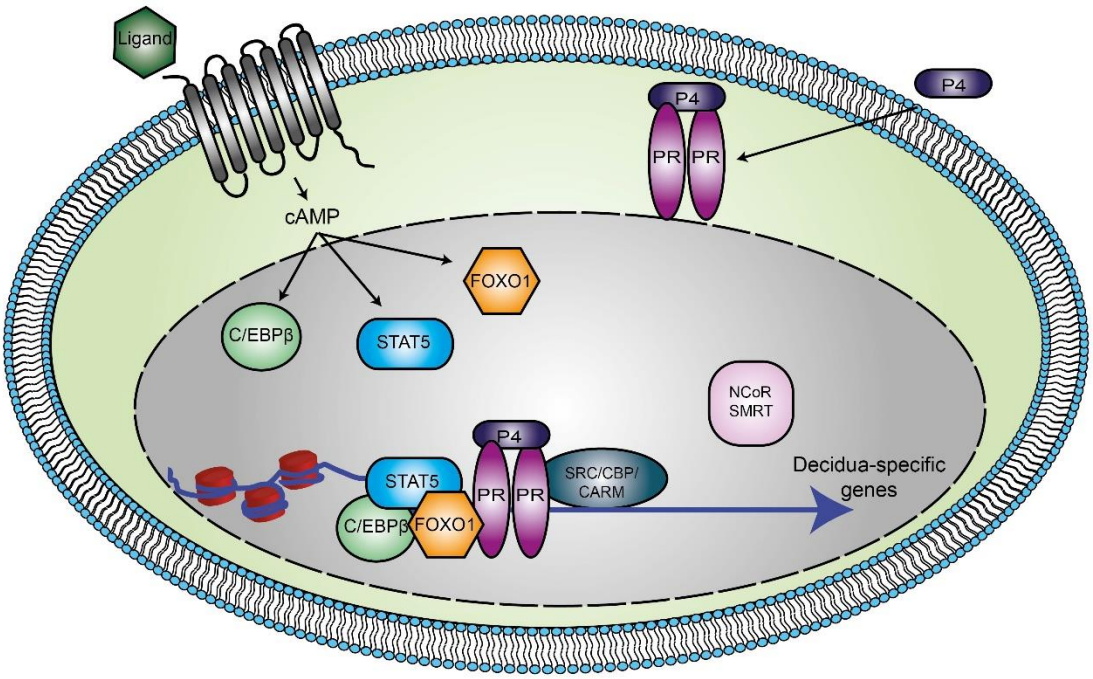

Figure 1.4: ***Convergence of cAMP and progesterone signalling during decidualization.*** Ligand binding to G-protein coupled receptors results in increased cAMP production and subsequent activation of the PKA-dependent and -independent pathways. These cascades result in the nuclear accumulation of CEBP/β, FOXO1 and STAT5. Liganded PR-A is able to interact with these factors resulting in transcription initiation of decidua-specific genes with co-activators (SRC, CBP, CARM) as binding to co-repressors (NCoR, SMRT) is disrupted. Figure adapted from Gellersen & Brosens (2003).

1.6 Implantation and Endometrial Receptivity

Embryo implantation denotes the most critical step of the reproductive process. In order to occur, a competent embryo must attach to a receptive endometrial lining and be accepted and surrounded by the underlying decidual stroma. The process of implantation is considered to be a stepwise process of apposition, adhesion and subsequent encapsulation by the stroma, and requires a synchronised dialogue between maternal and embryonic tissues. Traditionally, implantation has been described as an invasion of trophoblast cells into the decidua, whilst the endometrium remains passive. Endovascular extravillous trophoblast cells display such an aggressive invasion of the spiral arteries they have been likened to a metastasising tumour (Ferretti *et al.*, 2007). However, recent co-culture models have challenged this theory. When hatched blastocysts were placed onto a monoloayer of decidualized HESCs it was apparent that the decidual cells actively engulf and encapsulate the embryo (Grewal *et al.*, 2008; Teklenburg *et al.*, 2010b) highlighting the invasive and migratory capabilities of stromal cells.

Implantation is the rate-limiting step in artificial reproductive technologies (ART) and is a major cause of infertility in otherwise healthy women. The average implantation rate in IVF is approximately 25%. Much debate remains as to whether the primary cause of implantation failure is embryonic or maternal in nature. Poor embryo quality due to the high incidence of chromosomal abnormalities in human embryos has long been considered the major contributor to implantation failure. These abnormalities and specifically aneuploidies increase with age and arise due to errors during meiosis or from the first mitotic divisions (Delhanty, 2005; Vanneste *et al.*, 2009). However, recent studies have revealed genetic mosaicism affects up to 90% of human embryos during pre-implantation development, of which the majority appear to be euploid by the blastocyst stage (Santos *et al.*, 2010). This suggests that although chromosomal

abnormalities are prevalent during the early first mitotic divisions, many of these errors are transient and embryos will 'correct' themselves by implantation. As such, pre-implantation genetic screening of 139 recurrent implantation failure patients showed no increase in implantation rate using fluorescent *in situ* hybridisation (FISH) (Blockeel *et al.*, 2008).

On the other hand, the inability of the endometrium to become receptive to embryo implantation is a further cause of implantation failure. The phenomenon of implantation is contained to a self-limiting time-frame termed the 'window of implantation'. This spans between day 20 and 24 of a regular menstrual cycle (LH+6 to LH+10), and during this time the endometrium is primed for blastocyst attachment triggered by changes in ovarian steroid hormones discussed previously (Bergh & Navot, 1992; Koot *et al.*, 2012). The 'window of implantation' is time restricted to enable coordinated embryonic and endometrial development, thereby minimizing the risk of maternal investment in non-viable embryos. Many studies have examined putative biomarkers of endometrial receptivity. Table 1.2 summarises both morphological and molecular markers.

Furthermore, the recent meta-analysis of various microarray studies examining differential gene expression in the endometrium during the 'window of implantation' has been used to create a Human Gene Expression Endometrial Receptivity database (HGEx-ERdb), which has been used to identify receptivity associated genes. Table 1.3 highlights genes with highest up- and down-regulation upon endometrial acquisition of a receptive phenotype.

Table 1.2 : *Morphological and molecular biomarkers of endometrial receptivity and implantation.*

Biomarker	**Role in Implantation**	**References**
Pinopodes (Epithelial cell membrane projections)	- Thought to play a role in protection of the blastocyst from cilia on the endometrial wall. - Potentially facilitate molecular adhesion with the blastocyst - Studies have now identified pinopodes throughout the luteal phase and early pregnancy - Role remains unclear.	(Bentin-Ley *et al.*, 1999; Quinn *et al.*, 2007)
Prostaglandins (PGs)	- Prostaglandins known to possess vasoactive factors to provide the blastocyst access to maternal vascular system. - Enzymes cytosolic phospholipase A2 (cPLA2), COX-1 and COX-2 synthesise PGs are upregulated by P4. - cPLA2 knockout mice show delayed implantation, with exogenous PG administration able to rescue the phenotype. - Recurrent implantation failure (RIF) patients express reduced levels of cPLA2α and COX-2.	(Achache *et al.*, 2010; Song *et al.*, 2002; Wang *et al.*, 2010b)
Mucins	- High molecular weight glycoproteins that act as a barrier for implantation. - *In vivo* models suggest MUC-1 expression is increased during the implantation window but lost at implantation site. - Women suffering recurrent miscarriage shown to expressed reduced endometrial MUC-1.	(Aplin *et al.*, 1996; Meseguer *et al.*, 2001)
Integrins	- Family of transmembrane glycoproteins known for roles in cell-adhesions. - Expression of αVβ3 integrin coincides with the 'window of implantation' - Dysregulated αVβ3 integrin expression associated with unexplained infertility.	(Klentzeris *et al.*, 1993; Lessey *et al.*, 1995)
Cadherins	- Responsible for Ca^{2+} dependent cell-to-cell adhesions - E-cadherin expression is P4 dependent via calcitonin and its downregulation thought to play a role in embryo invasion	(Achache & Revel, 2006; Li *et al.*, 2002)

Leukaemia inhibitory factor (LIF)	-	Cytokine affecting proliferation, differentiation and cell survival. - Female mice with LIF gene deficiency display failed embryo implantation. - RIF patients display weakened induction of LIF from the proliferative to secretory phase. - However, clinical trials in which recombinant LIF was administered to RIF patients did not show any increase in implantation rate in the intervention group.	(Achache & Revel, 2006; Brinsden *et al.*, 2009; L Stewart, 1994)
Interleukin -1 (IL-1)	-	IL-1 deficient mice were able to reach pregnancy, however intraperiotoneal injections of IL-1 receptor antagonist was sufficient to prevent implantation. - Attributed to regulation of integrin expression. - IL-1 supplementation of culture media of endometrial epithelial cells results in increase integrin β3 expression.	(Simón *et al.*, 1994; Simón *et al.*, 1997)
Interleukin- 6 (IL-6)	-	IL-6 receptors are found both in the endometrium but also the blastocyst during implantation suggestive of a paracrine/autocrine role. - IL-6 deficient mice display reduced fertility due to impaired implantation. - Recurrent miscarriage patients reportedly have abnormal IL-6 expression during the late secretory phase.	(Achache & Revel, 2006; Lim *et al.*, 2000)
Uterine Natural Killer cells (uNK)	-	uNKs are the most abundant immune cells present in the endometrium. - Elevated uNK cells in the stroma are associated with deregulation of cortisol biosynthesis and poor induction of key enzymes involved in lipid biogenesis and retinoid transport. - Excessive uNK cells in the stroma serve as a biomarker of suboptimal decidualization. - Percentage uNK used as a clinical test for women a risk of recurrent miscarriage.	(Kuroda *et al.*, 2013; Quenby & Farquharson, 2006; Tang *et al.*, 2011)
Micro-RNA (miRNA)	-	Roles in post-translational regulation of gene expression by regulating mRNA stability. - RIF patients displayed differential expression of 13 miRNAs compared to controls. - miRNAs involved included regulation of Wnt signalling, cell cycle regulation and cell-to-cell adhesions.	(Kuokkanen *et al.*, 2010; Revel *et al.*, 2011)

GENE SYMBOL	GENE NAME	UPREGULATION SCORE
SPP1	Secreted phosphoprotein 1	18
GPX3	Glutathione peroxidase 3	14
PAEP	Progestogen-associated endometrial protein	12
IGFBP7	Insulin-like growth factor binding protein 7	12
IL15	Interleukin 15	12
CD55	CD55 molecule, decay accelerating factor for complement	10
CLDN4	Claudin 4	6
DPP4	Dipeptidyl-peptidase 4	8
COMP	Cartilage oligomeric matrix protein	6
LAMB3	Laminin, beta 3	6
TIMP1	TIMP metallopeptidase inhibitor 1	4
DCN	Decorin	4
LIF	Leukaemia inhibitor factor	2
TCN1	Transcobalamin I	4
C4BPA	Complement component 4 binding protein alpha	4
IL6ST	Interleukin 6 signal transducer	4
MAOA	Monoamine oxidase A	4
MFAP5	Microfibrillar associated protein 5	4
TSPAN8	Tetraspanin 8	4
FAM148B	Family with sequence similarity 148, member B	4
GADD45A	Growth arrest and DNA damage inducible, alpha	4
S100P	S100 calcium binding protein P	4
IGFBP3	Insulin like growth factor binding protein 3	4
FXYD2	FXYD domain containing ion transport regulator 2	4

GENE SYMBOL	GENE NAME	DOWN-REGULATION SCORE
EPHB3	EPH receptor B3	4
CDC20	Cell division cycle 20 homolog	4
PTTG1	Pituitary tumour transforming 1	4
E2F2	E2F transcription factor 2	2
CDC45L	Cell division cycle 45 homolog	2
BMP7	Bone morphogenetic protein 7	2
KCNG1	Potassium voltage gated channel, subfamily G, member 1	2
S100Z	S100 calcium binding protein Z	2
EFNA2	Ephrin A2	2
S100A2	S100 calcium binding protein A2	2
S100G	S100 calcium binding protein G	2
PLA1A	Phospholipase A1 member A	2
TRH	Thyrotropin releasing hormone	2
FOXM1	Forkhead box M1	2
S100A5	S100 calcium binding protein A5	2
GJB6	Gap junction protein beta 6	2
TACC3	Transforming, acidic coiled coil containing protein 3	2
KIF20A	Kinesin family member 20A	2
PAQR4	Progestin and adipoQ receptor family member 4	2
CALB2	Calbindin 2	2

Table 1.3: ***HGEx-ERdb top 25 and 20 genes with highest up- and down-regulation upon endometrial acquisition of a receptive phenotype respectively (Bhagwat et al., 2013).***

1.7 Cell Fate Decisions

The processes of decidualization and endometrial receptivity both rely upon coordinated integration of various signalling pathways which cumulatively result in the molecular basis of life and death decisions in response to ovarian steroid hormones. These key cell fate decisions each cycle are able to shift the endometrial reaction to an appropriate response determined by the presence or absence of a competent or incompetent embryo. The role of key transcription factors and other proteins underpin these decisions and often lie at the junctions of various signalling pathways. For example, the balance between the progesterone induced promyelocytic leukaemia zinc finger protein (PLZF) and cAMP induced C-terminal fragment of heparin-binding epidermal growth factor-like growth factor (HB-EGF-C) is thought to participate endometrial stromal fate by the balancing anti- and pro-apoptotic signals respectively (Brosens & Gellersen, 2006; Nanba *et al.*, 2003).

FOXO1 is markedly induced upon decidualization and participates as part of multimeric transcription factor complexes driving expression of key decidual genes including *PRL* and *IGFBP1.* FOXO1 plays a critical role in proapoptotic pathway upon progesterone withdrawal in the absence of an implanting conceptus. FOXO1 nuclear accumulation is cAMP dependent, however progesterone treatment results in FOXO1 translocation to the cytoplasm rending it inactive. In turn, progesterone withdrawal at the end of the menstrual cycle results in rapid nuclear re-accumulation of FOXO1, enabling it to target proapoptotic mediators such as BIM and Fas ligand (FASLG) (Brosens & Gellersen, 2006; Labied *et al.*, 2006).

Furthermore, cAMP induced protein stabilisation of p53 may also regulate cell fate in the endometrium. It is hypothesised that increased p53 protein during decidualization may be transcriptionally inert but still able to exert repression via protein:protein

interactions; however upon withdrawal of progesterone, p53 transcriptional activity is then released resulting in endometrial breakdown (Brosens & Gellersen, 2006; Christian *et al.*, 2002a; Christian *et al.*, 2002b) Thus, the balance between activated and non-activated p53 may serve as a critical decision making molecule in the endometrium.

1.8 Recurrent Pregnancy Loss

In humans, the incidence of embryo wastage and pregnancy loss is remarkably high. It is estimated that 30% of embryos are lost prior to implantation, 30% result in early pregnancy loss, and a further 10% in clinically recognised pregnancies (Rai & Regan, 2006). Moreover, 1-2% of couples experience recurrent pregnancy loss (RPL), which is defined in Europe as three or more consecutive miscarriages and in the USA as two or more consecutive miscarriages (Quenby *et al.*, 2002). By probability alone, the RPL rate in fertile couples would be 0.3-0.4%, therefore it appears that some couples are more susceptible to miscarriage than others. Alongside numerous anatomical, endocrine, immunological and thrombophilic perturbations, traditionally it was presumed that RPL was a result of maternal rejection of normal embryos. However a fairly recent shift in paradigm now suggests that RPL is the result of a failure to prevent 'poor quality' embryos implanting in the endometrium, and as such RPL can be thought of a defect of endometrial quality control (Aplin *et al.*, 1996; Quenby *et al.*, 2002). This is supported by the finding that RPL and time to pregnancy (TTP) rates are linked. Retrospective analysis of RPL patients revealed up to 40% could be classed as 'superfertile' defined as a TTP of ≤ 3 months (Salker *et al.*, 2010). As such, the lower levels of endometrial quality control result in the implantation and subsequent miscarriage of karyotypically abnormal embryos. Supporting this hypothesis is the finding that uterine receptivity is enhanced and prolonged in RPL patients as demonstrated by significantly higher and protracted PROK1 expression

(a promoter of embryo-uterine interactions by induction of LIF) (Salker *et al.*, 2010) and a prolonged pro-inflammatory response (Salker *et al.*, 2012). Furthermore, expression of the anti-adhesion molecule MUC-1 was found to be attenuated in RPL endometrium (Aplin *et al.*, 1996). It is now assumed that both endometrial receptivity programming and endometrial responses to embryonic signals are deregulated in RPL, acting to extend the 'window of implantation' and thus permits out-of-phase implantation in an unsupportive uterine environment.

1.9 The Central Circadian Clock

The circadian clock is a molecular pacemaker, central to the temporal organisation of physiological, behavioural and biochemical activities of a vast array of organisms. Standard terminology states that a circadian rhythm is an endogenous biological rhythm that persists under constant environmental conditions with a period length of approximately 24 hours. Circadian rhythms permeate all aspects of mammalian physiology from sleep-wake cycles to mating behaviour (Jin *et al.*, 1999; Sakai & Ishida, 2001); from hormone regulation to redox state (Karman & Tischkau, 2006; Merrow & Roenneberg, 2001). Circadian oscillations allow for the anticipation of environmental changes during the day and hence adaptation of multiple physiological processes. The presence of circadian pacemakers in cyanobacteria is suggestive of a conserved role of the clock throughout evolution (Dvornyk *et al.*, 2003). It is thought circadian rhythms served to time DNA replication to darkness to protect DNA from UV radiation (Gehring & Rosbash, 2003).

In mammals, the biological basis of the central pacemaker is a cell-intrinsic molecular clock within a region of the anterior hypothalamus called the suprachiasmatic nucleus (SCN). This is a small structure consisting of approximately 20,000 neurons and glial cells. It is situated dorsal to the optic chiasm and is responsible for the establishment

of the daily rhythm (Moore *et al.*, 2002). It is classically divided into ventral and dorsal regions, known as the SCN shell and the SCN core respectively. The ventral shell region contains vasoactive intestinal peptide (VIP) producing neurons as well as other non-VIP cell types inducing Gastrin-Releasing Peptide (GRP) producing neurons. The dorsal core, however, is known to contain neurons producing arginine vasopressin (AVP) and receives input from the VIP neurons (Ueyama *et al.*, 1999). The spatial distribution of these subpopulations is highly specific and conserved across species, suggesting a localisation for the processing of circadian information (Abrahamson *et al.*, 2001).

The SCN is required for behavioural rhythmicity in mammals as it contains the most robust molecular clockwork in the body, and therefore is critical for many free-running rhythms in the absence of light (Husse *et al.*, 2014). In other words, the SCN generates daily time autonomously. Explanted SCN tissue from mice is able to maintain circadian oscillations in both gene expression and neural activity (Abe *et al.*, 2002). Interestingly, studies have revealed that although SCN neurons are synchronised, they are not in phase with one another. Dorsal neurons are shown to peak 2-3 hours prior to ventral cells, creating a spatiotemporal wave throughout the SCN, critically dependent on synaptic integration. Specific SCN inhibition of voltage-gated sodium channels dampens the phase relationship between neurons impairing the circadian wave (Yamaguchi *et al.*, 2003).

The second function of the SCN is to entrain biological rhythms to external cues, termed zeitgebers in order to adjust the rhythm to the environment. The strongest of these zeitgebers is light, which entrains the circadian rhythm via direct neural input from the eyes via the optic tract (Roenneberg *et al.*, 2013). Emerging evidence suggests the involvement of melanopsin receptors for circadian entrainment. Light induced phase shifts of the SCN, as well as light induced inhibition of melatonin are

mediated by a mechanism independent of rods and cones (Lucas, 2001). Light information reaches the SCN via the retinohypothalamic tract (RHT) from the retina. In the SCN, VIPergic neurons integrate light input to confer intrinsic synchronisation of the SCN neurons (Antle & Silver, 2005). This is achieved by signalling to the rhythmic AVP neurons in the dorsal region via VPAC2 receptors. VIP or VPAC deficient mice display an 8 hour behavioural phase shift and lose rhythmicity in constant darkness due to defective synchrony between SCN neurons (Harmar *et al.*, 2002).

As well as pace-making in the absence of external stimuli and entraining to light signals, the SCN must also convey temporal cues to the rest of the body ensuring rhythmic behavioural output appropriate to environmental conditions. This is thought to be directed from the AVP neurons which display high amplitude oscillations in neuronal firing, neuropeptide expression, and release. Interestingly, however, exogenous addition of AVP does not result in any measurable changes in circadian gene expression or behaviour (Arima *et al.*, 2002). Output from the SCN is achieved directly by secreted factors and multisynaptic neural pathways. The SCN neurons project into the medial hypothalamus surrounding the SCN. Activity of these autonomic and neuro-endocrine target neurons are controlled by circadian timed release of vasopressin, GABA and glutamate. (Kalsbeek et al., 2006). The SCN is also known to secrete factors into the cerebrospinal fluid (CSF) including AVP, transforming growth factor, (TGFα) and prokineticin 2 (PK2) (Kennaway, 2005). PK2 has been shown to influence sleep/wake cycles in mice (Cheng *et al.*, 2002), whilst AVP is thought to be implicated in circadian temperature regulation. Additionally, hormonal signals are able to target peripheral organs as shown by the ability of glucocorticoids to re-set the circadian phase in multiple organs (Balsalobre *et al.*, 2000a)

One of the most studied outputs from the SCN is melatonin secretion from the pineal gland. Melatonin secretion at night is controlled by noradrenaline, which is secreted from sympathetic neurons in the superior cervical ganglion which in turn, project onto the pineal gland. Information from the SCN reaches the sympathetic system via the paraventricular nuclei and intermediolateral column of the spinal cord (Teclemariam-Mesbah *et al.*, 1999). Fluctuations in melatonin act to regulate day-night cycles with levels peaking in the middle of the night. Aberrations in melatonin regulation have been implicated with ageing and sleep disorders (Brzezinski *et al.*, 2005). Interestingly, exogenous addition of melatonin is able to dampen the SCN neural firing rate, suggesting melatonin receptors in the SCN are able to mediate negative feedback, or phase-shifting events in the central clock (Dubocovich *et al.*, 2005).

1.10 Peripheral Clocks

The SCN, as well as directly influencing circadian output, also synchronizes and influences multiple peripheral circadian clocks found throughout the body. Originally thought of as ‘slave’ oscillators, these peripheral clocks have been shown to be endogenous and self-sustained, maintaining up to 20 circadian cycles upon explant (Yoo *et al.*, 2004). Ablation studies of the SCN in mice have shown that many organs continue to be rhythmic but no longer in time with each other. This suggests that peripheral oscillators are not connected in a paracrine manner and rely upon the SCN for synchronisation (Ripperger & Brown, 2010). Furthermore, experiments from Guo et al. (2006) demonstrated that signals derived from the SCN were able to entrain the circadian phase of both the liver and kidney.

Current opinion describes an ‘orchestra’ model of the circadian clock in which the SCN behaves as a conductor, whilst each peripheral clock acts as a musician. Therefore, each peripheral oscillator is able to be influenced by its own environmental

conditions and is also able to influence circadian output, whilst the SCN is able to guide and adjust both the input to and the output of these peripheral clocks (Dibner *et al.*, 2010). Circadian oscillations in gene expression have been found in tissue explants from nearly every peripheral organ, including heart, lung, cornea, pancreas and adrenal gland (Yamazaki *et al.*, 2000; Yoo *et al.*, 2004) which in turn leads to circadian regulation of key physiological functions such as lipid metabolism (Turek *et al.*, 2005), endobiotic detoxification (Gachon *et al.*, 2006), urine production (Nørgaard *et al.*, 1985) and regulation of blood pressure (Millar-Craig *et al.*, 1978). For example, anti-phase circadian regulation of glycogen synthase and glycogen phosphorylase ensures efficient glucose conversion in the liver (Ishikawa & Shimazu, 1980). A fully functional circadian clock is required for blood pressure regulation via rhythmic regulation of plasminogen activator inhibiot-1 (PAI-1) (Naito *et al.*, 2003), and pathogenic recognition by Toll-like receptor 9 (TLR9) is disrupted upon circadian mutation (Silver *et al.*, 2012). It is estimated that up to 10% of the human transcriptome and 20% of the proteome have rhythmic oscillations. The output of circadianally driven genes differs from tissue to tissue, allowing tissue-specific responsiveness to various cues both externally and internally via the SCN (Boden *et al.*, 2013b; Oster *et al.*, 2006).

Entrainment and synchronisation of peripheral oscillators is influenced by both hormonal and neuronal signalling from the SCN. For example, plasma glucose and insulin concentrations are affected by treatment with GABAergic antagonists in mouse models. However, this effect is absent in SCN-ablated mice, suggestive of a requirement for GABAergic SCN inputs for liver regulated outputs (Kalsbeek *et al.*, 2008). Zeitgebers are also important for peripheral clocks. Daily feeding-fasting cycles are proposed to be the dominant environmental input for several peripheral oscillators. Restricted daytime feeding in mice results in an inverted phase of gene expression in the liver, while gene expression in the SCN remains unchanged,

effectively uncoupling the peripheral and central clocks (Damiola *et al.*, 2000). Multiple signalling molecules and pathways including ghrelin, leptin and glucose concentrations as well as intracellular redox balance are all proposed to act as entraining signals for peripheral organs (Jaworek *et al.*, 2005; Rutter *et al.*, 2002).

Single cell recordings have demonstrated that presence of functional oscillators in cultured cells including Rat-1 fibroblasts and NIH-3T3 cells (Akashi & Nishida, 2000; Balsalobre *et al.*, 2000b). The circadian oscillations produced by cultured cells are both robust and self-sustained, although unsynchronised. Synchronisation can be achieved through activation of several signalling pathways including glucocorticoids, insulin or retinoic acid (Balsalobre *et al.*, 2000a; Hirota & Fukada, 2004). Importantly, peripheral oscillations must be resistant to changes in temperature and must persist during cell division. Research has demonstrated that circadian gene expression passes on to daughter cells with minimal disruption to the phase. This is further exemplified in resilience to temperature fluctuations. In contrast to most biochemical processes, which will increase in speed upon rising temperature, the period of the circadian oscillations are temperature compensated and remain constant even in cultured fibroblasts (Takeuchi *et al.*, 2007).

The effectiveness of peripheral clocks is critically dependent upon their robustness. Small alterations in period length can result in larger phase-shifts causing deviations in circadian physiological behaviour. Evidence is still emerging concerning the organisation of the circadian system and the relationship between the SCN and multiple peripheral oscillators. What is becoming increasingly apparent is the high levels of redundancy and complexity within the system, integrating signals from multiple pathways. However, in order to appreciate the circadian system as a whole, one must understand the molecular mechanism underlying this daily cycle.

1.11 Molecular Basis of the Circadian Clock

The circadian clock is constituted of temporally regulated activities of a core set of genes, resulting in a robust and stable transcriptional/translational feedback/feedforward loop (Figure 1.5) (Reppert & Weaver, 2002). The two key transcriptional activator genes are *BMAL1* (brain muscle arnt-like 1, encoded by *ARNTL*) and *CLOCK* (circadian locomoter output cycle kaput). The protein products of these genes bind together via a PAS domain forming a heterodimer. This heterodimer binds to specific DNA motifs (termed E-boxes) in the promoter regions of many genes. Additionally, CLOCK possesses an intrinsic acetylase activity (Doi *et al.*, 2006), which acts upon both histones and its binding partner, BMAL1. Chromatin immunoprecipitation studies have evidenced rhythmic daily binding of the CLOCK/BMAL1 heterodimer to E-box motifs, resulting in circadianally regulated expression of target genes.

The CLOCK/BMAL1 heterodimer drives expression of the Period (*PER1, PER2* and *PER3*) and Cryptochrome (*CRY1* and *CRY2)* genes, causing their protein products to accumulate in the cytoplasm. Phosphorylation by Casein Kinase 1δ/ε (CK1δ/ε) targets PER proteins for degradation via the proteasome. This acts to limit the availability of PER proteins for association with CRY and CK1δ/ε in a stable complex. However, once formed, this complex translocates back to the nucleus where it inhibits the activity of the BMAL1/CLOCK dimer and in turn limits its own transcription. The PER/CRY/CK1δ/ε complex is degraded at night, thereby re-setting the oscillator for the following day (Pegoraro & Tauber, 2011).

Additionally, the CLOCK/BMAL1 heterodimer also drives an auxiliary loop helping to maintain a 24 hour period. This is achieved by driving expression of two orphan nuclear receptors, *REV-ERBα* and *RORα*. *REV-ERBα* and *RORα* gene products bind

to ROR response elements (RREs) in the *BMAL1* promoter and act to supress or induce transcription respectively (Guillaumond *et al.*, 2005). The complete molecular feedback/feedforward loop takes approximately 24 hours to complete, and establishes itself as a robust, temperature insensitive and cell division independent oscillator. Due to the interlocking arms of the circadian oscillator and evolutionary conservation, it is unsurprising that many aspects show redundancy. Ablation studies of several of the core clock genes show minimal disruptive effects on circadian rhythms with many changes compensated for by alterations in other genes or post-translational modifications (Ripperger & Brown, 2010). For example, redundancy is shown with multiple PER and CRY proteins in mammals. An exception is made with PER2, which appears to be essential for the continuation of circadian rhythms, however, it should be noted, a PER2 deletion can be rescued by an additional CRY2 deletion (Albrecht *et al.*, 2007).

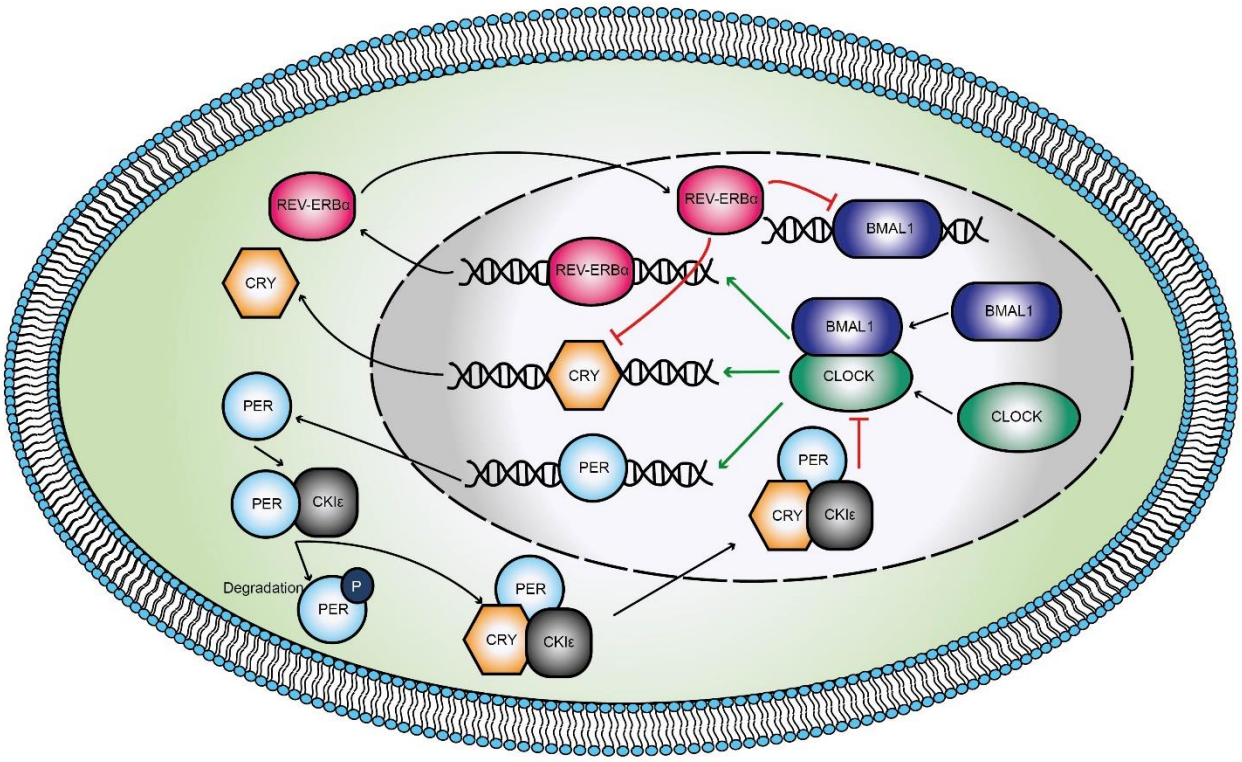

Figure 1.5: ***Transcriptional/translational feedback loop of core clock genes*****.**

Accumulating levels of BMAL1 at the start of the subjective day promote BMAL1-CLOCK heterodimer formation. These bind to E-box elements in promoter regions of *PER*, *CRY* and *REV-ERBα* genes activating their transcription. Accumulating PER proteins in the cytoplasm are phosphorylated by CK1ε, targeting them for degradation. However, as CRY proteins also accumulate in the cytoplasm, they promote formation of stable CKIε/PER/CRY complexes, which are translocated into the nucleus, where they act to disrupt the CLOCK/BMAL1 complex, inhibiting their own transcription. REV-ERBα acts to inhibit *BMALl1* and *CRY* transcription via an auxiliary loop. Figure adapted from Fu & Lee (2003).

1.12 Circadian Post-transcriptional and Post-translational Modifications.

In order to establish and maintain circadian oscillations, as well as rhythmic transcription, the action of the core clock proteins must be tightly controlled. A sufficient delay between transcription and repression is required in order to maintain a 24 hour period. A major mechanism to achieve this is by post-translational modifications of core clock proteins including protein phosphorylation, acetylation, ubiquitination and sumoylation (Vanselow *et al.*, 2006). The majority of the core clock proteins are phosphorylated *in vivo,* and additionally, these phosphorylation events have been found to be circadian in pattern. Phosphorylation events regulate stability, proteasomal degradation and nuclear translocation of clock proteins (Figure 1.6).

Casein kinase epsilon and delta (CK1ε/δ) are essential regulators of the negative feedback loop, with both isoforms widely assumed to have redundant roles. Phosphorylation of PER proteins by CK1ε/δ targets them for degradation via recruitment of the ubiqutin ligase adaptor protein β-TrCP (Vanselow *et al.*, 2006). CK1ε/δ also has a role in PER and CRY cellular localisation, whereby phosphorylation masks the nuclear localisation signal, retaining PER proteins in the cytoplasm (Miyazaki *et al.*, 2007). Furthermore, even when *Per* genes are constitutively expressed in rat-1-fibroblasts, PER protein abundance is still rhythmic (Fujimoto *et al.*, 2006), suggesting post-translational modifications are sufficient to cause oscillatory protein abundance. Similarly, BMAL1 is phosphorylated by both CK1ε/δ and mitogen-activated protein kinase (MAPK) leading to opposing results. CK1ε/δ mediated phosphorylation of BMAL1 promotes its transcriptional activity (Eide *et al.*, 2002) whereas phosphorylation by MAPK acts to reduces it (Sanada *et al.*, 2002).

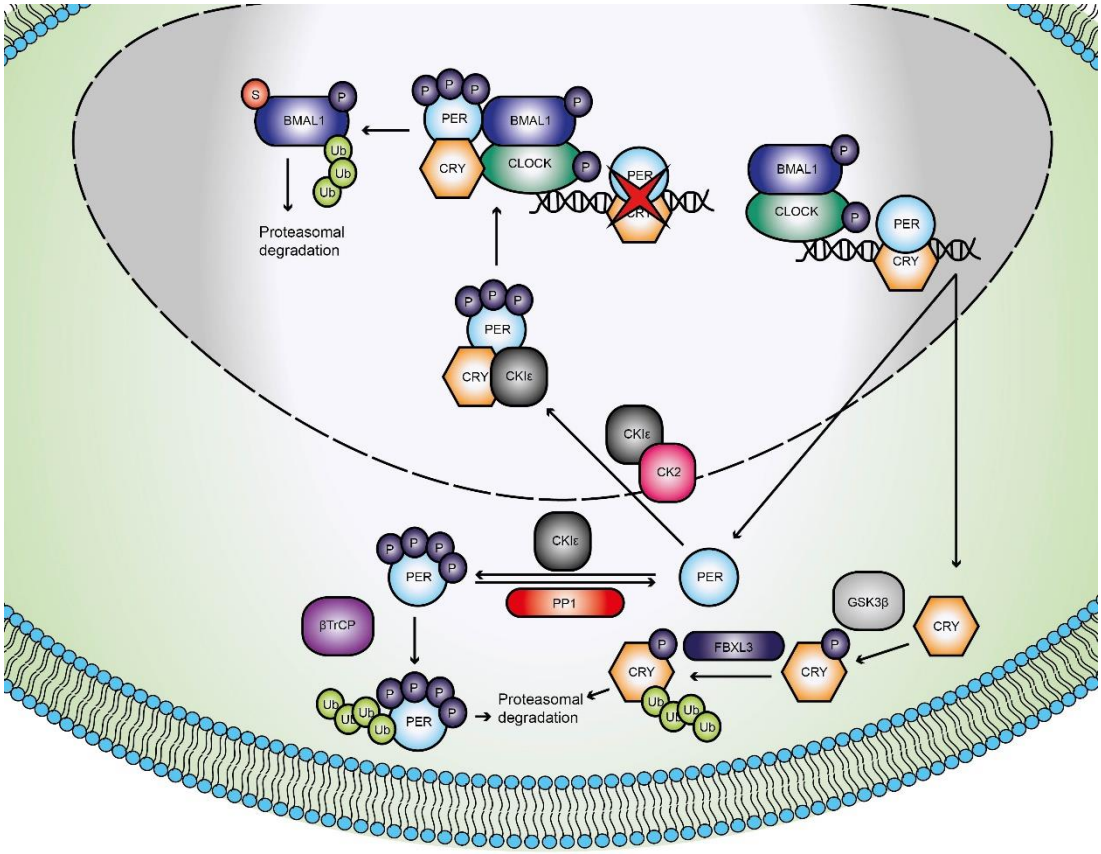

Figure 1.6: ***Post-translational modifications of core clock machinery.***

Phosphorylation of CLOCK and BMAL1 is coincident with their highest transcriptional activity. After CLOCK:BMAL1 mediated transcription PER and CRY proteins accumulate in the cytoplasm. PER proteins are phosphorylated by CKI which triggers ubiquitinisation by β-TrCP leading to proteasomal degradation. CRY proteins are phosphorylated by GSK3β permitting FBXL3 mediated ubiquitinisation again leading to degradation. PP1 acts to dephosphorylate and stabilise PER proteins. CKI and CK2 are involved in the nuclear localisation of PER proteins by differential phosphorylation, allowing the formation of the repressive complex. BMAL1 is SUMOylated and ubiquitinated facilitating proteasomal degradation. Figure adapted from Vanselow & Kramer (2010).

Other kinases are also known to phosphorylate core circadian clock genes, including casein kinase 2 (CK2) and glycogen synthase kinase 3β (GSK3β). CK2 phosphorylates PER2, and increases protein stability and influences nuclear localisation (Smith *et al.*, 2008). GSK3β phosphorylation targets include PER2, CRY2 and REV-ERBα. Interestingly, its own activity, as determined by phosphorylation status is circadianally regulated (Iitaka *et al.*, 2005).

Opposing actions of kinases and phosphatases result in intricate temporal and spatial regulation of the molecular mechanism of the core clock genes. Phosphatases including PP5, PP2A and PP1 counteract the action of kinases. PP5 has been shown to bind to and activate CK1ε by releasing an auto-inhibitory tail domain (Partch *et al.*, 2006). CLOCK and BMAL1 are also phosphoproteins, and dimerise upon phosphorylation. Increasing CLOCK protein levels leads to hyperphosphorylation of BMAL1, which in turn is required for nuclear localisation of CLOCK (Kondratov *et al.*, 2003).

Epigenetic modifications also alter protein activity. CLOCK itself has an internal histone acetyl transferase activity. It acetylates both histone H3 and H4, as well as its binding partner BMAL1 (Doi *et al.*, 2006), which appears necessary for CRY2 repressor activity. The histone deacetylase sirtuin 1 (SIRT1) counteracts CLOCK, and targets both BMAL1 and PER2. SIRT1 catalytic activity is NAD+ dependent, linking metabolic state to circadian oscillations (Rutter *et al.*, 2002). Additionally, sumoylation of BMAL1 at lysine 259 facilitates BMAL1 ubiquitin mediated proteasomal degradation (Cardone *et al.*, 2005).

Emerging evidence also indicates an important role for post-transcriptional regulation including splicing, mRNA stability and regulation by microRNAs. This added level of complexity within the circadian system is thought to enhance both the robustness and

adaptability of the system. Use of alternative splicing of a single gene results in the generation of multiple isoforms with distinct structure and/or function from the full length transcript. RNA-sequencing has revealed tissue specific alternative splicing in both mouse and *Drosophila.* For example alternative splicing of *per3* in *Drosophila* is clock regulated and permits temperature sensitive circadian regulation during changing seasons (Majercak *et al.*, 2004).

Micro-RNAs have recently been identified within mouse, rat, *Arabidopsis* and *Drosophila* as important for the functioning of the circadian clock. Within the mouse CREB targets miR132, whilst CLOCK targets miR219-1 resulting in circadian regulation of the two miRNAs. Disruption of miR219-1 caused a lengthening of wheel-running rhythms (Cheng *et al.*, 2007). Additionally, miR-192 and miR-194 have been implicated in the regulation of *Per* genes (Nagel *et al.*, 2009), whilst miR-494 and miR-142-3p in *Bmal1* expression (Luo & Sehgal, 2012). Furthermore, mRNA half-life will drastically impact upon functional protein abundances. *Per* mRNA transcripts in *Drosophila* show rhythmic abundance in the absence of circadian transcription indicative of circadian regulation of mRNA stability (So & Rosbash, 1997).

In summary, combinations of rhythmic transcription coupled with post-transcriptional and post-translational modifications of just a small number of core clock genes provide a highly regulated and precise timing system that is able to regulate the circadian system throughout the organism.

1.13 Circadian Regulation of Reproduction.

In the majority of mammals, the circadian system needs to detect changes in the seasons to ensure reproduction occurs at the appropriate time of year. However non-seasonal reproduction also involves many temporally regulated activities, from

oestrous cycles, ovulation, implantation, placentation and parturition. Peripheral clocks have been identified throughout reproductive tissues including the ovary, oviduct and uterus. Interestingly, the testis, along with the thymus is one of the two tissues shown to express constant rather than rhythmic expression of circadian clock genes (Alvarez & Sehgal, 2005). Female reproduction on the other hand is increasingly thought of as a circadianally regulated process (Figure 1.7).

Firstly, in order for successful pregnancy, primordial follicles need to mature and ovulation must occur in concert with appropriate mating behaviour. During the late follicular phase, estradiol concentrations increase, stimulating gonadotrophin-releasing hormone (GnRH) secretion resulting in sustained LH release from the anterior pituitary. This in turn, results in oocyte release from the ovary. Evidence suggests that the central circadian system impacts on these events. Tract-tracing identified direct SCN-GnRH neural connections which were found to be critical for driving the pre-ovulatory GnRH surge. Whilst elevated estradiol levels are mandatory for this hormone release, a time-restricted signal from the SCN is also required. Therefore, rats exposed to chronically high estradiol levels exhibited an LH surge on multiple successive days (Norman *et al.*, 1973). As such, the LH surge of rats and mice is restricted to the late-afternoon of pro-oestrous with ovulation and mating occurring approximately 6 hours after darkness (Barbacka-Surowiak *et al.*, 2003). In humans, the LH surge generally occurs between midnight and 8am with ovulation occurring 12-48 hours later (Luciano *et al.*, 1990). Additionally, the sensitivity of the ovary to LH is also rhythmic with maximal receptiveness apparent in the middle of the night during pro-oestrous in rats (Sellix & Menaker, 2010). Next, the fertilised egg must traverse the oviduct, which also displays the molecular components of autonomous clocks. *PAI* expression in the oviduct is oscillatory and is proposed to protect the embryo from protease damage. Perturbed *PAI* rhythms may render the

embryo vulnerable to increased environmental damage and thus decrease embryonic viability (Kennaway *et al.*, 2003a).

In mice, the coupled timing of ovulation and mating are important for successful reproductive outcome. A delay in mating after ovulation causes deleterious effects on pre-implantation embryos (Sakai & Endo, 1988). This is also noted in humans whereby intrauterine insemination is most successful 24-42 hours post LH surge, with live birth rates almost halving when insemination is delayed to post 42 hours (Khattab *et al.*, 2005). Experiments in which mouse uterine horns were flushed with soluble signals produced from day 4 decidual HESCs demonstrate histologically normal implantation, however, when soluble signals were derived from day 10 decidual HESCs, implantation was significantly impaired (Salker *et al.*, 2012). Studies such as this are indicative of the 'window of implantation' which is critically timed for optimal reproductive outcome. Core clock genes have been identified as rhythmically expressed in the luminal epithelium, stroma and myometrial compartments of the uterus (Akiyama *et al.*, 2010; Nakamura *et al.*, 2005) and appear to be affected by both the menstrual cycle and stimulation with ovarian hormones (Nakamura *et al.*, 2008).

Due to the requirement for synchronised embryonic development and maternal receptivity, implantation can be considered as a 'chrono-event'. In humans the window of implantation is generally thought to be 6 to 10 days post-ovulation, whereas murine endometrium is receptive to implanting blastocysts on day 4. A study conducted by (Uchikawa *et al.*, 2011) identified down-regulation of *Per2* mRNA in endometrial stromal cells of rats during decidualization. ESCs from pregnant transgenic rats, in which the *Per2* promoter was fused to a destabilized luciferase reporter gene, were prepared during the implantation window (day 4.5 of gestation) and during decidualization (day 6.5 of gestation). Rhythmic oscillations of both *Per2*

transcripts and protein were enhanced in cells from day 4.5, but attenuated during day 6.5 (during decidualization). This evidence suggests that the circadian oscillator may be impaired during decidualization in the endometrial stroma. With further regard to implantation, exposure of mice to an altered photoperiod (both phase advances and delays) between fertilisation and implantation led to an acute reduction in successful pregnancy outcome (Summa *et al.*, 2012). Furthermore, entrainment of mice to photoperiods of 26 hours throughout pregnancy reduced the number of successful implantation sites (Endo & Watanabe, 1989).

Due to medical interventions, the timing of labour and parturition in humans is unclear; however consistent observations show that the timing of birth is unevenly distributed over the circadian day with higher birth rates apparent late at night and early in the morning, even in pre-term births (Lindow *et al.*, 2000). Selective advantage means parturition is timed to the night or daytime phase depending on the temporal niche of the species. Rats commonly give birth during day-light hours; however, ablation of the SCN disrupts this timing (Boden *et al.*, 2013a; Reppert *et al.*, 1987). Furthermore, this effect was shown to be mediated by melatonin. Pinealectomised rats (who do not produce melatonin) failed to deliver pups exclusively during daylight hours, and instead delivered randomly throughout the day. Appropriately timed melatonin administration was able to rescue the phenotype (Takayama *et al.*, 2003). The role for melatonin signalling during human parturition is less well characterised. However, parallel up-regulation of the melatonin receptor alongside the canonical oxytocin receptor has been identified in labouring women, when compared to pregnant, non-labouring women. Furthermore, melatonin acted to enhance oxytocin induced contractility and facilitate gap junction activity in term labour *in vitro* myometrium biopsies (Sharkey *et al.*, 2009).

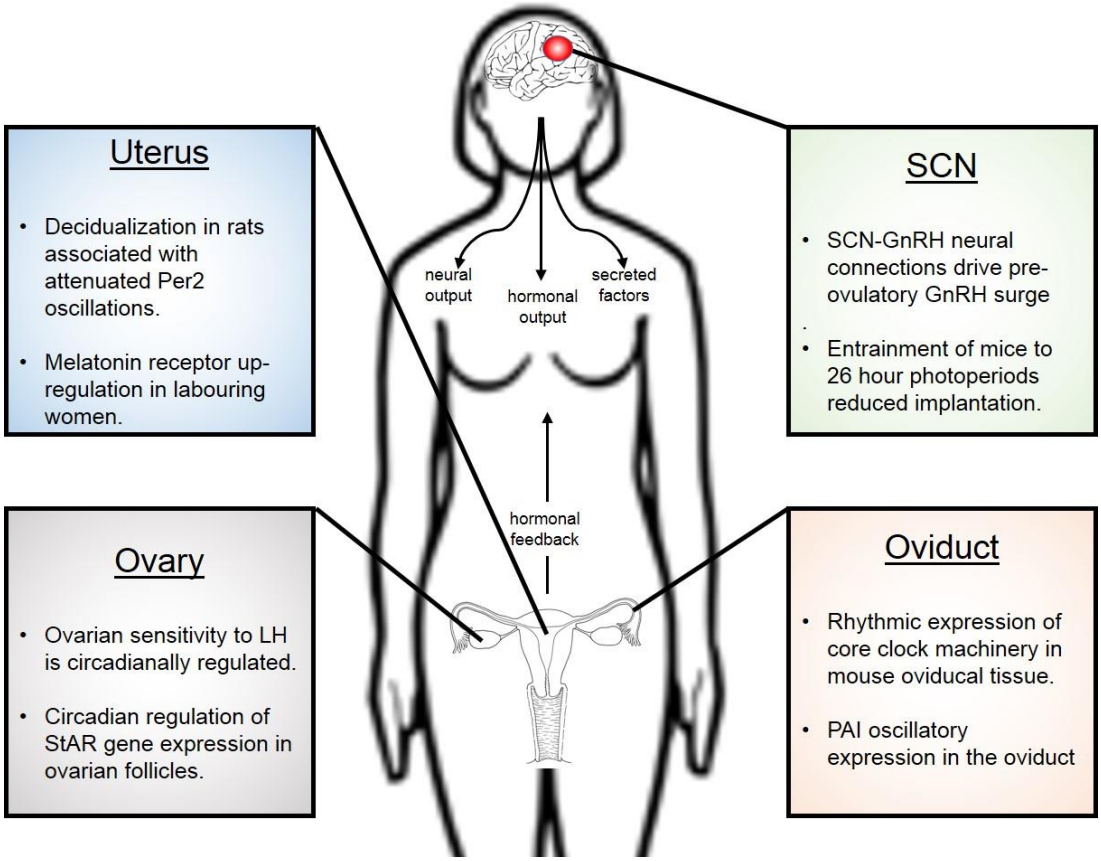

Figure 1.7: ***Circadian clock function in peripheral tissues of the female reproductive system.***

The central SCN clock drives rhythmic GnRH secretion from GnRH neurons in the hypothalamus. In addition to these neuroendocrine pacemakers, clocks are also present in peripheral tissues including the ovary, uterus and oviduct where they have been implicated in ovulation, steroid hormone synthesis, embryo protection, implantation, decidualization and parturition. Synchronisation of central and peripheral oscillators is mediated by hormonal, neural and humoral cues. Furthermore, feedback signals from the periphery are able to fine tune the clock of the HPG axis. Figure adapted from Sellix (2013)..

1.14 Circadian Rhythms in the Embryo.

Mammalian oocytes express core circadian clock genes, however, post fertilisation expression of these genes decreases to very low levels. It is therefore likely the transcripts are maternal mRNAs and are not translated by the embryo. This suggests that during early embryonic development there is an absence of a molecular clock (Amano *et al.*, 2010). During foetal development the prenatal environment is innately circadian in nature. The developing foetus is exposed to the maternal circadian milieu including daily rhythms of temperature, maternal feeding patterns and melatonin concentrations- melatonin being one of the few maternal hormones found to cross the foetal-maternal interface unaltered. Development of circadian rhythms are demonstrated by the entrainment of 24 hour oscillations of foetal heart rate, foetal movement and respiratory movements (Seron-Ferre *et al.*, 2007). However, it is currently unclear as to whether these rhythms are foetal or maternally controlled.

In both rodents and humans, the SCN is histologically apparent by mid-gestation and displays day and night-time regulation of metabolic activity and AVP mRNA expression before birth. (Shibata & Moore, 1988). However, little data has been found to support rhythmic expression of core clock genes during foetal development. Data from foetal rat and hamster tissues demonstrate constitutive expression of the clockwork genes in the liver and heart (Dolatshad *et al.*, 2009) However, observations of SCN-driven rhythms of oxygen consumption and body temperature in human preterm infants born post 32 weeks gestation suggests the foetal SCN is functional in late gestation (Bauer *et al.*, 2009). Interestingly, melanopsin receptors in the retina are thought to be accountable for circadian entrainment in infants. Cots in a neonatal wards fitted with a circadian filter (on for 12 hours, off for 12 hours) specifically targeting the wavelength of light detected by melanopsin receptors, were shown to increase weight gain and head circumference in preterm infants (Watanabe *et al.*,

2013). It could be proposed that the circadian arrangement in the foetus in similar to that of a peripheral clock and is entrained by maternal circadian signals allowing the conceptus to maintain synchrony with the mother.

1.15 Clock Gene Disruption and Fertility.

As there is accumulating evidence of a critical role for circadian output during reproduction, it could be assumed that disruption of core clock genes would lead to profound reproductive deficient phenotypes. Surprisingly, mutation of clock genes seems to have subtle effects on reproductive outcome, suggestive of compensatory mechanisms in order to maintain reproductive function under an altered circadian timing system. Studies examining core gene disruption are summarized in Table 1.4.

Remarkably, there are only a handful of studies addressing the involvement of circadian rhythms in human reproduction. This is likely due to the invasive nature that such studies would require, however, some data is available concerning women working shifts and/or travelling across time zones. The evidence of the impact of shift work on female reproduction is fairly inconclusive with conflicting conclusions from a number of studies. (Bisanti *et al.*, 1996) reported an association between female shift work and subfecundity (adjusted odds ratio (AOR): 2.0; 95% confidence interval: (CI) 0.9-2.3). However, a larger study concluded there was no causal association between shift work and prolonged time to pregnancy (AOR: 0.99; 95% CI: 0.91-10.7) (Zhu *et al.*, 2003). A recent meta-analysis reported a significant association between shift work and menstrual disruption (AOR: 1.22; 95% CI: 1.15-1.29) and infertility (AOR: 1.80; 95% CI: 1.01-3.20), but not miscarriage (AOR: 0.96; 95% CI: 0.88-1.05). However, night shifts (starting between 8pm and 10pm and lasting 10-12 hours) were associated with an increased incidence of early spontaneous pregnancy loss (adjusted odds ratio: 1.41; 95% confidence interval: 1.22-1.63) (Stocker *et al.*, 2014).

Additionally, small adverse effects of shift work on risk of low birth weight (AOR: 1.27: 95% CI: 0.93-1.74) and small for gestational age infants (AOR 1.12: 95% CI: 1.03-1.22) have been observed (Bonzini *et al.*, 2011). Overall, these findings suggests that reproductive risk arising from shift work is small, and there is 'currently insufficient evidence for clinicians to advise restricting shift work in women of reproductive age' (Stocker *et al.*, 2014). Interestingly, although there has been no association observed between circadian disruption and pre-eclampsia, the protective property of administration of low dose aspirin appears to be influenced by ingestion time. Administration at night time is effective in lowering blood pressure; however, when taken in the morning, this effect is lost. The authors propose that this may be related to the circadian secretion pattern of blood pressure regulators (Ditisheim *et al.*, 2013). This chronotherapy approach may also be applied in the future with regard to assisted reproductive technologies.

At a molecular level, women with a single-nucleotide polymorphism in *BMAL1* were found to have a greater rate of implantation; however, this was accompanied by an increased incidence of miscarriages, consistent with data observed in mice. Furthermore, a polymorphism in Neuronal PAS domain-containing protein 2 (*NPAS2),* a CLOCK analogous gene, may be protective as it is associated with a reduced number of pregnancy losses (Kovanen *et al.*, 2010).

Table 1.4: ***Reproductive phenotype of disrupted circadian core genes.***

Circadian Gene	*Mutation*	*Reproductive Effects*	*References*
Clock	Clock$^{\Delta 19}$ 51 amino acid deletion in transcriptional activation domain. Unable to bind E-box motifs	- Normal steroid hormone levels, follicular development and ovulation. - Higher proportion irregular oestrous cycles with a greater time spent in oestrous - Failure to initiate an LH surge in response to estradiol - High proportion of reabsorbed embryos by day 11 post-conception.	(Dolatshad *et al.*, 2006) (Miller *et al.*, 2004)
Per 1	Per1^{Bdrm} Per1 protein non functional	- Normal reproductive phenotype as young adults - Aged mice demonstrated smaller litter sizes and abnormal parturition - Higher loss of implanted embryos	(Pilorz & Steinlechner, 2008)
Per 2	Per2^{Brdm} Per 2 protein non functional	- Normal reproductive phenotype as young adults - Aged mice demonstrated smaller litter sizes and abnormal parturition - Higher loss of implanted embryos - Dampened glucocorticoid secretion rhythms - Altered sex behaviour	(Pilorz & Steinlechner, 2008)
Bmal1	Knock out	- Delayed puberty, irregular oestrous cycles, and small ovaries. - Still able to ovulate - Complete implantation failure due to impaired steroidogenesis and loss of StAR enzyme	(Ratajczak *et al.*, 2009)

1.16 Hormonal Regulation of Circadian Rhythms.

Rhythms of *Per1, Per2* and *Bmal1* have been shown to be influenced by the stage of the oestrous cycle in rat uteri, supporting the hypothesis that the oestrous cycle drives changes in the timing of the clock in reproductive tissues. However, these changes were variable in other tissues including the kidney and liver (Nakamura *et al.*, 2008). This suggests there are tissue specific effects of oestrogen on clockwork gene expression. A putative explanation for this observation is the differential tissue distribution of oestrogen receptors, which, furthermore, are known to be modified by clock genes (Urlep & Rozman, 2013). Thus, on one hand, oestrogen is able to influence the clock machinery, whilst on the other, the clock proteins are able to influence oestrogenic effects by mediating its receptors. Little is known about the influence of progesterone upon circadian clock expression, however exogenous application of progesterone acutely induces clock gene expression in MCF-7 human cancer cells via activation of the *Per1* gene (Nakamura *et al.*, 2010). This is supported by the finding of a PRE half site in the 5' region of the mouse *Per1* gene. Taken together, it can be proposed that oestrogen and progesterone act both independently and in concert to regulate circadian oscillations in reproductive tissues.

1.17 Research Justification and Aims.

Recently chronotherapy has been used in the treatment of many disorders including depression, cancer and kidney disease amongst others. Chronotherapy acts to coordinate treatment and/or drug delivery with circadian rhythms in order to enhance effectiveness or reduce side effects of the given treatment. Due to increasing demand for ART, it is important to understand the contribution of circadian rhythms to reproductive outcome. It seems counterintuitive that for such temporally regulated events as ovulation, fertilisation, implantation and parturition, circadian rhythms are largely ignored. *In vitro* technologies tend to overlook the fact that the embryo is cultured in a non-circadian environment, and will be returned to an 'out of sync' uterus. Therefore, the temporally regulated characteristics of reproduction need to be considered and understood more in depth.

The specific aims of this project are:

- To determine the role of both overall circadian rhythms and circadian dependent genes in the context of decidualization and implantation.
- To define the mechanism of circadian rhythm regulation during decidualization in HESCs.
- To utilise and validate transcriptomic analysis to visualise the impact of knockdown of a core clock gene.
- Examine relevant clock gene dependent transcripts in the context of key cell fate decision pathways critical for reproductive success.
- Characterise important mechanistic pathways that define the organisation of HESC decidualization by manipulation of key genes.
- To establish the clinical relevance of these pathways.

Chapter 2

Materials and Methods

2.1 Materials

2.1.1 Cell Culture Materials

Reagent	***Manufacturer***
Dulbecco's Modified Eagle Medium (DMEM)/F12 (1:1) with L-glutamine with phenol red	Fisher Scientific
Dulbecco's Modified Eagle Medium (DMEM)/F12 (1:1) with L-glutamine, phenol free	Fisher Scientific
Charcoal	Sigma-Aldrich
Collagenase type IA	Sigma-Aldrich
Dextran	Fisher Scientific
Deoxyribonuclease I (DNAse I)	Roche
Foetal bovine serum (FBS) heat inactivated	Gibco
Insulin	Sigma-Aldrich
L-Glutamine	Gibco
Penicillin (10,000 µg/ml)- Streptomycin (10,000µg/ml) solution	Invitrogen
RNA-later	Sigma-Aldrich
Trypsin-EDTA solution	Gibco
Plastic-ware	VWR

2.1.2 Cell Culture Treatments

Hormone	***Concentration***	***Manufacturer***
8-br-cAMP	0.5mM	Sigma-Aldrich
Basic fibroblast growth factor	10ng/ml	Merck-Millipore
Estradiol	1nM	Sigma-Aldrich
Dexamethasone	0.1µM	Sigma-Aldrich
Medroxyprogesterone acetate (MPA)	1µM	Sigma-Aldrich
Progesterone	1µM	Sigma-Aldrich

2.1.3 siRNA

All siRNA reagents were purchased from Dharmacon GE Healthcare.

SMARTpool ON-TARGETplus for human PER2.

SMARTpool ON-TARGETplus for human BRE-AS1.

SMARTpool ON-TARGETplus for human PRIP-1.

ON-TARGETplus Non-targeting Pool 1.

2.1.4 Antibodies

Primary

Antibody	***Dilution***	***Manufacturer***
CLOCK	1:3000	Abcam
BMAL1	1:400	Abcam
CRY1	1:500	Abcam
CRY2	1:2000	Abcam
PER1	1:300	Abcam
PER2	1:300	Abcam
PRIP-1	1:500 (Western blotting) 1:100 (Immunohistochemistry)	Sigma-Aldrich
Total AKT	1:1000	Cell Signalling
Phospho-AKT (Ser473)	1:1000	Cell Signalling
FOXO1A	1:1000	Cell Signalling
FOXO3A	1:1000	Cell Signalling
BIM	1:1000	Cell Signalling
IgG	1:2000	Sigma-Aldrich
β-ACTIN	1:100,000	Abcam

Secondary

Antibody	***Dilution***	***Manufacturer***
Horseradish peroxidase (HRP)-conjugated goat anti-rabbit	1:2000	Dako
Horseradish peroxidase (HRP)-conjugated goat anti-mouse	1:6000	Dako

2.1.5 Chemical Reagents

Reagent	***Manufacturer***
Actinomycin D	Sigma-Aldrich
30% acrylamide/Bis solution	Bio-rad
Agarose powder	Sigma-Aldrich
Ammonium Persulphate (APS)	Fisher Scientific
Ampicillin	Sigma-Aldrich
Bovine serum albumin (BSA)	Sigma-Aldrich
Bromophenol blue	Sigma-Aldrich
2-Butanol	VWR
Coelenterazine	Invitrogen
Chloroform	AnalaR
Deoxycholate	Fisher Scientific
Dimethyl sulphoxyde (DMSO)	Life Technologies
Dithiothreitol (DTT)	Sigma-Aldrich
DPX mountant	Sigma-Aldrich
Ethidium bromide	Sigma-Aldrich
Ethylenediaminetetraacetic acid (EDTA)	Fisher Scientific
Fluo-4-AM	Life Technologies
Formaldehyde	J.T. Baker
Formalin	Leica
Glycerol	Sigma-Aldrich
Glycine	Fisher Scientific
Haematoxylin	Leica

Hydrochloric acid	Sigma-Aldrich
Hydrogen peroxide solution (30%)	Fisher Scientific
Histo-clear	Sigma-Aldrich
Isopropanol	Sigma-Aldrich
Lithium Chloride	VWR
m-3M3FBS	Tocris Bioscience
Magnesium chloride	Sigma-Aldrich
Methanol	Fisher Scientific
NP-40	Calbiochem
N,N,N,N'-tetramethyl-ethane-1,2-diamine (TEMED)	Sigma-Aldrich
(4-(2-hydroxyeyhyl)-1-piperazineethanesulphonic acid (HEPES)	Sigma-Aldrich
Paraformaldehyde (PFA)	Sigma-Aldrich
Potassium chloride	Fisher Scientific
Propidium Iodide	Sigma-Aldrich
Ribonuclease-A	Qiagen
RNase	Invitrogen
Sodium butyrate	Fisher Scientific
Sodium chloride	Fisher Scientific
Sodium dodecyl sulphate (SDS)	Thermo
Sodium hydroxide	Fisher Scientific
Tris base	Sigma-Aldrich
Tris-borate	Sigma-Aldrich
Tris HCl	Sigma-Aldrich
Triton X-100	Sigma-Aldrich
Trypan blue	Invitrogen
Tween 20	Sigma-Aldrich
β-mercaptoethanol	Fisher Scientific

2.1.6 Miscellaneous Reagents

Reagent	***Manufacturer***
Bio-Rad Protein Assay Dye	Bio-Rad
Bioruptor sonicator	Diagenode
cOmplete EDTA free protease inhibitors	Roche

ECL hyperfilm	GE Healthcare
Fibronectin	Sigma-Aldrich
gDNA wipeout	Qiagen
Hybond PVDF membrane	GE Healthcare
Milk powder	AppliChem
Phosphatase inhibitor cocktail	Sigma-Aldrich
Primers	Sigma-Aldrich
Protease K	Sigma-Aldrich
Protein A Dynabeads	Life Technologies
Protein ladders	Life Technologies
RIPA	Millipore
RNA ladders	Sigma-Aldrich
RNAse free tubes	Life-Technologies
RNAse free water	Life Technologies
RNase ZAP	Fisher Scientific
Stat-60	AMS Biotechnology
SYBR Green Mastermix	Life Technologies

2.1.7 Kits

Kit	***Manufacturer***
ApoOne Caspase 3/7 Assay Kit	Promega
ECL Prime Western Blotting detection system	GE Healthcare
IGFBP1 ELISA Kit	R&D Systems
jetPRIME Transfection Kit	VWR
Novolink Polymer Detection System	Leica Biosystems
PRIP-1 ELISA Kit	Antibodies-Online
PRL ELISA Kit	R&D Systems
Proteome Human Phospho MAPK Array Kit	R&D Systems
QIAquick Gel Extraction Kit	Qiagen
QIAquick PCR Purification Kit	Qiagen
QuantiTECT Reverse Transcription Kit	Qiagen
XTT Assay Kit	Cell Signalling

2.1.8 Buffers and Solutions

2.1.8.1 General

TBS

130mM NaCl

20mM Tris, pH 7.6

TBS-Tween

0.1% Tween in 1x TBS

TBE

0.9M Tris-borate

2mM EDTA, pH8.0

4% Paraformaldehyde

4% PFA (W/v) in PBS

pH 7.4 with NaOH

RIPA Buffer

50mM Tris HCl pH 7.4

1% NP40

0.5% deoxycholate

0.1% SDS

150mM NaCl

2mM EDTA

50mM NaF

DNA Loading Buffer

0.2% (w/v) Bromophenol blue

40% (v/v) glycerol

0.25M EDTA pH8.0

Laemmli Buffer

50mM Tris-HCl, pH 6.8

1% (w/v) SDS

10% (v/v) glycerol

2% (v/v) β-mercaptoethanol

0.002% (w/v) Bromophenol blue

2.1.8.2 Immunohistochemistry

Blocking and Antibody Incubation Solution

3% BSA (w/v) in PBS

2.1.8.3 Western Blotting

Running Buffer (10x)

250mM Tris Base

192mM glycine

1% (w/v) SDS

Transfer Buffer

250mM Tris Base

192mM glycine

20% (v/v) methanol

Blocking and Antibody Incubation Solution

5% BSA (w/v) in TBS-Tween *or*

5% skimmed milk powder (w/v) in TBS-Tween (antibody dependent)

Stripping buffer

100mM β-mercaptoethanol

2% (w/v) SDS

62.5mM Tris-HCl, pH6.7

2.1.8.4 ChIP

SDS Lysis Buffer

1% SDS

1% Triton X-100

0.5% deoxycholate

10mM EDTA

500mM Tris HCl pH 8.1

Swelling Buffer

25mM 4-(2-hyroxyethyl)-1-piperazineethanesulphonic acid pH 7.9

1.5mM $MgCl_2$

10mM KCl

0.1% NP40

Immunoprecipitation Buffer

0.01% SDS

1.1% Triton X-100

1.2mM EDTA

16.7mM Tris HCl pH 8.1

167mM NaCl

Low Salt Solution

0.1% SDS

1% Triton X-100

2mM EDTA

20mM Tris-HCl pH 8.1

150mM NaCl

High Salt Solution

0.1% SDS

1% Triton X-100

2mM EDTA

20mM Tris-HCl pH 8.1

500mM NaCl

Lithium Chloride Solution

250mM LiCl

1% NP40

1% deoxycholate

1mM EDTA

10mM Tris-HCl pH 8.1

Tris-EDTA Buffer

10mM Tris-HCl pH 8.0

1mM EDTA

Elution Buffer

1% SDS

100mM $NaHCO_3$

2.1.8.4 Calcium Profiling

Krebs'-Heinselet Buffer

133mM NaCl

4.7mM KCl

11.1mM Glucose

1.2mM $MgSO_4$

1.2 KH_2PO_4

2.5mM CaCl

10mM TES pH 7.4

2.2. Methods

2.2.1 Human Endometrial Biopsies

Endometrial biopsies were obtained from patients recruited from the Implantation Clinic, a dedicated research unit at University Hospitals Coventry and Warwickshire National Health Service Trust. All patients gave informed written consent and the study was approved by the NHS National Research Ethics Committee of Hammersmith and Queen Charlotte's Hospital NHS Trust. All biopsies were timed to the mid-secretory phase, 5 to 11 days after the post-ovulatory LH surge and none of the patients were taking hormonal treatments for at least 3 months prior to the biopsy. For immediate isolation of endometrial stromal cells, biopsies were placed in 7ml 10% dextran-coated charcoal treated foetal bovine serum (DCC-FBS) supplemented DMEM-F12. For protein analysis, biopsies were snap frozen in liquid nitrogen and

stored at -80˚C, and for RNA studies, small tissue pieces were immersed in RNA later and stored at -80˚C.

2.2.2 Cell Culture

2.2.2.1 Preparation of Dextran Coated Charcoal Treated Stripped Foetal Calf Serum

FBS was stripped of various small molecules including endogenous hormones by DCC treatment. 500ml of FBS was treated with 1.25g of charcoal and 125mg of dextran and incubated at 57C for 2 hours with regular mixing. Supernatant was collected following a 30 minute centrifugation at 400 x g, sterile filtered and aliquoted for future use.

2.2.2.2 Preparation of Isolated Endometrial Stromal Cells

Endometrial biopsies were collected in 10% DCC-FBS supplemented DMEM-F12. Excess media was removed, and biopsies were finely minced with scalpels in a Petri dish and enzymatically digested with 0.5mg/ml collagenase type 1A and 0.1mg/ml DNAse I in 10ml phenol free DMEM-F12 for 1 hour at 37°C, with vigorous shaking every 20 minutes. Collagenase activity was stopped by addition of 10ml 10% DCC-FBS supplemented DMEM followed by centrifugation at 400*g* for 5 min. Cell pellets were resuspended in DMEM/F12, 10% DCC-FBS, 1% penicillin-streptomycin, 2mM L-glutamine, 1nM estradiol and 2mg/ml insulin and transferred to an appropriately size tissue culture flask and incubated at 37°C and 5% v/v CO_2. Endometrial stromal cells were isolated from epithelial cells by attachment timings, by removing any suspension cells (epithelial and blood cells), washing attached cells with warmed PBS and replacing with fresh 10% DCC-FBS supplemented media.

2.2.2.3 Primary Cell Culture

All HESCs were managed under standard cell culture incubation conditions using a Heracell CO_2 incubator which provided a humid atmosphere with 5% v/v CO_2 maintained at 37˚C. A class II microbiological safety cabinet was used for all cell culture. HESCs were maintained in 10% DCC-FBS supplemented DMEM-F12 media which was changed every other day. Confluent monolayers of endometrial stromal cells were passaged by treatment with 3ml trypsin-EDTA for 5 min at 37°C. Flasks were tapped to dislodge any remaining attached cells. Trypsin treatment was subsequently inhibited by the addition of 7ml 10% DCC-FBS supplemented media. Cells were collected by centrifugation at 400g for 5 min. Cells were split at a ratio of 1 in 3 and resuspended in 10% DCC-FBS supplemented media.

2.2.2.4 Hormone Treatment

For experimental assays confluent monolayers were placed in phenol red-free 2% DCC-FBS supplemented DMEM-F12 overnight and hormonal treatments completed the following day. For standard decidualization treatment, HESCs were treated in phenol red-free DMEM/F12 containing 2% DCC-FBS with 0.5mM 8-bromo-cAMP alone or in combination with and 1µM medroxyprogesterone acetate, 0.1µM dexamethasone, 1µM dihydrotestosterone or 1µM P4. All experimental treatments were carried out before the fourth cell passage.

2.2.2.5 Dexamethasone Mediated Circadian Synchronization

In order to achieve circadian oscillatory synchronization in culture, 100nM dexamethasone was added to confluent monolayers of HESCs in additive and

phenol-free DMEM/F12 media for 30 minutes. This treatment was carried out either post-transfection or post-differentiation.

2.2.3 Transient Transfections

Primary HESCs were transfected using jetPRIME Polyplus transfection kit, a non-liposomal, cationic polymer based transfection reagent. Transfections were performed at approximately 80% confluency and in the presence of 10% DCC-FBS supplemented media. 50nM of siRNA was diluted in jetPRIME buffer and vortexed. JetPRIME reagent was added at an appropriate volume, vortexed and incubated at room temperature for 10 minutes 1/10th of the volume of culture media of the transfection solution was added dropwise to cells. Media was changed 24 hours post-transfection. All targeted siRNA used were siGENOME SMARTpool duplexes, with siGENOME Non-Targeting siRNA Pool 1 used as a control.

2.2.4 Protein Analysis

2.2.4.1 Protein Extraction

Whole cell protein extracts were obtained by direct lysis in RIPA buffer. RIPA buffer was supplemented with cOmplete EDTA-free protease inhibitor. Media was aspirated from cells and cells washed with PBS. 60µl RIPA solution was added per well (in a 6 well plate, scaled volumes were applied for other plasticware). Cells were scraped using a silicon scraper and collected in microcentrifuge tubes. Samples were centrifuged at 12,000 x g for 15 minutes at 4°C and supernatant containing protein lysates collected and stored at -80°C.

2.2.4.2 Assessment of Protein Concentration

Protein concentration was determined via Bradford assay. Bradford assay reagent contains a Coommassie dye which exhibits an absorbance shift when bound to specific amino acid residues in proteins, observable by a colour shift from red to blue. Stock Bovine Serum Albumin (BSA) was diluted to a concentration range of 0, 0.5, 1.0, 1.5, 2.0, 2.5, 3.0 and 3.5µg/well in a 96 well plate format. 20µl of Biorad protein dye was pipetted into each well for the protein standard and sample wells in triplicate. The protein samples to be quantified were diluted 1:400 in distilled water and added to each well. Plates were loaded onto the Multiskan Ascent plate reader and absorbance measured at 595nm. Protein concentrations of the samples were calculated by reference to known standards.

2.2.4.3 SDS-PAGE

Appropriate concentrations of protein were diluted in Laemmli buffer and heated to 100˚C for 5 minutes and quickly cooled on ice. Proteins were resolved on discontinuous polyacrylamide gels using the Invitrogen XCell SureLock Mini-cell apparatus. Gels were prepared in disposable plastic cassettes from two solutions to form an upper stacking gel (usually 5%) and a lower resolving gel (variable % depending on protein size). The stacking gel was prepared to pH 6.8 and the resolving gel to pH 8.8. Polymerisation in the gel was instigated by the addition of TEMED and 10% APS. The resolving gel was poured into the cassette, overlayed with 100% isopropanol and left to polymerise. Once set, isopropanol was rinsed off with distilled water and the stacking gel overlayed and combs inserted.

Gels were inserted into the electrophoresis tank with running buffer. Equal concentrations of proteins were loaded into the wells, along with a pre-stained

molecular weight marker. A constant voltage of 100V was applied until separation had occurred. The cassette was opened and gel removed for Western blotting.

2.2.4.4 Western Blotting

Protein samples resolved by SDS-Page were transferred to PVDF membrane for immunoprobing using a wet-blot method. Gel/membrane sandwiches were made consisting of pre-soaked blotting pads on the cathode shell, followed by a pre-soaked Whatman filter paper. The gel and the 100% methanol activated PVDF membrane were orientated next, followed by another filter paper and finally two pre-soaked blotting pads towards the anode shell. Once assembled the sandwich was rolled to eliminate any bubbles and placed in the transfer tank with transfer buffer enriched with variable volumes of methanol dependent upon protein size. Transfer was performed at a constant voltage of 30V for 2 hour. Following transfer, the PVDF membrane was air dried, reactivated in 100% methanol, and blocked in 5% w/v milk powder in TBS-Tween for 1 hour. The membrane was subsequently incubated with the primary antibody diluted in 5% milk TBS-Tween overnight at 4˚C. The membrane was washed 5 x in TBS-Tween, and subsequently incubated in the secondary antibody conjugated to horseradish peroxidise in the appropriate species diluted in 5% milk TBS-Tween for 1 hour at room temperature. Following three washes in TBS-Tween, the membrane was washed finally in distilled water. Chemiluminescent signals were visualized by using ECL Plus Western Blotting Detection System either onto autoradiography film or using a G:Box Chemie XX6.

2.2.4.5 Phospho-MAPK Array

Relative phosphorylation of 26 phospho-kinases was determined by Proteome Profiler Human Phospho-MAPK array kit. The array was performed according to

manufacturer's specifications using 250µg total protein lysates. Briefly, cell lysates are diluted and mixed with a cocktail of biotinylated detection antibodies. The lysates are then incubated overnight with the phosphor-MAKP array blot. The membrane was washed several times to remove any unbound material. Streptavidin-HRP and chemiluminsence detection reagents were applied producing a signal at each capture spot corresponding to the amount of phosphorylated protein bound. Densitometry was performed with individual phospho-proteins expressed as a percentage of reference dots.

2.2.4.6 Enzyme-linked Immunosorbent Assay (ELISA)

Several ELISA kits were used throughout the study for detection of PRIP1, sST2, PRL and IGFBP1. For detection of PRIP1, total protein lysates were used, for the detection of sST2, PRL and IGFBP1, supernatant from cell culture was used. All ELISA kits used were solid phase sandwich ELISAs.

In brief, a serial dilution of known protein concentration was added to an antibody specific pre-coated microplate along with unknown samples. The plate was sealed and incubated for 2 hours at 37˚C. Following incubation, the samples are aspirated and biotinylated detection antibody was added to each well and again sealed and incubated for 1 hour at 37˚C. Following three washes, horseradish peroxidase (HRP) conjugated streptavidin was added to each well and incubated for 1 hour at 37˚C. Again, following three wash steps, a substrate solution was added to the wells and colour develops in proportion to the amount of protein bound in the initial step. The colour development was stopped and the intensity of the colour measured immediately using a PheraStar microplate reader at 450nm with correction deducted from 540nm. Results were derived using a 4-paramenter logistic regression analysis and normalised to total protein concentration as determined by Bradford assay.

2.2.5 RNA Extraction

To minimize risks of RNA degradation, RNase-free plastic-ware and nuclease free water was used throughout and in combination with RNase ZAP. Supernatant was removed from the cells and frozen at -80C for future analysis. Total RNA was extracted from cells and tissues using STAT-60 reagent; a monophasic solution of phenol and guanidine isothiocyanate, which maintains RNA integrity whilst simultaneously disrupting other cellular components. 400µl of reagent RNA Stat-60 reagent was added per well in a 6 well plate ensuring all cells were covered and left to stand at room temperature for 5-10mins. Cells were scraped thoroughly using a Corring Cell Scraper and transferred to pre-chilled RNase-free 1.5ml eppendorfs and placed on ice. 20% volume of ice cold 100% chloroform was added to the Stat-60 solution and mixed well by vortexing. Samples were snap frozen and placed at -80°C overnight. Samples were defrosted on ice and centrifuged at 12,000 x g at 4°C for 30 minutes in order to separate the sample into an aqueous and an organic phase. RNA remains exclusively in the colourless upper aqueous phase. The aqueous phase was carefully transferred into 50% volume of 100% ice cold isopropanol, incubated at room temperature for 10 minutes to precipitate the RNA. RNA was pelleted by centrifugation at 12,000 x g at 4°C for 15 minutes, washed twice with 1ml 75% ice cold ethanol and air-dried and dissolved in an appropriate volume of nuclease free water. RNA concentration and quality was assessed by nanodrop. Satisfactory values were considered equal to or greater than 1.80 on the 260/280 absorbance scale, indicating pure RNA without contamination of protein. Samples were stored at -80°C.

2.2.6 RNA Analysis

2.2.6.1 Actinomycin D Assay

Actinomycin D is a known inhibitor of transcription by binding DNA at the transcription initiation complex and interfering with the elongation of growing RNA chains. It was therefore used to assess changes in mRNA stability.

Confluent HESCs were treated with 2µM Actinomycin D in DMSO or with a DMSO vehicle control in additive and phenol-free media. RNA was harvested as per protocol. RNA stability was expressed as a percentage of vehicle treated control. Results were analysed using a single phase exponential decay function.

2.2.7 Gene Expression Analysis by qRT-PCR

2.2.7.1 cDNA Synthesis

QuantiTech Reverse Transcription Kit was used for cDNA synthesis. All reagents were thawed on ice, mixed and centrifuged briefly to prevent any concentration gradients. 2µl of 7x gDNA wipeout buffer was added to 1µg template RNA made up to a total volume of 14µl with RNase-free water. This was done to remove any traces of genomic DNA. The samples were incubated at 42°C for 2 minutes and placed immediately on ice. A reverse-transcription master mix was prepared to a volume of 10% greater than that required. Per reaction, 1µl of Quantiscript Reverse Transcriptase was added to 4µl 5x Quantiscript RT Buffer, along with 1µl RT Primer Mix. This was then added to the 14µl template RNA, reactions were mixed and stored on ice. Minus RT controls were also used in which 1µl nuclease free water replaced the 1µl of Quantiscript Reverse Transcriptase. All other stages were identical. Reactions were incubates at 42°C for 30 minutes, then inactivated by incubation at

95˚C for 3 minutes. cDNA samples were diluted with 30µl nuclease free water to give a final volume of 50µl.

2.2.7.2 Primer Design

Sequences were obtained from the Enseml Human Genome datatbase (www.ensenbl.org). Primers were designed to the following requirements:

Melting temperature (Tm) is calculated with the formula Tm = 69.3 + (41(GC/L)) - (650/L), where GC is the number of G and C bases in the primer and L is the number of nucleotides in the primer.

a) Tm to be between 58.0°C and 59.9°C
b) Total amplicon length to be between 75 and 110 base pairs
c) Tms shouldn't differ from the forward and reverse primer by greater than 1˚C
d) At the 3' end of the primer, of the last five bases, 2 bases should be either G or C
e) There is no more than four of the same base consecutively
f) Primer length should be between 18-24 bases
g) Primers are required to be exon spanning (to distinguish between cDNA and gDNA)
h) Amplicon Tm is calculated by the following = 64.9+(0.41*(((C+G)/L)*100))-(500/L)

Designed primers were cross-referenced using the Primer 3 Output Programme to screen for primer dimer formation and secondary structure formation. See Appendix 1 for primer sequences.

2.2.7.3 Primer Optimization

Primers were optimized to determine efficiencies. Forward and reverse primers were used at 300nM in a total volume of 19µl in a SYBR Green master mix and loaded

onto a 96 well plate. 1µl of pooled cDNA or 1µl nuclease free water was added per well in triplicate. The amplified product of the triplicate well combined, mixed with loading dye and ran on a 1% agarose gel, which was ran for approximately 50 minutes at 100V. The purified product was excised from the gel using Qiagen Gel Extraction Kit (as described below) and cDNA concentration measured.

Purified cDNA was serially diluted between 100pg/µl to 10ag/µl in 1/10 dilution factor providing 8 dilutions. The serial dilutions were amplified using the appropriate primers and a SYBR Green Master Mix and Ct Values measured. The log of the concentration of cDNA was plotted against average Ct values. To calculate primer efficiencies the following calculation was used. See Figure 2.1 for examples.

$$Primer\ Efficiency = 10^{\frac{-1}{Gradient\ of\ the\ line}}$$

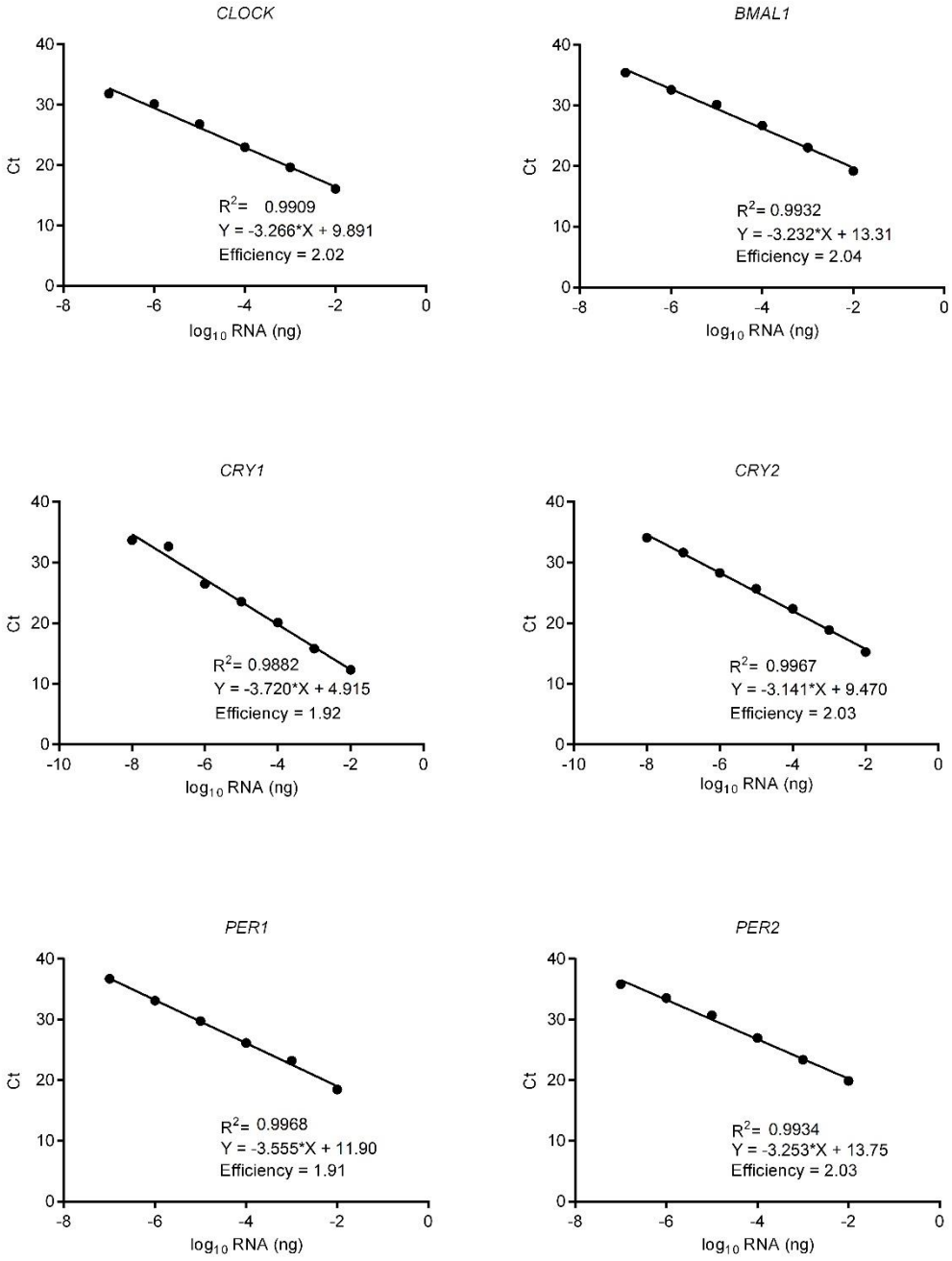

Figure 2.1. ***Primer Optimization of core circadian clock genes***

300nM of designed primers were tested using pooled cDNA samples. The amplified products was purified, serially diluted, and amplified using the appropriate primers and a SYBR Green Master Mix. Ct Values were measured and from this data primer efficiencies were calculated.

2.2.7.4 Agarose Gels and Gel Extraction

Gels were made by dissolving powered agarose in 1x TBE solution in a conical flask and microwaving. 1µl per 50ml gel of ethidium bromide was added. Gel was allowed to cool slightly and poured into the gel tank and left to set. Gels were run in 1x TBE buffer at 10V per cm of gel. Purified products were visualised under the UV transilluminator.

Gel Extraction was carried out using the Qiagen Quick Gel Extraction Kit. Briefly, gel slices were weighed and 3 volumes buffer QC added per 1 volume of gel and incubated at 50°C for 10 min until the gel had dissolved fully. 1 volume of 100% isopropanol was added and sample placed in a QIAquick spin column and centrifuged at 12,000 x g for 1 min. Flow through was discarded and 0.5ml buffer QC added and centrifuged at the above conditions again. The product was washed by adding 0.75ml buffer PE and samples left to stand at room temperature for 3 minutes, then centrifuged as above. The column was placed into an RNase-free eppendorf, 30µl of nuclease free water added, left to stand for 3 minutes then centrifuged as above to elute the cDNA.

2.2.7 5 Real Time Quantitative Polymerase Chain Reaction (qRT-PCR)

Genes of interest were amplified using SYBR Green detection reagent. Reactions were carried out on a 96 well plate in a total volume of 20µl. Primers were used at a concentration of 300nM and at a 50:50 ratio between forward and reverse primers. 1µl of cDNA template was added to the well and set up in triplicate for technical replicate. Non-template controls in which 1µl nuclease free water replaced the cDNA were also used. The optical plate was sealed with an optical cover, briefly centrifuged to remove air bubbles and placed in the qRT-PCR machine.

Thermocycling conditions were as follows:

1) 50°C for 2 mins

2) 95°C for 10 mins
3) 95°C for 15 seconds
4) 60°C for 1 min

Dissociation curves were also ran to determine that the amplified products were specific, and that SYBR Green I fluorescence is a direct measure of accumulation of the product of interest.

Real time analysis

Real time quantitative polymerase chain reaction was used to determine mRNA abundance, indicative of gene expression, using the ABI PRISM 7500 Sequence Detection System. A SYBR Green based assay was used in which a fluorescent signal is emitted once SYBR Green is incorporated into double stranded DNA. Therefore as the PCR progresses, higher quantities of double stranded DNA accumulated, and is measured at each cycle, thus allowing DNA concentrations to be quantified and assigned a Ct (cycle threshold) value. Ct values are defined as the number of cycles required for the fluorescent signal to cross a given threshold (i.e. exceeds background level).

Analysis was carried out using the Delta Delta Ct Method, by which comparisons between the Ct values of the samples of interest with a control or normaliser such as a non-treated sample. The Ct values of both the normaliser and the samples of interest are adjusted to the housekeeping gene L19. This results in a fold change value indicating the relative fold change of expression between the sample of interest and the normaliser.

2.2.8 Chromatin Immunoprecipitation (ChIP)

2.2.8.1 ChIP

Confluent HESC cultured in 10-cm dishes were fixed with 1% formaldehyde for 10 minutes at 37°C. Fixation was stopped with 125 mM glycine and nuclei were isolated by incubating at 4°C for 10 min in 1ml of Swelling buffer. Stromal cells were scraped, homogenized, and centrifuged for 3 minutes at 16,000 × g at 4°C. Pelleted nuclei were resuspended in 500µl of SDS lysis buffer and sonicated for 30 minutes at 4°C on high power in a Diagenode Bioruptor sonicator. The resulting suspension was centrifuged for 15 minutes at 16,000 × g at 4°C and supernatant diluted in IP buffer, and subsequently pre-cleared at 4°C for 3 hours with Protein A Dynabeads. The chromatin was then complexed overnight at 4°C with the appropriate antibody bound to Protein A Dynabeads. Post complexing, samples were washed with low salt buffer, high salt buffer, LiCl buffer, and Tris-EDTA buffer respectively before eluting the chromatin with 250µl of Elution buffer and incubating at room temperature for 15 minutes. 200 mM NaCl was added to reverse cross-link the proteins and the DNA. After an overnight incubation at 65°C, 10 mM EDTA, 40 mM Tris-HCl (pH 8), and 40 µg/ml Protease K were added and the sample incubated for a further hour at 55°C before proceeding with the DNA purification using QIAquick PCR Purification kit. Buffers were supplemented with protease and phosphatase inhibitor cocktails and 10 mM sodium butyrate. The following antibodies were used in the ChIP experiments: CLOCK, BMAL1 and as negative control the rabbit polyclonal antimouse IgG was used. The purified DNA was amplified by qRT-PCR.

2.2.8.2 DNA Purification

The QIAquick Spin kit was used for DNA purification following ChIP. This using selective binding to a silica membrane and appropriate salt buffers to remove

contaminants from previous procedures. PCR products were diluted in 5 volumes of isopropanol containing guanidinium chloride buffer (buffer PB) and applied to a silica membrane and centrifuged at 17,900 x g for 1 minute. DNA was washed with 0.75ml ethanol containing buffer (buffer PE) to remove salt contaminants by centrifugation as above. Purified DNA was eluted with 50µl of 10mM Tris-Cl (pH 7.0) and stored at -20˚C for assessment by qRT-PCR. Primer sequences can be found in Appendix 2.

2.2.9 Calcium Profiling

HESCs were cultured on 35mm glass bottomed dishes and transfected and treated as appropriate. For calcium profiling, HESCs were washed in modified Krebs'-Heinselet buffer and loaded with 5µM Fluo-4-AM for 1 hour at room temperature. Cells were washed and incubated in 2ml Krebs'-Heinselet buffer on the stage of a Zeiss Axiovert 200M inverted microscope and visualized with a 40x objective lens. Temperatures were maintained at 37ºC with a peltier unit. Using a Zeiss LSM 510 confocal imaging system, cells were excited with a krypton/argon laser at 488nm and emitted light was collected above 510nm. Cells were challenged with 5µM *m*-3M3FBS or control DMSO vehicle by direct addition into the cell chamber and imaged for 10 minutes. Fluorescence was captured by a cooled charge-couple device (CCD) camera at a rate of approximately one frame per second and used as an indication of changes in $[Ca^{2+}]_i$. Videos were visualised with LSM work station image analysis software, whereby changes in regions of interest within cells were expressed as a fold increase from time 0 (F/F_0). Data was analysed and expressed graphically where peak response, area under the curve, and oscillatory frequency were calculated.

2.2.10 Microscopy

2.2.10.1 Immunohistochemistry

Paraffin-embedded, formalin fixed endometrial specimens were immunostained for PRIP-1 immunoreactivity using the Novolink polymer detection system. 5µm sections were sliced by microtome. Sections were dewaxed in histoclear, rehydrated in descending ethanol solutions and rinsed with water. Slides were exposed to 30% v/v hydrogen peroxide for 5 minutes, rinsed with TBS and blocked in immunohistochemistry blocking solution, using serum from the species in which the secondary antibody was raised, in a humidified chamber for 5 minutes at room temperature. Immunostaining was carried out using primary antibodies against PRIP-1 (1:100 dilution), in a humidified chamber overnight at 4˚C. For negative controls, the primary antibody was omitted and replaced by the corresponding IgG isotype. Slides were rinsed twice in TBS and incubated with a post primary solution (Rabbit anti Mouse IgG) for 30 minutes. Slides were once again rinsed in TBS and incubated with Novolink Polymer, which detected rabbit immunoglobulins for 30 minutes and rinsed in TBS again. Peroxidase activity was developed using a diaminobenzidine (DAB) solution to produce a visible brown precipitate at the antigen site. Sections were counterstained with Hematoxylin and coverslipped.

2.2.10.2 Immunofluorescence

HESCS were cultured on 4 well chamber slides. Following media aspiration, cells were washed with PBS and fixed in 4% paraformaldehyde for 1 hour at room temperature. The slides were washed with filtered PBS and permeabilized in 0.1% v/v Triton X-100 for 1 hour at room temperature with rocking. Cells were washed again 3 times with filtered PBS (3 x 5 minutes). 1% w/v BSA in PBS was added to block unspecific binding of antibodies and incubated for 1 hour at 4˚C with rocking. Primary

antibodies against PRIP-1 were diluted 1:100 in 1% w/v BSA and incubated with cells overnight at 4˚C. As a negative control, primary antibodies were omitted. The slides were then washed in cold 1% w/v BSA for 30 minutes at 4˚C. Secondary goat Alex Fluor-388 conjugated anti-rabbit antibody was diluted 1:200 in 1% w/v BSA and incubated with cells for 2 hours at 4˚C. The slides were washed with PBS and mounted in Vectashield with DAPI for nuclear counterstain. Staining was visualized with a Zeiss LSM 510 confocal imaging system.

2.2.11 *In vitro* Colony-forming Assay

2.2.11.1 Staining

Transfected HESCs were seeded at a clonal density of 50 cells/cm^2 to ensure equal loading onto fibronectin-coated 60mm culture dishes and cultured in normal growth medium supplemented with 10ng/ml basic fibroblast growth factor. Culture medium was first changed was after 7 days. Colonies were monitored microscopically to ensure that they were derived from single cells. Cultures were terminated at 10 days. Media was aspirated and cells washed 3 times with 3ml PBS. Colonies were fixed with 2ml 10% v/v formalin for 10 minutes at room temperature and subsequently washed again 3 times in 3ml sterile distilled water. 2ml filtered haematoxylin was added to colonies for 4 minutes to stain and then washed again 3 times in 3ml sterile distilled water. 2ml of PBS was added to colonies to intensify the staining for 4 minutes at room temperature, aspirated and dishes allowed to dry. Staining was visualized using the G:Box Chemie XX6.

2.2.11.2 Image Analysis

Images were analysed using Image J software. Brightness and contrast was adjusted to set levels for all images. Colony area was calculated using the 'analyse particles' function.

2.2.12 Viability and Proliferation Assays

2.2.12.1 Trypan Blue Exclusion

Transfected cells were trypsinised and resuspended in 1ml of 2% DCC-FBS supplemented media. To 10µl of cells, 10µl of trypan blue stain was added. Cell counts were measured using a Luna cell counter and conducted in quadruplet. Percentage viability was calculated.

2.2.12.2 Caspase 3/7 Apoptosis Assay

Caspase 3/7 activity was measured using the Apo-ONE Homogenous Caspase 3/7 Assay kit. The buffer supplied with this kit rapidly lyses cultured cells. The caspase 3/7 substrate rhodamine 110, bis(N-CBZ-L-aspartyl-L-glutamyl-L-valyl-L-aspartic acid amide) exits as a profluorescent substrate. Upon sequential cleavage by caspase 3/7 activity and excitation at 499nm, the rhodamine 110 group becomes intensity fluorescent. The amount of fluorescent product is proportional to the amount of caspase 3/7 activity in the sample, indicative of apoptosis.

100µl of Apo-ONE Caspase 3/7 reagent was added to 100µl of cultured cells in normal 10% DCC-FBS supplemented media a 96 well format. Blank wells with no cells were used as a negative control. Contents of the wells were mixed on a plate shaker and the plate incubated at room temperature. The assay incubation time was

optimized empirically to 4 hours. Fluorescence was measured at 530nm emission and 490nm excitation on the PHERAStar FS microplate reader.

2.2.12.3 XTT assay

Cellular viability is determined by the cell's ability to reduce tetrazolium salts (XTT) into coloured formazan compounds by mitochondrial enzymes. These coloured formazan compounds can then be detected colorimetrically. 50µl of XTT detection solution was added to 100µl of cultured cells in normal 10% DCC-FBS supplemented media in a 96 well format. The plate was incubated at 37˚C for 4 hours. Dye absorbance was measured at 450 nm on the PHERAStar FS microplate reader and is proportional to the number of viable cells per well.

2.2.12.4 Real-time Adherent Cell Proliferation

Real-time adherent cell proliferation was determined by the label-free xCELLigence Real-Time Cell Analyser (RTCA) DP instrument, which utilizes specialized microtitre culture plates containing an interdigitized gold microelectrode on which cells attach and proliferate. Cell contact with the electrode increases the impedance across these gold arrays and reported as an arbitrary 'cell index' value as an indication of confluency and adherence. HESCs were seeded into 16-well E-plates at a density of 10,000 cells per well and cultured in 10% DCC-FBS supplemented media until ~80% confluent. The RTCA DP instrument was placed at 37°C in a humidified environment with 95% air and 5% CO_2. Cells were either left undifferentiated or decidualized following transient transfection as per standard protocols. Individual wells within the E-plate were referenced immediately and monitored first every 15 min for 3 hours and then hourly for 4 days. Changes in cell index were captured and analysed using the RTCA Software v1.2 supplied with the instrument.

2.2.13 Flow Cytometry

Transfected HESCs were harvested from T25 plastic culture-ware by trypsinization and centrifugation at 300 x g for 5 minutes. Cell pellets were resuspended in 600µl of sterile filtered cold PBS. 1400µl of ice cold 100% ethanol was added drop wise whilst concurrently mixing. Samples were stored on ice for at least 1 hour. For propidium iodide staining, cells were collected by centrifugation at 300 x g for 5 minutes. Ethanol solution was removed and pellets washed twice in 2ml 1% w/v BSA in PBS with centrifugation between each wash. Pellets were resuspended in 1ml PBS supplemented with 100µg/ml RNse and 100µg/ml propidium iodide. Samples were incubated in this solution for 30 minutes at 37˚C in the dark. 50,000 cells per sample were subjected to flow cytometry analysis using a FACScaliber with CellQuestPro software. Cell cycle distribution was assessed using FlowJo software using the Watson (Pragmatic) model.

2.2.14 RNA Sequencing

2.2.14.1 Sample Preparation and Selection

Primary HESCs cultures were transfected with either PER2 or non-targeting siRNA and then decidualized with 8-br-cAMP and MPA for 24 hours. Three biological repeat experiments were performed. To ensure samples had sufficient levels of gene knockdown and responded appropriately to decidualization stimuli, aliquots of RNA were used for cDNA synthesis followed by qRT-PCR to assess expression of PER2 mRNA, as well as decidualization markers prolactin and IGFBP1. All samples showed reduced PER2 expression upon PER2 siRNA transfection. All samples transfected with non-targeting siRNA showed normal induction of decidual markers.

2.2.14.2 RNA Quality Control

RNA quality was analysed on an Agilent 2100 Bioanalyser and assessed with the Eukaryotic Total RNA Nano program according to the manufacturer's instructions. RNA integrity number (RIN) score for all samples was ≥ 8.9.

2.2.14.3 Library Preparation

TruSeq stranded mRNA library preparation was carried out by Source Bioscience from the RNA provided. In principal mRNA in total RNA in converted into a library of template molecules suitable for sequencing. Poly-A containing mRNA molecules are first purified by separation using oligo-dT conjugated magnetic beads. Following purification, mRNA is fragmented using divalent cations under elevated temperatures. The cleaved mRNA fragments are then copied into first strand cDNA using reverse transcription and random primers. This is followed by second strand cDNA synthesis using DNA Polymerase I and RNase H. The cDNA fragments are subjected to end repair, addition of a single 'A' base and ligation of adapters. The fragments are finally purified and enriched by PCR to create the cDNA library suitable for sequencing.

2.2.14.4 Sequencing

Illumina HiSeq was carried out by Source Bioscience. Single end next generation sequencing was utilized with a read length of 100 base pairs.

2.2.14.5 Data Analysis and Quality Control

Transcriptomic alignments were identified using bowtie-0.12.8, samtools-0.1.18, and tophat-2.0.4 against the University of California Santa Cruz (UCSC) hg19 reference transcriptome from the Illumina iGenomes resource. Gene counts were estimated

using HTSeq-0.5.3p3 (http://wwwhuber.embl.de/users/anders/HTSeq/) and transcripts per million (TPM) calculated. Count data from the TopHat-HTSeq pipeline were analysed using two different methods for differential expression detection; DESeq and edge R. Gene transcript abundances were considered to be significantly different if the false discovery rate (FDR) value (edgeR) or adjusted P value (DESeq) was < 0.01. Differentially expressed genes were retained if they were detected by at least two of the methods used.

2.2.15 Data Mining

Datasets from the GEO repository were data-mined for expression data of various genes. The following data sets were used;

Endometrium through the menstrual cycle: GDS2052

Preimplantation embryonic development (HG-UG133_Plus_2): GDS3959

2.2.16 Statistical Analysis

Data was analysed using the statistical package GraphPad Prism. Where appropriate, a 2-tailed paired Student's t-test or one-way analysis of variance (ANOVA) was applied. Variables that were not normally distributed were analysed using the Kruskal-Wallis test. Mann-Whitney U test was used for paired comparisons. Spearman's' rank test was utilised for correlative analysis. Results were expressed as means ± standard error of the mean (SEM). Values of $P<0.05$ were considered statistically significant.

Chapter 3

The Circadian Protein PER2 Synchronises Mitotic Expansion and Decidualization in HESCs.

3.1 Introduction

As discussed in the chapter 1, mammalian reproduction is critically dependent upon precisely timed interconnecting signalling networks. These networks act in concert to control the onset of puberty, timing of ovulation, blastocyst implantation and parturition (Boden *et al.*, 2013a). The circadian system is highly evolutionary conserved and acts as an exquisitely accurate internal biological clock, timing daily events. The finding that most peripheral organs and tissues express circadian oscillations has unlocked a series of questions concerning the role of rhythms as well are the architecture of circadian clocks in the reproductive system (Dolatshad *et al.*, 2009; Karman & Tischkau, 2006; Kennaway *et al.*, 2003b). It is now increasingly evident that oscillators within individual cells are able to respond diversely to entraining signals, control various physiological outputs and interact cooperatively with each other and within the circadian system as a whole. Within the human uterus, the action of ovarian steroid hormones have been shown to influence clock gene expression in all of the major tissue types including the epithelium, stroma and myometrium (Czeisler & Klerman, 1998; Nakamura *et al.*, 2008).

Decidualization, the most prominent feature in the human reproductive cycle, defines a cellular differentiation process which is both highly dynamic and temporally regulated. Emerging evidence highlights the role for a biphasic inflammatory response. This begins with a tightly defined acute pro-inflammatory phase, characterised by the production of free radicals, chemokines, interleukins and other inflammatory mediators. This is then critically followed by a profound anti-inflammatory response during the late luteal phase of the cycle in which stromal cells acquire a characteristic secretory phenotype (Salker *et al.*, 2010; Salker *et al.*, 2012). Timings of these inflammatory phases define the ‘window of implantation’ and are critical for successful embryonic implantation. Disruption of the temporal organization

of the decidual response is associated with reproductive failure. For example, endometriosis is associated with uterine progesterone resistance, an attenuated decidual response, implantation failure and conception delay (Al-Sabbagh *et al.*, 2012). Conversely, a protracted pro-inflammatory response prolongs the window of endometrial receptivity, which in turn increases the risk of developmentally delayed embryo implantation and early pregnancy loss. Thus synchronised endometrial receptivity and embryonic development are critical to prevent pregnancy related pathologic events.

Disruption of clock genes either through mutation or knockout have highlighted the importance of cell autonomous peripheral clocks in reproduction. Conditional deletion of *Bmal1* in rat pituitary gonadotrophs affects oestrous length (Chu *et al.*, 2013), whilst deletion in the ovary results in complete implantation failure due to impaired steroidogenesis (Ratajczak *et al.*, 2012; Ratajczak *et al.*, 2009). Other studies have demonstrated that mice lacking both *Per1* and *Per2* have more embryonic implantation sites, yet fewer live offspring when compared to wild type controls (Pilorz & Steinlechner, 2008). It is suspected that these *Per* gene deletions result in an accelerated ageing reproductive phenotype in mice.

In this chapter I aim to establish the role of circadian rhythms in primary HESCs and their effects upon the differentiation programme. Primarily, it was observed that alike in rats, circadian oscillations are highly temporally regulated during the differentiation programme in the human endometrium. I will further investigate the precisely timed down-regulation of the core clock gene *PER2*, and its ability to create a ‘pause’ in the circadian programme, permissive for successful decidualization. I will additionally discuss the critical timing of this event, and investigate the effects of premature loss of *PER2* in HESCs during the initial stages of the decidual response by utilising RNA-sequencing. The importance of this transitional pathway was emphasised by analysis

of mid-luteal endometrial biopsies from 70 women suffering consecutive miscarriage, showing significant correlations between *PER2* mRNA levels with both age and the number of preceding pregnancy losses. The results discussed within this chapter highlight the significance of circadian coordination within female reproduction.

3.2 Results

3.2.1 *In vivo* Expression of Core Circadian Clock Genes.

I speculate that circadian rhythms may have an important role in the regulation of decidual transformation of HESCs and therefore implantation. In other words, circadian genes may act to influence the monthly menstrual cycle as well as critically maintain the daily circadian cycle. To test this hypothesis, data mining of the Gene Expression Omnibus (GEO) revealed changes in expression levels of six of the core clock genes over the course of the menstrual cycle (GDS2052). Transcript levels of *CLOCK* (circadian locomoter output cycles kaput), *BMAL1* (brain muscle arnt-like 1), *CRY1, CRY2* (cryptochrome 1 and 2), *PER1* and *PER2* (period 1 and 2) were investigated, as their gene products establish the basis of a robust and stable circadian transcriptional and translational feedback loop.

Data revealed transcript levels of these 6 genes from the proliferative, early secretory, mid secretory and late secretory stages from a total of 27 samples (Figure 3.1). Expression levels of *CLOCK* and *CRY1* showed no significant changes over the course of the menstrual cycle. mRNA transcript levels of *BMAL1* and *CRY2* displayed significant increases during the secretory phase, whilst both *PER* gene transcripts revealed a biphasic response. *PER1* and *PER2* increased 2 fold and 4 fold respectively between the proliferative and early-secretory phase. Elevated levels are maintained during the mid-secretory phase, but then fall in concert during the late secretory phase when known decidual marker genes such as *LEFTY2* and *IGFBP1*

are sharply induced. These results highlight significant gene regulation of circadian transcripts during the menstrual cycle.

Further data mining of the GEO revealed changes in expression levels of 6 of the core clock genes during preimplantation human embryonic development (GDS3959). Data from the microarray revealed transcript levels of these six genes from the 1 cell to blastocyst stage from a total of 18 samples (Figure 3.2). Expression profiles of *CLOCK, BMAL1*, *CRY1* and *PER2* display high expression during the very early stages of development but decline rapidly. This is likely attributable to the degradation of stored maternal transcripts. No induction during embryonic gene activation is apparent. Interestingly *CRY2* and *PER1* expression profiles show an up-regulation of transcripts during embryonic development, with increased transcripts apparent at the morula and blastocysts stages. This suggests these genes are actively transcribed by the zygotic genome, as opposed to the maternal genome.

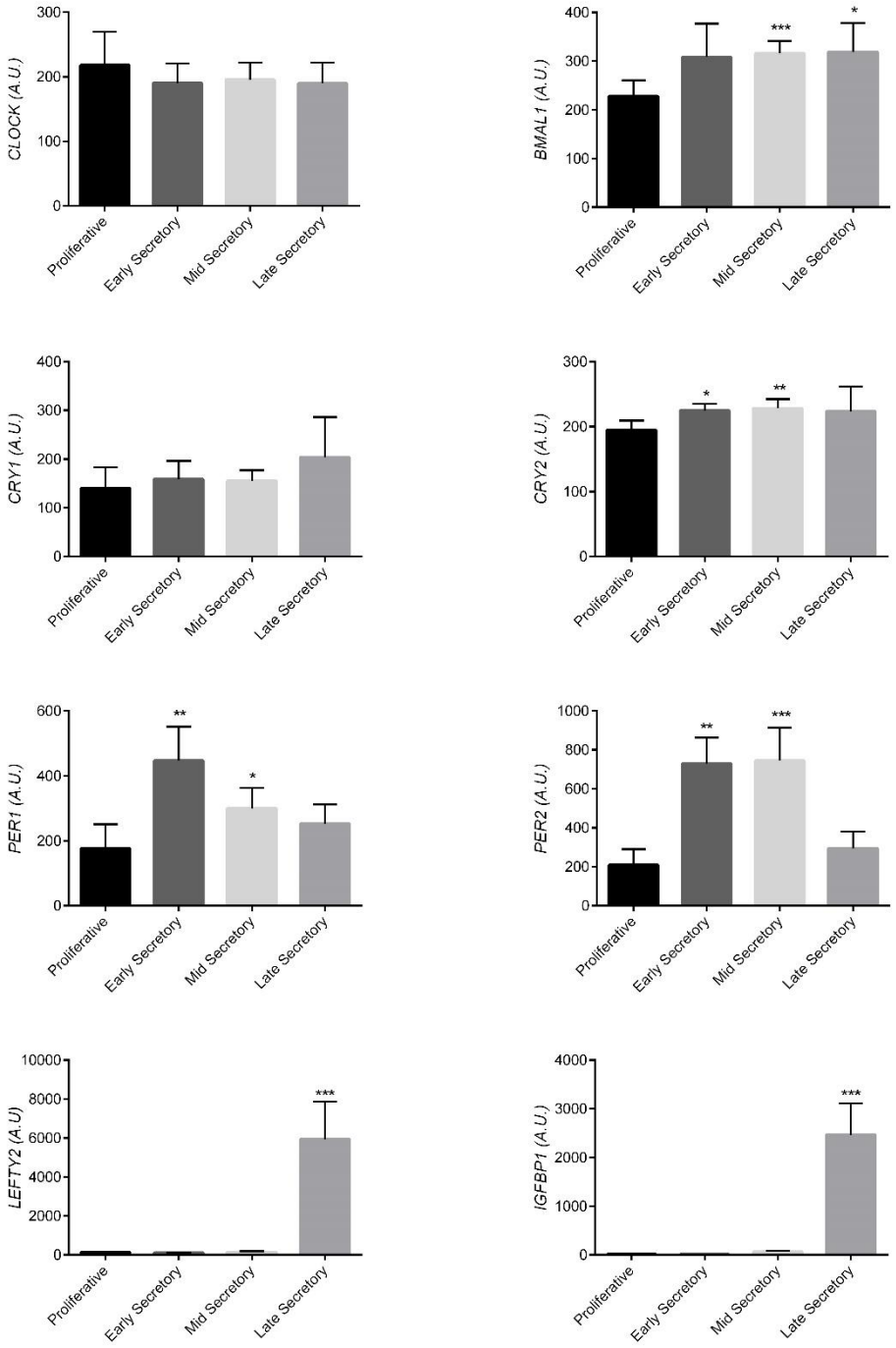

Figure 3.1 ***Expression of core circadian clock genes through the menstrual cycle.*** GEO profile microarray of circadian transcripts, *CLOCK, BMAL1, CRY1, CRY2, PER1* and *PER2* and decidual markers *LEFTY2* and *IGFBP1* during the proliferative, early secretory, mid-secretory and late secretory phases of the menstrual cycle in 28 subjects using Affymetrix Human Genome U133 Array. *P<0.05; ** P<0.01; ***P<0.001. Data are presented as means ± S.E.M.

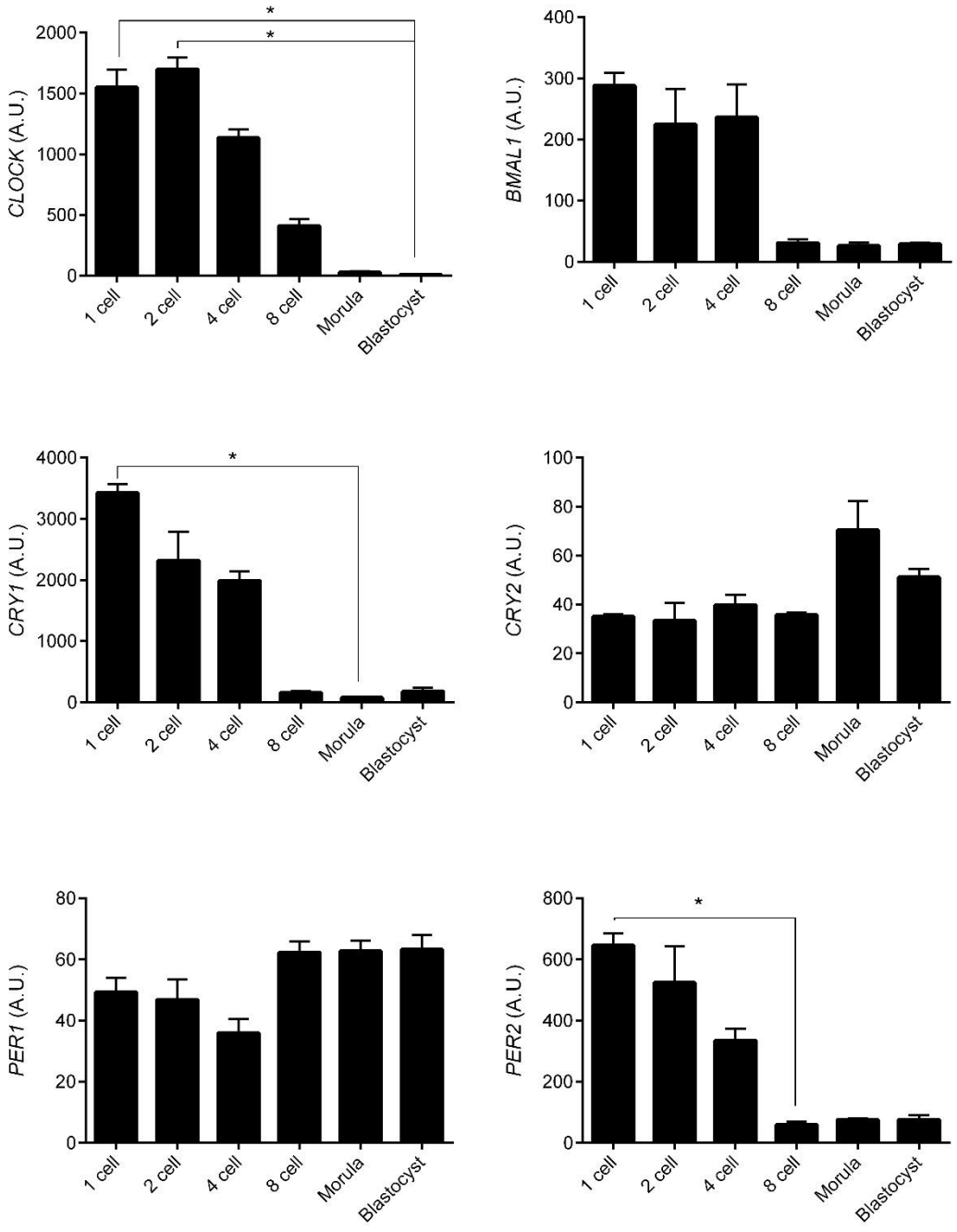

Figure 3.2 In vivo *expression of core circadian clock genes during human pre-implantation embryonic development.* GEO profile microarray of *CLOCK, BMAL1, CRY1, CRY2, PER1* and *PER2* transcripts from the 1 cell, 2 cell, 4 cell, 8 cell, morula and blastocyst stages of embryonic development from 18 samples using Affymetrix Human Genome U133 Array. *P<0.05. Data are presented as means ± S.E.M.

3.2.2 Loss of Circadian Oscillations upon Decidualization of HESCs.

Decidualization of stromal cells in the rat uterus has been shown to be associated with the loss of circadian rhythmicity (Uchikawa *et al.*, 2011). I therefore speculated that this phenomenon may be conserved in humans and acts to synchronize maternal and embryonic gene expression at implantation. To investigate this hypothesis, transcript levels of the 6 core clock genes were measured in primary undifferentiated HESCs and cells that had first been decidualized for 4 days with 8-br-cAMP and MPA, representing the window of implantation.

In vitro, single cells have been shown to harbour self-sustained and cell autonomous circadian oscillations (Nagoshi *et al.*, 2004), however once isolated they are no longer in synchrony. In other words, each cell will by cycling independently. In order to detect changes in circadian oscillations within a whole culture, circadian rhythms must first be synchronized. This was achieved with a short dexamethasone pulse, which is known to act as a resetting stimulus *in vitro*. As shown in Figure 3.3, all 6 clock genes exhibited circadian regulation in undifferentiated cells with amplitude of gene expression varying up to 5 fold over a 26 hour period. However, upon decidualization, expression was uniformly aperiodic across the circadian time-course. These results indicate that differentiation of HESCs is associated with a concurrent loss of circadian rhythmicity.

Given the positive and negative transcriptional/translational feedback loop the circadian system is centred around, it was concerning that all of the core clock genes measured were approximately in phase with one another. Peak transcript levels were all focused between 2-10 hours post synchronization, whereas it is known that several transcripts are anti-phase to each other, including *BMAL1* and *PER2*. I speculated

that measurement of RNA transcript levels within the 26 hours immediately post dexamethasone treatment may have contributed to this ‘in phase’ phenomenon. In order to confirm normal circadian rhythms in undifferentiated cultures, *BMAL1* and *PER2* expression was measured in an extended time-course. RNA was extracted every 4 hours between 12 and 48 hours post dexamethasone synchronization and subjected to qRT-PCR. Over this timeframe, *BMAL1* and *PER2* were shown to be anti-phase to each other, confirming the presence of normal circadian oscillations in undifferentiated HESCs (Figure 3.4).

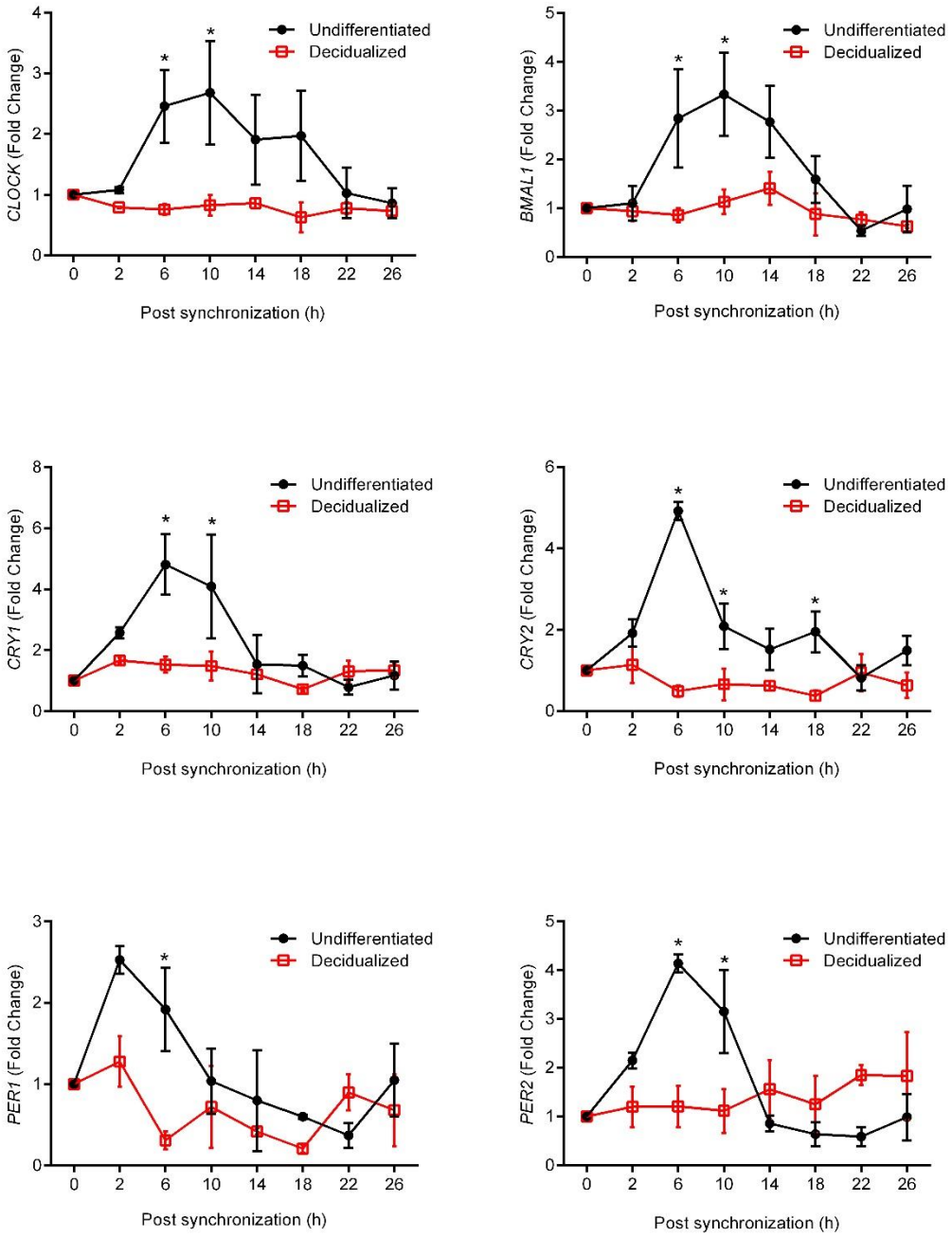

Figure 3.3 ***Decidualization of primary endometrial stromal cells is associated with loss of rhythmic expression of core clock genes***. Expression of *CLOCK, BMAL1, CRY1, CRY2*, *PER1* and *PER2* mRNA transcripts in undifferentiated HESCs or cells decidualized for 6 days with 8-br-cAMP and MPA, Both cultures were synchronized with dexamethasone for 30 minutes. mRNA was collected at indicated time points and transcript expression analysed using qRT-PCR. *P<0.05. Data are presented as mean fold change ± S.E.M.

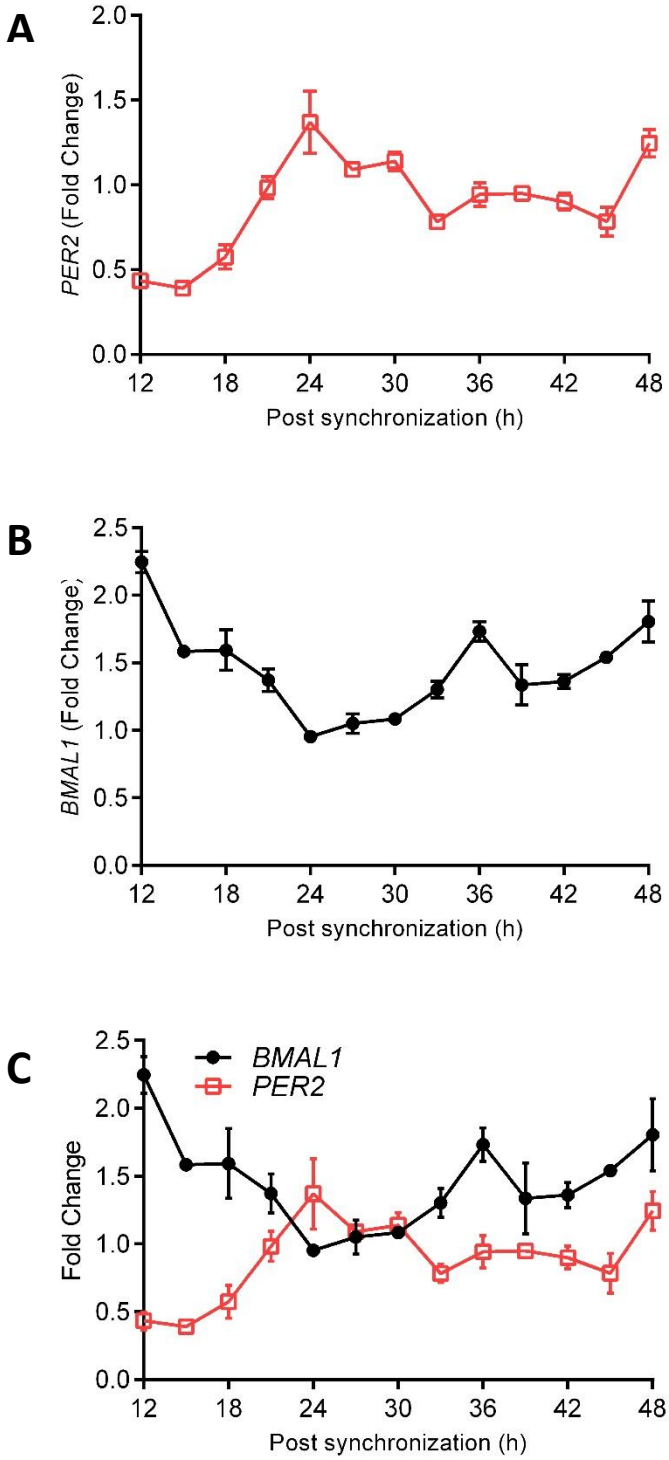

Figure 3.4 ***Confirmation of anti-phase expression pattern of*** **PER2** ***and*** **BMAL1.** Expression of (a) *PER2* and (b) *BMAL1* mRNA transcripts in undifferentiated HESCs over an extended timeframe. (c) Overlay of *PER2* and *BMAL1* expression to indicate anti-phase expression. Cultures were synchronized with dexamethasome for 30 minutes and mRNA was collected at indicated time points, transcript expression was analysed using qRT-PCR. Data are presented as mean fold change ± S.E.M.

3.2.3 Resumption of Circadian Oscillations.

It is known that circadian rhythms are present at the time of parturition in humans (Honnebier & Nathanielsz, 1994; Longo & Yellon, 1988; Srinivasan *et al.*, 2009), therefore I speculated that oscillations of the core clock machinery are potentially only 'paused' upon decidualization of HESCs. Whilst it was observed that circadian oscillations are switched off at day 4 of decidualization, it was unknown as to when circadian oscillations resume. To investigate this, transcript levels of the same 6 core clock genes were measured in primary undifferentiated HESCs and cells that had first been decidualized for 12 days with 8-br-cAMP and MPA. Results unfortunately were inconclusive (Figure 3.5). Oscillations in undifferentiated HESCs were inconsistent with previous data, whilst those from HESCs decidualized for 12 days were present in *CRY1* but erratic in all other genes. I hypothesise that this inconclusive data is a result of cells being maintained in reduced serum media for a prolonged period of time. Alternatively, it is possible that resumption of circadian cyclicity is dependent upon embryonic signals.

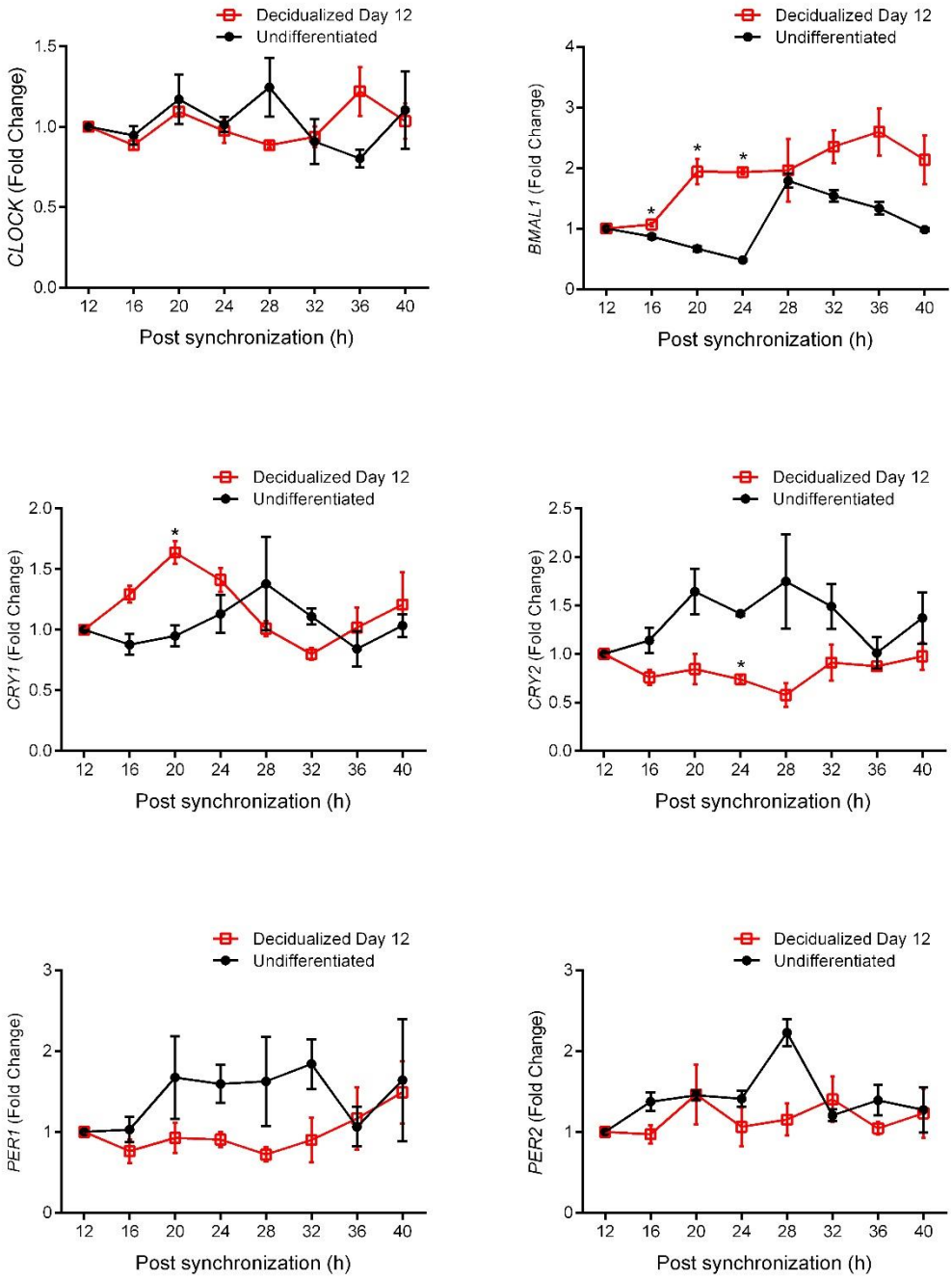

Figure 3.5 The resumption of rhythmic expression of core clock genes at decidual day 12 is inconclusive. mRNA transcript expression of the six core clock genes in undifferentiated HESCs or cultures decidualized for 12 days with 8-br-cAMP and MPA. Both sample sets were synchronized with 100nM dexamethasone for 30 minutes. mRNA was harvested at indicated time points and transcript expression analysed by qRT-PCR. Data are presented as mean fold change ± S.E.M.

3.2.4 Expression of Core Clock Genes in Decidualized HESCs.

To investigate the underlying mechanism of the observed loss of rhythmicity, expression profiles of the same core clock genes were examined in unsynchronized HESCs, which were either undifferentiated or decidualized for 2, 4 or 8 days. qRT-PCR analysis revealed modest but consistent changes in the expression of several transcripts upon differentiation (Figure 3.6a). *CLOCK* is known to be stably transcribed over the circadian cycle, and expression both at RNA and protein level remained constant over the 8-day time-course. *BMAL1* and *PER1* transcripts were both increased by day 2, and maintained over the 8 day period, although this response did not reach statistical significance. By contrast, protein expression demonstrated a lag and accumulated as decidual transformation unfolded, reaching maximal expression by day 8 (Figure 3.6b). Down-regulation of both *CRY1* and *CRY2* was observed both at mRNA and protein level. Once again, protein expression exhibited a time lag following transcript loss. Circadian genes are known to be post-translationally modified (Lee *et al.*, 2008; O'Neill *et al.*, 2013; Stojkovic *et al.*, 2014), which may account for observed delays in protein expression. The most striking observation, however, was the rapid and profound inhibition of *PER2* expression with transcript levels falling by 80% within 2 days of differentiation. Western blot analysis confirmed the dramatic decline in *PER2* levels upon decidualization. Furthermore, *PER2* mobility on SDS-PAGE became more focused and noticeably enhanced, suggesting that decidualization also impacts on the post-translational modification status of this component of the circadian machinery.

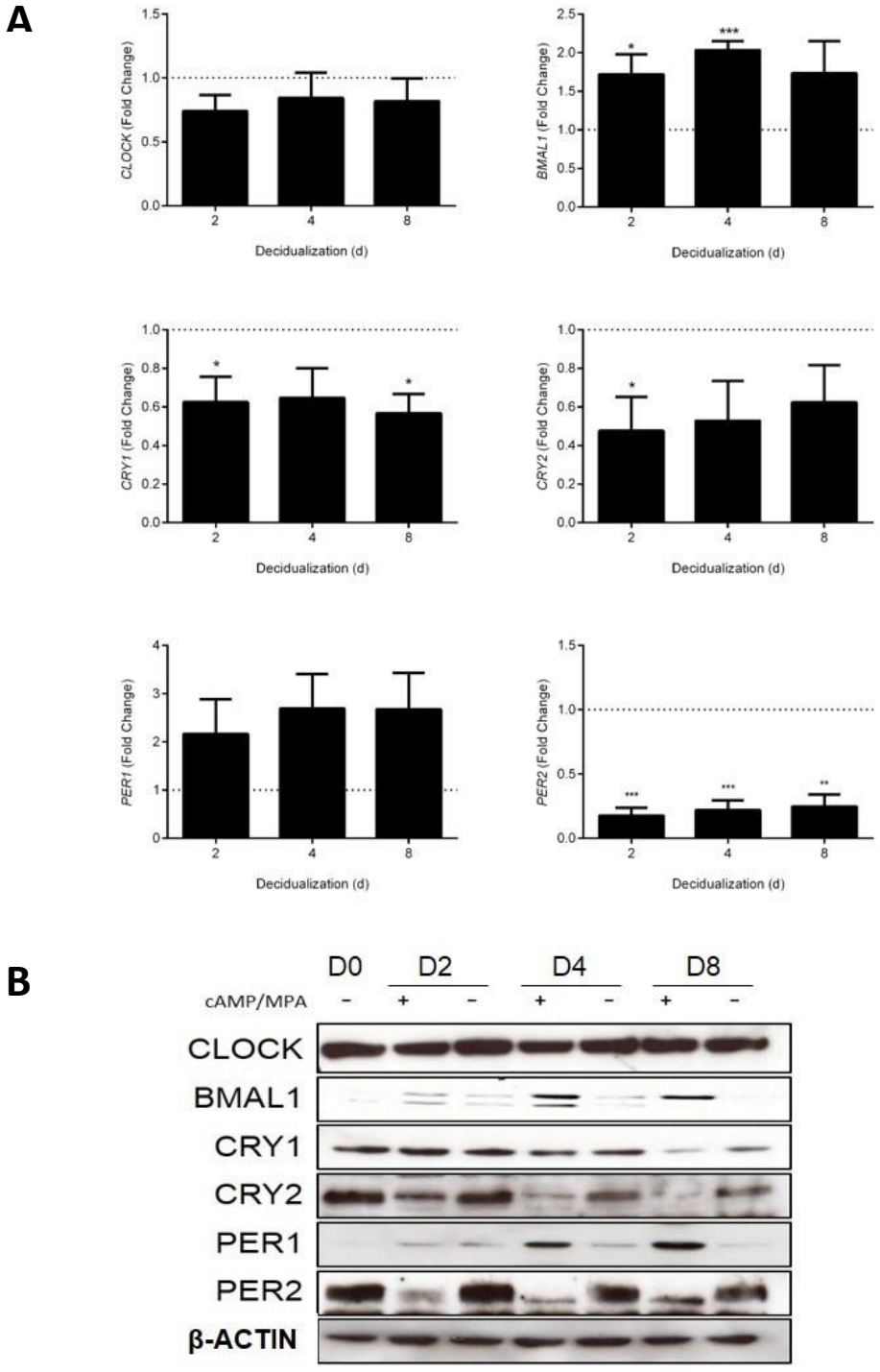

Figure 3.6 ***Uterine stromal decidualization is associated with attenuation of PER2.*** (a) Core clock gene expression in cultures decidualized with 8-br-cAMP and MPA for 2-8 days. Transcript expression was normalized to that of undifferentiated cells (Day 0). *P<0.05; ** P<0.01; ***P<0.001. Data are presented as mean fold change ± S.E.M. (b) Western blot analysis of total cell lysates of timed paired undifferentiated or decidualized HESCs (2-8 days).

3.2.5 Investigations into *PER2S*, a Splicing Variant of *PER2.*

Splicing variants have been reported for *BMAL1* and *PER1* (Ikeda & Nomura, 1997; Yu et al., 1999*)*. *PER2S*, has been recently identified as a novel splicing variant of the human *PER2* gene. *PER2S* is 1215 base pairs long, corresponding to a protein of 404 amino acids, whilst canonical *PER2* is much longer at 3767 base pairs, producing a protein of 1255 amino acids. Studies have highlighted sequence homology between the two isoforms in nucleotides 1-1046 and 1155-1215, whilst nucleotides spanning 1047-1154 and 1616-3767 were only present in the full length variant (Avitabile *et al.*, 2014). Using ExPASy software, it was calculated that the protein product of the *PER2S* isoform would have a molecular weight of 45kDa, whilst the known molecular weight of the full length *PER2* isoform is 140kDa.

Upon western blot analysis, whilst the full length isoform confirmed the decline in *PER2* levels during decidualization, a band also appeared at approximately 50kDa which showed an inverse pattern, with clear up-regulation upon differentiation (Figure 3.7a). I therefore speculated that this product may be the result of the *PER2S* isoform, and the balance between the protein products of these may regulate circadian function in HESCs during decidualization. Primers were designed that were able to distinguish between the two isoforms (Figure 3.7b). qRT-PCR analysis revealed that the *PER2S* variant was only very lowly expressed within HESCs, whilst the full length isoform was consistent with the results previously observed (Figure 3.7c). Additionally, the abundance of the lower molecular weight band in decidualizing cells was constant throughout the time-course indicting that it is likely non-specific; therefore I conclude that the full length isoform is the critical variant subject to regulation in these cells.

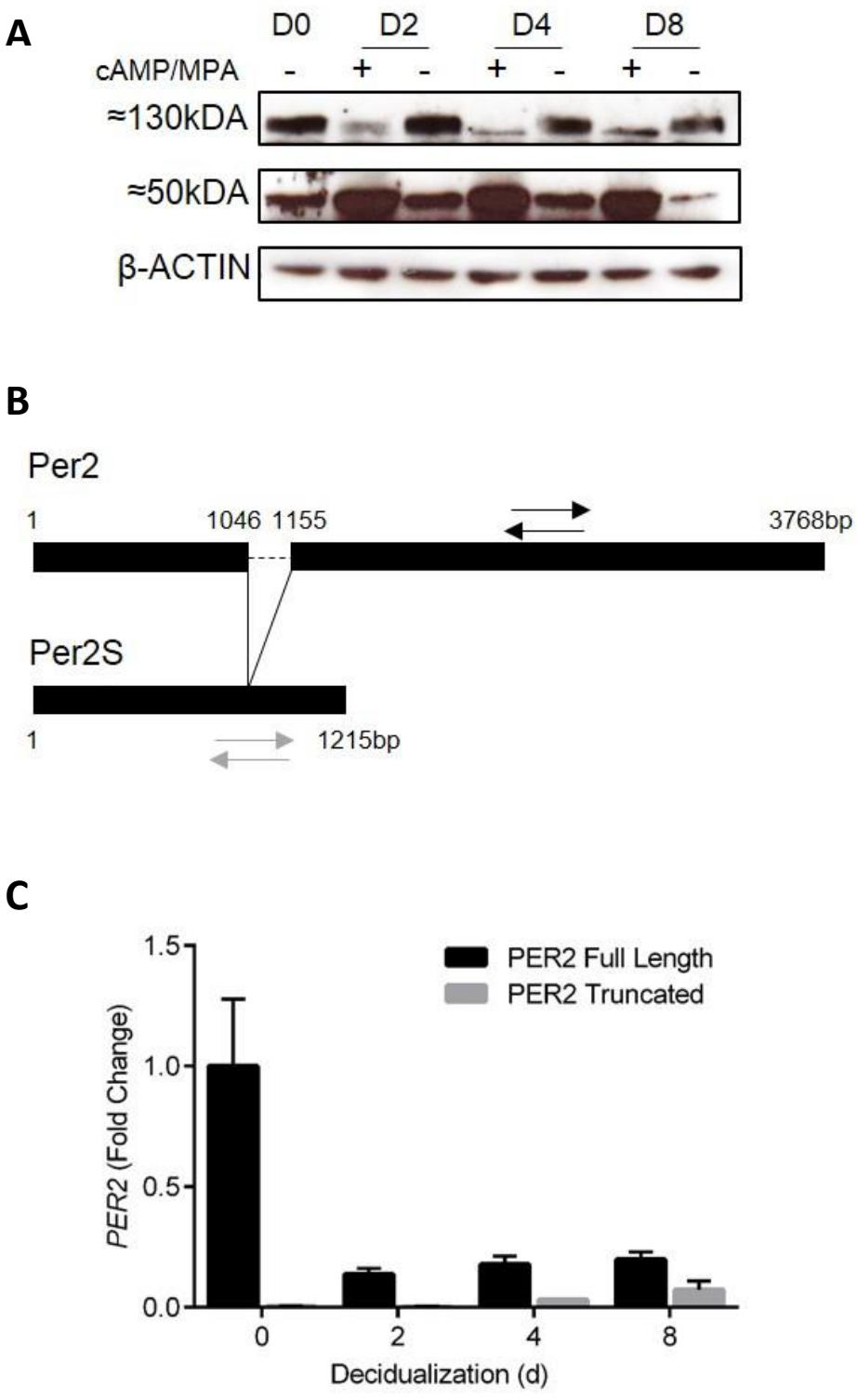

Figure 3.7 ***Down-regulation of*** **PER2** ***is driven by the full length isoform.*** (a) Representative western blot analysis of total cell lysates of timed paired undifferentiated or decidualized HESCs, identifying the full length 132kDa PER2 protein and an additional band at approximately 50kDa with inverse expression. (b) *PER*2 and *PER2S* cDNA coding sequences. Arrows indicated location of amplicons. (c) Full length *PER2* and truncated *PER2S* expression in decidualizaed HESCs (0-8 days) as analysed by qRT-PCR. Data are presented as mean fold change ± S.E.M.

3.2.6 Convergence of cAMP and P4 Signalling Downregulates *PER2.*

The convergence of the cAMP and progesterone pathways drives the decidual phenotype in HESCs (Brar *et al.*, 1997). To further explore the regulation of *PER2*, HESCs were treated with either 8-br-cAMP or MPA alone or in combination for a total of 2 days. The decline in *PER2* expression was more pronounced with MPA compared to 8-br-cAMP, although the level of inhibition was not statistically significant with either treatment. By contrast, combined treatment elicited an 80% reduction in *PER2* expression after 48 hours when compared to vehicle-treated control (Figure 3.8). This is indicative of a synergistic response common in many decidual associated genes.

3.2.7 *PER2* Regulation is Independent of RNA Stability.

In addition to evidence demonstrating circadian control of transcription, results from various studies have suggested posttranscriptional regulatory mechanisms at the RNA level (Woo *et al.*, 2010; Woo *et al.*, 2009). I therefore speculated that *PER2* expression could be differentially controlled by the stability of its RNA transcripts. To test this hypothesis, undifferentiated and HESCS decidualized for 4 days were subjected to actinomycin D treatment, a known potent transcription inhibitor, for 30 minutes, 1, 2, 4 or 8 hours. Using qRT-PCR analysis, the rate of decay of *PER2* mRNA transcripts was measured. Exponential decay analysis resulted in comparable non-significant half-lives in undifferentiated and decidualized cells (2.93 hours in undifferentiated cells versus 3.39 hours in decidual cells).

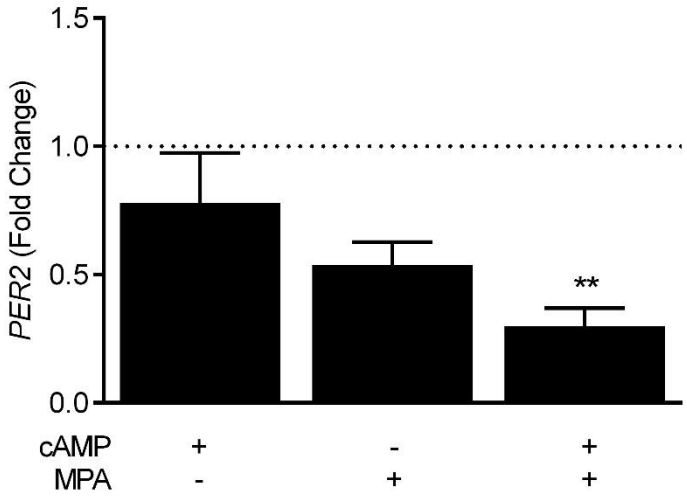

Figure 3.8 PER2 *downregulation is driven by coordinating cAMP and progesterone signalling pathways.* Primary HESC cultures were treated with either 8-br-cAMP or MPA for 48 hours as indicated and *PER2* transcript levels measured. Transcript expression was normalized to that of undifferentiated control. **P<0.01. Data is presented as mean fold change ± S.E.M.

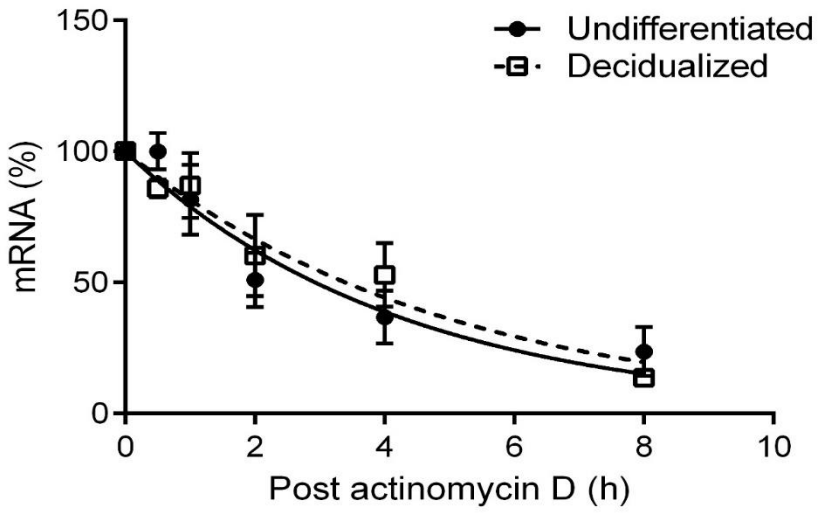

Figure 3.9 *Reduction if* PER2 *expression is not associated with alterations in RNA stability.* Undifferentiated or decidualized HESC (2 days) were treated with 2µM actinomycin D. RNA was harvested at indicated time points and *PER2* mRNA expression quantified by qRT-PCR. Exponential decay analysis was used to determine RNA half-life. Data are presented as means ± S.E.M

3.2.8 *PER2* Down-regulation is Dependent upon Attenuated CLOCK Binding to an E2 Enhancer Element.

Sustained expression of circadian oscillations in peripheral tissues requires the integrity of the transcriptional/translational feedback loop. In the mouse, *Per2* expression is critically dependent upon a non-canonical 5'-CACGTT-3' E-box enhancer element, termed E2, located 20 base pairs upstream of the transcriptional start site (Yoo *et al.*, 2005). This enhancer element and its flanking regions corresponding to the core CLOCK:BMAL1 heterodimer M34 core binding site are conserved at the human *PER2* locus on chromosome 2q37.3. I therefore speculated that disruption of CLOCK:BMAL1 binding to this specific E2 enhancer may contribute to the down-regulation of *PER2* expression observed upon decidualization.

In order to investigate this possibility, ChIP analysis was optimised using CLOCK, BMAL1 and control IgG antibodies, followed by qRT-PCR, with primers specifically targeting the E2 element. In undifferentiated HESCs, results indicated that CLOCK antibody pulldown resulted in a near 3% enrichment of the E2 locus, compared to ≈ 1% with BMAL1. Rabbit IgG antibody was used a negative control, and showed very little (<0.07%) enrichment. (Figure 3.10a). Due to the increased E2 locus enrichment upon CLOCK pulldown, this antibody was used for future assays.

HESC cultures from three independent patients were either undifferentiated, or decidualized with 8-br-cAMP and MPA for 12, 24, 48, 96 or 192 hours. Results show that decidualization was associated with a rapid and sustained loss of CLOCK binding at the E2 enhancer locus (amplicon -301 to -162 base pairs). After 12 hours of treatment, CLOCK binding was reduced by 59%, and this level of reduction was maintained throughout the whole time-course. In order to validate results, primers targeted to the *PER2* gene body (off target), were employed. This locus showed no

enrichment. Additionally, primers were designed to target the E-box located in the *PER1* promoter (E5, amplicon -142 to -54 base pairs) to prove specificity (Figure 3.10b). The *PER1* gene was shown to be upregulated slightly upon decidualization. This response was again mirrored by enriched CLOCK binding over the decidual time-course (2.8 fold increase by 24 hours), however, results did not reach significance. *PER1* gene body (off target) primers showed no enrichment (Figure 3.10c). Thus, the attenuated binding of CLOCK to the E2 enhancer element in the *PER2* promoter cannot be accounted for by a general reduction in the DNA-binding activity of the CLOCK:BMAL1 heterodimer.

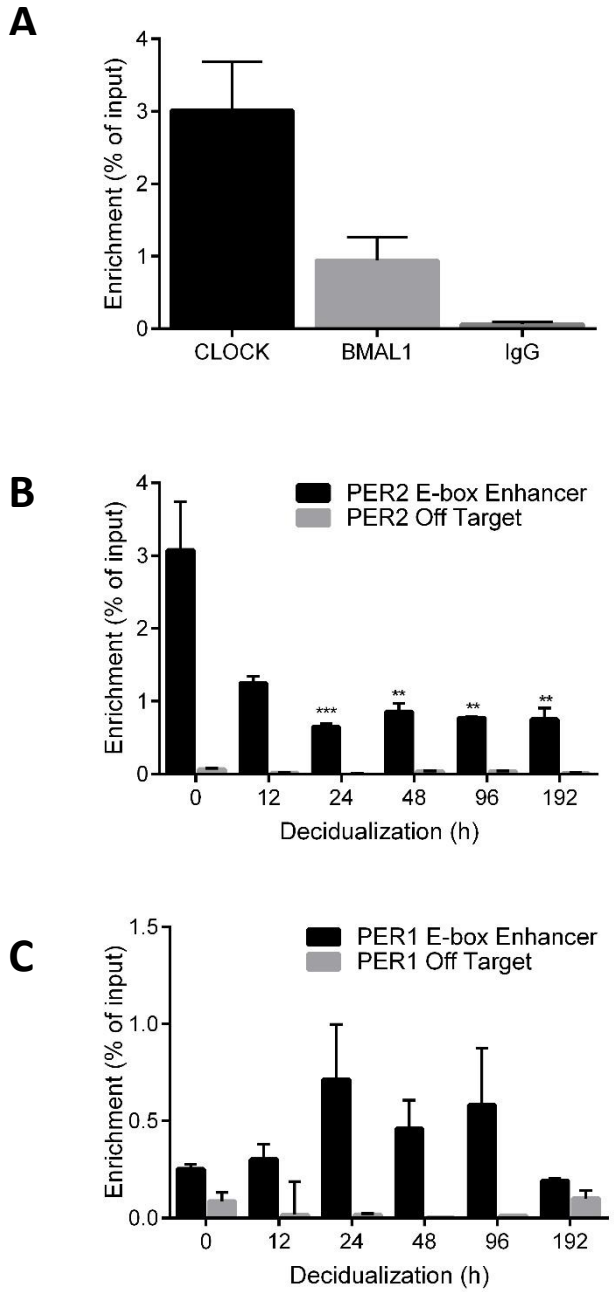

Figure 3.10. ***Reduction in* PER2 *expression is associated with a reduction in CLOCK promoter binding*.** (a) ChIP enrichment for the *PER2* E2 enhancer element when chromatin is immunoprecipitated with CLOCK, BMAL1 and control IgG antibodies in primary HESCs decidualized for indicated time points. (b) ChIP enrichment of the *PER2* enhancer element and *PER2* gene body upon CLOCK binding in HESCs during a decidual time course. (c) Enrichment of *PER1* E5 E-box element and *PER1* gene body in HESCs described above. Data are mean percentage of input ± S.E.M. ** P<0.01; ***P<0.001

3.2.9 *PER2* Knockdown Disrupts other Core Circadian Components.

Circadian oscillations are predicated on the basis of autoregulatory feedback loops, therefore I speculated that *PER2* knockdown by siRNA in undifferentiated HESCs may recapitulate the changes observed in other core clock components associated with decidualization. In order to investigate this, three independent HESC cultures were transfected with either non targeting control siRNA or *PER2* siRNA. RNA and protein were harvested 4 days post transfection. Analysis by qRT-PCR confirmed *PER2* transcriptional knockdown by 77% (Figure 3.11a). Western blot analysis additionally confirmed *PER2* loss of expression at functional protein level (Figure 3.11b). *CLOCK* expression was previously shown to be stable throughout decidualization. *PER2* knockdown did not alter *CLOCK* expression at either mRNA or protein level. *BMAL1* expression was induced 2-fold during decidualization. *PER2* knockdown resulted in a modest, non-significant up-regulation in *BMAL1* mRNA, but no changes in protein expression were observed. Both *CRY1* and *CRY2* were down-regulated during HESC differentiation. Upon *PER2* knockdown, *CRY1* transcripts were strikingly upregulated by over 6 fold; however, changes at the protein level were modest. In regards to *CRY2* expression, no real changes were observed at RNA level; however, CRY2 protein appeared heightened upon treatment with *PER2* siRNA. *PER2* knockdown recapitulated the changes observed in *PER1* expression upon decidualization, with a reciprocal up-regulation confirmed by qRT-PCR and western blot analysis. However, this induction in *PER1* mRNA was enhanced upon *PER2* knockdown as compared to decidualization. Therefore, although *PER2* knockdown resulted in recapitulation of some decidual changes in core clock component expression, it did not result in a complete reproduction of the phenotype. This suggests that multiple clock regulators are modulated in response to HESC

decidualization. Additionally, due to the highly redundant nature of the circadian system, perturbations in one gene are likely to cause alterations in other core genes.

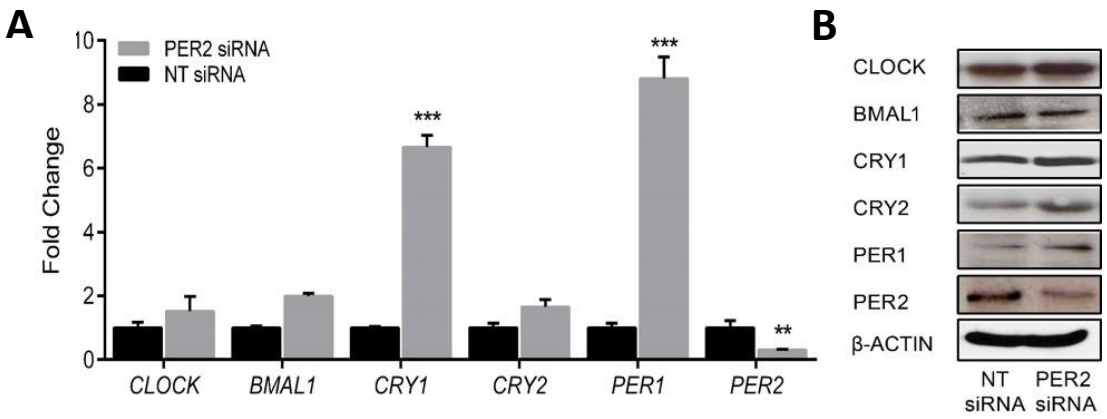

Figure 3.11 ***siRNA mediated knockdown of* PER2 *is associated with compensatory modifications in other core clock genes*** (a) Core clock gene expression in primary HESC cultures transfected with NT or *PER2* siRNA for 48 hours and analysed by qRT-PCR. (b) Western blot analysis of total cell lysates of primary HESC cultures transfected as indicated for 48 hours. ** P<0.01; ***P<0.001. Data are presented as mean fold change ± S.E.M.

3.2.10 *PER2* Knockdown Silences Circadian Oscillations and Disrupts HESC Decidualization.

Next, I investigated if *PER2* knockdown in undifferentiated HESCs would suffice to disturb circadian rhythm generation and phenocopy the silencing of core clock oscillations observed upon decidualization. To do this, three independent paired primary cultures were transfected with either NT or *PER2* siRNA and synchronized as previously described with a dexamethasone pulse. Following 12 hours post glucocorticoid shock, total RNA was harvested at 4 hour intervals over a 28 hour period. Cells transfected with NT siRNA demonstrated robust circadian oscillations in the 6 core clock genes, with normal anti-phase observed between *BMAL1* and *PER2* transcript profiles (Figure 3.12). In HESCs transfected with *PER2* siRNA, gene expression in core clock components was uniformly non-oscillatory. This indicates that the down-regulation of *PER2* observed during HESC differentiation is both necessary and sufficient to cause the loss of autonomous circadian rhythms in decidual cells.

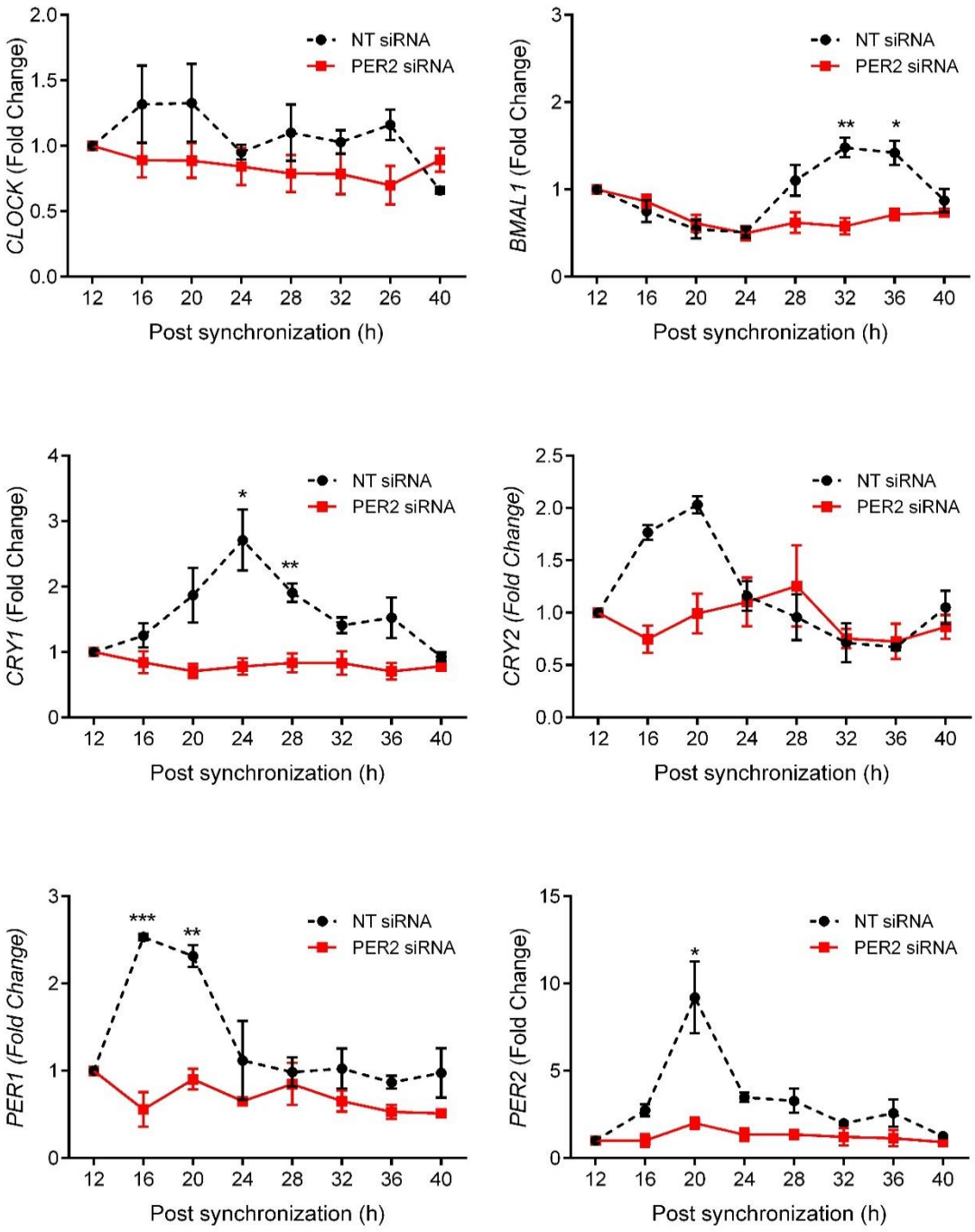

Figure 3.12 ***Knockdown of* PER2** ***expression is sufficient to cause the loss of oscillatory expression in core clock genes.*** mRNA transcript expression of *CLOCK, BMAL1, CRY1, CRY2, PER1* and *PER2* in undifferentiated HESCs transfected with NT siRNA or *PER2* siRNA for 48 hours. Cultures were synchronized with 100nM dexamethasone for 30 minutes. mRNA was harvested at indicated time points. qRT-PCR was utilised for transcript expression analysis. *P<0.05; ** P<0.01; ***P<0.001. Data are presented as mean fold change ± S.E.M.

Next, it was therefore hypothesized that *PER2* down-regulation may sensitize HESCs to differentiation signals. In order to investigate this, HESCs were transfected with either NT or *PER2* siRNA and subsequently decidualized for 2 days. Expression of four cardinal decidual markers (*PRL*, *IGFBP1, WNT4* and *11HSD*) were quantified using qRT-PCR. Surprisingly, instead of the hypothesized sensitization, *PER2* knockdown severely attenuated the induction of these genes. *PRL* induction was suppressed by 63%, *IGFBP1* by 82%, *WNT4* by 52% (non-significant) and *11HSD* by 78% (Figure 3.13). This indicates that although PER2 down-regulation is a striking feature of decidual cells, this core clock protein is somehow critically required for the initial responsiveness of HESCs to deciduogenic cues.

In order to examine the role of *PER2* during the initial decidualization of HESCs, investigations were undertaken into the earlier kinetics of this core clock gene after deciduogenic treatment. The previous data has shown that *PER2* gene expression is already suppressed by 82% by day 2 of a decidual time-course. HESCs were therefore subjected to 8-br-cAMP and MPA for 6, 12, 24 or 48 hours, or left untreated. Expression of *PER2* was shown to be biphasic in its response. Transcript levels transiently increased at early stages of decidualization, with levels peaking at 12 hours. This was followed by a sharp drop at 24 hours which was maintained at 48 hours. It is well established that induction of *PRL* expression upon decidualization is also biphasic. It is characterized by an initial cAMP dependent, rapid but modest response, followed by an accelerated rise in promoter activity after 12 hours of stimulation. Quantification by qRT-PCR revealed *PRL* and *IGFBP1* were induced as anticipated: a modest increase in expression during the first 12 hours of stimulation (in concert with increased *PER2* expression), and a further rapid increase in expression after 24 hours (in concert with falling *PER2* transcript levels). From figure 3.14 it can be seen there is an intriguing partial inverse correlation between expression of *PER2* and these key decidual marker genes.

To investigate further the consequences of *PER2* knockdown on the activation of decidualization, previous knockdown assays were repeated at 12 and 24 hours. Briefly, three independent HESC cultures were transfected with NT or *PER2* siRNA and then treated with decidualizing stimuli for 12 or 24 hours. RT-PCR confirmed a 74% and 76% reduction in *PER2* expression at 12 and 24 hours respectively. Interestingly, *PER2* knockdown had no significant impact on expression of *PRL* or *IGFBP1* transcripts in the first 12 hours of decidualization. However, knockdown did inhibit the accelerated induction of these decidual markers as measured at 24 hours, thereby halting functional decidualization. This is suggests that *PER2* may act as a precise timing mechanism during the initiation of HESC differentiation (Figure 3.15).

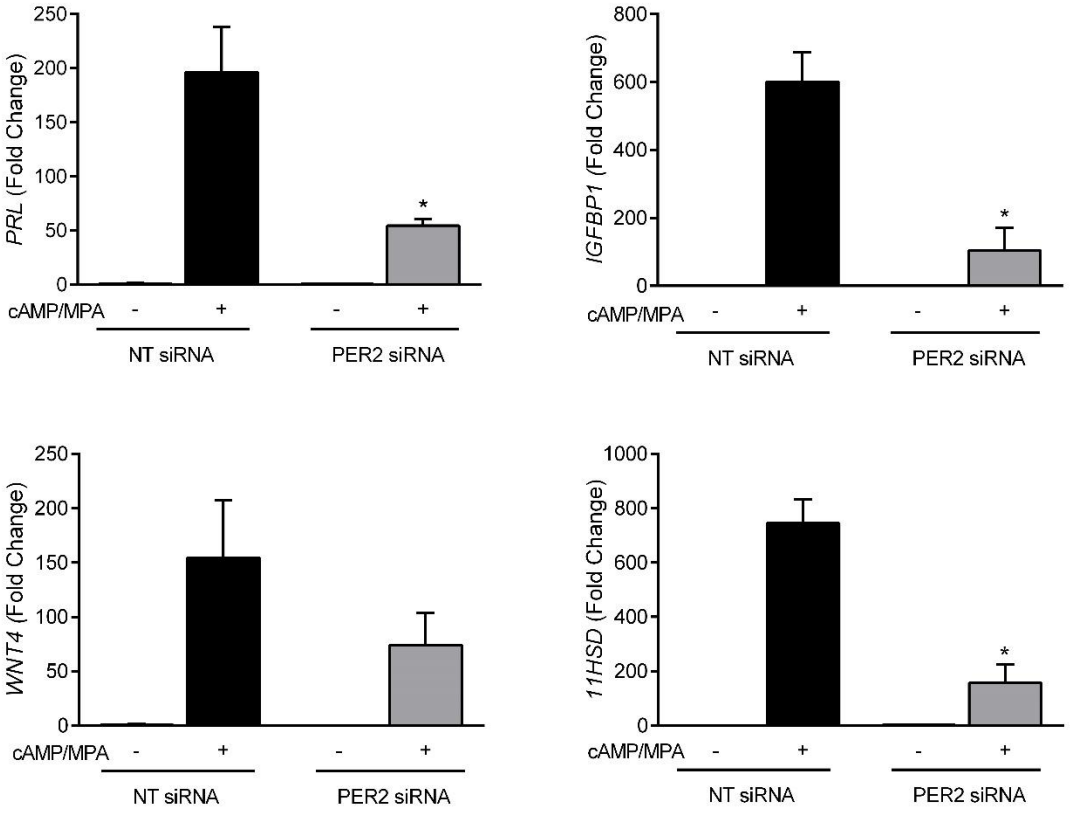

Figure 3.13 ***Expression of*** **PER2** ***is vital for functional decidualization of HESCs*****.** Transcript expression of key decidualization markers *PRL, IGFBP1*, *WNT4* and *11HSD* in primary HESCs transfected with NT siRNA or *PER2* siRNA. HESCs were subsequently undifferentiated or decidualized for 2 days with 8-br-cAMP and MPA. Expression was normalised to the undifferentiated control within the group. *P<0.05. Data are presented as mean fold change ± S.E.M.

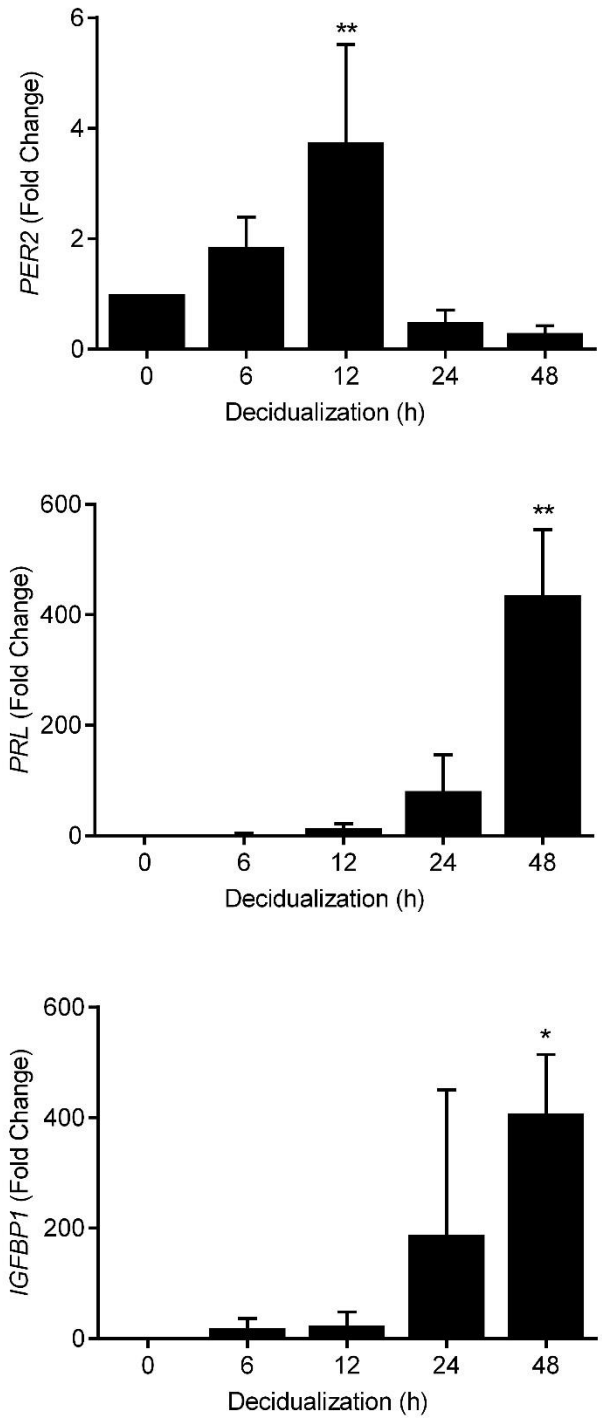

Figure 3.14 ***Early decidual kinetics of*** **PER2** ***and key decidual marker genes.*** The gene expression kinetics of *PER2* and the decidual marker genes *PRL* and *IGFBP1* in primary HESCs decidualized for 6, 12, 24 or 48 hours. Transcript levels were normalised to that of undifferentiated cells (0 hour). *P<0.05; **P<0.01. Data represent fold change ± S.E.M.

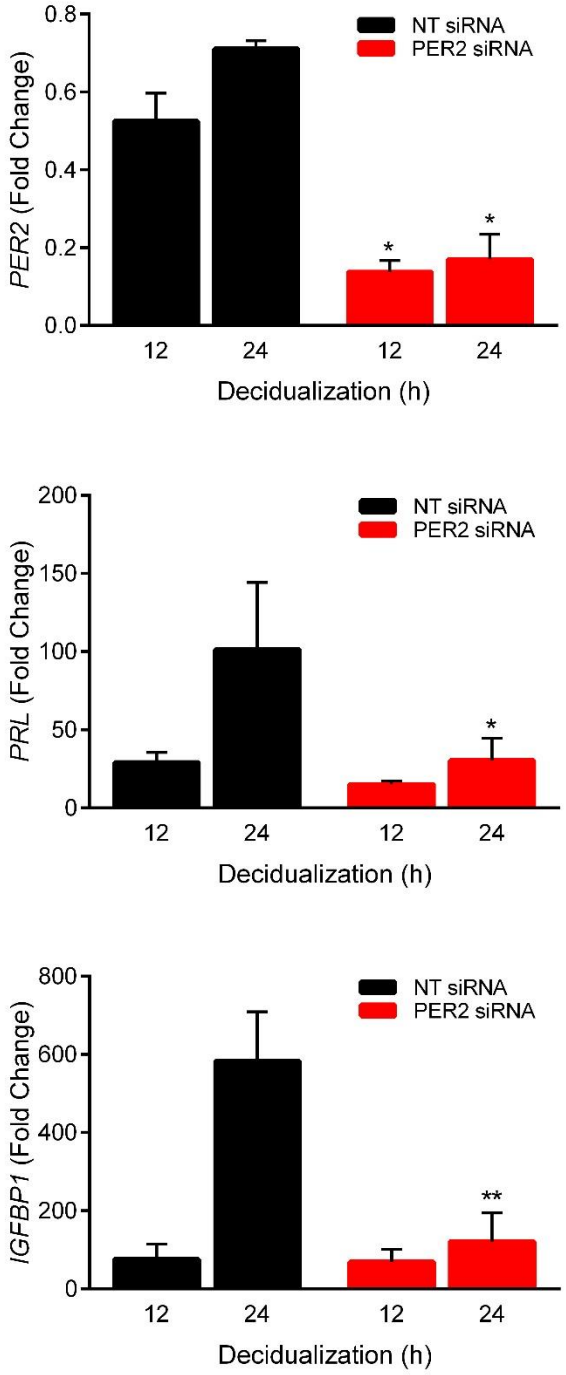

Figure 3.15 ***Timed*** **PER2** ***regulation is critical for induction of decidualization.*** Primary HESCs from three independent cultures were transfected with NT or *PER2* siRNA. 48 hours post transfection, cultures were treated with 8-br-cAMP and MPA for 12 or 24 hours. Transcript levels of *PER2* and the decidual marker genes *PRL* and *IGFBP1* were assessed by qRT-PCR. Transcript levels were normalised to those of undifferentiated cells.. *P<0.05; **P<0.01. Data represent mean fold change ± S.E.M.

3.2.11 Premature *PER2* Down-regulation Deregulates Decidualization.

To further this hypothesis, I established paired NT and *PER2* knockdown cultures from three mid-luteal biopsies, and then decidualized the cells for 24 hours. Transcriptomes were profiled by RNA sequencing. On average, 25 million single end reads were sequenced per sample. Of 19,721 expressed genes, 1,202 and 2,398 were identified as significantly different between NT and *PER2* knockdown cultures by edgeR and DESeq differential expression analyses, respectively. Combining these analyses, we identified a robust list of 1121 differentially expressed genes detected by both methods. 572 (51%) of which were up-regulated (≥ 2 fold induction) and 549 (49%) down-regulated (≥ 2 fold repression). Lists of differentially expressed genes can be found in Appendix 3 and 4 (up- and down-regulated respectively). To assess further the relatedness of the cultures, we calculated z scores of the transcripts-per-million values for the differentially expressed genes and depicted as a heat map (Figure 3.16a)

The most up-regulated genes encoded for secretogranin II (SCG2), a peptide hormone packaging gene (40-fold induction); brain and reproductive organ expressed anti-sense I (*BRE-AS1*), a novel long non-coding RNA antisense to BRE (a known component of the DNA damage response complex) (33-fold induction); and solute carrier family 6 member 12 (SLC6A13), a sodium dependent GABA transporter (28-fold induction). The most down-regulated genes were ATPase calcium transporting plasma membrane 3 (ATP2B3), a critical component in intracellular calcium homeostasis (10-fold repression); insulin receptor-related receptor (INSRR), an AKT activating pH sensing receptor (7-fold repression); and claudin 20 (CLDN20), a cell adhesion gene involved in tight junction strands (7-fold repression).

Amongst the list of down-regulated genes upon *PER2* siRNA mediated knockdown were *PRL* and *IGFBP1,* confirming qRT-PCR results. However, *PER2* knockdown actually upregulated various other decidual genes. These included key transcription factors such as *CREM*, *CEBPβ*, *CEBPα*, and *NURR1*, kinases and phosphatases including *SGK1* and *MKP1*, the cell surface receptor for IL33 (*IL1RL1*, also known as *ST2*), and *BMP2*, a key decidual morphogen. Strikingly, also observed were the induction of several genes coding metabolic regulators, including peroxisome proliferator-activated receptor *γ* (*PPARG*) and PPARG coactivator 1-*α*, following *PER2* inhibition were also observed. Taken together, these results suggest that rather than preventing or halting differentiation, premature loss of *PER2* expression predisposes HESCs to a disordered decidual phenotype.

Gene Ontology (GO) enrichment analysis was applied to the list of up- and down-regulated genes to discover which biological processes associated with the differentially expressed genes were over-represented. The top 15 processes are shown in the pie chart in Figure 3.16b. Signal transduction, anatomical development and metabolic process were the most over-represented biological functions upon *PER2* siRNA mediated knockdown at 24 hours decidualization. Cell differentiation, apoptosis, cell cycle and cell proliferation were all also prominently affected, indicative of a key role for *PER2* in cell fate decisions.

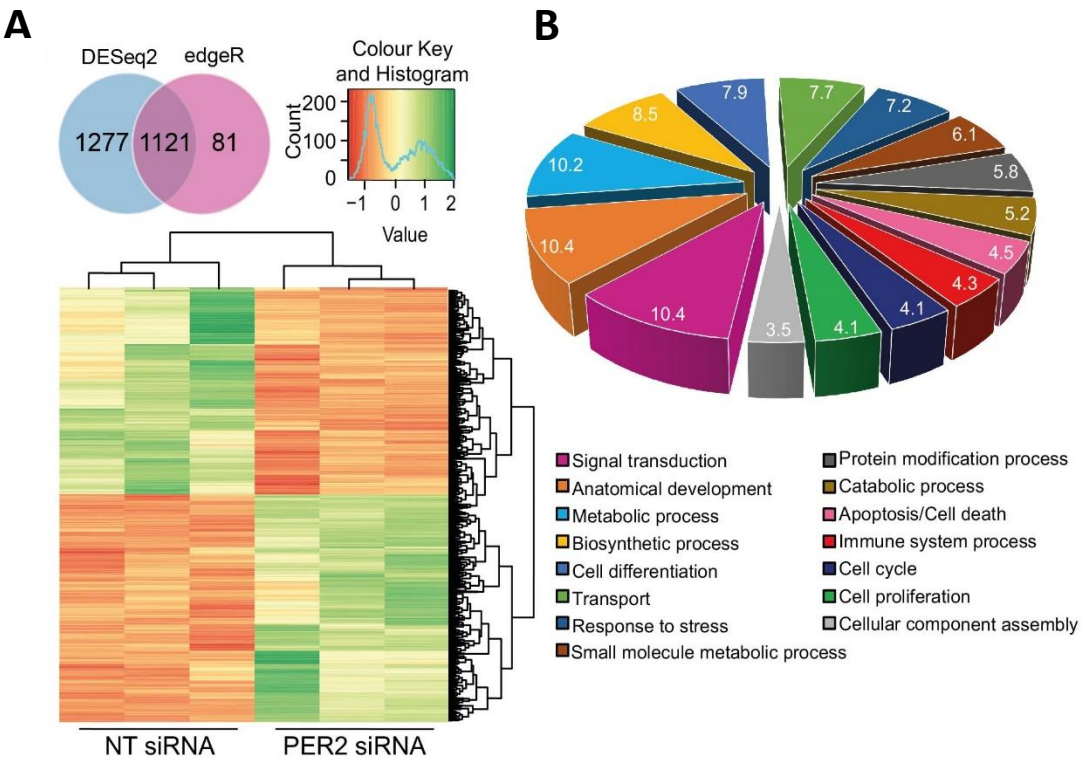

Figure 3.16 ***Premature loss of*** **PER2** ***mediated by siRNA results in a disordered decidual phenotype.*** Three paired independent biopsies were transfected with either NT or *PER2* siRNA and subsequently decidualized for 24 hours. Samples were subjected to Illumina HiSeq RNA-Sequencing analysis. (a) Venn diagram comparison of differentially expressed transcripts identified by DESeq2 and edgeR. Clustered heat map shows relatedness of top-ranked differentially expressed transcripts. (b) Pie chart representing the top 15 GO annotations of biological processes of the differentially expressed genes.

3.2.12 Loss of *PER2* Prevents HESC Clonal Expansion by Cell Cycle Arrest.

Gene ontology analysis revealed proliferation was significantly influenced by *PER2* loss. Previous studies have shown that prior to decidual transformation, HESCs undergo a round of cell division. Stromal cells have been observed to synthesize DNA preceding the development of uterine sensitivity to deciduogenic stimuli (Moulton & Koenig, 1983; Moulton & Koenig, 1984). It was therefore supposed that *PER2* expression may be required for this mitotic expansion. Transfected HESCs were consequently seeded in triplicate at low density (50 cells/cm^2) onto culture plates and cultured over a prolonged time, in order to permit colony formation. Results show that the ability of HESCs to form colonies was severely attenuated upon knockdown of *PER2* as compared to controls (colony area; 2% to 24% respectively, Figure 3.17). This suggests that premature *PER2* inhibition acts to deregulate decidual gene expression by interrupting the proliferative ability of HESCs prior to the onset of differentiation.

Similarly, gene ontology analysis also revealed ‘cell cycle’ as another biological process over represented upon *PER2* knockdown. To further elucidate the role of *PER2* within the cell cycle, HESCs were once again transfected with NT or *PER2* siRNA and then subjected to propidium iodide staining. This intercalating dye stains DNA quantitatively, and the fluorescent intensity emitted upon flow cytometric analysis at certain wavelengths corresponds to the amount of DNA contained within the nucleus. This can then be attributed to a particular stage of the cell cycle. This study critically revealed an accumulation of HESCs within the G2/M portion of the cell cycle upon *PER2* knockdown when compared to NT controls (22.1% and 8.8% respectively). This was correlated with a reduced proportion of cells in mitotic S phase (11.6% compared to 17.6%). Of note, the <2N, or apoptotic fraction was also

significantly smaller upon *PER2* knockdown (Figure 3.18a and b). This data demonstrates that the lack of mitotic proliferation observed upon *PER2* knockdown is, at least in part, due to imposition of a cell cycle block at the G2/M stage. This observation correlates well with the RNA sequencing data which revealed that 52 of the 73 cell cycle related genes disturbed upon *PER2* knockdown are involved in the G2/M checkpoint. For cell cycle genes differentially regulated upon *PER2* knockdown see Appendix 5.

To further confirm these results, real-time monitoring of cell proliferation over 100 hours using microelectronic sensor technology was utilised. 10,000 HESCs from three independent biopsies were plated in triplicate into 16 well E-plates containing interdigitized gold microelectrodes. Cells were grown until 80% confluent and then transfected within the E-plate with either NT or *PER2* siRNA. Mock transfected HESCs were used as growth controls and maintained in either 10% DCC-FBS supplemented media or 0% un-supplemented media. HESCs transfected with siRNA were maintained in 10% DCC-FBS. Adherence to the gold microelectrodes was recorded over the following 100 hours. The data confirmed that knockdown of *PER2* resulted in a significant growth inhibition of HESCs as analysed by ANOVA. (Figure 3.19) Transfection with NT siRNA additionally resulted in growth retardation when compared to mock transfected cells in 10% DCC-FBS media, although this can be attributed to the presence of transfected siRNA and off target effects.

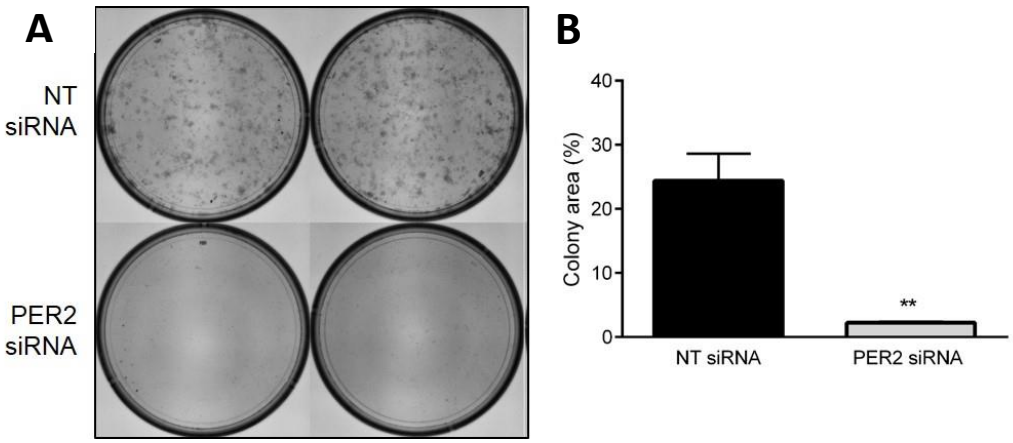

Figure 3.17 PER2 *knockdown prevents clonal expansion of HESCs.* (a) Haematoxylin stained representative colonies of 2 independent primary HESC cultures first transfected with NT or *PER2* siRNA. Cells were plated at low density to permit colony formation and terminated at 10 days. (b) Total colony area as quantified by ImageJ analysis. **P<0.01. Data represent mean ± S.E.M.

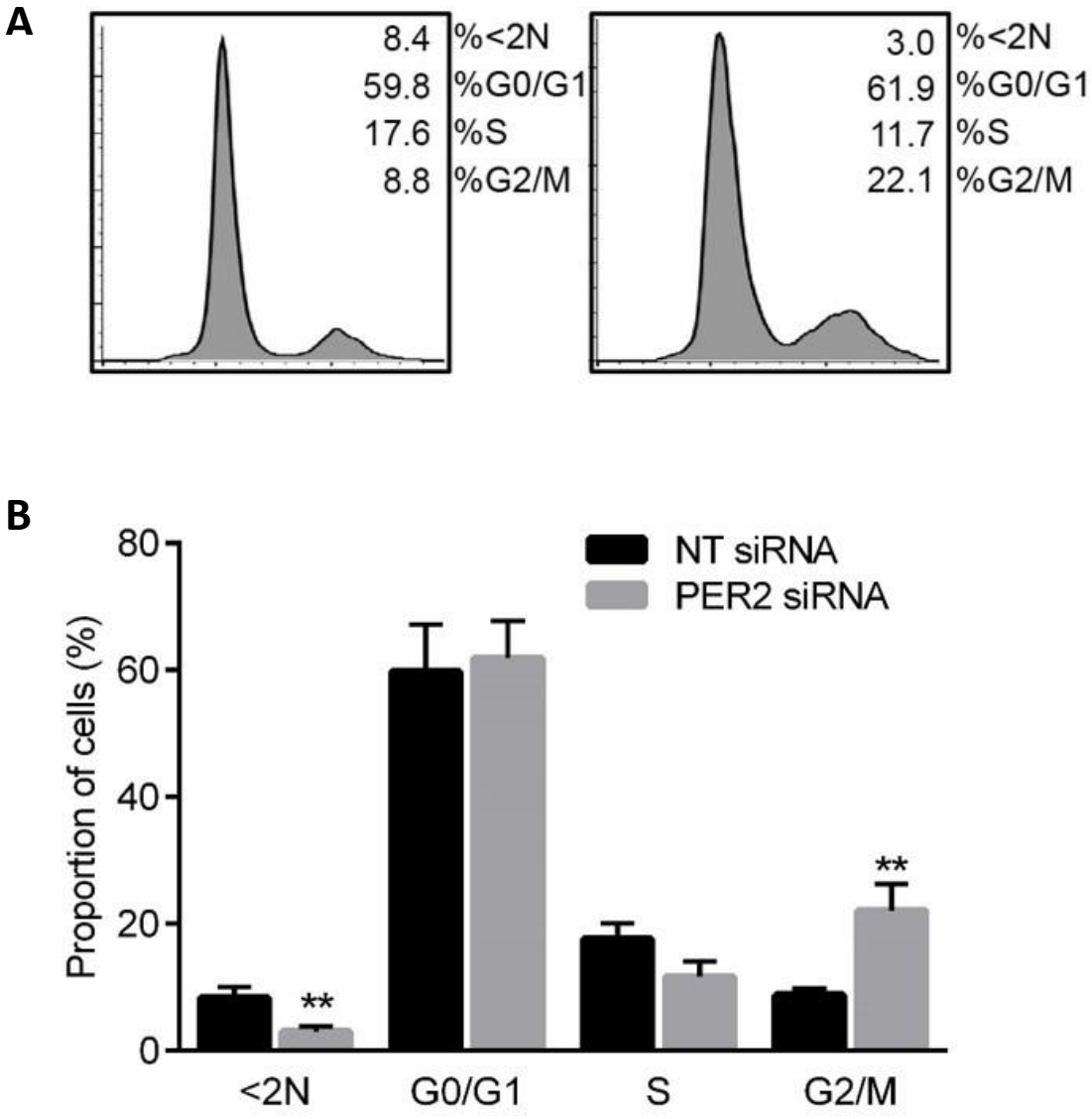

Figure 3.18 PER2 *knockdown induces a G2/M cell cycle block.* (a) Representative gated cell cycle histograms obtained 48 hours post transfection with NT or *PER2* siRNA in primary HESCs. Cell cycle distribution was assessed using the Watson model. (b) Graphical representation of cell cycle distribution from 3 independent HESC cultures transfected and treated as above. **P<0.01. Data represent mean ± S.E.M.

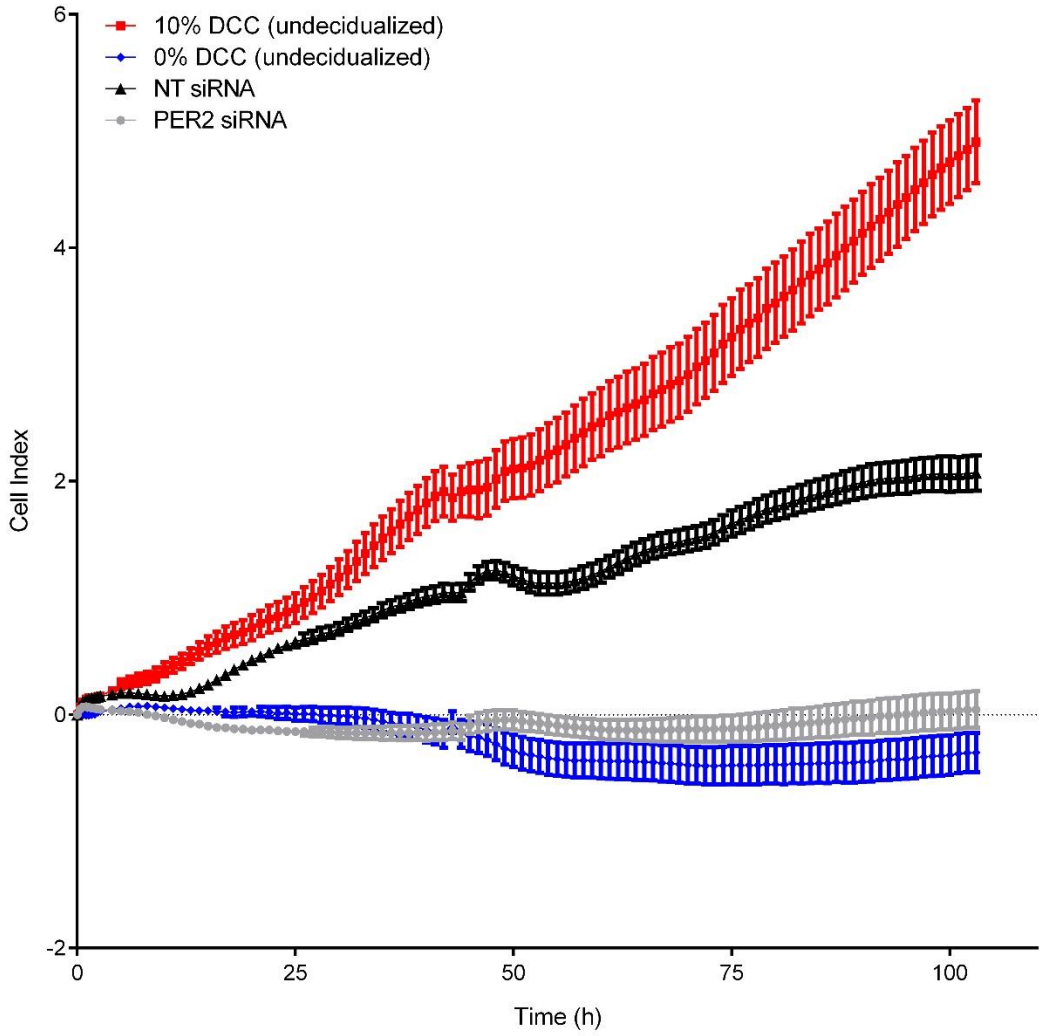

Figure 3.19 PER2 *loss prevents mitotic expansion of HESC cultures.* Real-time monitoring of cell growth and adherence as measured by electrical impedance using an xCelligence analyser. HESCs were seeded into 16 well plates and transfected within the plate with NT or *PER2* siRNA. Untransfected HESCs cultured in 10 or 0% DCC-FBS supplemented media were used as controls. Cell index measurements were captured over 100 hours.

3.2.13 Partial Rescue of Decidual Phenotype by Double Knockdown of *PER2* and *BRE-AS1*.

Results from RNA-seq data revealed that one of most upregulated genes upon *PER2* knockdown was for a long non-coding RNA called *BRE-AS1* (brain and reproductive organ expressed anti-sense 1). Expression was consistently up-regulated with a mean 33-fold increase upon *PER2* loss in HESCs decidualized for 24 hours. In order to confirm these results, primers were designed to specifically target *BRE-AS1*. Confirmation of primer specificity was confirmed using melt curve analysis and primer efficiency calculated as previously described (Figure 3.20a). Firstly I examined if *BRE-AS1* displayed rhythmic circadian oscillations. Results showed that variation in transcript expression over 28 hours was not sufficient to indicate circadian regulation. (Figure 3.20b).

In order to confirm the up-regulation in *BRE-AS1* upon *PER2* knockdown observed in RNA-seq, transcripts levels were measured in three independent cultures transfected with NT or *PER2* siRNA and subjected to deciduogenic stimuli for 48 hours. Whilst transcript levels were comparable in undifferentiated HESCs transfected with either NT or *PER2* siRNA, upon decidualization *BRE-AS1* expression was induced by 66-fold in *PER2* siRNA transfected cells, compared to only 15 fold in NT siRNA transfected HESCs (Figure 3.20c). Next, confluent HESCs were transfected with either NT, *PER2* or a combination of *PER2* and *BRE-AS1* siRNA. Transfected cells were then decidualized for 24 or 48 hours. Transfected undifferentiated cells were used as controls. To confirm knockdown, RNA was extracted and subjected to qRT-PCR analysis. *BRE-AS1* expression showed a small increase upon decidualization in NT HESCs (D4; 1.44 fold, D8; 2.23 fold). As expected, *PER2* knockdown resulted in increased expression of *BRE-AS1* both in undifferentiated HESCs and upon decidualization, although this increase was smaller than previously observed (D4;

12.85 fold, D8; 13.95 fold). Upon double knockdown, *BRE-AS1* expression was reduced to levels comparable with NT controls (Figure 3.20d). Furthermore, *PER2* knockdown was confirmed in samples transfected with both *PER2* siRNA and *PER2*/*BRE-AS1* siRNA (Figure 3.20e). As *BRE-AS1* is antisense to the gene BRE, this coding transcript was also quantified. Results demonstrated a small increase in BRE expression upon decidualization in both controls and cells transfected with *PER2* siRNA alone. Double knockdown resulted in a small but significant increase in BRE transcripts in the undifferentiated state (P=0.002), but no change was observed once HESCs were subjected to differentiation signals (Figure 3.20f).

As *BRE-AS1* was only upregulated upon *PER2* knockdown when cells were decidualized, it was hypothesized that it may play a role in the sensitization of HESCs to early deciduogenic stimuli. Experiments were designed to determine if appropriate decidual responses would return upon double knockdown of *PER2* and *BRE-AS1*. The same four key decidual markers were used, *PRL, IGFBP1, WNT4* and *11HSD*. Confirming previous results, single *PER2* knockdown severely attenuated the induction of these genes upon decidualization. PRL induction was suppressed by 35% and 69%, IGFBP1 by 75% and 81%, WNT4 by 37% and 43%, and 11HSD by 59% and 55% at 24 and 48 hours respectively, further confirming the critical requirement of *PER2* for normal decidual initiation (Figure 3.21). Interestingly, upon concurrent *PER2* and *BRE-AS1* knockdown, near complete phenotypic rescue was observed. No statistical significance was observed in any of the decidual markers genes between NT controls and double knockdowns. This suggests that *PER2* siRNA mediated increased expression in *BRE-AS1* is at least partially responsible for the disordered decidual phenotype observed.

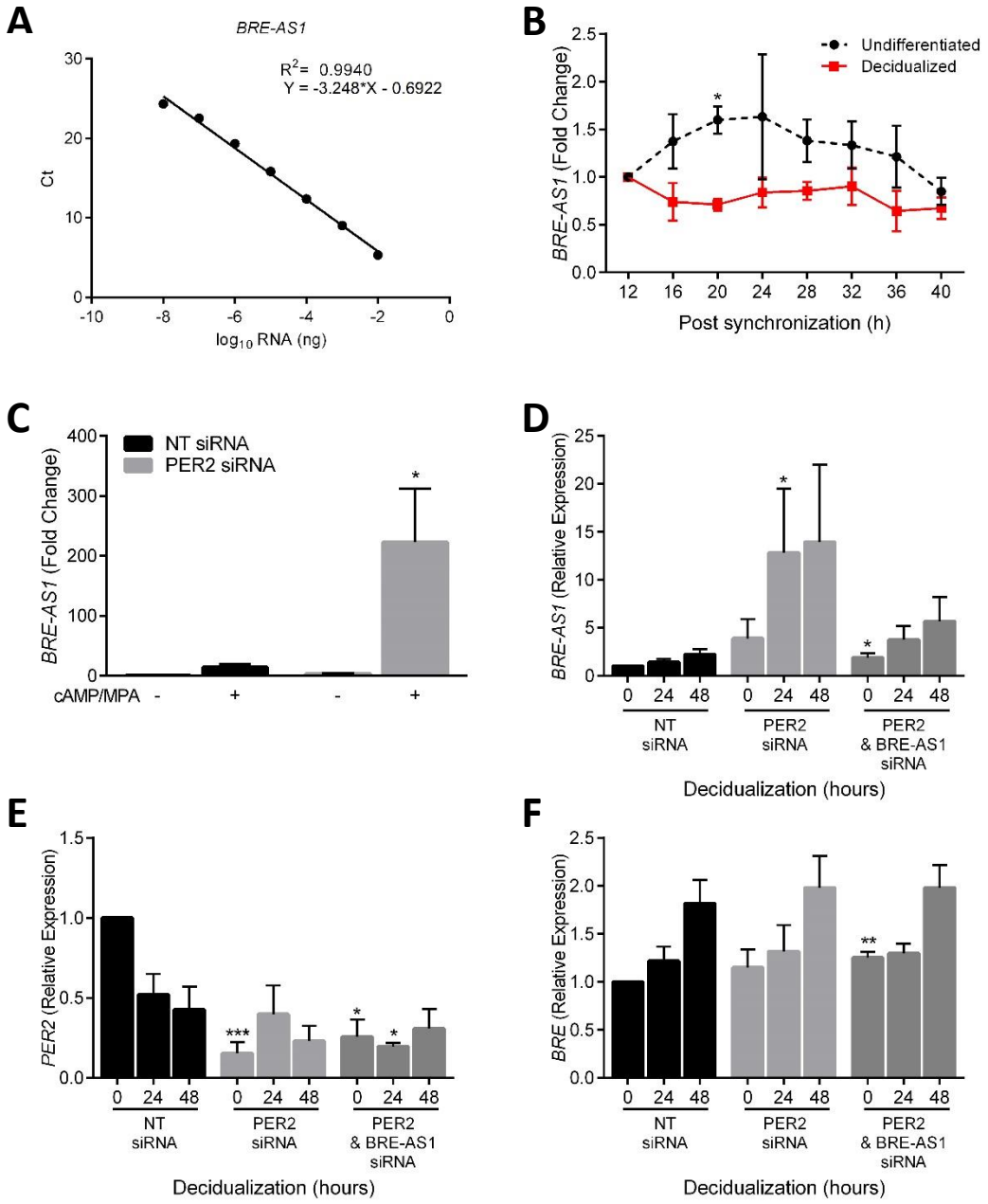

Figure 3.20 ***Expression of the long non-coding transcript*** **BRE-AS1.** (a) Optimization of *BRE-AS1* primers to determine primer efficiency for the long non-coding transcript. (b) Rhythmic assessment of mRNA transcript expression of *BRE-AS1* in synchronized undifferentiated or decidualized HESCs. (c) HESCs transfected as indicated were subjected to deciduogenic stimuli for 48 hours or left untreated. *BRE-AS1* transcript expression assessed by qRT-PCR. Transcript expression of (d) *BRE-AS1*, (e) *PER2* and (f) *BRE* in primary HESCs transfected with NT siRNA, *PER2* siRNA alone or *PER2* and *BRE-AS1* siRNA combined. HESCs were subsequently undifferentiated or decidualized for 24 or 48 hours with 8-br-cAMP and MPA. Expression was normalised to NT 0 hour *P<0.0; **P<0.01; ***P<0.001. Data are presented as means ± S.E.M

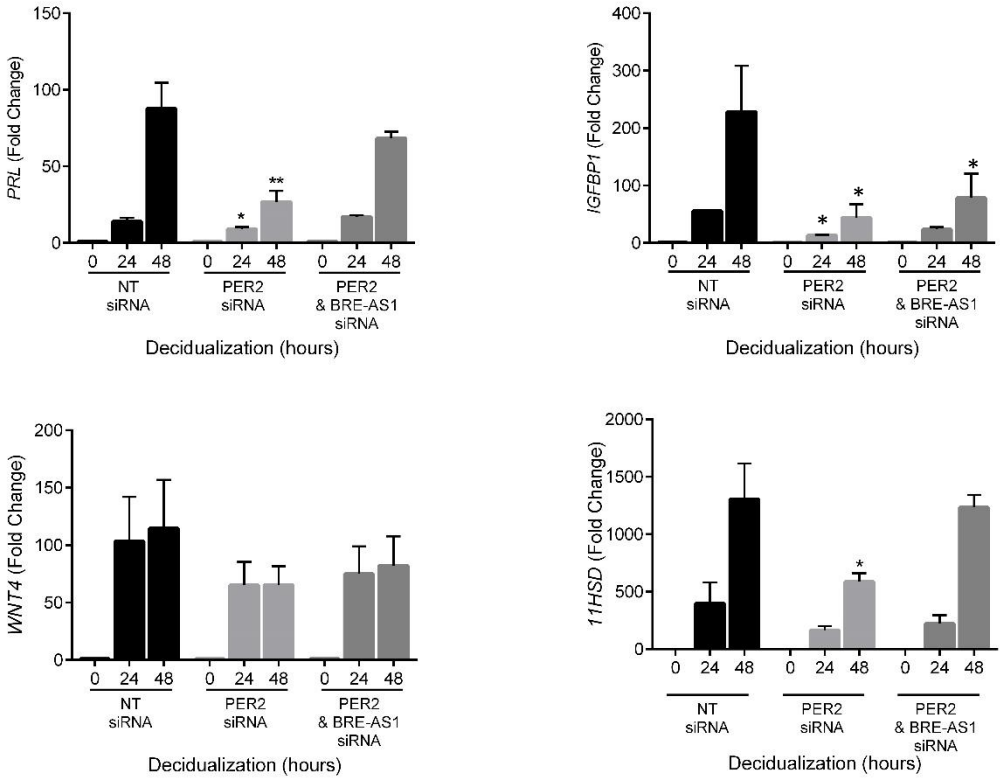

Figure 3.21 ***Partial rescue of functional decidualization following double knockdown of*** **PER2** ***and*** **BRE-AS1** Transcript expression of key decidualization markers *PRL, IGFBP1, WNT4* and *11HSD* in primary HESCs transfected with NT siRNA, *PER2* siRNA alone or *PER2* and *BRE-AS1* siRNA combined. HESCs were subsequently undifferentiated or decidualized for 24 or 48 hours with 8-br-cAMP and MPA. Expression was normalised to the undifferentiated control within the group. *P<0.0; **P<0.01. Data are presented as mean fold change ± S.E.M

3.2.14 Mid-luteal Endometrial *PER2* Expression in Recurrent Miscarriage.

Finally, I examined the expression levels of *PER2* transcripts in timed mid-luteal endometrial biopsies from 70 women with ovulatory cycles attending a dedicated miscarriage clinic. All of the patients examined suffered consecutive miscarriages, ranging between 2 and 11 pregnancy losses. Other patient demographics associated with miscarriage were also collected, including age, BMI, percentage of uterine natural killer cells (Kuroda *et al.*), and the day of cycle (post LH surge). Small tissue pieces were collected and stored in RNA later. RNA was subsequently extracted as previously described and *PER2* mRNA transcript levels quantified using qRT-PCR. Statistical analysis revealed none of the patient demographics correlated with *PER2* levels in a Gaussian distribution, therefore linear regression analysis was applied and statistical significance determined using Spearman's rank test. Within this cohort BMI (Spearman's rank test ρ=0.0107, P= 0.9315), uNK % (ρ=0.0624, P= 0.5998) and the day of cycle (ρ=-0.1879, P= 0.1165) showed no association with *PER2* transcript levels (Figure 3.22b-d). Patient age was inversely correlated with *PER2* expression (ρ=-0.2588, P= 0.0240), as was the number of previous pregnancy losses (ρ=0.3260, P=0.0046, [Figure 3.22a and e]). To investigate this further, biopsies from 5 control and 5 recurrent pregnancy loss patients were taken. Stromal cells were grown *in vitro* and decidualized for 2, 4 or 8 days, or remained undifferentiated. *PER2* transcript levels were assessed by qRT-PCR. As previously observed, *PER2* transcript levels were attenuated in all ten patients upon decidualization. Additionally, in accordance with the previous correlative data, *PER2* transcript levels were consistently lower in RPL patients compared to controls (Figure 3.22f). The disparity between the two cohorts increased over the differentiation time-course, reaching statistical significance at day 4 and day 8 (P=0.040 and P=0.024 respectively). See Appendix 6 for patient demographics.

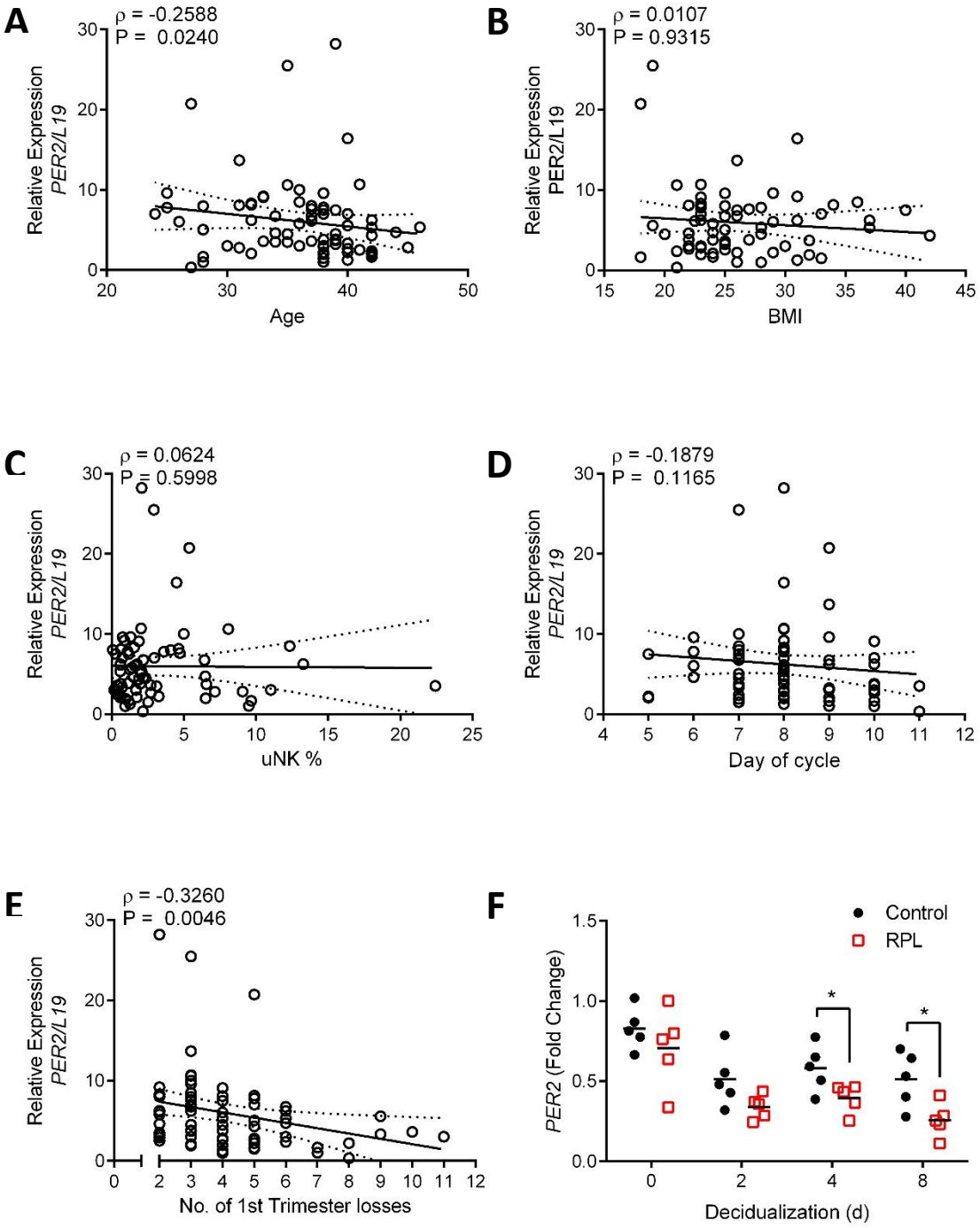

Figure 3.22 ***Timed mid-luteal endometrial expression of*** **PER2** ***in a recurrent miscarriage cohort.*** Endometrial *PER2* expression in a cohort of 70 recurrent miscarriage patients. Correlation between *PER2* expression in mid-luteal endometrial biopsies and (a) age, (b) BMI, (c) uterine NK cell percentage, (d) day of cycle (post LH surge) and (e) the number of previous pregnancy losses, using regression analysis. Dotted lines represent 95% confidence intervals. Spearman's ρ value and probability (P) shown. (f) *PER2* expression in primary HESC cultures from 5 control and 5 RPL patients decidualized with 8-br-cAMP and MPA for 2, 4 or 8 days, or left untreated. *P<0.05. Data presented as mean fold change.

3.3 Discussion

Circadian rhythms permeate a vast array of biological processes by permitting anticipation of environmental change (Ko & Takahashi, 2006). Decidualization is a spatiotemporally controlled event initiated during the mid-secretory phase of the menstrual cycle, preceded by proliferation in the superficial endometrial layer. Differentiating cells then pass though tightly defined phenotypic changes, which control endometrial receptivity, embryo selection and ultimately resolution via pregnancy or menstrual shedding (Gellersen & Brosens, 2014).

Successful implantation is dependent upon coordinated two-way communication between a competent embryo and a receptive endometrium. It is therefore not beyond speculation that circadian rhythms in the female reproductive system provide timing cues required for successful decidualization and successive implantation. It is shown in this chapter that core clock machinery is temporally regulated throughout the menstrual cycle. Additionally, human pre-implantation embryos do not express the majority of the core circadian genes, except for maternal transcripts which are degraded prior to implantation (Boden *et al.*, 2013b). Here, I demonstrate that rhythmic oscillations of the core clock machinery are halted (or potentially 'paused') upon decidualization of HESCs. One possible explanation of this phenomenon is to permit functional embryo-maternal synchronisation, thus allowing the maternal environment to dictate the daily clock, preventing out of phase oscillations between mother and foetus.

Evidently, although there is loss of overall circadian oscillations, both mRNA and protein of the core clock components are still expressed. This may suggest that the endometrium is poised, ready to resume circadian oscillations once the blastocyst has implanted. It is conceivable that the blastocyst may provide such an entraining

signal to the endometrium to resume 'in sync' rhythms. Unfortunately, data from day 12 decidual cells was inconsistent, likely due to prolonged serum starvation. Therefore, although it is known circadian rhythms are present in the endometrium at parturition, further work is required to establish when they are switched back on after decidualization associated silencing.

As a core circadian gene, *PER2* shows a high degree of temporal regulation in response to deciduogenic stimulants. The data provided here support previous studies in rats, where *PER2* down-regulation signals the transition from an oscillatory receptive endometrium to a non-oscillatory post receptive decidual endometrium (Uchikawa *et al.*, 2011). It is reported here that a similar expression profile is recapitulated in human cells, where declining *PER2* transcript levels signal the progression from mid- to late-secretory endometrium. Concordant *PER2* regulation between the two species is indicative of an evolutionary conserved mechanism. This is striking given the vast dissimilarities between human and rodent reproduction. Whilst both are mammals, rodent decidualization is initiated by the presence of an implanting embryo, whereas human decidualization is under maternal control and hence initiated each cycle, irrespective of the presence or absence of a conceptus.

In this study, dexamethasone was used as a synchronizing agent enabling measurement of rhythms within a culture of cells. As a glucocorticoid, dexamethasone binds to the glucocorticoid receptor (GR) which in turn activates genes with a glucocorticoid response elements (GREs) within their promoters. Multiple clock genes have been shown to contain GREs and be directly regulated by GR (So *et al.*, 2009). As decidualization is associated with a gradual decrease in GR expression and a concurrent increase in mineralocorticoid receptor (MR) expression (Kuroda *et al.*, 2012) it could be argued that the loss of rhythmicity observed upon decidualization is an artefact due to a decreased ability to be synchronized by dexamethasone.

However, as shown here, PER2 siRNA mediated knockdown in undifferentiated HESCs is sufficient to silence circadian oscillations, recapitulating conditions observed upon differentiation. Furthermore, the downstream effects mediated by PER2 knockdown including cell cycle arrest, provide a rational explanation for this observed loss of rhythmicity. Further work would be designed to include assessment of GR levels in the various conditions.

This study provides evidence that down-regulation of *PER2* is attributed to the full length 3768 base pair transcript and expression synergistically mediated by cAMP and progesterone. Previous reports indicate *PER2* is acutely responsive to hormonal signals that converge onto a cAMP-response element (CRE) in its promoter region (Koyanagi *et al.*, 2011; O'Neill *et al.*, 2008). Additionally, progesterone-response element (PRE) – half sites have been located upstream of the *PER2* transcriptional start site indicative of cis- acting regulation (Rubel *et al.*, 2012). These pathways provides a likely explanation for the initial transient rise in *PER2* transcript levels in differentiating HESCs. However, in this chapter data is provided to show that the loss of *PER2* expression in decidualizing HESCs coincided with specific attenuated CLOCK binding to the highly conserved non-canonical E2 enhancer element in the *PER2* promoter. The data further shows that this attenuation could not be accounted for by a general reduction in the DNA binding activity of the CLOCK:BMAL1 heterodimer as demonstrated by constitutive binding to the *PER1* E5 E-box. It has previously been suggested that binding of p53 to a response element found in the promoter region of *PER2* which overlaps the E2 enhancer, prevents heterodimer binding, leading to repression of *PER2* expression (Sun *et al.*, 2010). Further work is required to determine if this phenomenon is occurring during decidualization.

Furthermore, due to the high level of redundant and compensatory mechanisms within the circadian machinery (Erzberger *et al.*, 2013; Reppert & Weaver, 2002), it

was suspected that decidual associated repression of *PER2* alone would not be adequate to cause the overall cessation of rhythms during decidualization. However, data shown in this chapter shows that siRNA mediated *PER2* repression is sufficient to cause loss of circadian oscillations in the core clock machinery. *PER2* knockdown in undifferentiated HESCs results in a complete aperiodic expression profile reminiscent of a decidual circadian phenotype.

The data here shows that regulation of *PER2* expression occurs within a precise timeframe. Loss of expression observed 2 days after treatment with deciduogenic stimuli is preceded by a transient increase in expression between 6-12 hours post treatment. This corresponds to the known induction of *PRL*; whilst a weak induction up to 12 hours is dependent upon a non-palindromic cAMP response element (CRE), a much more intense induction is observed from 24 hours via an enhancer region. Thus, initially the data suggested that *PER2* acts as a major repressor of decidual gene expression; therefore, it was hypothesised that knockdown may act to sensitise HESCs to deciduogenic signals. However, paradoxically siRNA knockdown demonstrated that this core clock protein is critically required for successful HESC differentiation as measured by transcript expression of *PRL, IGFBP1, WNT4* and *11HSD*, four key decidual marker genes. Further analysis via RNA-sequencing indicated that rather than preventing differentiation, *PER2* knockdown actually results in a wholly disordered decidual response.

Moreover, data provided here goes some way to explain this chaotic differentiation observed upon *PER2* knockdown. Several lines of evidence show that HESCs undergo an obligatory round of mitotic proliferation prior to decidualization (Wang *et al.*, 2010a). This study demonstrates *PER2* is functionally required for this event. Knockdown resulted in a complete failure of HESCs to form colonies, growth retardation and imposition of a G2/M cell cycle block. These results are contrary to

the widely regarded nature of *PER2* as a tumour suppressor (Fu *et al.*, 2002; Sun *et al.*, 2010; Thoennissen *et al.*, 2012). In leukaemia cell lines, *PER2* overexpression induces growth arrest in G2/M by inhibition of c-MYC and cyclin B1 and upregulation of p53 (Sun *et al.*, 2010). The ability of *PER2* to promote or inhibit cell cycle progression therefore seems to be tissue or cell type specific.

Additionally, in this chapter I demonstrate that the aberrant decidual phenotype observed upon premature *PER2* loss by siRNA is at least partially rescued by co-knockdown of *BRE-AS1*. This is a poorly characterised long non-coding RNA, antisense to *BRE*, both of which are located on overlapping regions of chromosome 2. *BRE-AS1* was demonstrated to be amongst the most induced transcripts upon *PER2* knockdown. Findings of up-regulation during the late secretory phase of the menstrual cycle suggest that this long non-coding RNA may play an important role during HESC decidualization. Concurrent siRNA mediated knockdown of *PER2* with *BRE-AS1* acts to rescue induction of key decidual marker genes. Further research is required to determine if double knockdown is also able to rescue other *PER2* knockdown mediated phenotypes, including the G2/M cell cycle block. However, this preliminary data suggests that long non-coding RNAs may be unknown key regulators of human decidualization.

Finally, the finding that *PER2* transcript levels inversely correlate with age lends credence to previous studies reporting age related decline in circadian output (Jud *et al.*, 2009; Nakamura *et al.*, 2011). It is feasible that low *PER2* expression in the mid-luteal phase of the cycle may contribute to an accelerated ageing phenotype as observed upon mutation in mice, resulting in poor reproductive fitness (Pilorz & Steinlechner, 2008). Critically, the observation of a significant inverse correlation between mid-luteal *PER2* transcript levels and the number of previous miscarriages strongly implicate that deregulation of this core clock gene increases the likelihood of

persistent miscarriages. These findings were further supported with data showing reduced *PER2* expression in cultured HESCs from RPL patients upon decidualization. Taken together, these observations demonstrate that disruption of circadian clock output predisposes for reproductive failure.

Chapter 4

PRIP-1 acts as a Molecular Switch Promoting HESC Survival via Regulation of the AKT Pathway.

4.1 Introduction

During decidualization the endometrial stromal compartment is extensively remodelled in order to establish maternal immunological tolerance to foetal antigens, ensure tissue integrity during trophoblast invasion, and, significantly, to actively encapsulate the implanting conceptus (Brosens & Gellersen, 2010; Hanna *et al.*, 2006; Trowsdale & Betz, 2006). In order to protect the blastocyst from environmental insults, decidualization acts to uncouple the stroma from the environmental stressors. For example, stress-induced signalling through JNK and p38 pathways are selectively inactivated upon differentiation when potentially harmful concentrations of reactive oxygen species (ROS) are present (Leitao *et al.*, 2010). Moreover, as shown, circadian oscillations within the endometrium are firmly disabled upon decidualization, further isolating the decidua from the peripheral environment (Muter *et al.*, 2015).

An interesting observation obtained from the *PER2* knockdown sequencing data was the emergence of *PRIP-1* [Phospholipase C (PLC)-Related, but catalytically Inactive Protein-1], also known as *PLCL1,* amongst down-regulated genes. As such, *PRIP-1* expression is *PER2* dependent. *PRIP-1* has previously been implicated in a reproductive deficient phenotype in mice via its control of gonadotrophin secretion (Matsuda *et al.*, 2009), as well as being found to be a P4 responsive gene in the human myometrium (Chan *et al.*, 2014).

Two non-catalytic phospholipase C-like enzymes (PRIP-1/2) have been identified with structural homology to the phospholipase C protein family (Matsuda *et al.*, 1998; Uji *et al.*, 2002). Structural organisation closely mirrors PLC-enzymes and contains a pleckstrin homology (PH) domain allowing it to bind inositol 4,5 bisphosphate (IP_3) and other phosphoinositides. Further similarities include the presence of EF hands, catalytic X and Y domains and a C2 domain. (Figure 4.1) However, 2 key amino-acid

mutations within the catalytic domain abolish enzymatic activity and thus the catalysis of phosphatidylinositol 4,5-bisphosphate (PIP_2) to IP_3 and DAG is abated, as is the subsequent ability of IP_3 to release Ca^{2+} from endoplasmic reticulum (Murakami *et al.*, 2006). Interestingly, both overexpression and knockdown of *PRIP-1* have been shown to reduce IP_3 mediated Ca^{2+} release, indicative of a requirement for precise expression of *PRIP-1* for functional IP_3/Ca^{2+} signalling (Harada *et al.*, 2005) (Figure 4.1). Further studies have identified *PRIP-1* as a novel protein scaffold with the ability to bind and regulate key protein phosphatases 1 and 2A (PP1 and PP2A) as well as the serine/threonine kinase Akt (Fujii *et al.*, 2010; Sugiyama *et al.*, 2013). Through this phospho-regulatory function, PRIP-1 has been shown to modulate γ-aminobutyric acid type A ($GABA_A$) receptor function and trafficking (Kanematsu *et al.*, 2007; Terunuma *et al.*, 2004), as well as SNAP-25-phosphoregulated exocytosis (Zhang *et al.*, 2013). As mentioned, gene deletions in mice have highlighted the importance of both PRIP-1 and 2 in reproduction. Double *Prip-1* and *Prip-2* knockout mice display reduced litter sizes and exhibit prolonged intervals between litters. Furthermore, mutant female mice demonstrated smaller uteri at puberty, increased time spent in oestrous, and higher serum LH concentrations - attributed to increased gonadotrophin secretion (Matsuda *et al.*, 2009) . These findings suggest that PRIP proteins are essential for optimal regulation of the HPG axis in female mice.

This chapter investigates the role and regulation of *PRIP-1* during decidual transformation of HESCs. Here I report that endometrial expression of PRIP-1 is induced and maintained by progesterone signalling and contributes to decidual cell survival via the Akt pathway. Furthermore, I show PRIP-1 is a chelator of IP_3 signalling within the decidua, positioning it as a central mediator of multiple signalling pathways ensuring cellular homeostasis under adverse environmental conditions.

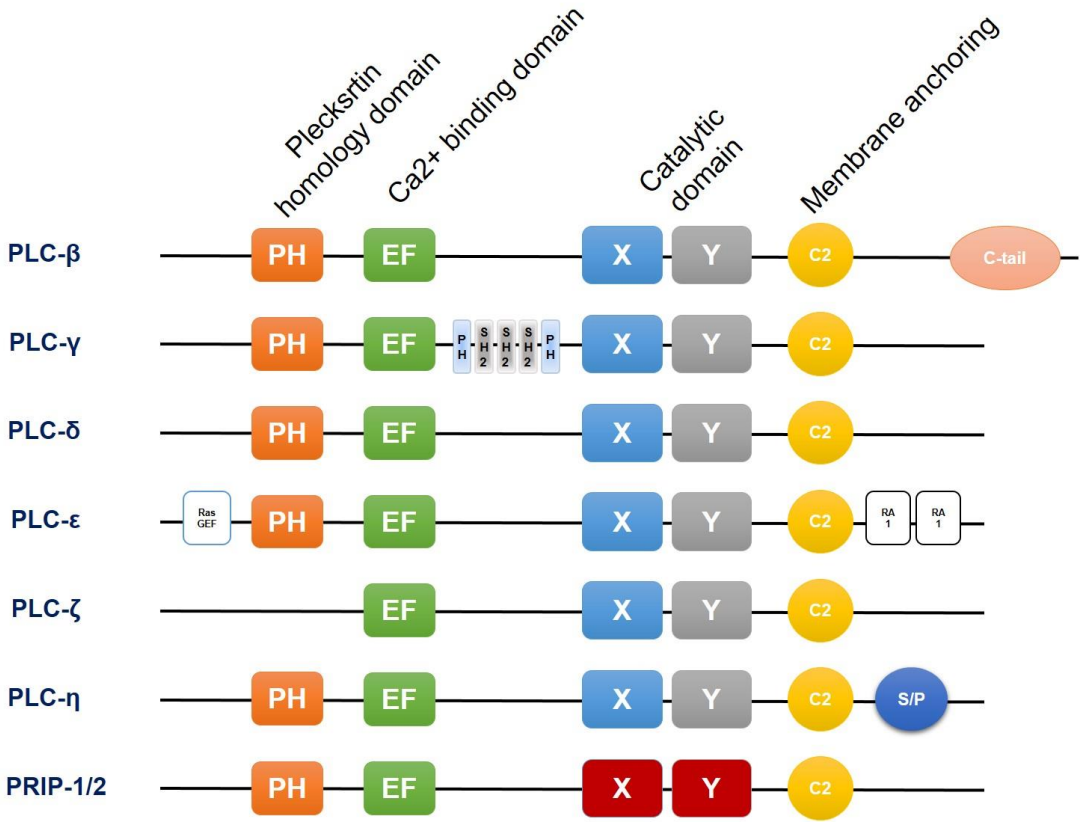

Figure 4.1 ***Structure of the Phospholipase C family of proteins.*** Schematic representation of structural motifs in phospholipase C family of proteins and PRIP-1/2. Note the mutations in the catalytic domain of PRIP-1/2.

4.2 Results

4.2.1 Endometrial *PRIP-1* Expression is Strongly Correlated with *PER2* Expression.

RNA-seq data from *PER2* knockdown revealed a 59% reduction of *PRIP-1* transcript levels. In order to elucidate the relationship between the two genes, expression was measured in a cohort of 101 mid-luteal endometrial biopsies. Regression analysis showed expression of *PRIP-1* and *PER2* exhibited a robust positive correlation. [P=<0.0001] (Figure 4.2a). I therefore hypothesised that *PRIP-1* may be a putative clock controlled gene (CCG). To test this, *PRIP-1* mRNA expression was measured over a circadian period of 28 hours. Three independent undifferentiated primary HESC cultures were synchronized using a dexamethasone pulse and RNA harvested over a 28 hour period. As previously described, *PER2* expression is robustly rhythmic, whereas *PRIP-1* oscillations are weak. However as shown in Figure 4.2b, both *PER2* and *PRIP-1* oscillate within the same phase with peak gene expression 16-20 hours post-synchronization.

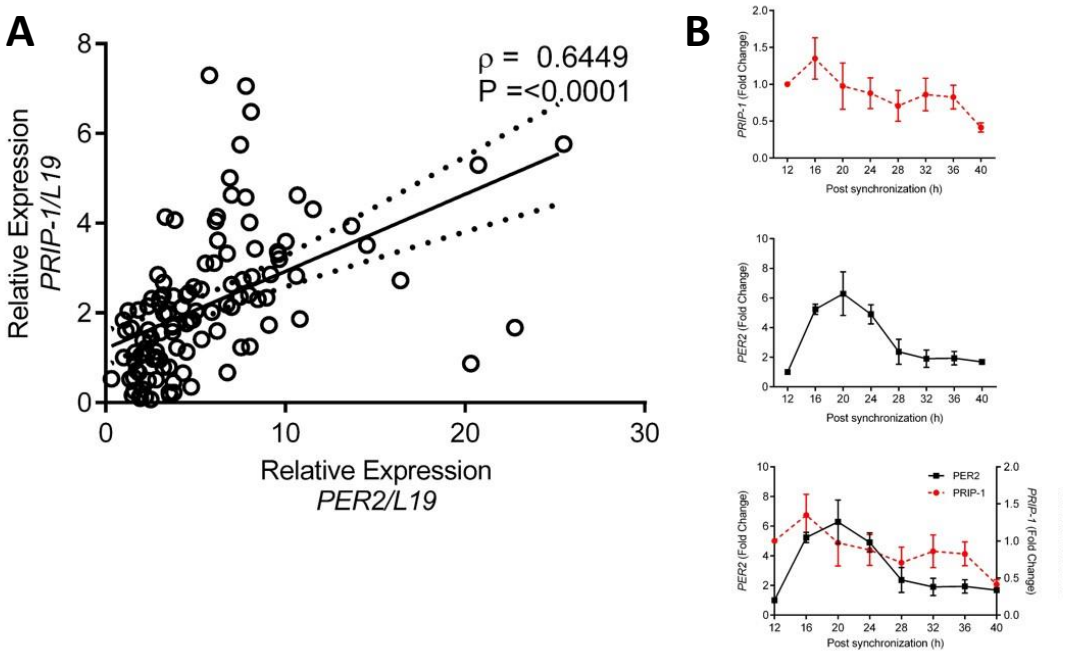

Figure 4.2 ***Endometrial*** **PRIP-1** ***expression strongly correlates with*** **PER2** ***expression in mid-luteal samples.*** (a) Spearman's rank correlation of *PRIP-1* and *PER2* mRNA transcripts in timed endometrial biopsies. Spearman's ρ value and probability (P) shown. (b) Triplicate cultures of primary undifferentiated HESCs were synchronized with dexamethasone for 30 minutes, mRNA collected at indicated time points and transcript expression of *PRIP-1* and *PER2* analysed using qRT-PCR. Overlay shows fold change in gene expression of the two transcripts. Data are presented as mean fold change ± S.E.M.

4.2.2 *PRIP-1* is Up-regulated upon Decidualization by P4.

To provide insight into the regulation of *PRIP-1* within the human endometrium, transcript levels were measured in undifferentiated HESCs and cells decidualized first for either 2, 4, or 8 days. Notably, decidualization elicited an up-regulation in *PRIP-1* mRNA, with transcript levels rising >30 fold by day 2, and this was maintained throughout the 8 day decidual time-course (Figure 4.3a). Western blot analysis confirmed the increase in PRIP-1 during decidualization. However, it also revealed a lag in the induction of protein when compared to mRNA (Figure 4.3b). PRIP-1 protein gradually accumulated in HESCs over the course of decidualization, with maximal expression apparent at day 8. In order to understand the mechanism involved in *PRIP-1* up-regulation, primary HESCs were treated with either 8-br-cAMP, MPA or in combination. Treatment with a cAMP analogue resulted in weak induction of *PRIP-1* transcripts. In contrast, MPA treatment in 3 biological repeat experiments resulted in an induction >24-fold. Combined treatment resulted in an up-regulation of *PRIP-1* mRNA nearly identical to that of MPA alone, indicating a critical dependence upon progesterone signalling (Figure 4.3c). Conversely, protein expression demonstrated a disparate synergistic response. Whilst treatment with 8-br-cAMP only resulted in a slight up-regulation of PRIP-1 protein, combined treatment elicited a greater induction of PRIP-1 than that of MPA alone (Figure 4.3d).

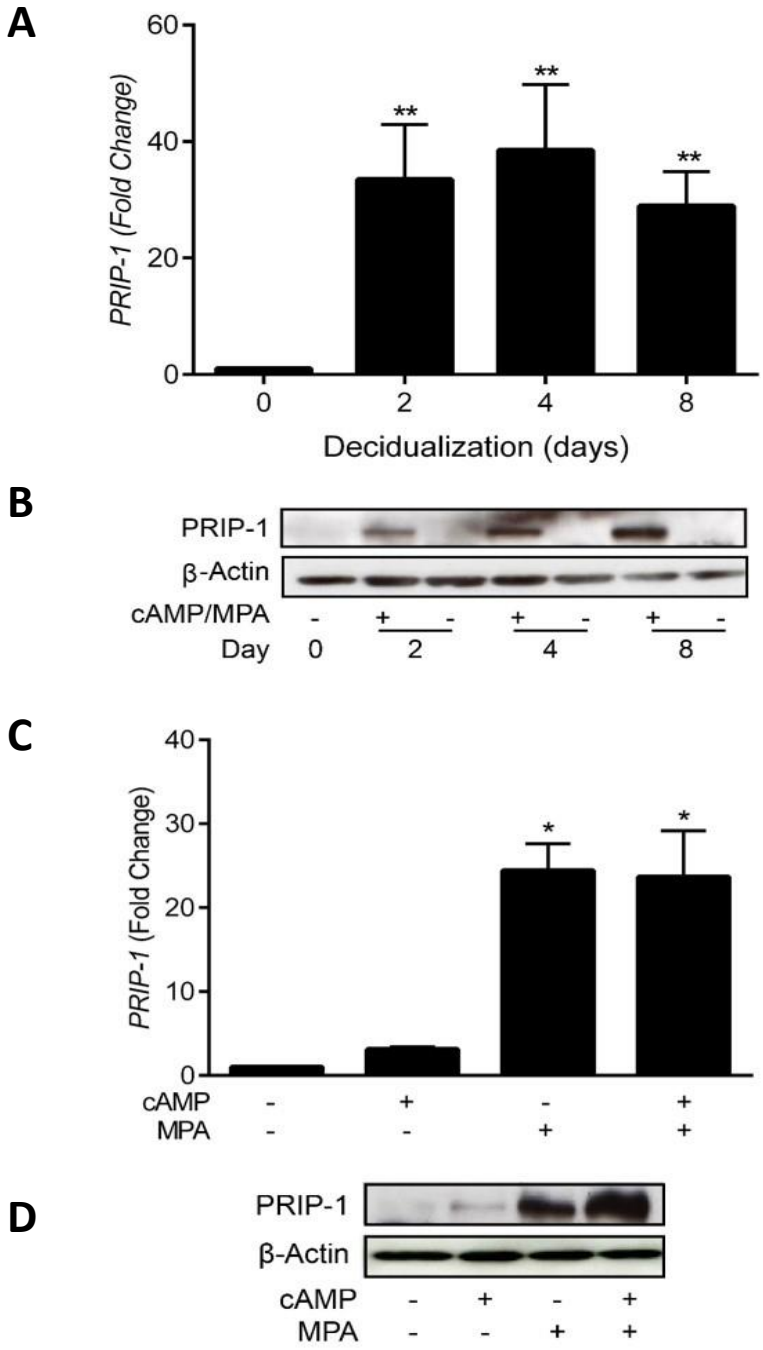

Figure 4.3 ***Uterine stromal decidualization is associated with up-regulation of*** **PRIP-1**. (a) *PRIP-1* expression in cultures decidualized with 8-br-cAMP and MPA for 2-8 days. Transcript expression was normalised to that of undifferentiated HESCs (Day 0). (b) Western blot analysis of total cell lysates of timed paired undifferentiated or decidualized HESCs. (c) Primary HESC cultures were treated with 8-br-cAMP or MPA as indicated for 4 days. *PRIP-1* expression measured by qRT-PCR. (d) Total protein lysates from parallel cultures were subjected to Western blotting. *P<0.05; **P<0.01. Data are presented as means ± S.E.M.

In order to establish if maintenance of PRIP-1 expression is also dependent upon P4 signalling, *PRIP-1* RNA and protein expression was measured in the hours following deciduogenic stimuli withdrawal. Briefly, triplicate cultures of HESCs were decidualized as above for 4 days and subsequently had cAMP and MPA withdrawn from culture media for 12, 24, 48 or 72 hours. *PRIP-1* RNA and protein expression was assessed by qRT-PCR and ELISA respectively. Stimuli withdrawal resulted in a reduction in *PRIP-1* transcripts by 29%, 50% and 35% at 24, 48 and 72 hours respectively (Figure 4.4a). Protein expression of PRIP-1 was reduced slightly upon withdrawal at 48 and 72 hours compared to D4 decidualized HESCs (10% and 20% respectively, Figure 4.4b). These results show that although *PRIP-1* induction is acutely responsive to P4, withdrawal does not result in a sharp decline in *PRIP-1* protein abundance.

GEO data mining revealed a biphasic expression profile of *PRIP-1* over the course of the menstrual cycle (Accession number GDS2052). During the proliferative phase, *PRIP-1* expression is low. It is subsequently induced during the early secretory phase, followed by progressively declining levels during the mid- and late-secretory phases (Figure 4.5a). Detailed analysis of the peri-implantation window revealed that within this defined period *PRIP-1* expression is also biphasic. *PRIP-1* transcript levels were measured in 73 women with ovulatory cycles 5-12 days post LH surge. Low transcript levels are apparent between days 5 and 6, increased expression between days 6 and 8 and reduced levels between days 9 and 12 post LH surge (Figure 4.5b). Confirming previous observations of disparate expression between mRNA transcripts and protein, ELISA analysis of 25 biopsies obtained 6 to 10 days post LH surge showed a significant positive correlation of PRIP-1 protein levels with increasing day of cycle (Figure 4.5c). Taken together, these results highlight a lag period between the induction of mRNA and upregulation of protein of approximately 48 hours. This

indicates additional levels of regulation by post-transcriptional modifications, and/or degradation in the determination of protein concentration.

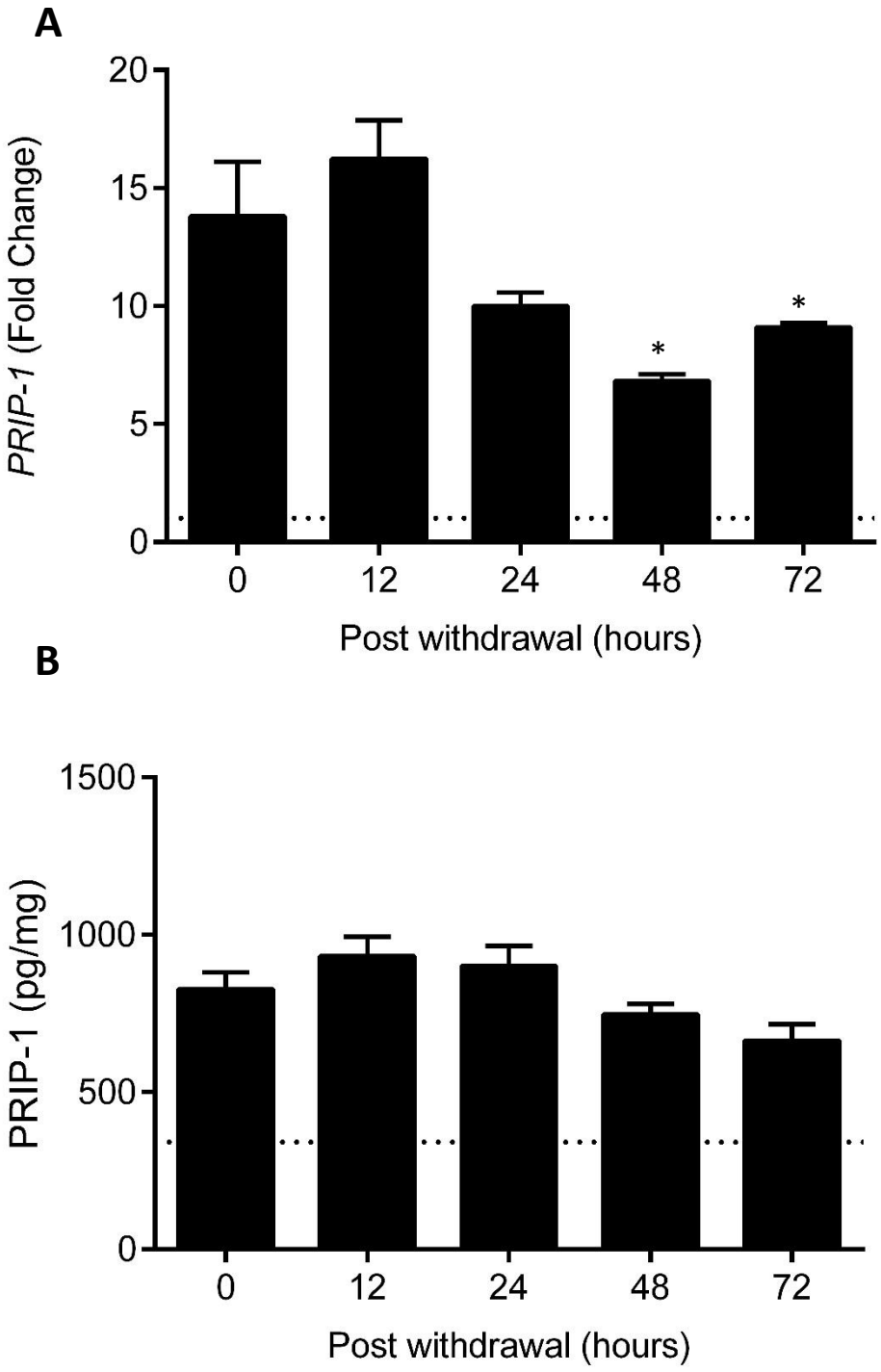

Figure 4.4 *Progesterone withdrawal leads to loss of* PRIP-1. (a) *PRIP-1* transcript expression in cultures which were decidualized with 8-br-cAMP and MPA for 4 days and then had cAMP and MPA withdrawn for indicated time-points. Transcript expression was normalised to that of undifferentiated HESCs. (b) PRIP-1 protein expression as measured by ELISA on total cell lysates of decidualized HESCs which then had cAMP and MPA withdrawn for indicated time-points. Dotted line indicated undifferentiated HESCs. Data was normalised to total protein concentration. *P<0.05; **P<0.01. Data are presented as means ± S.E.M.

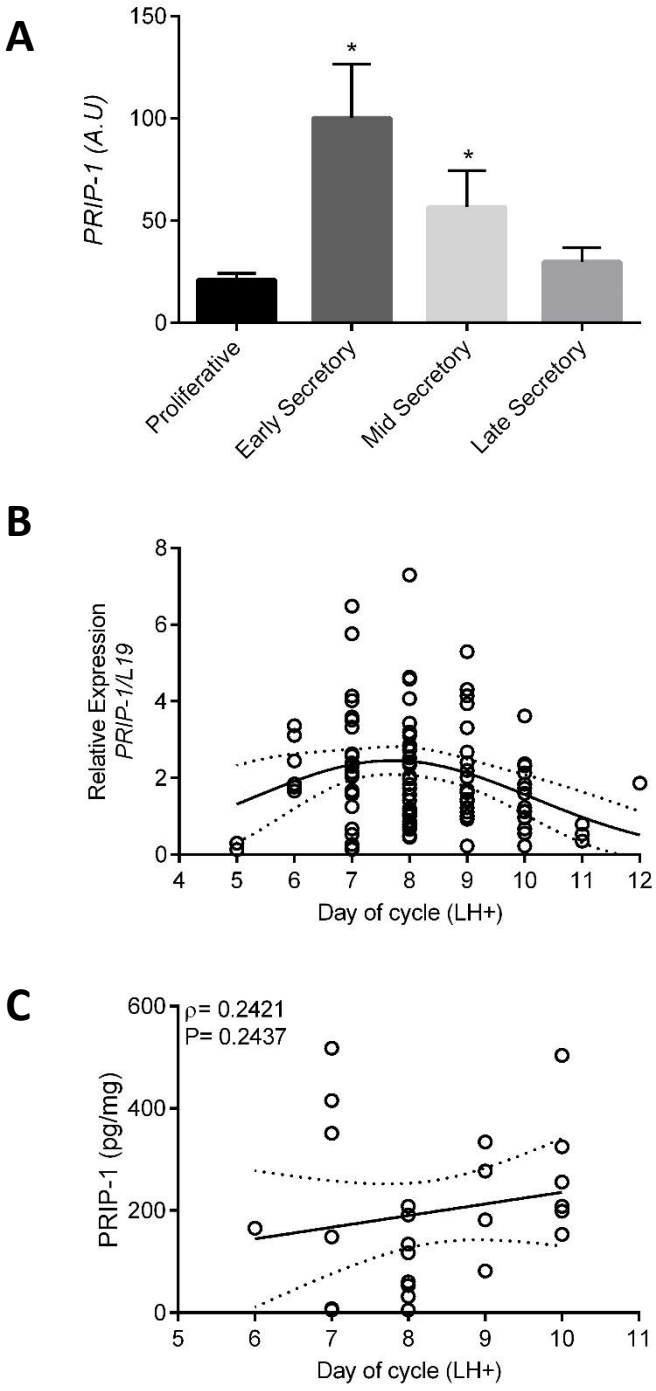

Figure 4.5 PRIP-1 *expression is regulated throughout the menstrual cycle* (a) GEO profile microarray of *PRIP-1* transcripts during the proliferative, early-, mid- and late-secretory phases of the menstrual cycle in 28 subjects using Affymetrix Human Genome U133 Array. *P<0.05. Data are presented as means ± S.E.M. (b) Endometrial *PRIP-1* gene expression in a cohort of 73 patients correlated with day of menstrual cycle (post LH surge). Data is fitted to a Guassian distribution. (c) PRIP-1 protein expression by ELSIA from 25 patients correlated with day of cycle. Data is analysed using regression analysis. Dotted lines represent 95% confidence intervals. Spearman's ρ value and probability (P) shown.

4.2.3 Tissue Distribution of *PRIP-1* in Mid-luteal Endometrium.

To examine the localisation of expression of PRIP-1 in the endometrium, mid-luteal biopsies were stained with PRIP-1 antibody. H and E staining shows normal mid-luteal physiology. Uterine glands, spiral arteries, luminal and glandular epithelia and the underlying stroma can all be observed (Figure 4.6a). Absence of primary antibody was used as a negative control (Figure 4.6b). PRIP-1 immunoreactivity can be observed predominantly in the luminal and glandular epithelium, however staining is also apparent in the stromal compartment and surrounding the spiral arteries (Figure 4.6c&d).

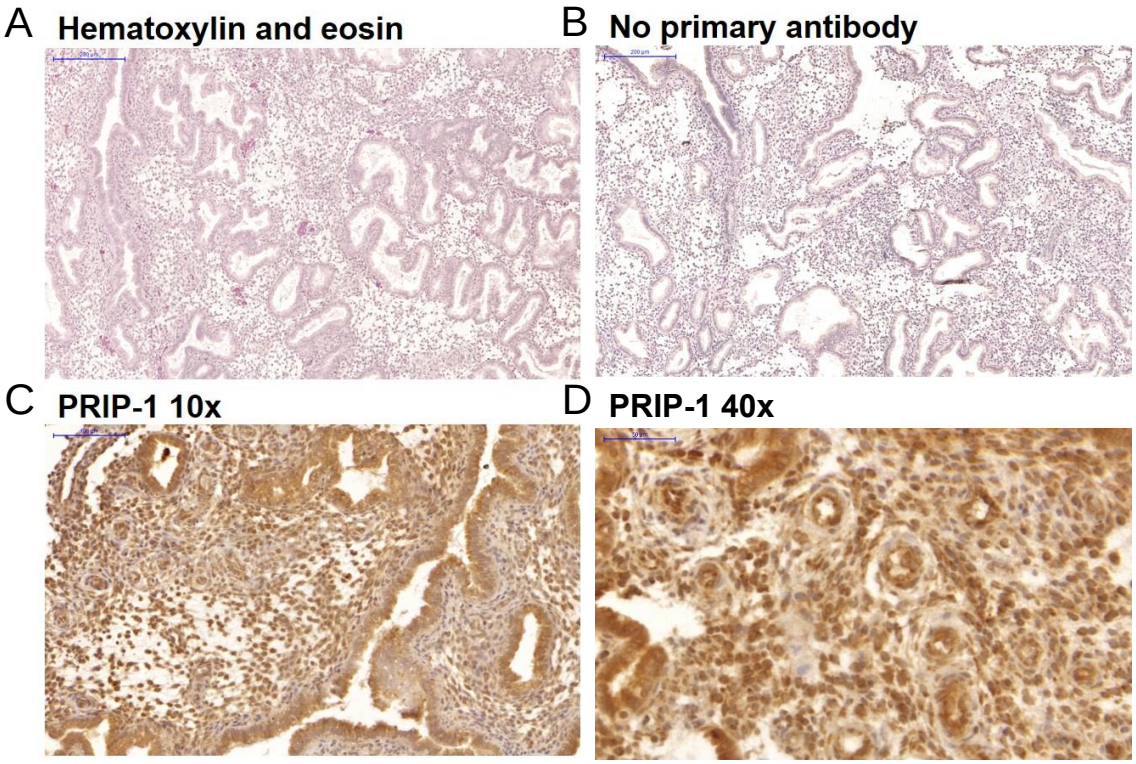

Figure 4. 6 PRIP-1 *expression in mid-luteal endometrium* (a) H and E staining of mid-luteal endometrium. Magnification x 10 (b) Negative control showing a lack of unspecific staining (c) *PRIP-1* immunoreactivity in mid-luteal endometrium. Staining was apparent not only in luminal and glandular epithelial cells, but also in the stromal compartment. (d) Higher magnification (x40) of the area also shows *PRIP-1* staining especially close to the spiral arteries.

4.2.4 *PRIP-1* Loss Reduces Basal Expression of Decidual Markers but does not Impact Their Induction upon Decidualization.

I hypothesised *PRIP-1* knockdown in HESCs may disrupt the expression of key decidual regulators. Therefore primary cultures were transfected with either NT or *PRIP-1* siRNA prior to differentiation for 4 days. Proof of knockdown was confirmed both at mRNA and protein levels (Figure 4.7a). PRIP-1 knockdown lowered the basal expression levels of both *PRL* and *IGFBP1* in undifferentiated HESCs (Figure 4.7b); however, the induction of these genes upon decidualization (as indicated by fold change, Figure 4.7c) remained unchanged and, in the case of *PRL,* was relatively increased.

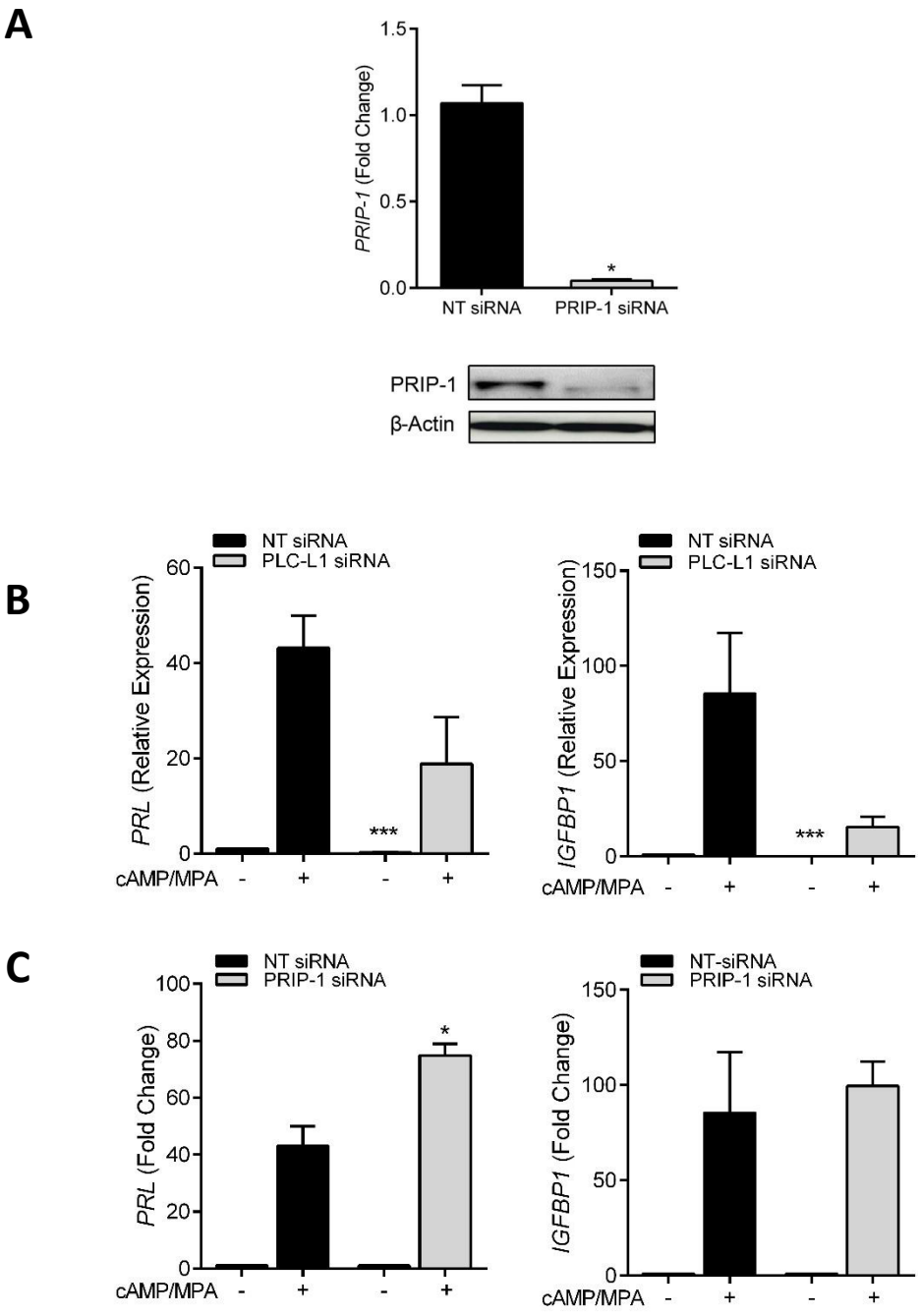

Figure 4.7 PRIP-1 ***is not required for induction of decidual markers***. (a) mRNA levels of *PRIP-1* were determined 48 hours following transfection of primary cultures with NT or *PRIP-1* siRNA. Total protein lysates from parallel cultures were subjected to Western blotting. β-Actin served as a loading control. (b) Primary HESCs were transfected with NT or *PRIP-1* siRNA. The cultures remained untreated or were decidualized for 4 days. The data show both relative expression and fold induction (means + SEM) of the decidual marker genes *PRL* and *IGFBP1* from cultures established from 3 independent biopsies. *P < 0.05; ***P < 0.001.

4.2.5 PRIP-1 is Not Essential for Secretory Transformation of HESCs.

PRIP-1 plays a role in exocytosis function via regulation of the phospho-status of SNAP-25, a component of the SNARE complex necessary for vesicle fusion (Zhang *et al.*, 2013). As decidualization is defined as the acquisition of a secretory phenotype, *PRIP-1* may serve in the exocytosis of critical decidual factors required for the creation of a rich extracellular environment for embryo implantation. To test this hypothesis, secretion of three key decidual genes were measured from the supernatant of transfected HESCs. Cultures were transfected with NT or *PRIP-1* siRNA and decidualized for 8 days or left undifferentiated. Cell supernatant was collected at day 2, 4 and 8 of the decidual time-course and applied in ELISAs for sST2, IGFBP1 and PRL. As expected, secretion of all three factors was increased upon decidualization when compared to undifferentiated cells. However, no change was observed in the secretion of any of the decidual factors upon *PRIP-1* knockdown in comparison to controls (Figure 4.8a-c).

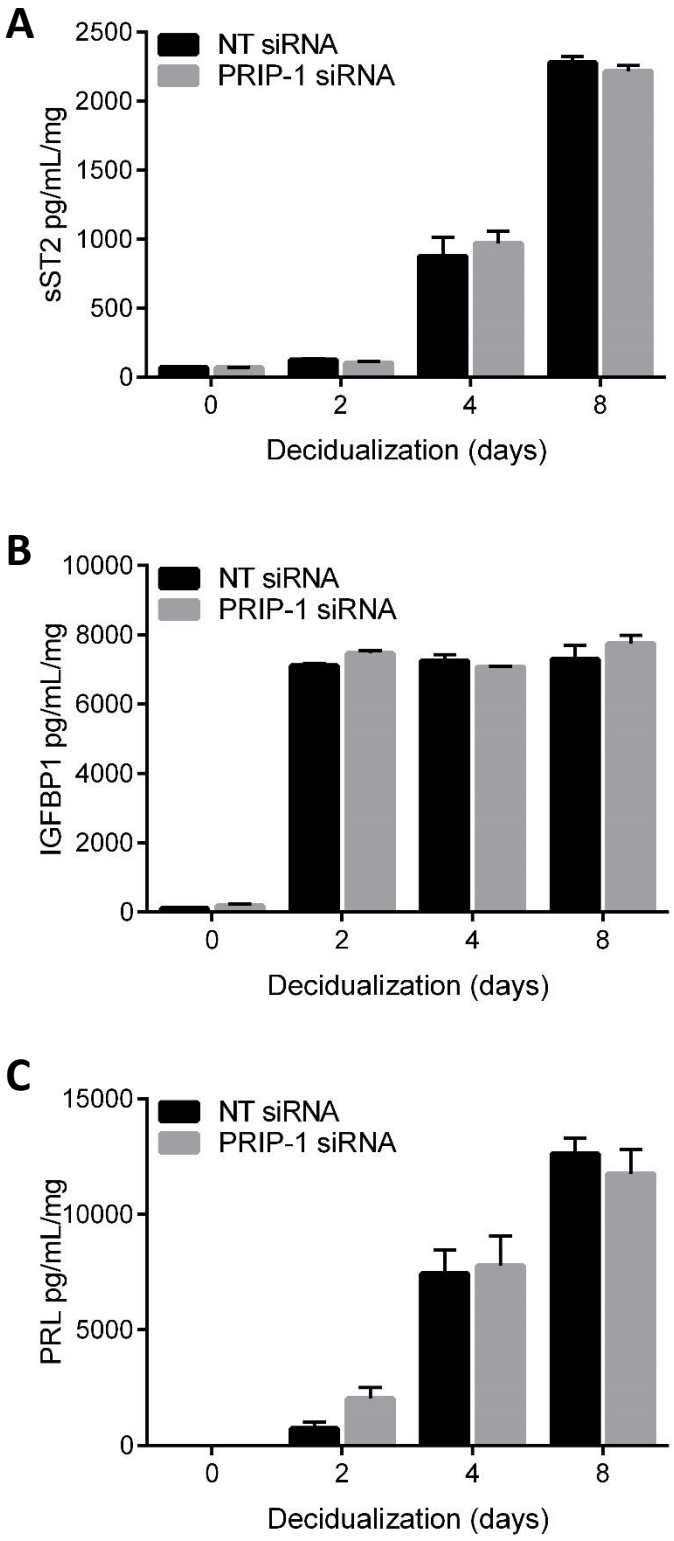

Figure 4.8 PRIP-1 *does not influence secretion in HESCs.* Protein expression of (a) sST2, (b) IGFBP1 and (c) PRL as measured by ELISA in supernatant from transfected HESCs as indicated which were subsequently decidualized for 0, 2, 4 or 8 days with 8-br-cAMP and MPA. Data show mean normalised to total protein concentration.

4.2.6 *PRIP-1* Acts as a Chelator of Calcium Signalling.

Investigations into *PRIP-1* have previously demonstrated its role as a regulator of Ca^{2+} signalling via its known interaction with IP_3 (Harada *et al.*, 2005). To test if this function is maintained in human endometrial cells, Ca^{2+} oscillations were assessed. Briefly, cells were transfected with either NT or *PRIP-1* siRNA, decidualized, and loaded with the fluorescent calcium indicator Fluo-4-AM. Samples were subsequently challenged with the PLC activator *m*-3M3FBS or DMSO vehicle. *PRIP-1* knockdown was confirmed by qRT-PCR (Figure 4.9a). Decidualized HESCs transfected with NT siRNA displayed limited fluorescence over a 10 minute exposure, indicative of an absence of Ca^{2+} signalling (Figure 4.9b). However, cells transfected with *PRIP-1* siRNA exhibited robust and sustained fluorescence over the entirety of the time-course, signifying the presence of Ca^{2+} fluxes (Figure 4.7c). Analysis of these traces revealed a 3-fold increase in area under the curve, 2-fold increase in oscillation frequency and a 2-fold increase in maximal fluorescence upon *PRIP-1* knockdown (Figure 4.9d-f). These results demonstrate *PRIP-1* expression in the endometrial stroma during decidualization acts to sequester phosphoinositides and limit functional Ca^{2+} signalling pathways.

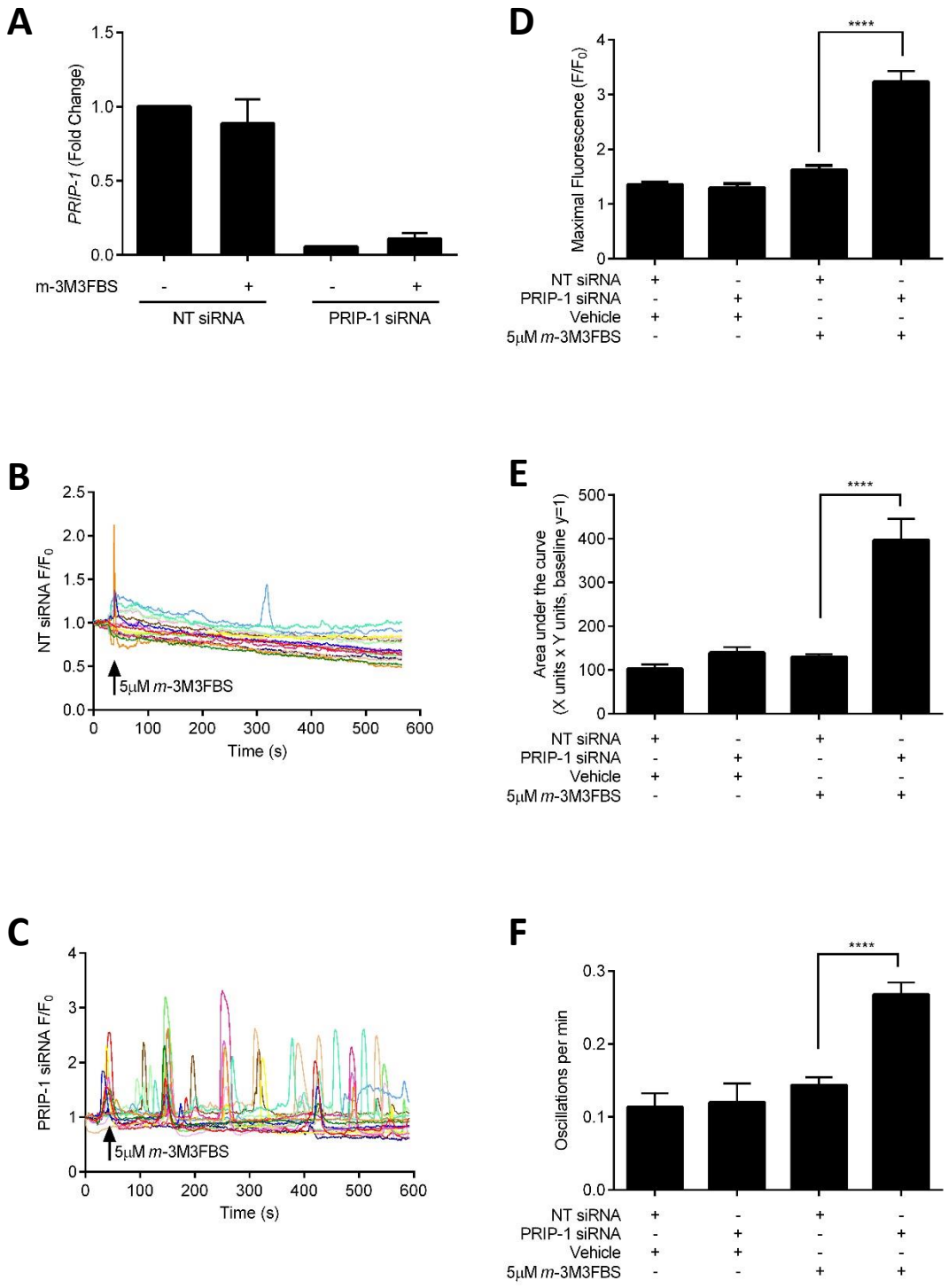

Figure 4.9 *m*-3M3FBS-mediated Ca^{2+} signalling in decidualized HESCs. (a) HESCs were transfected with NT and *PRIP-1* siRNA and decidualized for 4 days and challenged with 5μM m-3M3FBS. *PRIP-1* expression quantified by qRT-PCR. HESCs transfected with (b) NT siRNA or (c) *PRIP-1* siRNA were loaded with 5μM Fluo-4-AM and imaged by confocal microscopy with cytosolic fluorescence used as an index of $[Ca^{2+}]_i$. Cells were then challenged with 5μM m-3M3FBS at t-30s and imaged for 10min. Traces showing fluorescence within individual cells are expressed as a fold increase over fluorescence at time-0 (F/F_0). Data are representative of n=4. (d) Traces were analysed to assess the maximal changes in fluorescence, (e) the area under the curve (baseline = y=1) and (f) oscillation frequency (oscillations per minute). Data show mean + SEM., n=4, **** denotes $P < 0.0001$.

4.2.7 *PRIP-1* Promotes HESC Survival.

Decidual cells are highly resistant to environmental stressors, yet are poised to undergo apoptosis in response to P4 withdrawal. Visual observations upon *PRIP-1* knockdown indicated a recurrent partial loss of cellular viability. To investigate this phenomenon further I used a range of viability assays to quantify this effect. A trypan blue exclusion assay revealed a 28% reduction in live cell numbers in decidualized HESCs upon *PRIP-1* knockdown (Figure 4.10a). This was accounted for by an increase in apoptosis as measured by caspase 3/7 activity in decidual cells. Knockdown of *PRIP-1* resulted in a 3.4-fold increase in fluorescence, indicating caspase 3/7 sequential cleavage of a pro-fluorescent substrate. (Figure 4.10b). Additionally, real-time monitoring of cell proliferation > 100 hours using xCELLigence technology was used. Once again, HESCs were transfected with NT or *PRIP-1* siRNA and then subjected to deciduogenic stimuli for 4 days. Mock transfected undifferentiated cells were used as growth controls and maintained in either 10% or 0% DCC-FBS supplemented media. Triplicate biological repeat experiments revealed knockdown of *PRIP-1* resulted in complete growth inhibition. (Figure 4.10c).

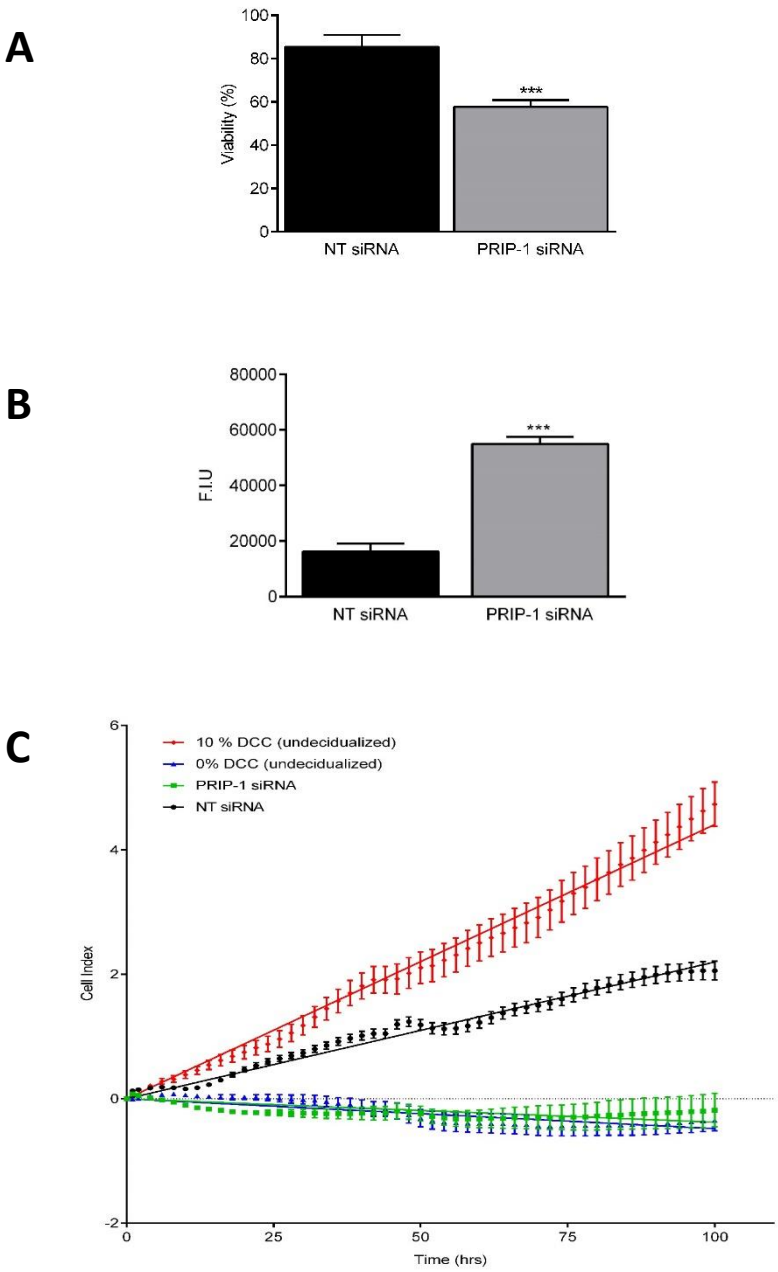

Figure 4.10 PRIP-1 *is a critical survival factor in HESCs.* (a) Cell viability as measured by trypan blue exclusion assay in 3 independent primary cultures first transfected with wither NT or *PRIP-1* siRNA. The cultures were decidualized for 4 days. (b) Triplicate undifferentiated HESC cultures were transfected as indicated and decidualized for 4 days. Caspase 3/7 activity measured in fluorescent intensity units (F.I.U). (c) **.** Real-time monitoring of cell growth and adherence as measured by electrical impedance using an xCelligence analyser over 100 hours. HESCs were seeded into 16 well plates and transfected within the plate with NT or *PRIP-1* siRNA. Untransfected HESCs cultured in 10 or 0% DCC-FBS supplemented media were used as controls. Cell index measurements were captured.

4.2.8 *PRIP-1* Acts as a Survival Factor Through AKT Signalling.

PRIP-1 is a known binding partner of active AKT (Sugiyama *et al.*, 2013), therefore, I speculated that *PRIP-1* loss may compromise the activity of the PI3K/AKT/FOXO1 survival pathway. To investigate this, I ran a proteome array to detect the relative levels of phosphorylation of 26 kinases on lysates obtained from HESCs first transfected with either control or *PRIP-1* siRNA (Figure 4.11a). This revealed a dramatic yet specific inhibition of active phosphorylated-AKT upon *PRIP-1* knockdown. Levels of phospho-AKT1 (S473), phospho-AKT2 (S474), phospho-AKT3 (S472) and pan-phospho-AKT (S473, S474, S472) were all attenuated upon *PRIP-1* loss by 69%, 59%, 46% and 58% respectively. Phospho-status of any other kinases in the array did not demonstrate any significant regulation upon *PRIP-1* knockdown (Figure 4.11b and c), highlighting the specific impact upon AKT. To confirm these results western blot analysis was undertaken on total cell lysates from NT or PRIP-1 siRNA transfected decidual HESCs. Total un-phosphorylated AKT levels did not change upon knockdown; however, confirmation of a loss of phospho-AKT can be observed. Furthermore, the downstream AKT effector FOXO1A was shown to be induced upon PRIP-1 loss as well as the pro-apoptotic regulator BIM. Taken together, these results indicate that *PRIP-1* acts as a critical survival factor during decidualization, mediated via AKT signalling.

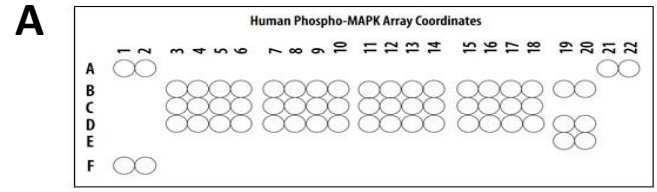

Coordinate	Target	Phosphorylation site detected
A1, A2, A21, A22	Reference Spots	
B3, B4	Akt1	S473
B5, B6	Akt2	S474
B7, B8	Akt3	S472
B9, B10	Akt pan	S473, S474, S472
B11, B12	CREB	S133
B13, B14	ERK1	T202/Y204
B15, B16	ERK2	T185/Y187
B17, B18	GSK-3α/β	S21/S9
B19, B20	GSK-3β	S9
C3, C4	HSP27	S78/S82
C5, C6	JNK1	T183/Y185
C7, C8	JNK2	T183/Y185
C9, C10	JNK3	T221/Y223
C11, C12	JNK pan	T183/Y185, T221/Y223
C13, C14	MKK3	S218/T222
C15, C16	MKK6	S207/T211
C17, C18	MSK2	S360
D3, D4	p38α	T180/Y182
D5, D6	p38β	T180/Y182
D7, D8	p38δ	T180/Y182
D9, D10	p38γ	T183/Y185
D11, D12	p53	S46
D13, D14	p70 S6 kinase	T421/S424
D15, D16	RSK1	S380
D17, D18	RSK2	S386
D19, D20	TOR	S2448
E19, E20	PBS	
F1, F2	Reference Spots	

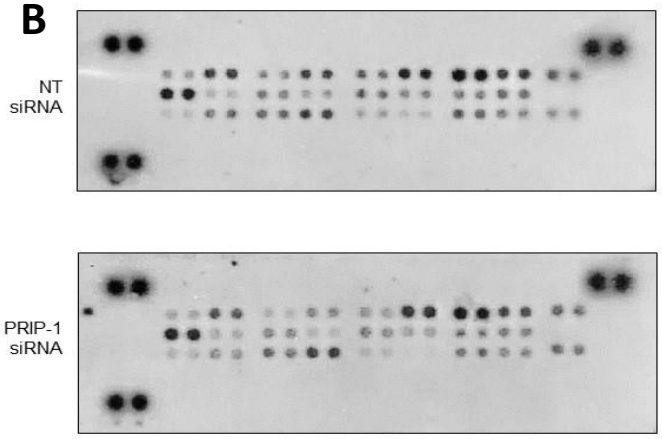

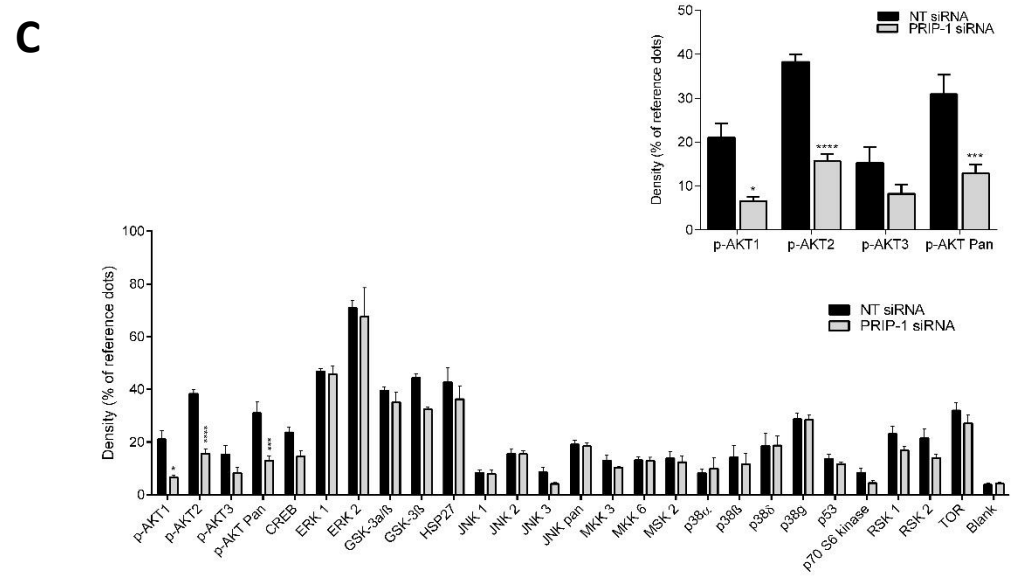

Figure 4.11 PRIP-1 ***acts to influence the AKT pathway***.(a) Location and list of phosphorylated genes analysed by array. (b) Blot array membranes of primary HESCs were transfected with NT or *PRIP-1* siRNA. Cultures were harvested at 48 hours post transfection and protein lysates subjected to Proteome Profiler MAPK array membranes (c) Densitometry analysis of above blots; inset highlights differential regulation of the AKT pathway upon *PRIP-1* knockdown. The data show mean ± SEM; **P < 0.01; ***P < 0.001

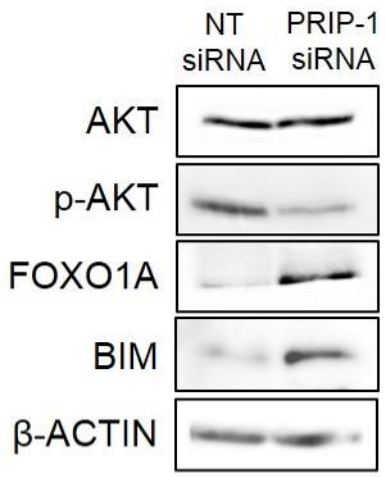

Figure 4.12 ***Expression of*** **AKT** ***and its downstream effectors upon*** **PRIP-1** ***loss.*** Western blots of total protein lysates from HESCs transfected with NT siRNA or PRIP-1 siRNA as indicated and decidualized for 4 days. β-Actin serves as a loading control.

.

4.2.9 *PRIP-1* Expression in Mid-luteal Biopsies.

Finally, I examined the expression levels of *PRIP-1* transcripts in mid-luteal endometrial biopsies. This cohort consisted of 101 patients with varying fertility issues (Appenidx 7). Once again, statistical analysis revealed none of the patient demographics correlated with *PRIP-1* levels in a Gaussian distribution; therefore, linear regression analysis was applied and statistical significance determined using a Spearman's rank test. Findings demonstrate that neither age (Spearman's rank test ρ=-0.0640, P= 0.4945), BMI (ρ=-0.0498, P= 0.6154) nor uNK % (ρ=0.0385, P= 0.6939) showed association with *PRIP-1* mRNA levels during the mid-luteal phase (Figure 4.13a-c). To determine if any correlation was observed within a sub-cohort of miscarriage patients, correlation was assessed between *PRIP-1* transcript levels and number of previous pregnancy losses in women who had suffered consecutive miscarriages, ranging between 2 and 11 losses. Once again, no association with *PRIP-1* expression was observed (ρ=-0.1901, P= 0.1073, Figure 4.13d). Due to the disparate expression of *PRIP-1* mRNA and protein, I also examined correlations between patient demographics relevant to reproduction and PRIP-1 protein levels by ELISA. As with mRNA, in a cohort of 25 women no significant associations were found between age (ρ=-0.1559, P= 0.4283), BMI (ρ=-0.0010, P= 0.9613), uNK% (ρ=-0.2379, P= 0.2834) or previous number of miscarriages (sub-cohort of 15 patients (ρ=-0.2379, P= 0.2834)) with PRIP-1 protein expression (Figure 4.14a-d).

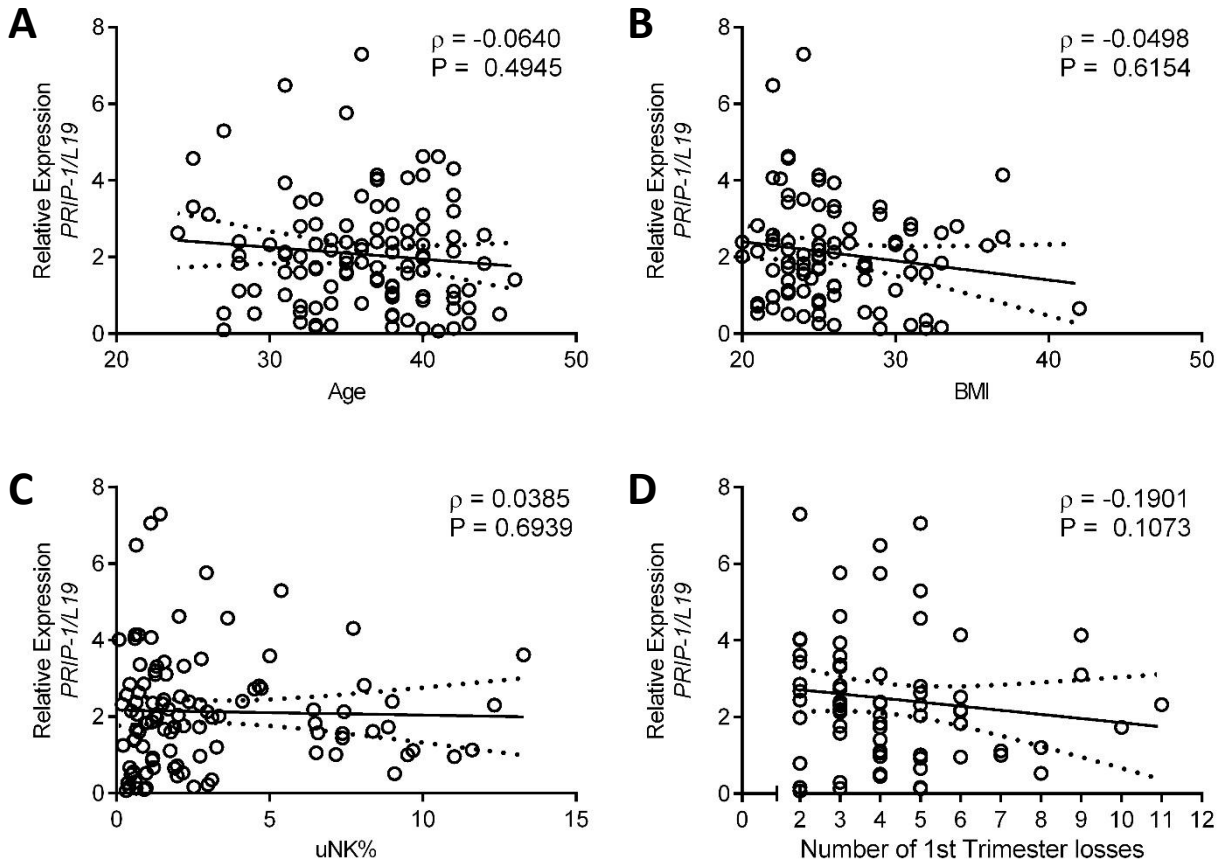

Figure 4.13 ***Timed mid-luteal endometrial mRNA expression of*** **PRIP-1** ***in a cohort of 101 women.*** Correlation between *PRIP-1* expression in mid-luteal endometrial biopsies and (a) age, (b) BMI, (c) uterine NK cell percentage, and (d) the number of previous pregnancy losses in a sub-cohort of recurrent miscarriage patients using regression analysis. Dotted lines represent 95% confidence intervals. Spearman's ρ value and probability (P) shown.

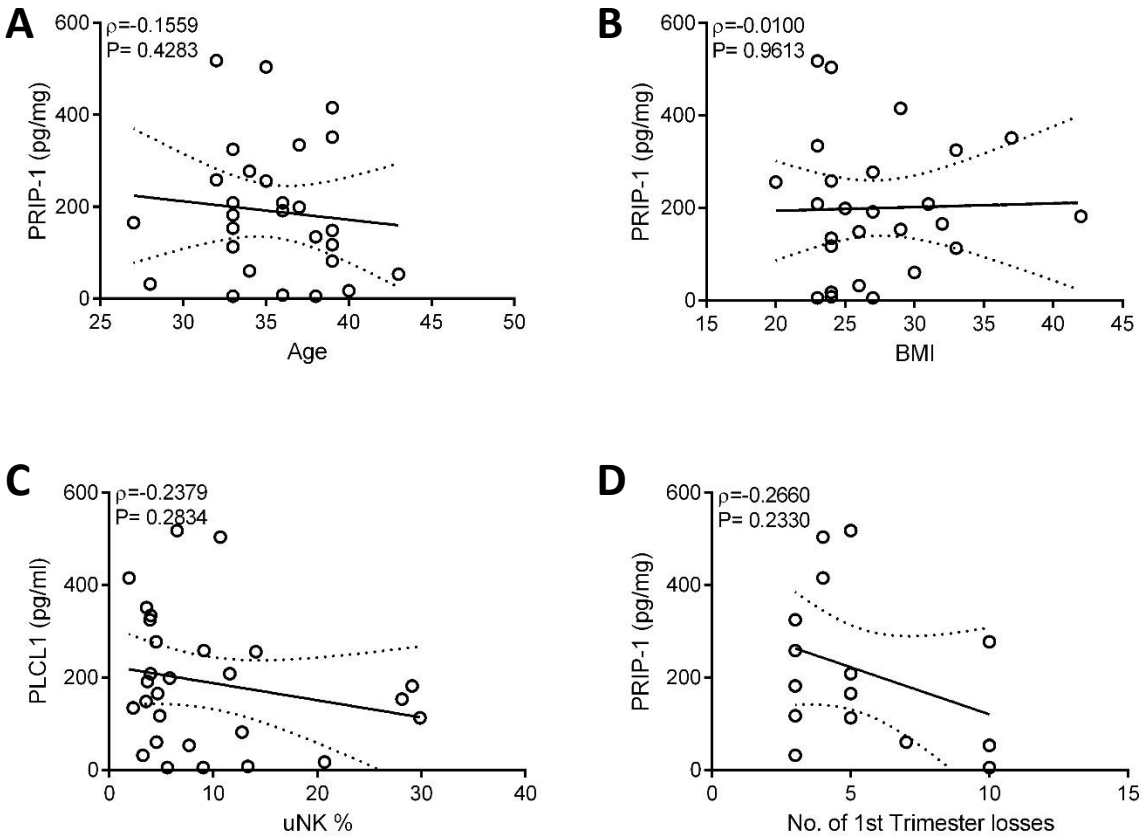

Figure 4.14 ***Timed mid-luteal endometrial protein expression of PRIP-1 in a cohort of 25 women.*** Correlation between PRIP-1 protein expression in endometrial biopsies and (a) age, (b) BMI, (c) uterine NK cell percentage, and (d) the number of previous pregnancy losses in a sub-cohort of recurrent miscarriage patients using regression analysis. Dotted lines represent 95% confidence intervals. Spearman's ρ value and probability (P) shown.

4.3 Discussion

This study was initiated by the observation that *PRIP-1* expression is *PER2* dependent in undifferentiated HESCs. *PRIP-1* promoter analysis reveals the presence of an E-box, a motif typically associated with circadian regulation. However, although both genes showed expression peaks during the same circadian phase, the amplitude of *PRIP-1* oscillations was very weak, and therefore unlikely to be circadianally regulated. As both genes are located on the long arm of chromosome 2 (40 mega base pairs apart), *PER2* and *PRIP-1* may be expressed as a single unit of co-regulated genes that are not otherwise functionally related. Importantly, however, *PER2* and *PRIP-1* display opposite responses during HESC decidualization. Whilst *PER2* expression is critically down-regulated, *PRIP-1* is induced. This suggests that whilst *PRIP-1* expression is *PER2* dependent in undifferentiated HESCs, the impact of deciduogenic signals is sufficient to drive independent regulation.

In this chapter, divergent regulation of *PRIP-1* mRNA and protein is shown. Protein abundance is controlled by the balance of both RNA and protein production and turnover rates. 3' UTR analysis of *PRIP-1* demonstrates the presence of a K-box motif, known to interact with miRNA and exert transcriptional repression, which may account for some of the lagging expression patterns. Protein post-translational modifications are likely to mediate disparate expression. PRIP-1 is known to be phosphorylated by protein kinase A (Sugiyama *et al.*, 2013). However, due to the prolonged period between peak mRNA and protein expression in HESCs, this is more likely attributed to the lengthy protein turnover rate as calculated by ExPASY analysis as above 30 hours (http://web.expasy.org/protparam/).

Data provided here demonstrates that although *PRIP-1* knockdown does not affect induction or secretion of key decidual factors, it acts to reduce basal levels of *PRL* and *IGFBP1.* As such, *PRIP-1* may act to augment the decidual phenotype.

Importantly, *PRIP-1* sequesters IP_3. Challenge with a PLC activating compound revealed sustained calcium flux upon *PRIP-1* knockdown, not apparent in control transfected decidual HESCs. Decidualizing cells are known to mount an endoplasmic reticulum (ER) stress response associated with acquisition of a secretory phenotype (Leitao *et al.*, 2010). This is characterised by up-regulation of various chaperones including protein disulphide isomerase (PDI), BIP and calnexin. ER stress is also associated with calcium release which then accumulates in mitochondrial matrices (Deniaud *et al.*, 2008). Sustained Ca^{2+} accretion can act to trigger pro-apoptotic signals leading to cell death (Orrenius *et al.*, 2003). As such, it may be speculated that up-regulation of *PRIP-1* during decidualization acts to maintain Ca^{2+} homeostasis during a decidual ER stress response. This is further supported by data showing that *PRIP-1* acts as a survival factor during decidual transformation, as shown by increased apoptosis and attenuated real time proliferation upon gene knockdown. The demonstrated association between *PRIP-1* and the AKT pathway further supports this hypothesis. AKT is known to influence multiple factors involved in apoptosis by transcriptional regulation or direct phosphorylation, including inhibition of the caspase cascade, phosphorylation of the forkhead family of transcription factors, and activation of the pro-survival genes *CREB* and *MDM2* (Brunet et al., 1999). The data provided here shows active phospho-forms of AKT are reduced upon *PRIP-1* loss. Furthermore, western blot analysis shows up-regulation of both FOXO1 and BIM upon *PRIP-1* knockdown. This further supports the hypothesis of an anti-apoptotic role for *PRIP-1,* acting to protect the implanting conceptus from damaging input signals. As PRIP-1 is known to act as a protein scaffold to PP1 and PP2A, it is tempting to speculate that during decidualization PRIP-1 acts a regulatory switch

controlling the phospho-status of AKT. This may be achieved by either binding and presenting AKT to appropriate kinases, or by sequestering PP2A, thus preventing AKT dephosphorylation and deactivation.

Up-regulation of *PRIP-1* in the endometrium is critically dependent upon progesterone signalling. This is unusual as very few genes are acutely responsive to progesterone treatment alone and often require convergent activation of the cAMP pathway(Gellersen & Brosens, 2003)(Gellersen & Brosens, 2003). The P4 specific up-regulation of *PRIP-1* during the mid-secretory phase, and continued PRIP-1 protein expression past the window of implantation, suggests that it is required for the post-implantation environment. Continued progesterone signalling is critical for ongoing pregnancy, as once decidualized, constant P4 is required to maintain the integrity of the decidua (Brosens & Gellersen, 2006). In the absence of successful implantation, declining P4 levels trigger breakdown of the superficial endometrial layer leading to focal bleeding and menstruation. I show here *PRIP-1* expression drops during the late-secretory phase when P4 levels are declining, suggesting maintenance of *PRIP-1* expression is dependent upon P4. This is supported by evidence demonstrating *PRIP-1* transcript induction by low dose hCG during the follicular phase of the cycle (Blockeel *et al.*, 2011), as hCG acts to signal to the corpus luteum to secrete P4 to maintain the decidual phenotype. P4 withdrawal is associated with FOXO1 reactivation, PLZF down-regulation and p53 mediated cell death (Brosens & Gellersen, 2006). I therefore propose that PRIP-1 functions as a molecular switch within this pathway. As such, high *PRIP-1* levels present during decidualization lead to AKT and IP_3 mediated cell survival, whilst declining levels upon P4 withdrawal reverse this cell-fate decision. This leads to calcium influx and deactivation of the AKT pathway, ultimately leading to tissue destabilisation surrounding the spiral arteries, and the breakdown of the superficial endometrium. Finally, although *PRIP-1* expression was not correlated with demographics

associated with miscarriage, these results do not suggest that *PRIP-1* is not vital for decidualization and ongoing pregnancy.

Chapter 5

General Discussion

5.1 The Challenges of Human Reproduction.

Human implantation presents unique challenges that must be overcome for successful pregnancy. The balance between endometrial receptivity and selectivity is central to this. The vast majority of foetal loss occurs prior to placental perfusion, thereby limiting maternal investment in poor quality embryos. Human reproduction is typified by a high rate of embryo wastage, which can be attributed to the vast embryological diversity required for evolution (Bielanska *et al.*, 2002). Pre-implantation human embryos are characterised by mosaicism, aneuploidies, and result in deeply invading placenta (Delhanty *et al.*, 1997). Genomic studies have found genes associated with reproduction are amongst the most rapidly evolving in the human genome (Swanson & Vacquier, 2002). As such, the ability of the decidua to detect and select high quality embryos, or destroy low quality embryos represents a maternal adaptation to these conditions.

Assisted reproductive technologies are increasingly in demand as maternal age upon childbearing rises. Failed outcomes of both infertility and pregnancy loss are often associated with psychological distress including anxiety and depression (Lok & Neugebauer, 2007). As such it is important that we expand our knowledge regarding the molecular mechanisms that control early embryo–maternal interactions as implantation remains the least understood key rate-limiting step in human reproduction. Whilst implantation cannot be studied directly in humans, mouse models, primary and cell line cultures, and the analysis of IVF treatment successes and failures provide insight into these critical mechanisms determining reproductive outcome. Recent work has proposed a spectral model balancing endometrial receptivity and selectivity at opposing poles. Women who fall at the high receptivity/low selectivity extremity demonstrate rapid time to pregnancy (superfertility), and may have increased likelihood of recurrent miscarriage. On the

other hand, women with extreme low receptivity/high selectivity are more likely to present as infertile, and have recurrent implantation failure during IVF as their 'quality control' mechanism is too stringent. Thus, normal implantation relies upon a balance of receptivity and selectivity giving rise to a defined 'window of implantation' (Salker *et al.*, 2011)(Salker *et al.*, 2011)(Brosens *et al.*, 2014; Salker *et al.*, 2011; Teklenburg *et al.*, 2010a). However, what is unknown is the role the internal body clock plays in how this window is temporally defined within the decidual transformation. Furthermore, implantation relies upon synchrony between endometrial and embryonic development and how this synchrony is achieved is also unknown. This thesis has investigated the circadian molecular mechanisms underpinning the precise timing of stromal decidualization, and cell fate decisions in the endometrium controlling receptivity and selectivity.

In summary, I provide data showing that:

i. Circadian rhythms are silenced at the time of implantation via down-regulation of the core clock gene *PER2.*
ii. PER2 acts to synchronise endometrial proliferation with the initiation of decidual gene expression.
iii. Women who have suffered previous miscarriage are more likely to have deregulated levels of *PER2*, and as such may not be able to adjust decidual synchrony within the endometrium.
iv. Although *PRIP-1* is a *PER2* dependent gene in undifferentiated cells, this dependency becomes uncoupled in decidualizing cells, rendering *PRIP-1* under the control of P4.
v. P4-dependent induction of *PRIP-1* is essential for autonomous functioning of decidual cells in early pregnancy.

5.2 PER2 and PRIP-1 are Mediators of Cell Fate Decisions in Decidualizing HESCs.

The maternal ability to abort non-viable pregnancies via miscarriage is functionally linked to the mechanism of monthly spontaneous decidualization and menstrual shedding in the absence of a viable embryo. Menstrual preconditioning suggests that cyclical endometrial shedding serves to sensitise uterine tissues to inflammatory and oxidative stressors associated with deep placentation, and to coordinate an appropriate spatio-temporal decidual response (Brosens *et al.*, 2009). Paracrine signalling from decidualizing HESCs results in tissue wide reorganisation to form a decidual matrix receptive to embryo implantation. Stromal cell differentiation represents the 'tipping point' of the superficial endometrium. HESCs will either give rise to the maternal portion of the placenta, or be lost by menstrual shedding or in early pregnancy loss via a menstrual shedding like event.

Both *PER2* and *PRIP-1* are important regulators of this tipping point, mediating cell fate decisions. PER2 acts to silence the circadian clock by signalling the progression from mid- to late-secretory endometrium in response to deciduogenic stimuli. By regulation of the G2/M cell cycle checkpoint, PER2 is required for the obligatory round of mitotic proliferation prior to decidualization. In the absence of PER2, cell cycle progression is halted, and as a consequence, a disorganised decidual phenotype is observed. This timed regulation of PER2 appears to be evolutionary conserved as it has been previously observed in mice (Uchikawa *et al.*, 2011). I show here that this temporal suppression was achieved via regulation of CLOCK binding to the PER2 enhancer element. Recent studies have shown further regulation of circadian components by epigenetic and RNA modifications including m^6-RNA methylation, which affects transcript production and nuclear retention (Fustin *et al.*, 2013). The level of complexity and redundancy within the circadian system indicate that the

specific silencing of *PER2* and the consequent suppression of the circadian clock at decidualization is significant. As such, I propose, *PER2* acts as a potential trigger mechanism defining the onset of decidualization.

PRIP-1 appears to act later in the decidual response, acting as an activating mechanism for apoptosis in a non-implanting cycle. However, as PRIP-1 protein shows minimal responsiveness to acute progesterone withdrawal, I hypothesise that although PRIP-1 may not trigger embryo rejection, but instead act to protect the conceptus from progesterone flux within the endometrium. This is supported by the finding of contrasting regulation of *PRIP-1* mRNA (fast) and protein (Bedaiwy *et al.*) upon P4 addition and withdrawal. As such, this enables a lag between *PRIP-1* mRNA and protein concentrations. I speculate that this enables flux in progesterone concentrations without activation of a potentially damaging apoptotic response.

These mechanisms act to define the window of implantation temporally. Failure to both initiate and terminate the window of receptivity is associated with reproductive failure. RPL is associated with a prolonged period of receptivity and thus permits out-of-phase implantation. It seems logical that central circadian components influence these timings. This is supported by the finding of an inverse correlation between *PER2* transcript levels and the previous number of miscarriages in women suffering reproductive failure. As such, these women may not be able to regulate decidual synchrony within the endometrium, which is critical to prevent pregnancy related pathologic events. Additionally, the small but significant association between *PER2* transcript levels and patient age suggests that the ability of the circadian system to appropriately time the onset of decidualization may decline with increasing age. It is well established that the amplitude of circadian rhythms decreases with age (Nakamura *et al.*, 2011), as well as reproductive function. Furthermore previous studies have identified an accelerated reproductive phenotype in Per1/Per2 deficient

mice (Pilorz & Steinlechner, 2008). As such, low levels of PER2 could represent an 'aged' reproductive phenotype and contribute to adverse outcome. Further work into this association may yield interesting results.

5.3 The Role of PER2 and PRIP-1 in Defining Cell Populations Within the Stroma.

The most remarkable characteristic of the endometrium is its inherent plasticity and regenerative capacity, with extensive remodelling apparent in response to menstruation, miscarriage or birth. Unsurprisingly, the basal layer of endometrium is rich in multipotent mesenchymal stem-like cells (Gargett, 2007; Meng *et al.*, 2007; Murakami *et al.*, 2014). One theory suggests that the ability to expand the endometrial stem cell niche is required as part of a pre-conditioning reaction in response to deep trophoblast invasion. It is therefore notable that the majority of adolescent menstrual cycles are anovulatory (Brosens *et al.*, 2009; Wheeler, 1991), and the risk of early pregnancy loss in very young mothers is raised (Fraser *et al.*, 1995). This is suggestive of an evolutionary response ensuring that stem cell mobilisation precedes pregnancy.

Emerging evidence suggest that the composition of the decidua itself is more complex than previously appreciated. Recent work has indicated that a balance between 'true' decidual cells and 'senescent' decidual cells is critical for the formation of a honey comb like structure required for the active envelopment of an implanting conceptus (unpublished data). Various networks of signalling pathways are presumed to critically define these subpopulations within the decidua, including cell to cell signalling via the Notch pathway (Murakami *et al.*, 2014). As *PER2* knockdown results in a disordered decidual gene expression profile, I speculate that the balance between

resident stromal cells may be affected by loss of this protein. Future work could be carried out to establish and assess the impact of PER2 loss on the balance of cell populations within the stroma. Furthermore, the ability of the long non-coding RNA BRE-AS1 to rescue the induction of key decidual markers may indicate that it acts to re-establish the balance of subpopulations. Further research is required to assess its ability to reverse other *PER2* knockdown mediated phenotypes, including failed endometrial proliferation.

5.4 PER2 and PRIP-1 Serve as Protectors Against Environmental Stressors.

One of the unique challenges of human implantation that must be overcome for successful pregnancy is one of protection. The implanting conceptus requires shielding from various environmental factors. This is achieved by the formation of a decidual matrix designed to buffer and absorb such stressors. Various mechanisms of protection have previously been described including inactivation of the JNK and p38 stress-responsive pathways via SUMO regulation (Feligioni *et al.*, 2011; Leitao *et al.*, 2011), and increased ROS scavenging by HESCs (Sugino *et al.*, 1996).

In this thesis, I report two further mechanisms for the isolation of the endometrium and protection of the implanting blastocyst. Firstly, *PER2* switches off the endometrial circadian clock, thereby protecting the embryo from daily oscillations in gene expression. As PER2 is known to influence circadian output by interaction with various nuclear receptors (Schmutz *et al.*, 2010), it can be envisaged that the absence of a functional circadian clock in the endometrium could act to stabilise steroid hormone receptor availability. As such, PER2 may create a hormonal steady state at implantation. As stated previously, PRIP-1 may have a similar functional protective role by enabling minor progesterone flux without activation of an apoptotic response.

As such, PER2 and PRIP-1 act as mediators of endometrial autonomy, isolating the endometrium from variations of environmental inputs. Further work examining the balance between PER2, PRIP-1 and daily endometrial progesterone concentrations would provide insight into how fluctuations in this steroid hormone affect reproductive outcome. It can be envisaged that an optimal ratio between PER2 and PRIP-1 exists and manipulation of this balance may help to determine endometrial receptivity. Conversely, aberrations in these pathways may predispose to adverse reproductive outcomes.

5.5 Implications of the Thesis.

Currently, the implications of this work are not fully apparent. However, recent successes of various chronotherapy trials suggests that timed drug delivery may reap certain benefits in various conditions (Hermida *et al.*, 2008; Levi, 2001; Wu *et al.*, 2009). As stated previously, the apparent disregard of circadian rhythms in the reproductive context seems counterintuitive, as manipulation of the clockwork may help to increase reproductive success. One theory meriting further investigation is that oscillations are inhibited at implantation to allow synchronisation between the embryo and endometrium. *In vitro* technologies maintain embryos in a non-circadian environment, and as such may be transferred to an 'out of sync' uterus. It would be interesting to investigate the effect of timed embryo transfer; however, as decidualization renders the endometrium non-oscillatory, I speculate that this may have minimal effect. Other circadian manipulations could potentially be implicated into artificial reproductive technologies. Timing of semen collection may be maximised as diurnal variations in semen quality in males has been observed with higher number and concentrations of spermatozoa apparent in specimens collected in the afternoon (Cagnacci *et al.*, 1999). Clinical trials of low dose melatonin supplements have

indicated a positive impact on the quality of oocytes and embryos, which is postulated to be attributed to an antioxidant effect (Rizzo *et al.*, 2010; Tamura *et al.*, 2008). Furthermore, removal of the pineal gland in female rats results in impaired implantation, which can be reversed by administration of melatonin (Dair *et al.*, 2008). This suggests melatonin has an active regulatory role in early pregnancy. Whilst the effect of melatonin on human stromal differentiation has not yet been investigated, melatonin receptors in mice are progressively down-regulated upon decidualization. As such, future work could assess the impact of melatonin administration on circadian rhythms within the endometrium, both across the menstrual cycle and during decidualization.

Currently, women with recurrent pregnancy loss can attend a dedicated miscarriage clinic to assess uNK cell levels in midluteal endometrial biopsies. Increased uNK cell density is associated with impaired corticosteroid signalling in the endometrium (Kuroda *et al.*, 2013), and thus, women with a greater than a 5% uNK density are offered steroid treatment. Although no association between *PER2* and uNK density was observed, *PER2* expression was inversely correlated with the number of previous pregnancy losses. Therefore, as release of glucocorticoids follows a circadian pattern (Chung *et al.*, 2011), and chronotherapeutic administration of steroids has shown to be beneficial in the treatment of asthma (Martin & Banks-Schlegel, 1998) and multiple sclerosis (Glass-Marmor *et al.*, 2007), timed drug delivery for the treatment of recurrent miscarriage may be advantageous. Further applications of chronotherapy could extend to IVF drug delivery and treatment of other reproductive pathologies, such as polycystic ovarian syndrome and endometriosis. In essence, clinical management of reproductive difficulties should include the recognition of circadian influence throughout human reproduction.

Although my work has begun to answer some important questions, many new questions arose. The role of epigenetic modifications is gaining recognition within the context of decidualization. This raises the possibility of genomic profiling examining changes in circadian and clock controlled gene modifications during the menstrual cycle and decidualization. Secondly, what and when are the signals to turn the molecular clockwork back on after implantation? Are these signals embryonically or placentally derived, and do they ensure synchrony between mother and baby? Additionally, what is the role of long non-coding RNAs in regulating decidualization specific pathways, and how do they interact with the circadian clockwork?

In conclusion, in this thesis I have characterised the mechanism of circadian regulation during decidualization for normal embryo implantation. Furthermore I have highlighted the importance of the anti-apoptotic role of the poorly characterised gene *PRIP-1.* Asynchrony during decidualization can lead to a cascade of events resulting in pregnancy complications. Only by further research into reproductive health, with especial focus on the endometrial environment, are we able to tackle the far-reaching ramifications of reproductive pathologies.

Appendices

Appendix 1: qRT-PCR primers

Gene	***Forward Primer***	***Reverse Primer***
11HSD	5’-caa tgg aag cat tgt ttg tcg-3’	5’-ggc agc aac cat tgg ata ag-3’
BMAL1	5′-gac att cct tcc agt ggc cta-3′	5′-tac cta tgt ggg ggt tct cac-3′
BRE	5’-ccc ctc agc ttt gca gaa t-3’	5’-ttg caca ag ttc ctt cac ca-3’
BRE-AS1	5’-gtg att tcg ggc agt cag g-3’	5’-acc tgg acg gtg acc tct-3’
CLOCK	5′-gac aaa gcg aaa aga gta tct ag-3′	5′-cat ctt tct agc att acc agg aa-3′
CRY1	5′-cat cct gga ccc ctg gtt-3′	5′-cac tga agc aaa aat cgc c-3′
CRY2	5′-ctg ttc aag gaa tgg gga gtg-3′	5′-ggt cat aga ggg tat gag aat tc-3′
IGFBP1	5’-cga agg ctc tcc atg tca cca-3’	5’-tgt ctc ctg cct tgg cta aac-3’
L19	5’-gcg gaa ggg tac agc caa-3’	5’-gca gcc ggg cgc aaa-3’
PER1	5′-atg gtt cca ctg ctc cat ctc-3′	5′-ccg gtc agg acc tcc tc-3′
PER2	5′-gtc cga aag ctt cgt tcc aga-3′	5′-gtc cac atc ttc ctg cag tg-3′
PER2S	5’-gag aga gtg cac tct ggt ta-3’	5’-tga ctg cag gac atc cac at-3’
PRIP-1	5’-gca gca gca tca tca agg-3’	5’-gct gct gaa aga cac ggt tt-3’
PRL	5′-aag ctg tag aga ttg agg agc aaa c-3′	5′-tca gga tga acc tgg ctg act a-3′
WNT4	5’-gca gag ccc tca tga acc t-3’	5’-cac cgc atg tgt gtc ag-3’

Appendix 2: qRT-PCR primers following ChIP

Gene	***Forward Primer***	***Reverse Primer***
PER1 E box	5′-cac gtg cgc ccg tgt gt-3′	5′-ccg att ggc tgg gga tct c-3′
PER1 Off target	5′-atg gtt cca ctg ctc cat ctc-3′	5′-ccg gtc agg acc tcc tc-3′
PER2 E box	5′-cag at gaga cgg agt cgc-3′	5′-ccc aca gct gca cgt atc-3′
PER2 Off target	5′-gtc cga aag ctt cgt tcc aga-3′	5′-gtc cac atc ttc ctg cag tg-3′

Appendix 3: Up-regulated genes: Fold Change >2.0

GENE SYMBOL	GENE NAME	FOLD CHANGE	P VALUE
SCG2	secretogranin II	40.35598	0.001753
BRE-AS1	BRE antisense RNA 1	32.68074	3.16E-05
SLC6A13	solute carrier family 6 (neurotransmitter transporter), member 13	27.9465	0.000936
RHCG	Rh family, C glycoprotein	27.79435	0.066707
IL10RA	interleukin 10 receptor, alpha	24.54574	0.065746
FOXQ1	forkhead box Q1	17.08307	0.020332
RASD2	RASD family, member 2	16.85334	0.001382
KLKB1	kallikrein B, plasma (Fletcher factor) 1	16.68146	0.090497
ALOXE3	arachidonate lipoxygenase 3	14.68952	0.043206
IRX2	iroquois homeobox 2	14.37181	0.012281
FREM2	FRAS1 related extracellular matrix protein 2	12.3521	0.032508
LPL	lipoprotein lipase	11.17344	0.314057
PHF21B	PHD finger protein 21B	9.97597	0.016302
MN1	meningioma (disrupted in balanced translocation) 1	9.971293	0.001172
KCNG3	potassium channel, voltage gated modifier subfamily G, member 3	9.665192	0.00186
SLC4A5	solute carrier family 4 (sodium bicarbonate cotransporter), member 4	9.335809	0.000133
AMH	anti-Mullerian hormone	9.308525	0.01427
C19ORF38	chromosome 19 open reading frame 38	9.026967	0.006509
NOXRED1	NADP-dependent oxidoreductase domain containing 1	8.561398	0.051487
C11ORF53	chromosome 11 open reading frame 53	8.389231	0.016988
DNAH17	dynein, axonemal, heavy chain 17	8.091413	0.011364
DNAH6	dynein, axonemal, heavy chain 6	7.558104	0.005469
HIST1H4E	histone cluster 1, H4e	7.546458	0.008295
EYA4	EYA transcriptional coactivator and phosphatase 4	7.511637	0.0572
SMOC1	SPARC related modular calcium binding 1	7.309043	0.1153
OASL	2'-5'-oligoadenylate synthetase-like	7.164212	0.000683
PDLIM3	PDZ and LIM domain 3	7.148204	0.03935
GEM	GTP binding protein overexpressed in skeletal muscle	7.08656	0.001013
BEX2	brain expressed X-linked 2	7.05143	0.002994
SPINK5	serine peptidase inhibitor, Kazal type 5	7.027469	0.003839
DNAH12	dynein, axonemal, heavy chain 12	6.98742	0.029408
NPPB	natriuretic peptide B	6.871499	0.005736
ACTN2	actinin, alpha 2	6.816899	0.045805
SPINK1	serine peptidase inhibitor, Kazal type 1	6.761275	0.020071
NEB	nebulin	6.417897	0.00741
ESM1	endothelial cell-specific molecule 1	6.385958	0.140299
NRARP	NOTCH-regulated ankyrin repeat protein	6.368778	0.002302
PKIB	protein kinase (cAMP-dependent, catalytic) inhibitor beta	6.319142	0.005423
P2RY11	purinergic receptor P2Y, G-protein coupled, 11	6.158358	0.631993
HLF	hepatic leukemia factor	5.961905	0.011033
HPX	hemopexin	5.913101	0.112248
HIST1H2BG	histone cluster 1, H2bg	5.853555	0.01341
MYH3	myosin, heavy chain 3, skeletal muscle, embryonic	5.818122	0.00038
ANKRD1	ankyrin repeat domain 1 (cardiac muscle)	5.692344	0.046822
PPARG	peroxisome proliferator-activated receptor gamma	5.684692	0.009657
KLF17	Kruppel-like factor 17	5.665481	0.00472
FOXD1	forkhead box D1	5.649442	0.065279
SLC28A3	solute carrier family 28 (concentrative nucleoside transporter), member 3	5.580816	0.159565
KRT36	keratin 36, type I	5.403947	0.036606
CBLN1	cerebellin 1 precursor	5.397832	0.018944
INHBA-AS1	INHBA antisense RNA 1	5.353157	9.62E-05
SNORA68	small nucleolar RNA, H/ACA box 68	5.32503	0.063758
CABLES1	Cdk5 and Abl enzyme substrate 1	5.24088	0.098239
WNT1	wingless-type MMTV integration site family, member 1	5.24029	0.059734
MYOM2	myomesin 2	5.207824	0.16913

ENOX1	ecto-NOX disulfide-thiol exchanger 1	5.160391	0.034179
SRRM5	serine/arginine repetitive matrix 5	5.11152	0.08521
CAPNS2	calpain, small subunit 2	5.107833	0.077856
PCSK1	proprotein convertase subtilisin/kexin type 1	5.054108	0.048695
ANKRD24	ankyrin repeat domain 24	4.962964	0.082959
KCTD16	potassium channel tetramerization domain containing 16	4.929545	0.024688
KCP	kielin/chordin-like protein	4.91864	0.187707
ARHGAP11B	Rho GTPase activating protein 11B	4.912781	0.119033
NBPF20	neuroblastoma breakpoint family, member 20	4.900556	0.093676
PTX3	pentraxin 3, long	4.854831	0.0003
TRABD2A	TraB domain containing 2A	4.854065	0.071245
COLCA2	colorectal cancer associated 2	4.847806	0.117956
ATF3	activating transcription factor 3	4.838741	0.02754
MARCH10	membrane-associated ring finger (C3HC4) 10, E3 ubiquitin protein ligase	4.816433	0.014606
CDKL2	cyclin-dependent kinase-like 2 (CDC2-related kinase)	4.743907	0.043887
PSAT1	phosphoserine aminotransferase 1	4.717655	0.046484
DNER	delta/notch-like EGF repeat containing	4.640589	0.027429
LINC00471	long intergenic non-protein coding RNA 471	4.610674	0.154331
FOXP2	forkhead box P2	4.592131	0.037046
BDNF	brain-derived neurotrophic factor	4.574596	0.005907
IRF8	interferon regulatory factor 8	4.53196	0.08196
S1PR1	sphingosine-1-phosphate receptor 1	4.527865	0.064783
HIST1H2AG	histone cluster 1, H2ag	4.526735	0.030329
AURKC	aurora kinase C	4.526693	0.038287
HILS1	histone linker H1 domain, spermatid-specific 1, pseudogene	4.509022	0.11596
PPARGC1A	peroxisome proliferator-activated receptor gamma, coactivator 1 alpha	4.503735	0.003463
LHX4	LIM homeobox 4	4.473903	0.048803
LINC01366	long intergenic non-protein coding RNA 1366	4.432831	0.003088
DDX43	DEAD (Asp-Glu-Ala-Asp) box polypeptide 43	4.431013	0.056892
IFIT2	interferon-induced protein with tetratricopeptide repeats 2	4.424701	0.000529
AKAP3	A kinase (PRKA) anchor protein 3	4.411586	0.011219
GATA4	GATA binding protein 4	4.404193	0.179117
TCP10L	t-complex 10-like	4.338226	0.290163
SERPINB5	serpin peptidase inhibitor, clade B (ovalbumin), member 5	4.336087	0.239519
TIGD3	tigger transposable element derived 3	4.293715	0.39965
CCSER1	coiled-coil serine-rich protein 1	4.290164	0.056126
DIRC3	disrupted in renal carcinoma 3	4.229444	0.001982
CGA	glycoprotein hormones, alpha polypeptide	4.195015	0.040765
CXCR4	chemokine (C-X-C motif) receptor 4	4.192616	0.004209
LRRN3	leucine rich repeat neuronal 3	4.156441	0.138117
KLF15	Kruppel-like factor 15	4.144916	0.019861
ATP2A3	ATPase, Ca++ transporting, ubiquitous	4.144021	0.028562
ITGA9	integrin, alpha 9	4.141512	0.002565
LEKR1	leucine, glutamate and lysine rich 1	4.136563	0.216708
BEX1	brain expressed, X-linked 1	4.128414	0.099792
HSPBAP1	HSPB (heat shock 27kDa) associated protein 1	4.099061	0.054849
FOS	FBJ murine osteosarcoma viral oncogene homolog	4.089312	0.075762
SMG1P3	SMG1 pseudogene 3	4.060144	0.021983
GATA3	GATA binding protein 3	4.040405	0.00482
PPP1R15A	protein phosphatase 1, regulatory subunit 15A	4.03289	0.003372
FGD4	FYVE, RhoGEF and PH domain containing 4	3.998585	0.007994
KIAA1045	KIAA1045	3.997659	0.055803
CEBPA	CCAAT/enhancer binding protein (C/EBP), alpha	3.987311	0.004566
KRTAP1-5	keratin associated protein 1-5	3.963987	0.007325
SMG1P5	SMG1 pseudogene 5	3.957599	0.014826
DDIT3	DNA-damage-inducible transcript 3	3.955194	7.6E-05
ADM2	adrenomedullin 2	3.930041	0.03292
ZNF90	zinc finger protein 90	3.914722	0.112753
C12ORF60	chromosome 12 open reading frame 60	3.871922	0.019929
SNORD68	small nucleolar RNA, C/D box 68	3.838061	0.001171
DUSP10	dual specificity phosphatase 10	3.834297	0.002378

FTO-IT1	FTO intronic transcript 1	3.833429	0.060607
CSGALNACT1	chondroitin sulfate N-acetylgalactosaminyltransferase 1	3.821244	0.000886
FAM24B	family with sequence similarity 24, member B	3.815758	0.024808
P2RX5-TAX1BP3	P2RX5-TAX1BP3 readthrough (NMD candidate)	3.805052	0.722621
SNORD83A	small nucleolar RNA, C/D box 83A	3.801698	0.237621
DLL4	delta-like 4 (Drosophila)	3.794204	0.038878
CDC25C	cell division cycle 25C	3.787476	0.004606
EPHA5-AS1	EPHA5 antisense RNA 1	3.76905	0.325557
IL11	interleukin 11	3.76375	0.187882
TACR2	tachykinin receptor 2	3.758076	0.059331
RPPH1	ribonuclease P RNA component H1	3.752795	0.554347
SLC7A5	solute carrier family 7 (amino acid transporter light chain, L system),	3.749372	0.002442
SLC7A5P2	solute carrier family 7 (amino acid transporter light chain, L system),	3.749122	0.099779
NBPF9	neuroblastoma breakpoint family, member 9	3.734495	0.020498
CLDN6	claudin 6	3.717031	0.076136
ALDH8A1	aldehyde dehydrogenase 8 family, member A1	3.712389	0.01495
CX3CR1	chemokine (C-X3-C motif) receptor 1	3.711898	0.32078
MATN1-AS1	MATN1 antisense RNA 1	3.703392	0.008789
ZNF695	zinc finger protein 695	3.696745	0.114876
EPHA6	EPH receptor A6	3.657505	0.37068
CYP19A1	cytochrome P450, family 19, subfamily A, polypeptide 1	3.632826	0.143731
SH2D5	SH2 domain containing 5	3.626265	0.002934
SYCE2	synaptonemal complex central element protein 2	3.617386	0.235453
NR4A2	nuclear receptor subfamily 4, group A, member 2	3.605151	0.002499
MAP1LC3B2	microtubule-associated protein 1 light chain 3 beta 2	3.593138	0.029082
UNC5B-AS1	UNC5B antisense RNA 1	3.588267	0.053386
TMEM88	transmembrane protein 88	3.583821	0.457157
SMG1P1	SMG1 pseudogene 1	3.58309	0.00938
PHKG1	phosphorylase kinase, gamma 1 (muscle)	3.582165	0.030849
CPNE7	copine VII	3.579597	0.001869
HLA-DRB1	major histocompatibility complex, class II, DR beta 1	3.558108	0.403745
CREBRF	CREB3 regulatory factor	3.551274	0.003898
GAD1	glutamate decarboxylase 1 (brain, 67kDa)	3.549436	0.059036
SLC46A2	solute carrier family 46, member 2	3.541732	0.128735
C9ORF169	cysteine-rich tail protein 1	3.536247	0.214178
FAM72B	family with sequence similarity 72, member B	3.533649	0.047567
ASGR1	asialoglycoprotein receptor 1	3.529779	0.060112
PKN2-AS1	PKN2 antisense RNA 1	3.527801	0.077111
SNRPN	small nuclear ribonucleoprotein polypeptide N	3.495639	0.995633
FAM86B2	family with sequence similarity 86, member B2	3.490673	0.071258
PLS3-AS1	PLS3 antisense RNA 1	3.481046	0.112948
KIF2C	kinesin family member 2C	3.465041	0.009244
LRRC70	leucine rich repeat containing 70	3.45518	0.060524
GRAP2	GRB2-related adaptor protein 2	3.452644	0.265733
TFAP2A	transcription factor AP-2 alpha (activating enhancer binding protein 2	3.446071	0.018679
FAM46A	family with sequence similarity 46, member A	3.436669	0.003308
TINCR	tissue differentiation-inducing non-protein coding RNA	3.431167	0.012816
HLA-DQA1	major histocompatibility complex, class II, DQ alpha 1	3.42158	0.261549
CHGB	chromogranin B	3.417227	0.018933
SLC6A9	solute carrier family 6 (neurotransmitter transporter, glycine), member 9	3.41713	0.079271
THBD	thrombomodulin	3.416427	0.005182
BACH2	BTB and CNC homology 1, basic leucine zipper transcription factor 2	3.41415	0.042734
C12ORF36	long intergenic non-protein coding RNA 1559	3.41364	0.51862
LINC00174	long intergenic non-protein coding RNA 174	3.411484	0.003242
ZNF844	zinc finger protein 844	3.404071	0.00087
TSLP	thymic stromal lymphopoietin	3.398721	0.135685
DGKI	diacylglycerol kinase, iota	3.385548	0.003711
MSR1	macrophage scavenger receptor 1	3.372855	0.232299
HIST1H3D	histone cluster 1, H3d	3.367563	0.073497
GLS2	glutaminase 2 (liver, mitochondrial)	3.36406	0.14138
HERC5	HECT and RLD domain containing E3 ubiquitin protein ligase 5	3.362692	0.043984

PDK4	pyruvate dehydrogenase kinase, isozyme 4	3.356822	0.003353
VLDLR-AS1	VLDLR antisense RNA 1	3.354724	0.040397
GLP2R	glucagon-like peptide 2 receptor	3.354036	0.413873
UBE2C	ubiquitin-conjugating enzyme E2C	3.341854	0.000386
NBPF8	neuroblastoma breakpoint family, member 8	3.334013	0.017878
ARHGEF4	Rho guanine nucleotide exchange factor (GEF) 4	3.33142	0.10563
LURAP1L	leucine rich adaptor protein 1-like	3.328002	8.5E-05
PHGDH	phosphoglycerate dehydrogenase	3.324223	0.023078
MIR1204	microRNA 1204	3.318889	0.065666
GPR158	G protein-coupled receptor 158	3.317338	0.406191
TLL1	tolloid-like 1	3.316414	0.025383
ENTPD3-AS1	ENTPD3 antisense RNA 1	3.315203	0.069427
LSMEM1	leucine-rich single-pass membrane protein 1	3.307779	0.012312
CYP21A2	cytochrome P450, family 21, subfamily A, polypeptide 2	3.307422	0.16019
KLF4	Kruppel-like factor 4 (gut)	3.298949	0.070299
TRPM6	transient receptor potential cation channel, subfamily M, member 6	3.297833	0.005948
HGF	hepatocyte growth factor (hepapoietin A; scatter factor)	3.292272	0.06738
TRPA1	transient receptor potential cation channel, subfamily A, member 1	3.277529	0.082234
GJA4	gap junction protein, alpha 4, 37kDa	3.259821	0.140384
PTPRR	protein tyrosine phosphatase, receptor type, R	3.259629	0.027492
EREG	epiregulin	3.244596	0.155931
CFL1P1	cofilin 1 (non-muscle) pseudogene 1	3.235453	0.104329
ZNF331	zinc finger protein 331	3.220076	0.005526
PDE2A	phosphodiesterase 2A, cGMP-stimulated	3.217862	2.02E-05
CSRNP1	cysteine-serine-rich nuclear protein 1	3.212832	0.015226
SGCG	sarcoglycan, gamma (35kDa dystrophin-associated glycoprotein)	3.198142	0.044676
TSPAN8	tetraspanin 8	3.196236	0.022856
PILRA	paired immunoglobin-like type 2 receptor alpha	3.19339	0.235682
DNM1P46	dynamin 1 pseudogene 46	3.184432	0.153544
C14ORF105	chromosome 14 open reading frame 105	3.161444	0.468984
ULBP1	UL16 binding protein 1	3.15282	0.001193
GABBR2	gamma-aminobutyric acid (GABA) B receptor, 2	3.150347	0.116238
KRT86	keratin 86, type II	3.136028	0.051083
PLK1	polo-like kinase 1	3.128484	0.018114
JMY	junction mediating and regulatory protein, p53 cofactor	3.115133	0.005135
HIF1A-AS2	HIF1A antisense RNA 2	3.111121	0.00835
USP6	ubiquitin specific peptidase 6	3.093671	0.656691
HIST2H2AC	histone cluster 2, H2ac	3.082679	0.083428
CLEC4E	C-type lectin domain family 4, member E	3.066077	0.455286
DCAF4L1	DDB1 and CUL4 associated factor 4-like 1	3.063424	0.012132
MS4A7	membrane-spanning 4-domains, subfamily A, member 7	3.055027	0.293386
CDCA8	cell division cycle associated 8	3.052697	0.009945
TMEM178B	transmembrane protein 178B	3.049165	0.220627
LINC00242	long intergenic non-protein coding RNA 242	3.040287	0.127377
SYT16	synaptotagmin XVI	3.028402	0.379503
FLRT3	fibronectin leucine rich transmembrane protein 3	3.023931	0.000168
BMP6	bone morphogenetic protein 6	3.023781	0.142744
IL33	interleukin 33	3.021821	0.266084
GLDC	glycine dehydrogenase (decarboxylating)	3.020976	0.735582
BCL2L10	BCL2-like 10 (apoptosis facilitator)	3.020695	0.016494
MT2A	metallothionein 2A	3.013131	0.080466
KLK1	kallikrein 1	3.012437	0.581218
LAT2	linker for activation of T cells family, member 2	3.011897	0.020368
BOK-AS1	BOK antisense RNA 1	3.00487	0.571666
C4ORF19	chromosome 4 open reading frame 19	3.001861	0.002093
FGF7	fibroblast growth factor 7	2.998131	0.040102
IL17B	interleukin 17B	2.997338	0.18843
CHRM2	cholinergic receptor, muscarinic 2	2.995387	0.159552
ESAM	endothelial cell adhesion molecule	2.986536	0.439963
PTGIS	prostaglandin I2 (prostacyclin) synthase	2.98525	0.044228
LRRC37B	leucine rich repeat containing 37B	2.975165	0.001956

CCT6P3	chaperonin containing TCP1, subunit 6 (zeta) pseudogene 3	2.972086	0.00036
RPL13AP20	ribosomal protein L13a pseudogene 20	2.969018	0.028632
C10ORF10	chromosome 10 open reading frame 10	2.967802	0.009181
CHL1	cell adhesion molecule L1-like	2.967166	0.072234
SLC6A2	solute carrier family 6 (neurotransmitter transporter), member 2	2.963779	0.171125
RPSAP52	ribosomal protein SA pseudogene 52	2.963653	0.225569
C2ORF66	chromosome 2 open reading frame 66	2.962743	0.00748
AGAP11	ankyrin repeat and GTPase domain Arf GTPase activating protein 11	2.94869	0.025456
SMG1P2	SMG1 pseudogene 2	2.943823	8.05E-06
ALS2CR12	amyotrophic lateral sclerosis 2 (juvenile) chromosome region, candidate	2.941992	0.198586
ZGLP1	zinc finger, GATA-like protein 1	2.934546	0.087072
MAP7	microtubule-associated protein 7	2.933407	0.000628
ADAMTS9-AS2	ADAMTS9 antisense RNA 2	2.923742	0.010753
KLF2	Kruppel-like factor 2	2.920857	0.027027
DEPDC1	DEP domain containing 1	2.916187	0.093451
HSD17B2	hydroxysteroid (17-beta) dehydrogenase 2	2.899715	0.058877
KDR	kinase insert domain receptor	2.894599	0.132142
CXCL2	chemokine (C-X-C motif) ligand 2	2.89343	0.052264
SLC7A5P1	solute carrier family 7 (amino acid transporter light chain, L system),	2.888839	0.058606
SNORD16	small nucleolar RNA, C/D box 16	2.885772	0.150891
SLC1A3	solute carrier family 1 (glial high affinity glutamate transporter), member 3	2.882991	0.893452
MEF2BNBMEF2B	MEF2BNB-MEF2B readthrough	2.880342	0.0022
FGF9	fibroblast growth factor 9	2.866673	0.08697
UPK1A	uroplakin 1A	2.864375	0.210993
TRIB1	tribbles pseudokinase 1	2.863277	0.001133
LRRC37A	leucine rich repeat containing 37A	2.860609	0.19199
LINC00941	long intergenic non-protein coding RNA 941	2.848847	0.992183
MAST1	microtubule associated serine/threonine kinase 1	2.834263	0.073894
TMEM74	transmembrane protein 74	2.833628	0.767981
S100A14	S100 calcium binding protein A14	2.832583	0.001147
S100A14	S100 calcium binding protein A11 pseudogene 1	2.830217	0.147091
OLAH	oleoyl-ACP hydrolase	2.828839	0.493026
FAM83F	family with sequence similarity 83, member F	2.817513	0.001935
KIT	v-kit Hardy-Zuckerman 4 feline sarcoma viral oncogene homolog	2.817387	0.170283
C1ORF162	chromosome 1 open reading frame 162	2.813095	0.001614
HIST1H4H	histone cluster 1, H4h	2.811635	0.469863
SERPINF2	serpin peptidase inhibitor, clade F (alpha-2 antiplasmin, pigment	2.811199	0.000438
ZNF670	zinc finger protein 670	2.807234	0.151184
FCER1G	Fc fragment of IgE, high affinity I, receptor for; gamma polypeptide	2.806785	0.003494
FAM83D	family with sequence similarity 83, member D	2.806312	0.070823
TLR9	toll-like receptor 9	2.801498	0.043087
CYP26B1	cytochrome P450, family 26, subfamily B, polypeptide 1	2.791304	0.150797
FGF17	fibroblast growth factor 17	2.789151	0.177747
PATL2	protein associated with topoisomerase II homolog 2 (yeast)	2.779975	0.00028
ITPRIP	inositol 1,4,5-trisphosphate receptor interacting protein	2.778692	0.098644
FAM160A1	family with sequence similarity 160, member A1	2.777415	0.002822
PTHLH	parathyroid hormone-like hormone	2.77606	0.001137
STC2	stanniocalcin 2	2.775216	0.001636
HMOX1	heme oxygenase 1	2.772826	0.00456
PMAIP1	phorbol-12-myristate-13-acetate-induced protein 1	2.772025	0.533701
UPK2	uroplakin 2	2.768118	0.225917
ZMAT1	zinc finger, matrin-type 1	2.764995	0.199847
C9	complement component 9	2.762244	0.026707
KIF4A	kinesin family member 4A	2.761674	0.000178
STX3	syntaxin 3	2.761272	0.140042
PRSS27	protease, serine 27	2.759722	0.355863
USP2-AS1	USP2 antisense RNA 1 (head to head)	2.75144	0.209125
SAMD13	sterile alpha motif domain containing 13	2.746362	0.000804
AEN	apoptosis enhancing nuclease	2.742265	0.017433
SKA1	spindle and kinetochore associated complex subunit 1	2.738621	0.219965
CHIT1	chitinase 1 (chitotriosidase)	2.738621	0.125632

SCARNA9	small Cajal body-specific RNA 9	2.738621	0.105394
STOX2	storkhead box 2	2.738218	0.002465
PLD6	phospholipase D family, member 6	2.736885	0.100641
TCF21	transcription factor 21	2.733878	0.000183
OTUD1	OTU deubiquitinase 1	2.732984	0.345331
ADRB2	adrenoceptor beta 2, surface	2.731529	0.206695
GDF6	growth differentiation factor 6	2.729113	0.013053
GATM	glycine amidinotransferase (L-arginine:glycine amidinotransferase)	2.726154	0.016816
SPATA25	spermatogenesis associated 25	2.719146	0.005007
FAM181B	family with sequence similarity 181, member B	2.717419	0.007078
UTS2B	urotensin 2B	2.716809	0.23684
LINC00622	long intergenic non-protein coding RNA 622	2.711801	0.23181
MMP27	matrix metallopeptidase 27	2.701506	0.01495
BUB1B	BUB1 mitotic checkpoint serine/threonine kinase B	2.699532	0.878053
CATSPERG	catsper channel auxiliary subunit gamma	2.697429	0.297261
SLC22A1	solute carrier family 22 (organic cation transporter), member 1	2.696197	0.071979
ANGPTL4	angiopoietin-like 4	2.695557	0.006628
AURKA	aurora kinase A	2.695076	0.042552
RRAGD	Ras-related GTP binding D	2.692067	0.047623
BMP7	bone morphogenetic protein 7	2.688387	0.587287
NPFFR2	neuropeptide FF receptor 2	2.687333	0.124757
NETO1	neuropilin (NRP) and tolloid (TLL)-like 1	2.68374	0.16071
KIF18A	kinesin family member 18A	2.681873	0.254663
IL12A	interleukin 12A	2.681686	0.190047
ASCL2	achaete-scute family bHLH transcription factor 2	2.678214	0.675292
PCLO	piccolo presynaptic cytomatrix protein	2.669993	0.00954
CDC20	cell division cycle 20	2.667545	0.225836
FOXF2	forkhead box F2	2.665554	0.000382
NR4A3	nuclear receptor subfamily 4, group A, member 3	2.664375	0.030398
NUF2	NUF2, NDC80 kinetochore complex component	2.663668	0.00047
AVPI1	arginine vasopressin-induced 1	2.660481	0.112498
KCNH1	potassium channel, voltage gated eag related subfamily H, member 1	2.656892	0.000328
BMP2	bone morphogenetic protein 2	2.650371	0.140596
ACVR2B-AS1	ACVR2B antisense RNA 1	2.648724	0.190385
VWCE	von Willebrand factor C and EGF domains	2.642559	0.003169
KRT81	keratin 81, type II	2.641219	0.237881
HAS2	hyaluronan synthase 2	2.640043	0.420347
PILRB	paired immunoglobin-like type 2 receptor beta	2.638555	0.004119
CDK1	cyclin-dependent kinase 1	2.637401	0.062174
USP44	ubiquitin specific peptidase 44	2.631198	0.187157
GSG1	germ cell associated 1	2.631082	0.104538
NALCN	sodium leak channel, non selective	2.627576	0.443859
MYH7B	myosin, heavy chain 7B, cardiac muscle, beta	2.626637	0.243178
TBX18	T-box 18	2.626302	0.071711
GEMIN8P4	gem (nuclear organelle) associated protein 8 pseudogene 4	2.626182	0.033863
PKD1L1	polycystic kidney disease 1 like 1	2.61998	0.208156
ASPM	asp (abnormal spindle) homolog, microcephaly associated (Drosophila)	2.617089	0.089505
CCDC11	cilia and flagella associated protein 53	2.615061	0.005585
USP36	ubiquitin specific peptidase 36	2.614838	0.026783
MAFF	v-maf avian musculoaponeurotic fibrosarcoma oncogene homolog F	2.613701	0.252083
PXDNL	peroxidasin-like	2.61145	0.092769
HTR1B	5-hydroxytryptamine (serotonin) receptor 1B, G protein-coupled	2.611387	0.19888
KIF14	kinesin family member 14	2.607657	0.161715
EBF3	early B-cell factor 3	2.607335	0.150129
HK2	hexokinase 2	2.604334	0.050532
DEPDC1B	DEP domain containing 1B	2.596975	0.874854
CALB1	calbindin 1, 28kDa	2.593534	0.657529
TBX4	T-box 4	2.5875	0.009518
DTNA	dystrobrevin, alpha	2.58688	0.085829
CCDC62	coiled-coil domain containing 62	2.586776	0.085929
GFRA2	GDNF family receptor alpha 2	2.586028	0.010237

MYPN	myopalladin	2.585581	0.043464
CD177	CD177 molecule	2.576405	0.041124
CCDC150	coiled-coil domain containing 150	2.574954	0.01177
JMJD1C-AS1	JMJD1C antisense RNA 1	2.571052	0.116094
NBPF10	neuroblastoma breakpoint family, member 10	2.568466	0.035398
C7ORF61	chromosome 7 open reading frame 61	2.565686	0.831401
LRRN4	leucine rich repeat neuronal 4	2.563496	0.310325
SCARNA17	small Cajal body-specific RNA 17	2.553329	0.026275
IDNK	idnK, gluconokinase homolog (E. coli)	2.552774	0.03603
LINC00673	long intergenic non-protein coding RNA 673	2.552298	0.000728
MAP3K7CL	MAP3K7 C-terminal like	2.551774	0.344523
SCGB1D2	secretoglobin, family 1D, member 2	2.551659	0.085988
C16ORF96	chromosome 16 open reading frame 96	2.55022	0.003179
PIWIL4	piwi-like RNA-mediated gene silencing 4	2.545824	0.015438
RASGRP3	RAS guanyl releasing protein 3 (calcium and DAG-regulated)	2.54453	0.053963
C19ORF18	chromosome 19 open reading frame 18	2.542031	0.186088
HIST2H2BA	histone cluster 2, H2ba (pseudogene)	2.54135	0.00087
TMEM79	transmembrane protein 79	2.540579	0.00139
CLEC4A	C-type lectin domain family 4, member A	2.539739	0.000101
ABHD17C	abhydrolase domain containing 17C	2.539493	0.053977
GPR183	G protein-coupled receptor 183	2.536257	0.134906
SOX11	SRY (sex determining region Y)-box 11	2.536084	0.146917
KIAA1875	KIAA1875	2.533882	0.306065
CENPE	centromere protein E, 312kDa	2.533435	0.105337
SLC4A4	solute carrier family 4 (sodium bicarbonate cotransporter), member 4	2.532326	0.194606
INHBA	inhibin, beta A	2.530978	0.058933
ENTPD2	ectonucleoside triphosphate diphosphohydrolase 2	2.529541	0.625072
SCNN1B	sodium channel, non voltage gated 1 beta subunit	2.52658	0.108667
KLRD1	killer cell lectin-like receptor subfamily D, member 1	2.526456	0.352309
RNF39	ring finger protein 39	2.517664	0.025083
RGS6	regulator of G-protein signaling 6	2.513074	0.003273
NUAK1	NUAK family, SNF1-like kinase, 1	2.507613	0.009007
OVGP1	oviductal glycoprotein 1, 120kDa	2.507483	0.026761
GTSE1	G-2 and S-phase expressed 1	2.506531	0.361392
CIB4	calcium and integrin binding family member 4	2.504769	0.058158
KLHL7-AS1	KLHL7 antisense RNA 1 (head to head)	2.50334	0.051407
SLC6A12	solute carrier family 6 (neurotransmitter transporter), member 12	2.502656	0.252082
VMO1	vitelline membrane outer layer 1 homolog (chicken)	2.500073	0.069923
PLD5	phospholipase D family, member 5	2.500004	0.00559
TGFB2	transforming growth factor, beta 2	2.499759	0.015629
NANOS1	nanos homolog 1 (Drosophila)	2.498525	0.125088
STAC	SH3 and cysteine rich domain	2.496651	0.137428
GDF5	growth differentiation factor 5	2.492046	0.642754
KLK11	kallikrein-related peptidase 11	2.492012	0.001748
SLC3A2	solute carrier family 3 (amino acid transporter heavy chain), member 2	2.490633	0.196897
CENPF	centromere protein F, 350/400kDa	2.488301	6.92E-05
PVT1	Pvt1 oncogene (non-protein coding)	2.482566	0.063677
GK	glycerol kinase	2.48128	0.03617
EN2	engrailed homeobox 2	2.472678	0.30871
PPM1E	protein phosphatase, Mg2+/Mn2+ dependent, 1E	2.468831	0.046382
FOSB	FBJ murine osteosarcoma viral oncogene homolog B	2.467385	0.093423
AOC2	amine oxidase, copper containing 2 (retina-specific)	2.466604	0.021875
ATP6AP1L	ATPase, H+ transporting, lysosomal accessory protein 1-like	2.466266	0.447371
CDKN2B-AS1	CDKN2B antisense RNA 1	2.465602	0.214359
BATF3	basic leucine zipper transcription factor, ATF-like 3	2.462767	0.894741
LINC01301	long intergenic non-protein coding RNA 1301	2.459661	0.044289
B4GALNT2	beta-1,4-N-acetyl-galactosaminyl transferase 2	2.459601	0.032996
C2ORF82	chromosome 2 open reading frame 82	2.459247	0.902599
SNORD45C	small nucleolar RNA, C/D box 45C	2.45917	0.573722
C14ORF182	long intergenic non-protein coding RNA 1588	2.45604	0.028296
FIGN	fidgetin	2.455922	0.02084

KCNJ8	potassium channel, inwardly rectifying subfamily J, member 8	2.455736	0.008565
ABL2	ABL proto-oncogene 2, non-receptor tyrosine kinase	2.455698	0.013345
CCNB1	cyclin B1	2.454787	0.190681
VWA3A	von Willebrand factor A domain containing 3A	2.453681	0.57783
NHLH1	nescient helix loop helix 1	2.44586	0.017161
C11ORF87	chromosome 11 open reading frame 87	2.444549	0.039847
ASNS	asparagine synthetase (glutamine-hydrolyzing)	2.443798	0.000473
THUMPD2	THUMP domain containing 2	2.443342	0.120349
POLQ	polymerase (DNA directed), theta	2.443227	0.0583
MMP12	matrix metallopeptidase 12	2.442603	0.20469
SNORD23	small nucleolar RNA, C/D box 23	2.440868	0.033384
CDCA2	cell division cycle associated 2	2.440488	0.164396
MGAT4A	mannosyl (alpha-1,3-)-glycoprotein beta-1,4-N-	2.439903	0.29474
LEMD1	LEM domain containing 1	2.434859	0.006677
CFP	complement factor properdin	2.425606	0.336695
HNF4G	hepatocyte nuclear factor 4, gamma	2.424567	0.012321
FAM167A	family with sequence similarity 167, member A	2.420792	0.342234
ZNF560	zinc finger protein 560	2.419369	0.159992
SVILP1	supervillin pseudogene 1	2.417527	0.588531
NEK2	NIMA-related kinase 2	2.415884	5.83E-05
WNT10B	wingless-type MMTV integration site family, member 10B	2.4147	0.081497
NPIPB9	nuclear pore complex interacting protein family, member B9	2.413094	0.002909
SLC25A25	solute carrier family 25 (mitochondrial carrier; phosphate carrier), member	2.412549	0.000429
IFRD1	interferon-related developmental regulator 1	2.409321	0.279911
SCN9A	sodium channel, voltage gated, type IX alpha subunit	2.408863	0.082408
REREP3	arginine-glutamic acid dipeptide (RE) repeats pseudogene 3	2.407186	0.022653
IKZF3	IKAROS family zinc finger 3 (Aiolos)	2.401815	0.066283
TPI1P2	triosephosphate isomerase 1 pseudogene 2	2.398885	0.041891
TRIM54	tripartite motif containing 54	2.397828	0.039532
SHC2	SHC (Src homology 2 domain containing) transforming protein 2	2.397558	0.03579
FAM132B	family with sequence similarity 132, member B	2.386437	0.132016
CKAP2L	cytoskeleton associated protein 2-like	2.386357	0.00054
CCT6P1	chaperonin containing TCP1, subunit 6 (zeta) pseudogene 1	2.385375	0.163316
KRTAP20-2	keratin associated protein 20-2	2.384576	2.88E-05
ACKR3	atypical chemokine receptor 3	2.380998	0.05919
SIK1	salt-inducible kinase 1	2.380654	0.057035
PMF1-BGLAP	PMF1-BGLAP readthrough	2.377103	0.004636
DUSP16	dual specificity phosphatase 16	2.374763	0.882022
WNT10A	wingless-type MMTV integration site family, member 10A	2.374523	0.00369
LINC00473	long intergenic non-protein coding RNA 473	2.373688	0.003561
BBC3	BCL2 binding component 3	2.37103	0.366703
LRIT3	leucine-rich repeat, immunoglobulin-like and transmembrane domains 3	2.370031	0.025703
CENPA	centromere protein A	2.367542	0.268104
WWTR1-AS1	WWTR1 antisense RNA 1	2.36612	0.019376
ZNF521	zinc finger protein 521	2.358332	0.130349
C9ORF152	chromosome 9 open reading frame 152	2.356503	0.004066
CELF2	CUGBP, Elav-like family member 2	2.35591	0.000611
MYO16	myosin XVI	2.348411	0.038806
PBX4	pre-B-cell leukemia homeobox 4	2.348337	0.002861
YRDC	yrdC N(6)-threonylcarbamoyltransferase domain containing	2.348197	0.002295
DUSP1	dual specificity phosphatase 1	2.345399	0.941845
POU2F3	POU class 2 homeobox 3	2.345278	0.037734
ZNF442	zinc finger protein 442	2.343016	0.00143
PFKFB4	6-phosphofructo-2-kinase/fructose-2,6-biphosphatase 4	2.342982	0.014713
FGD5P1	FYVE, RhoGEF and PH domain containing 5 pseudogene 1	2.342419	0.231017
DDX12P	DEAD/H (Asp-Glu-Ala-Asp/His) box polypeptide 12, pseudogene	2.34183	0.466015
CXCL6	chemokine (C-X-C motif) ligand 6	2.341753	0.000259
WEE1	WEE1 G2 checkpoint kinase	2.341618	0.046812
PRC1	protein regulator of cytokinesis 1	2.339543	0.074948
ATE1-AS1	ATE1 antisense RNA 1 (head to head)	2.336419	0.010846
IQGAP3	IQ motif containing GTPase activating protein 3	2.334681	0.244914

FLRT1	fibronectin leucine rich transmembrane protein 1	2.331191	0.477853
VSIG2	V-set and immunoglobulin domain containing 2	2.330027	0.057526
HS3ST1	heparan sulfate (glucosamine) 3-O-sulfotransferase 1	2.329577	0.471514
TMC5	transmembrane channel-like 5	2.329472	0.350338
C20ORF26	cilia and flagella associated protein 61	2.324676	0.052592
KCNH5	potassium channel, voltage gated eag related subfamily H, member 5	2.322501	0.962657
RDH5	retinol dehydrogenase 5 (11-cis/9-cis)	2.321924	0.009577
RBKS	ribokinase	2.32021	0.330662
STAM-AS1	STAM antisense RNA 1 (head to head)	2.318868	0.176761
HERC2P4	hect domain and RLD 2 pseudogene 4	2.315731	0.309708
LRRC32	leucine rich repeat containing 32	2.315183	0.003547
EPB41L4A-AS1	EPB41L4A antisense RNA 1	2.313901	0.005432
SYCP2L	synaptonemal complex protein 2-like	2.312575	0.056284
ZNF763	zinc finger protein 763	2.310954	0.005003
ZNF625	zinc finger protein 625	2.309777	0.021094
BAMBI	BMP and activin membrane-bound inhibitor	2.307777	0.099217
SHISA2	shisa family member 2	2.306207	0.284491
PTGS2	prostaglandin-endoperoxide synthase 2 (prostaglandin G/H synthase and	2.302252	0.085859
TAS2R20	taste receptor, type 2, member 20	2.302012	0.275785
FAM189A1	family with sequence similarity 189, member A1	2.301338	0.143271
IL1RL1	interleukin 1 receptor-like 1	2.300686	0.008171
CCDC148	coiled-coil domain containing 148	2.300551	4.45E-05
DUSP5	dual specificity phosphatase 5	2.299975	0.039842
RUNX3	runt-related transcription factor 3	2.298745	0.550284
PTPRC	protein tyrosine phosphatase, receptor type, C	2.298133	0.076445
TMEM253	transmembrane protein 253	2.296439	0.332836
RGS18	regulator of G-protein signaling 18	2.295255	0.304232
GPR35	G protein-coupled receptor 35	2.292942	0.057361
SOX8	SRY (sex determining region Y)-box 8	2.290589	0.059043
RRAD	Ras-related associated with diabetes	2.289981	0.010769
CKS1B	CDC28 protein kinase regulatory subunit 1B	2.28855	0.020883
CPA4	carboxypeptidase A4	2.288268	0.413293
SCNN1G	sodium channel, non voltage gated 1 gamma subunit	2.287776	0.002352
TACC3	transforming, acidic coiled-coil containing protein 3	2.284766	0.187372
WNT11	wingless-type MMTV integration site family, member 11	2.277453	0.261846
NAPA-AS1	NAPA antisense RNA 1	2.277167	0.155573
LONRF3	LON peptidase N-terminal domain and ring finger 3	2.276886	0.139262
LINC00842	long intergenic non-protein coding RNA 842	2.275593	0.003982
TMEM9B-AS1	TMEM9B antisense RNA 1	2.270741	0.320306
PSG2	pregnancy specific beta-1-glycoprotein 2	2.270317	0.233545
C5AR1	complement component 5a receptor 1	2.270083	0.330286
NGFR	nerve growth factor receptor	2.267948	0.027037
SPAG5	sperm associated antigen 5	2.267825	0.172922
COLGALT2	collagen beta(1-O)galactosyltransferase 2	2.267676	0.043446
TMEM44-AS1	TMEM44 antisense RNA 1	2.267355	0.000555
MB21D2	Mab-21 domain containing 2	2.266913	0.270817
VAV3	vav 3 guanine nucleotide exchange factor	2.26685	0.255612
CD22	CD22 molecule	2.266595	0.167596
SLC11A1	solute carrier family 11 (proton-coupled divalent metal ion transporter),	2.264512	0.179058
KIF15	kinesin family member 15	2.261292	0.020101
IL1A	interleukin 1, alpha	2.257896	0.236211
KIF20B	kinesin family member 20B	2.25722	0.009362
CDH26	cadherin 26	2.257064	0.329296
LINC00643	long intergenic non-protein coding RNA 643	2.25227	0.530408
C9ORF135	chromosome 9 open reading frame 135	2.250492	0.088925
GTF2H2C_2	GTF2H2 family member C, copy 2	2.247436	0.38315
CYBB	cytochrome b-245, beta polypeptide	2.242709	0.329114
CNKSR1	connector enhancer of kinase suppressor of Ras 1	2.24263	0.114731
KYNU	kynureninase	2.241372	0.020501
PTTG1	pituitary tumor-transforming 1	2.240483	0.000586
HLX	H2.0-like homeobox	2.240463	0.009578

NFIL3	nuclear factor, interleukin 3 regulated	2.239077	0.027318
MT1L	metallothionein 1L (gene/pseudogene)	2.238269	0.263579
FAM86FP	family with sequence similarity 86, member F, pseudogene	2.236342	0.002069
UOX	urate oxidase, pseudogene	2.234357	0.021498
PROX1	prospero homeobox 1	2.23383	0.163992
HGFAC	HGF activator	2.232926	0.076288
NOG	noggin	2.232593	0.012179
GLCCI1	glucocorticoid induced 1	2.231947	0.003931
SMC5-AS1	SMC5 antisense RNA 1 (head to head)	2.231939	0.053677
WDR62	WD repeat domain 62	2.225934	0.19383
MT1M	metallothionein 1M	2.225534	0.001346
GDF15	growth differentiation factor 15	2.221188	0.061062
JADE1	jade family PHD finger 1	2.220952	0.122934
HMMR	hyaluronan-mediated motility receptor (RHAMM)	2.220346	0.018487
CCL26	chemokine (C-C motif) ligand 26	2.220251	5.23E-05
ADM	adrenomedullin	2.219307	0.90979
FAM106CP	family with sequence similarity 106, member C, pseudogene	2.214575	0.238022
RDH14	retinol dehydrogenase 14 (all-trans/9-cis/11-cis)	2.214338	0.298775
OTUD7A	OTU deubiquitinase 7A	2.211456	0.074679
CASC8	cancer susceptibility candidate 8 (non-protein coding)	2.207733	0.147376
ERN1	endoplasmic reticulum to nucleus signaling 1	2.207716	0.031409
ZNF620	zinc finger protein 620	2.206401	0.003268
HIST1H1C	histone cluster 1, H1c	2.205077	0.101382
SEMA3A	sema domain, immunoglobulin domain (Ig), short basic domain, secreted,	2.200258	0.701298
DDX11-AS1	DDX11 antisense RNA 1	2.199701	0.009246
TTC21A	tetratricopeptide repeat domain 21A	2.197934	0.29345
OSER1-AS1	OSER1 antisense RNA 1 (head to head)	2.197382	0.264623
LINC00933	long intergenic non-protein coding RNA 933	2.195371	0.201304
HTR2A	5-hydroxytryptamine (serotonin) receptor 2A, G protein-coupled	2.194944	0.182416
FAM129A	family with sequence similarity 129, member A	2.193413	0.174837
HLA-DRA	major histocompatibility complex, class II, DR alpha	2.193272	0.030935
SLC13A5	solute carrier family 13 (sodium-dependent citrate transporter), member 5	2.192081	0.00743
TG	thyroglobulin	2.191217	0.685064
SNORD69	small nucleolar RNA, C/D box 69	2.190781	0.630862
TXK	TXK tyrosine kinase	2.190208	0.07166
GRB14	growth factor receptor-bound protein 14	2.188137	0.038561
C11ORF96	chromosome 11 open reading frame 96	2.185818	0.481074
GREM2	gremlin 2, DAN family BMP antagonist	2.182463	0.03729
FANCD2	Fanconi anemia, complementation group D2	2.181591	0.06578
ATP2C2	ATPase, Ca++ transporting, type 2C, member 2	2.177762	0.009037
GKAP1	G kinase anchoring protein 1	2.176509	0.003273
LINC00312	long intergenic non-protein coding RNA 312	2.172506	0.111326
HOXD-AS2	HOXD cluster antisense RNA 2	2.169118	0.126575
IL13RA2	interleukin 13 receptor, alpha 2	2.165819	0.045398
FLVCR2	feline leukemia virus subgroup C cellular receptor family, member 2	2.165572	0.426014
TPTE2	transmembrane phosphoinositide 3-phosphatase and tensin homolog 2	2.165166	0.00726
OVOL2	ovo-like zinc finger 2	2.163228	0.002825
TBC1D15	TBC1 domain family, member 15	2.163224	0.260586
PSG6	pregnancy specific beta-1-glycoprotein 6	2.16269	0.013659
PGAP1	post-GPI attachment to proteins 1	2.160524	0.003891
IL4R	interleukin 4 receptor	2.157757	0.079133
CASP9	caspase 9, apoptosis-related cysteine peptidase	2.157693	0.01828
THSD1	thrombospondin, type I, domain containing 1	2.15706	0.032545
HGD	homogentisate 1,2-dioxygenase	2.156794	0.0737
BUB1	BUB1 mitotic checkpoint serine/threonine kinase	2.156388	0.002721
ELL2	elongation factor, RNA polymerase II, 2	2.152855	0.004498
SHBG	sex hormone-binding globulin	2.152652	0.045276
JUN	jun proto-oncogene	2.148369	0.358982
NPTX1	neuronal pentraxin I	2.143098	0.553208
GPR132	G protein-coupled receptor 132	2.143076	0.080764
TOP2A	topoisomerase (DNA) II alpha 170kDa	2.142692	0.017925

CREB5	cAMP responsive element binding protein 5	2.142303	0.048749
DYSF	dysferlin	2.141889	0.818732
TCTEX1D1	Tctex1 domain containing 1	2.140722	0.019389
DLGAP1-AS2	DLGAP1 antisense RNA 2	2.140428	0.062655
ABCC2	ATP-binding cassette, sub-family C (CFTR/MRP), member 2	2.138725	0.000157
TGIF1	TGFB-induced factor homeobox 1	2.137583	0.227825
PIWIL2	piwi-like RNA-mediated gene silencing 2	2.136086	0.113444
CHAC1	ChaC glutathione-specific gamma-glutamylcyclotransferase 1	2.135851	0.022689
MARC1	mitochondrial amidoxime reducing component 1	2.134405	0.006474
CDKL4	cyclin-dependent kinase-like 4	2.133749	0.130579
CHTF18	CTF18, chromosome transmission fidelity factor 18 homolog (S.	2.129102	0.72846
DDTL	D-dopachrome tautomerase-like	2.127849	0.117634
STX18-AS1	STX18 antisense RNA 1 (head to head)	2.127331	0.197896
ERVV-2	endogenous retrovirus group V, member 2	2.126191	0.103271
TAS2R5	taste receptor, type 2, member 5	2.126145	0.053322
IL18R1	interleukin 18 receptor 1	2.124003	0.861863
IFNLR1	interferon, lambda receptor 1	2.122404	0.001161
KRTAP5-AS1	KRTAP5-1/KRTAP5-2 antisense RNA 1	2.12007	0.022369
CMSS1	cms1 ribosomal small subunit homolog (yeast)	2.119727	0.327936
ANK2	ankyrin 2, neuronal	2.118739	0.11636
DUSP6	dual specificity phosphatase 6	2.118247	0.065508
OSER1	oxidative stress responsive serine-rich 1	2.117515	0.001153
FIBIN	fin bud initiation factor homolog (zebrafish)	2.116446	0.273208
SSTR1	somatostatin receptor 1	2.115884	0.144194
PROSER2	proline and serine rich 2	2.11511	0.006061
CCDC147	cilia and flagella associated protein 58	2.110141	0.059918
EID3	EP300 interacting inhibitor of differentiation 3	2.109674	0.063193
PID1	phosphotyrosine interaction domain containing 1	2.109563	0.267154
HSPA6	heat shock 70kDa protein 6 (HSP70B')	2.108911	0.092674
SNORA41	small nucleolar RNA, H/ACA box 41	2.108344	0.359851
SAMD5	sterile alpha motif domain containing 5	2.104043	0.294116
SLCO2B1	solute carrier organic anion transporter family, member 2B1	2.102214	0.902978
KCNJ15	potassium channel, inwardly rectifying subfamily J, member 15	2.099995	0.33138
NRK	Nik related kinase	2.098872	0.014514
MKX	mohawk homeobox	2.095703	0.169525
CBWD6	COBW domain containing 6	2.095603	0.007594
KIF18B	kinesin family member 18B	2.091011	0.004695
TSACC	TSSK6 activating co-chaperone	2.086825	0.875937
STX11	syntaxin 11	2.083951	0.025794
FAM209A	family with sequence similarity 209, member A	2.082286	0.078771
M1AP	meiosis 1 associated protein	2.082286	0.047692
ABCG1	ATP-binding cassette, sub-family G (WHITE), member 1	2.080872	0.02837
GABRA2	gamma-aminobutyric acid (GABA) A receptor, alpha 2	2.078895	0.594161
TAF1D	TATA box binding protein (TBP)-associated factor, RNA polymerase I, D,	2.078397	0.009115
BRCA2	breast cancer 2, early onset	2.077935	0.277313
HJURP	Holliday junction recognition protein	2.074836	0.011772
SH3RF2	SH3 domain containing ring finger 2	2.074048	0.176088
SIRT1	sirtuin 1	2.073554	0.000674
SYNPO	synaptopodin	2.07315	0.004453
RSPH4A	radial spoke head 4 homolog A (Chlamydomonas)	2.07083	0.09597
SGK1	serum/glucocorticoid regulated kinase 1	2.069261	0.554172
MND1	meiotic nuclear divisions 1 homolog (S. cerevisiae)	2.069118	0.001014
KIFC1	kinesin family member C1	2.06902	0.017454
AGTPBP1	ATP/GTP binding protein 1	2.068323	0.025333
KLHL24	kelch-like family member 24	2.066072	0.029773
C21ORF88	B3GALT5 antisense RNA 1	2.066051	0.003755
DYRK3	dual-specificity tyrosine-(Y)-phosphorylation regulated kinase 3	2.062762	0.302324
KLF6	Kruppel-like factor 6	2.061894	0.001958
ZNF582-AS1	ZNF582 antisense RNA 1 (head to head)	2.061819	0.001368
LINC00571	long intergenic non-protein coding RNA 571	2.060475	0.147205
PIK3CG	phosphatidylinositol-4,5-bisphosphate 3-kinase, catalytic subunit gamma	2.059149	0.306829

BCL6	B-cell CLL/lymphoma 6	2.058025	0.635482
KLHL41	kelch-like family member 41	2.057858	0.002811
SLC19A2	solute carrier family 19 (thiamine transporter), member 2	2.0567	0.34483
ZNF257	zinc finger protein 257	2.056224	0.017681
COBLL1	cordon-bleu WH2 repeat protein-like 1	2.054908	0.288691
LTB4R2	leukotriene B4 receptor 2	2.051448	0.777557
HSBP1L1	heat shock factor binding protein 1-like 1	2.049272	0.776186
FBXO32	F-box protein 32	2.048952	0.023585
MCF2	MCF.2 cell line derived transforming sequence	2.048733	0.001615
NKX3-1	NK3 homeobox 1	2.048291	0.093827
TNNT1	troponin T type 1 (skeletal, slow)	2.046834	0.119707
LINC00310	long intergenic non-protein coding RNA 310	2.046034	0.312179
LMNB1	lamin B1	2.044543	0.980749
KLF11	Kruppel-like factor 11	2.043974	0.001486
SNHG17	small nucleolar RNA host gene 17	2.043103	0.556727
ZC3H6	zinc finger CCCH-type containing 6	2.042724	0.005129
SPSB1	splA/ryanodine receptor domain and SOCS box containing 1	2.042645	0.054769
CIT	citron rho-interacting serine/threonine kinase	2.042483	0.004601
NR3C1	nuclear receptor subfamily 3, group C, member 1 (glucocorticoid receptor)	2.041658	0.105866
LOXL4	lysyl oxidase-like 4	2.039479	0.010183
PBK	PDZ binding kinase	2.039076	0.000329
PI3	peptidase inhibitor 3, skin-derived	2.034858	0.04962
BNC1	basonuclin 1	2.034791	0.165321
PHACTR1	phosphatase and actin regulator 1	2.034385	0.062542
AGR2	anterior gradient 2	2.033954	0.56953
ADORA3	adenosine A3 receptor	2.032531	0.170493
SLC25A33	solute carrier family 25 (pyrimidine nucleotide carrier), member 33	2.032524	0.127976
CD274	CD274 molecule	2.030926	0.006145
FLG	filaggrin	2.025603	0.007953
CTNNA2	catenin (cadherin-associated protein), alpha 2	2.025003	0.675819
CENPW	centromere protein W	2.024523	0.289229
PIGA	phosphatidylinositol glycan anchor biosynthesis, class A	2.02325	0.002616
VPREB3	pre-B lymphocyte 3	2.023111	0.005042
SH3GL1P1	SH3-domain GRB2-like 1 pseudogene 1	2.021666	0.087765
PPM1D	protein phosphatase, Mg2+/Mn2+ dependent, 1D	2.019539	0.165605
DNAJC6	DnaJ (Hsp40) homolog, subfamily C, member 6	2.019303	0.002092
KRT16	keratin 16, type I	2.018915	0.167412
MIR25	microRNA 25	2.017898	0.068395
SLC1A4	solute carrier family 1 (glutamate/neutral amino acid transporter), member	2.01723	0.147104
AFAP1L2	actin filament associated protein 1-like 2	2.014299	0.041546
RP9P	retinitis pigmentosa 9 pseudogene	2.012808	0.070512
FICD	FIC domain containing	2.011473	0.015746
C6ORF52	chromosome 6 open reading frame 52	2.011029	0.00216
OSGIN2	oxidative stress induced growth inhibitor family member 2	2.010896	0.338914
NCAPH	non-SMC condensin I complex, subunit H	2.010476	0.105437
TOX3	TOX high mobility group box family member 3	2.009449	0.066634
CPEB2	cytoplasmic polyadenylation element binding protein 2	2.009425	0.315551
EMILIN3	elastin microfibril interfacer 3	2.00934	0.042451
EMILIN3	multimerin 2	2.007223	0.005745
SUSD4	sushi domain containing 4	2.006658	0.764658
ARID3B	AT rich interactive domain 3B (BRIGHT-like)	2.00595	0.013243
TMEM71	transmembrane protein 71	2.004957	0.036808
CDC25A	cell division cycle 25A	2.003399	0.023231
TYMSOS	TYMS opposite strand	2.002887	0.344621
ZSCAN16	zinc finger and SCAN domain containing 16	2.002592	0.001873
SNORD63	small nucleolar RNA, C/D box 63	2.0017	0.301688
MMP10	matrix metallopeptidase 10	2.000415	0.130854

Appendix 4: Down-regulated genes: Fold Change <0.5

GENE SYMBOL	GENE NAME	FOLD CHANGE	P VALUE
ATP2B3	ATPase, Ca++ transporting, plasma membrane 3	0.098869	0.001708
INSRR	insulin receptor-related receptor	0.135885	0.019929
CLDN20	claudin 20	0.13821	0.000366
SLC8A1-AS1	SLC8A1 antisense RNA 1	0.140338	0.004357
MYLK3	myosin light chain kinase 3	0.142121	0.088042
IGDCC3	immunoglobulin superfamily, DCC subclass, member 3	0.143596	0.010158
NPAP1	nuclear pore associated protein 1	0.152822	0.234059
FXYD6	FXYD domain containing ion transport regulator 6	0.153192	0.072693
APOA1	apolipoprotein A-I	0.163728	0.065436
KIAA1210	KIAA1210	0.165262	0.127152
LRFN2	leucine rich repeat and fibronectin type III domain containing 2	0.168542	0.132257
STAR	steroidogenic acute regulatory protein	0.170075	0.000975
PNMA3	paraneoplastic Ma antigen 3	0.187661	0.000429
JAKMIP3	Janus kinase and microtubule interacting protein 3	0.193342	0.019728
PROK1	prokineticin 1	0.193583	0.172855
NRXN1	neurexin 1	0.199916	0.090250
RGS17	regulator of G-protein signaling 17	0.209787	0.053486
KCNIP2	Kv channel interacting protein 2	0.216627	0.000204
NUDT10	nudix (nucleoside diphosphate linked moiety X)-type motif 10	0.217543	1.25E-05
HTR1E	5-hydroxytryptamine (serotonin) receptor 1E, G protein-coupled	0.218103	0.015159
VCAM1	vascular cell adhesion molecule 1	0.21914	0.007359
TH	tyrosine hydroxylase	0.224251	0.014333
LDHD	lactate dehydrogenase D	0.23495	0.294131
AGAP2	ArfGAP with GTPase domain, ankyrin repeat and PH domain 2	0.2351	0.03005
SLC18A2	solute carrier family 18 (vesicular monoamine transporter), member 2	0.235357	0.105115
FAM124B	family with sequence similarity 124B	0.242967	0.113531
AGXT2	alanine--glyoxylate aminotransferase 2	0.248049	0.079055
SUSD5	sushi domain containing 5	0.249302	0.00202
ASTN1	astrotactin 1	0.250902	0.262441
CCL8	chemokine (C-C motif) ligand 8	0.250923	0.004559
TUB	tubby bipartite transcription factor	0.252774	0.134525
GRM7	glutamate receptor, metabotropic 7	0.258841	0.440666
TMEM35	transmembrane protein 35	0.260326	0.221635
CILP	cartilage intermediate layer protein, nucleotide pyrophosphohydrolase	0.261895	0.024731
TIE1	tyrosine kinase with immunoglobulin-like and EGF-like domains 1	0.263373	0.004527
IL12RB1	interleukin 12 receptor, beta 1	0.264821	0.012681
RNF112	ring finger protein 112	0.26599	0.003684
UNC5C	unc-5 homolog C (C. elegans)	0.266302	0.021621
PTGES2-AS1	PTGES2 antisense RNA 1 (head to head)	0.267006	0.079965
GNG2	guanine nucleotide binding protein (G protein), gamma 2	0.267549	0.034755
MIR1307	microRNA 1307	0.268323	0.24646
MSTN	Myostatin	0.268537	0.259197
NDRG4	NDRG family member 4	0.271667	0.128012
BAI1	adhesion G protein-coupled receptor B1	0.272441	0.003254
ENTPD1	ectonucleoside triphosphate diphosphohydrolase 1	0.27428	0.144811
SNORA55	small nucleolar RNA, H/ACA box 55	0.274979	0.00613
RIMBP2	RIMS binding protein 2	0.276509	0.07219
GPR20	G protein-coupled receptor 20	0.277769	0.294267
ADAM22	ADAM metallopeptidase domain 22	0.281613	0.150831
BCHE	butyrylcholinesterase	0.284942	0.005299
LRGUK	leucine-rich repeats and guanylate kinase domain containing	0.287656	0.008671
KCNB1	potassium channel, voltage gated Shab related subfamily B, member 1	0.289093	0.154694
FTCD	formimidoyltransferase cyclodeaminase	0.290813	0.044019
FAIM2	Fas apoptotic inhibitory molecule 2	0.293523	0.168667
CCR1	chemokine (C-C motif) receptor 1	0.295471	0.155518
CXCL14	chemokine (C-X-C motif) ligand 14	0.299891	0.007237

MAP2K6	mitogen-activated protein kinase kinase 6	0.307304	0.013021
MLC1	megalencephalic leukoencephalopathy with subcortical cysts 1	0.307557	0.05073
MIR641	microRNA 641	0.310459	0.212918
CRB2	crumbs family member 2	0.311363	0.044785
ENHO	energy homeostasis associated	0.31243	0.228595
CPB2-AS1	CPB2 antisense RNA 1	0.314	0.24014
SLC44A5	solute carrier family 44, member 5	0.315309	0.067067
LCNL1	lipocalin-like 1	0.31719	0.001536
MIR3605	microRNA 3605	0.317824	0.328648
CCDC116	coiled-coil domain containing 116	0.320042	0.00443
LCN1	lipocalin 1	0.321335	0.215772
TMEM229B	transmembrane protein 229B	0.321762	0.080368
IPCEF1	interaction protein for cytohesin exchange factors 1	0.321829	0.203266
AKAP5	A kinase (PRKA) anchor protein 5	0.322006	0.031401
NRTN	Neurturin	0.323115	0.092456
GABRG3	gamma-aminobutyric acid (GABA) A receptor, gamma 3	0.323749	0.002829
GCK	glucokinase (hexokinase 4)	0.32388	0.004024
SEC14L4	SEC14-like 4 (S. cerevisiae)	0.324021	0.015625
DACT3	dishevelled-binding antagonist of beta-catenin 3	0.324156	0.038714
PYGM	phosphorylase, glycogen, muscle	0.324452	0.24496
CLCN1	chloride channel, voltage-sensitive 1	0.32908	0.082666
OLFML2B	olfactomedin-like 2B	0.329419	0.098547
ARL9	ADP-ribosylation factor-like 9	0.330146	0.014419
DEFB124	defensin, beta 124	0.331061	0.038074
CDH23	cadherin-related 23	0.33263	0.260338
METTL7A	methyltransferase like 7A	0.333004	0.036769
MED14OS	MED14 opposite strand	0.33333	0.005049
KIAA1644	KIAA1644	0.334094	0.031833
KIAA0319	KIAA0319	0.33534	0.004567
NAT2	N-acetyltransferase 2 (arylamine N-acetyltransferase)	0.335671	0.291894
F2RL2	coagulation factor II (thrombin) receptor-like 2	0.340174	0.053122
COL4A6	collagen, type IV, alpha 6	0.342459	0.184529
H2BFM	H2B histone family, member M	0.34261	0.035432
EFHC2	EF-hand domain (C-terminal) containing 2	0.34342	0.038866
CRYGN	crystallin, gamma N	0.343552	0.198788
NDP	Norrie disease (pseudoglioma)	0.343828	0.248835
CORO1A	coronin, actin binding protein, 1A	0.34396	0.047852
SLC38A11	solute carrier family 38, member 11	0.345017	0.103141
ME1	malic enzyme 1, NADP(+)-dependent, cytosolic	0.345268	0.004179
ABCA13	ATP-binding cassette, sub-family A (ABC1), member 13	0.347566	0.001537
GPBAR1	G protein-coupled bile acid receptor 1	0.348361	0.016534
GPR155	G protein-coupled receptor 155	0.348389	0.009015
PCDHA10	protocadherin alpha 10	0.349549	0.043033
F13A1	coagulation factor XIII, A1 polypeptide	0.350272	0.377521
TDRD6	tudor domain containing 6	0.350369	0.16071
PTGIR	prostaglandin I2 (prostacyclin) receptor (IP)	0.351748	0.001184
KCNE2	potassium channel, voltage gated subfamily E regulatory beta subunit 2	0.35203	0.310514
JPH4	junctophilin 4	0.35304	0.005689
DOK5	docking protein 5	0.353363	0.118165
TAF7L	TAF7-like RNA polymerase II, TATA box binding protein (TBP)-associated factor, 50kDa	0.355122	0.000733
EPB41L3	erythrocyte membrane protein band 4.1-like 3	0.355208	0.000544
OGN	osteoglycin	0.35604	0.228826
EME2	essential meiotic structure-specific endonuclease subunit 2	0.356485	0.036861
KCNE3	potassium channel, voltage gated subfamily E regulatory beta subunit 3	0.356645	0.00553
ATP1B2	ATPase, Na+/K+ transporting, beta 2 polypeptide	0.357035	0.348153
TMEM63C	transmembrane protein 63C	0.359761	0.023393
DPYSL2	dihydropyrimidinase-like 2	0.36016	0.005037
TMED10P1	transmembrane emp24-like trafficking protein 10 (yeast) pseudogene 1	0.361826	0.009377
MFAP4	microfibrillar-associated protein 4	0.362302	0.068081
ANKRD34A	ankyrin repeat domain 34A	0.362467	0.000982

NNAT	Neuronatin	0.362918	0.017876
PRELP	proline/arginine-rich end leucine-rich repeat protein	0.365948	0.126195
LINC00894	long intergenic non-protein coding RNA 894	0.365952	0.052798
PLCD4	phospholipase C, delta 4	0.366218	0.00231
GCOM1	GRINL1A complex locus 1	0.366271	0.108009
NLGN1	neuroligin 1	0.366309	0.010425
SNORA71B	small nucleolar RNA, H/ACA box 71B	0.367075	0.022759
GALNT16	polypeptide N-acetylgalactosaminyltransferase 16	0.368068	0.056692
B4GALNT1	beta-1,4-N-acetyl-galactosaminyl transferase 1	0.368097	0.002055
SAMD9L	sterile alpha motif domain containing 9-like	0.369056	0.022038
CYP4B1	cytochrome P450, family 4, subfamily B, polypeptide 1	0.369263	0.110177
LSAMP	limbic system-associated membrane protein	0.3698	0.180642
LRP12	low density lipoprotein receptor-related protein 12	0.371104	0.001658
CES4A	carboxylesterase 4A	0.372345	0.019498
SELENBP1	selenium binding protein 1	0.372468	0.019709
PER2	period circadian clock 2	0.372579	0.002597
ENPP2	ectonucleotide pyrophosphatase/phosphodiesterase 2	0.372982	0.065713
WNT6	wingless-type MMTV integration site family, member 6	0.37304	0.157259
EPYC	Epiphycan	0.373514	0.168433
SOAT2	sterol O-acyltransferase 2	0.375926	0.001037
COL26A1	collagen, type XXVI, alpha 1	0.376523	0.2231
CPA1	carboxypeptidase A1 (pancreatic)	0.376603	0.041795
SEMA3G	sema domain, immunoglobulin domain (Ig), short basic domain, secreted, (semaphorin) 3G	0.377545	0.067579
GLT1D1	glycosyltransferase 1 domain containing 1	0.37767	0.012984
KLK3	kallikrein-related peptidase 3	0.378429	0.183928
ADAMTS9	ADAM metallopeptidase with thrombospondin type 1 motif, 9	0.378611	0.012479
C7	chemokine (C-X-C motif) ligand 10	0.379054	0.01652
CLEC3B	C-type lectin domain family 3, member B	0.379099	0.002208
PNMAL2	paraneoplastic Ma antigen family-like 2	0.380285	0.023818
GPD1L	glycerol-3-phosphate dehydrogenase 1-like	0.380534	0.00491
LRRC16B	leucine rich repeat containing 16B	0.380808	0.232462
PDGFD	platelet derived growth factor D	0.382451	0.0096
RGS11	regulator of G-protein signaling 11	0.383979	0.072987
LINC00908	long intergenic non-protein coding RNA 908	0.384759	0.050527
COL6A6	collagen, type VI, alpha 6	0.385698	0.02972
SCN2A	sodium channel, voltage gated, type II alpha subunit	0.386124	0.021629
MAP1A	microtubule-associated protein 1A	0.386755	0.049926
GSTA2	glutathione S-transferase alpha 2	0.387509	0.028191
GOLGA8O	golgin A8 family, member O	0.387509	0.120581
SLFN12L	schlafen family member 12-like	0.387509	0.208609
VAC14-AS1	VAC14 antisense RNA 1	0.387509	0.363239
ACY3	aminoacylase 3	0.389631	0.110946
ZNF208	zinc finger protein 208	0.390337	0.230132
LINC01123	long intergenic non-protein coding RNA 1123	0.390849	0.044634
CALML6	calmodulin-like 6	0.392717	0.047302
ERVK13-1	endogenous retrovirus group K13, member 1	0.393692	0.014464
CARNS1	carnosine synthase 1	0.39473	0.017233
BCAN	Brevican	0.39473	0.45256
SRI	Sorcin	0.395124	0.000586
B3GALNT1	beta-1,3-N-acetylgalactosaminyltransferase 1 (globoside blood group)	0.395294	0.008581
PNPLA3	patatin-like phospholipase domain containing 3	0.395731	0.028521
GALNT13	polypeptide N-acetylgalactosaminyltransferase 13	0.396511	0.30502
ALDH3A1	aldehyde dehydrogenase 3 family, member A1	0.397069	0.584979
ZNF883	zinc finger protein 883	0.397518	0.058367
GAB3	GRB2-associated binding protein 3	0.397974	0.004228
ANO7	anoctamin 7	0.399409	0.011404
CBLN4	cerebellin 4 precursor	0.399688	0.236214
ACOX2	acyl-CoA oxidase 2, branched chain	0.399977	0.008606
NACAD	NAC alpha domain containing	0.400526	0.000832
ZNF860	zinc finger protein 860	0.401293	0.024119

PHEX	phosphate regulating endopeptidase homolog, X-linked	0.401522	0.015585
ABCG4	ATP-binding cassette, sub-family G (WHITE), member 4	0.402874	0.176945
RIPPLY3	ripply transcriptional repressor 3	0.403747	0.10539
ADCY1	adenylate cyclase 1 (brain)	0.405111	0.234972
ANO2	anoctamin 2, calcium activated chloride channel	0.405573	0.027369
LGI2	leucine-rich repeat LGI family, member 2	0.405874	0.185637
FUCA1	fucosidase, alpha-L- 1, tissue	0.405911	0.029809
TMEM179	transmembrane protein 179	0.407101	0.011273
ASPN	Aspirin	0.407387	0.027794
GABRB3	gamma-aminobutyric acid (GABA) A receptor, beta 3	0.407669	0.196882
ROS1	ROS proto-oncogene 1 , receptor tyrosine kinase	0.408101	0.02168
TIAF1	TGFB1-induced anti-apoptotic factor 1	0.408342	0.06781
LINC00260	long intergenic non-protein coding RNA 260	0.408352	0.116038
RAB6B	RAB6B, member RAS oncogene family	0.40952	0.000213
TMOD2	tropomodulin 2 (neuronal)	0.410408	0.030245
C1QL1	complement component 1, q subcomponent-like 1	0.410594	0.012907
MIR29C	microRNA 29c	0.411126	0.014302
CORO2A	coronin, actin binding protein, 2A	0.411261	0.012579
PODNL1	podocan-like 1	0.411631	0.021094
DIRAS3	DIRAS family, GTP-binding RAS-like 3	0.411832	0.136993
IL17RD	interleukin 17 receptor D	0.411963	0.092121
VDAC3	voltage-dependent anion channel 3	0.413709	0.000712
CDON	cell adhesion associated, oncogene regulated	0.413937	0.047271
KCND1	potassium channel, voltage gated Shal related subfamily D, member 1	0.414327	0.002425
ZNF815P	zinc finger protein 815, pseudogene	0.414358	0.007193
PROSER2-AS1	PROSER2 antisense RNA 1	0.414876	0.057305
NAALAD2	N-acetylated alpha-linked acidic dipeptidase 2	0.415938	0.164584
CHST1	carbohydrate (keratan sulfate Gal-6) sulfotransferase 1	0.415986	0.329121
PLCL1	phospholipase C-like 1	0.41613	0.043636
MPP6	membrane protein, palmitoylated 6 (MAGUK p55 subfamily member 6)	0.416148	0.022909
ZP1	zona pellucida glycoprotein 1 (sperm receptor)	0.416541	0.054109
P2RX6	purinergic receptor P2X, ligand gated ion channel, 6	0.416621	0.002271
PRLR	prolactin receptor	0.416899	0.016699
PRUNE2	prune homolog 2 (Drosophila)	0.417636	0.019911
UBE2N	ubiquitin-conjugating enzyme E2N	0.417659	8.4E-05
LINC01016	long intergenic non-protein coding RNA 1016	0.418006	0.180946
ANXA13	annexin A13	0.418085	0.030516
SNORD35A	small nucleolar RNA, C/D box 35A	0.418125	0.023067
CORO2B	coronin, actin binding protein, 2B	0.418406	0.145299
GPRC5B	G protein-coupled receptor, class C, group 5, member B	0.418721	0.038715
ADD3	adducin 3 (gamma)	0.419387	0.00752
MPZ	myelin protein zero	0.419406	0.003314
STXBP6	syntaxin binding protein 6 (amisyn)	0.419933	0.004303
C21ORF67	long intergenic non-protein coding RNA 1547	0.421553	0.005522
NFIX	nuclear factor I/X (CCAAT-binding transcription factor)	0.421874	0.04146
ITGA6	integrin, alpha 6	0.422069	0.034479
RASA4B	RAS p21 protein activator 4B	0.422539	0.028664
RRAS	related RAS viral (r-ras) oncogene homolog	0.422821	0.000403
LRRTM1	leucine rich repeat transmembrane neuronal 1	0.423611	0.516123
CHGA	chromogranin A	0.423633	0.021171
MRAP2	melanocortin 2 receptor accessory protein 2	0.423646	0.194594
RASSF2	Ras association (RalGDS/AF-6) domain family member 2	0.424965	0.02866
PURG	purine-rich element binding protein G	0.425068	0.037608
IQSEC3	IQ motif and Sec7 domain 3	0.425332	0.000356
NBEAP1	neurobeachin pseudogene 1	0.42574	0.049376
GPR173	G protein-coupled receptor 173	0.426423	0.00255
DNAJC22	DnaJ (Hsp40) homolog, subfamily C, member 22	0.426821	0.087534
PCDHB11	protocadherin beta 11	0.427099	0.007548
FAM171A2	family with sequence similarity 171, member A2	0.42722	0.266227
GPR180	G protein-coupled receptor 180	0.427813	0.019914
ASB2	ankyrin repeat and SOCS box containing 2	0.427851	0.006277

PSD2	pleckstrin and Sec7 domain containing 2	0.42854	0.082224
TRIM14	tripartite motif containing 14	0.430429	0.001629
ANO3	anoctamin 3	0.432207	0.055591
CACNA2D2	calcium channel, voltage-dependent, alpha 2/delta subunit 2	0.433124	0.149673
PCDHGB3	protocadherin gamma subfamily B, 3	0.433695	0.103769
SH2D3C	SH2 domain containing 3C	0.433704	0.017317
PKD1L2	polycystic kidney disease 1-like 2 (gene/pseudogene)	0.434284	0.252857
NRG2	neuregulin 2	0.434355	0.073787
STAG3L3	stromal antigen 3-like 3 (pseudogene)	0.434908	0.058374
SGCE	sarcoglycan, epsilon	0.435682	0.00735
GAL3ST4	galactose-3-O-sulfotransferase 4	0.436786	0.03158
SERPIND1	serpin peptidase inhibitor, clade D (heparin cofactor), member 1	0.437221	0.076266
FABP3	fatty acid binding protein 3, muscle and heart	0.437652	0.215958
SNORD45A	small nucleolar RNA, C/D box 45A	0.43782	0.01663
CEND1	cell cycle exit and neuronal differentiation 1	0.437998	0.055063
CPAMD8	C3 and PZP-like, alpha-2-macroglobulin domain containing 8	0.438207	0.003453
VMA21	VMA21 vacuolar H+-ATPase homolog (S. cerevisiae)	0.438236	0.000456
ASIC1	acid sensing (proton gated) ion channel 1	0.438693	0.017652
RNF207	ring finger protein 207	0.438858	0.001842
RUSC1-AS1	RUSC1 antisense RNA 1	0.439346	0.146982
RFTN2	raftlin family member 2	0.439546	0.129576
LINC00924	long intergenic non-protein coding RNA 924	0.43956	0.675144
MAPK6	mitogen-activated protein kinase 6	0.440512	0.003602
SEPT6	septin 6	0.442488	0.035424
SSPO	SCO-spondin	0.442654	0.186779
TMEM119	transmembrane protein 119	0.442795	0.019395
PRSS30P	protease, serine, 30, pseudogene	0.442968	0.073497
PCSK9	proprotein convertase subtilisin/kexin type 9	0.443769	0.107103
NRN1L	neuritin 1-like	0.445217	0.093202
CPXM1	carboxypeptidase X (M14 family), member 1	0.445253	0.061474
HYAL1	hyaluronoglucosaminidase 1	0.445532	0.021313
IZUMO4	IZUMO family member 4	0.445568	0.085975
PSD	pleckstrin and Sec7 domain containing	0.445808	0.010259
PCAT6	prostate cancer associated transcript 6 (non-protein coding)	0.447544	0.002071
HEPH	hephaestin	0.447567	0.304443
C1ORF233	chromosome 1 open reading frame 233	0.447581	0.003255
KCNAB3	potassium channel, voltage gated subfamily A regulatory beta subunit 3	0.447959	0.098738
SYNDIG1	synapse differentiation inducing 1	0.448352	0.005183
CD81-AS1	CD81 antisense RNA 1	0.44858	0.094691
JAZF1-AS1	JAZF1 antisense RNA 1	0.448959	0.029533
SSBP2	single-stranded DNA binding protein 2	0.449184	0.000995
OSTM1	osteopetrosis associated transmembrane protein 1	0.449842	0.000323
SERHL2	serine hydrolase-like 2	0.451955	0.002111
TPTE2P1	transmembrane phosphoinositide 3-phosphatase and tensin homolog 2 pseudogene 1	0.452308	0.057568
EPB41L4A-AS2	EPB41L4A antisense RNA 2 (head to head)	0.452376	0.006197
SNORA69	small nucleolar RNA, H/ACA box 69	0.452376	0.023759
MAPT	microtubule-associated protein tau	0.453449	0.219509
GPR161	G protein-coupled receptor 161	0.453502	0.008976
ASB9	ankyrin repeat and SOCS box containing 9	0.454877	0.139141
HS2ST1	heparan sulfate 2-O-sulfotransferase 1	0.45504	0.002156
FAM43B	family with sequence similarity 43, member B	0.455836	0.004274
CCNG1	cyclin G1	0.456204	0.001686
TFF3	trefoil factor 3 (intestinal)	0.456531	0.229759
AIRE	autoimmune regulator	0.456576	0.132449
SCARF1	scavenger receptor class F, member 1	0.457005	0.034233
VN1R1	vomeronasal 1 receptor 1	0.457283	0.5525
ACAT2	acetyl-CoA acetyltransferase 2	0.457683	0.070981
CCL28	chemokine (C-C motif) ligand 28	0.457804	0.073004
ITIH1	inter-alpha-trypsin inhibitor heavy chain 1	0.458467	0.425543
LINC01305	long intergenic non-protein coding RNA 1305	0.458467	0.425543

CYP4F3	cytochrome P450, family 4, subfamily F, polypeptide 3	0.458467	0.412278
KERA	Keratocan	0.458467	0.546005
ATP9A	ATPase, class II, type 9A	0.45926	0.110276
PLEKHA6	pleckstrin homology domain containing, family A member 6	0.459402	0.02697
SUFU	suppressor of fused homolog (Drosophila)	0.460196	0.150243
PPFIA3	protein tyrosine phosphatase, receptor type, f polypeptide (PTPRF), interacting protein (liprin), alpha 3	0.46101	0.00434
DIRAS2	DIRAS family, GTP-binding RAS-like 2	0.46154	0.001375
FAM65C	family with sequence similarity 65, member C	0.463289	0.436337
C22ORF34	chromosome 22 open reading frame 34	0.463527	0.469117
EVL	Enah/Vasp-like	0.464386	0.06901
FAM71F2	family with sequence similarity 71, member F2	0.46449	0.007969
GAREM	GRB2 associated, regulator of MAPK1	0.464727	0.084988
LRRC75A	leucine rich repeat containing 75A	0.464816	0.030022
H19	H19, imprinted maternally expressed transcript (non-protein coding)	0.465214	0.01936
SLC29A4	solute carrier family 29 (equilibrative nucleoside transporter), member 4	0.465356	0.08886
ZNF491	zinc finger protein 491	0.465744	0.001406
MGAT3	mannosyl (beta-1,4-)-glycoprotein beta-1,4-N-acetylglucosaminyltransferase	0.465869	0.177274
HECW1	HECT, C2 and WW domain containing E3 ubiquitin protein ligase 1	0.466238	0.01047
STEAP4	STEAP family member 4	0.466304	0.038852
SNORD123	small nucleolar RNA, C/D box 123	0.466566	0.006511
TMSB15A	thymosin beta 15a	0.466994	0.029159
OTOF	Otoferlin	0.467057	0.016101
MARCKSL1	MARCKS-like 1	0.46706	0.056142
KIF3C	kinesin family member 3C	0.468013	0.002951
DFNB31	deafness, autosomal recessive 31	0.468067	0.018951
PCDHGA1	protocadherin gamma subfamily A, 1	0.468302	0.143704
ANKRD44	ankyrin repeat domain 44	0.468522	0.085212
HVCN1	hydrogen voltage gated channel 1	0.468598	0.001118
PRL	Prolactin	0.468645	0.085963
ELOVL6	ELOVL fatty acid elongase 6	0.468651	0.08156
MIR4697HG	MIR4697 host gene	0.46923	0.063817
CHRDL1	chordin-like 1	0.469503	0.059216
CPNE5	copine V	0.469544	0.149565
PAK3	p21 protein (Cdc42/Rac)-activated kinase 3	0.469748	0.180415
KCNQ4	potassium channel, voltage gated KQT-like subfamily Q, member 4	0.469967	0.032846
RASA4	RAS p21 protein activator 4	0.470116	0.03576
C6	complement component 6	0.471198	0.18538
KCTD14	potassium channel tetramerization domain containing 14	0.471298	0.027396
NUDT8	nudix (nucleoside diphosphate linked moiety X)-type motif 8	0.471591	0.023507
CROCCP3	ciliary rootlet coiled-coil, rootletin pseudogene 3	0.47165	0.003562
SARDH	sarcosine dehydrogenase	0.471881	0.145899
COL21A1	collagen, type XXI, alpha 1	0.472418	0.375665
PNMA2	paraneoplastic Ma antigen 2	0.472434	0.033757
SOBP	sine oculis binding protein homolog (Drosophila)	0.472825	0.268555
MTUS2	microtubule associated tumor suppressor candidate 2	0.472883	0.149522
PLIN4	perilipin 4	0.473089	0.067284
ST7-AS1	ST7 antisense RNA 1	0.473219	0.05056
ZYG11B	zyg-11 family member B, cell cycle regulator	0.473964	0.003407
CHURC1	churchill domain containing 1	0.474046	0.038121
DNM1P41	dynamin 1 pseudogene 41	0.474047	0.082849
KIRREL2	kin of IRRE like 2 (Drosophila)	0.474127	0.017784
C5ORF64	chromosome 5 open reading frame 64	0.474187	0.085744
SPEF1	sperm flagellar 1	0.474246	0.026844
INTS4L2	integrator complex subunit 4 pseudogene 2	0.475066	0.029673
TSPAN11	tetraspanin 11	0.475461	0.361051
CLMN	calmin (calponin-like, transmembrane)	0.475707	0.118588
BACE1	beta-site APP-cleaving enzyme 1	0.476148	0.027605
WNK2	WNK lysine deficient protein kinase 2	0.476487	0.213036
SEMA4G	sema domain, immunoglobulin domain (Ig), transmembrane domain (TM) and short cytoplasmic domain, (semaphorin) 4G	0.476664	0.212037

SMARCC2	SWI/SNF related, matrix associated, actin dependent regulator of chromatin, subfamily c, member 2	0.476729	0.011611
L3MBTL1	l(3)mbt-like 1 (Drosophila)	0.477108	0.067841
LAMP5	lysosomal-associated membrane protein family, member 5	0.477257	0.13946
C9ORF41	chromosome 9 open reading frame 41	0.477535	0.008264
LRRC17	leucine rich repeat containing 17	0.478473	0.063804
OMD	osteomodulin	0.478695	0.083174
NLGN3	neuroligin 3	0.479025	0.220931
METAP2	methionyl aminopeptidase 2	0.479153	0.002276
ZNF423	zinc finger protein 423	0.479187	0.369713
FAM32A	family with sequence similarity 32, member A	0.480214	5.53E-05
SCARA5	scavenger receptor class A, member 5	0.480365	0.038808
ESRRG	estrogen-related receptor gamma	0.480565	0.034137
PRG2	proteoglycan 2, bone marrow (natural killer cell activator, eosinophil granule major basic protein)	0.481555	0.002004
BHMT	betaine--homocysteine S-methyltransferase	0.482006	0.152955
SLC39A6	solute carrier family 39 (zinc transporter), member 6	0.482232	0.006232
LRRC29	leucine rich repeat containing 29	0.482587	0.001432
SNORA51	small nucleolar RNA, H/ACA box 51	0.482685	0.114144
ATP8A2	ATPase, aminophospholipid transporter, class I, type 8A, member 2	0.483	0.40961
EXTL1	exostosin-like glycosyltransferase 1	0.483018	0.082272
C2ORF16	chromosome 2 open reading frame 16	0.483041	0.498024
LRFN1	leucine rich repeat and fibronectin type III domain containing 1	0.483196	0.227532
TEKT4	tektin 4	0.483309	0.020047
CRABP2	cellular retinoic acid binding protein 2	0.483456	0.299121
INMT	indolethylamine N-methyltransferase	0.483769	0.754468
SLC38A4	solute carrier family 38, member 4	0.483833	0.236965
CD302	CD302 molecule	0.484378	0.000378
LMTK3	lemur tyrosine kinase 3	0.484406	0.067577
MAGI3	membrane associated guanylate kinase, WW and PDZ domain containing 3	0.484518	0.060058
SYT3	synaptotagmin III	0.484671	0.246265
USP3-AS1	USP3 antisense RNA 1	0.485092	0.069417
LINC00910	long intergenic non-protein coding RNA 910	0.485387	0.013346
PITRM1-AS1	PITRM1 antisense RNA 1	0.486084	0.180269
KCNIP1	Kv channel interacting protein 1	0.486084	0.333361
KIF26B	kinesin family member 26B	0.486162	0.159327
PPM1K	protein phosphatase, Mg2+/Mn2+ dependent, 1K	0.487087	0.027612
ADCY7	adenylate cyclase 7	0.487394	0.005609
RCOR1	REST corepressor 1	0.487836	0.007718
GSTM2	glutathione S-transferase mu 2 (muscle)	0.488045	0.000616
IGSF22	immunoglobulin superfamily, member 22	0.488351	0.13571
MIR497HG	mir-497-195 cluster host gene	0.488446	0.146457
RCOR2	REST corepressor 2	0.488796	0.022931
TNNT2	troponin T type 2 (cardiac)	0.488988	0.223074
GFAP	glial fibrillary acidic protein	0.489484	0.116144
PALD1	phosphatase domain containing, paladin 1	0.490346	0.045902
DPYD	dihydropyrimidine dehydrogenase	0.490563	0.014799
PTGES3L-AARSD1	PTGES3L-AARSD1 readthrough	0.490569	0.035594
ABI3BP	ABI family, member 3 (NESH) binding protein	0.490899	0.380921
CRMP1	collapsin response mediator protein 1	0.491699	0.003372
STAC2	SH3 and cysteine rich domain 2	0.491979	0.39548
ENPP4	ectonucleotide pyrophosphatase/phosphodiesterase 4 (putative)	0.492341	0.085458
SPRN	shadow of prion protein homolog (zebrafish)	0.492947	0.000285
ATP6V1G2	ATPase, H+ transporting, lysosomal 13kDa, V1 subunit G2	0.493067	0.065703
CFH	complement factor H	0.493913	0.020039
PCDHA12	protocadherin alpha 12	0.493959	0.110712
WT1	Wilms tumor 1	0.493999	0.003631
DNAJC4	DnaJ (Hsp40) homolog, subfamily C, member 4	0.494619	0.000752
KRT37	keratin 37, type I	0.494732	0.160559
KIAA1024	KIAA1024	0.494835	0.016429
EPHX2	epoxide hydrolase 2, cytoplasmic	0.495568	0.00444

PLXNA4	plexin A4	0.495635	0.202007
CSRNP3	cysteine-serine-rich nuclear protein 3	0.495762	0.015561
MIR3176	microRNA 3176	0.49592	0.349265
SPTBN4	spectrin, beta, non-erythrocytic 4	0.496179	0.020547
GSTM5	glutathione S-transferase mu 5	0.496239	0.006033
AVPR1A	arginine vasopressin receptor 1A	0.496311	0.074067
KALRN	kalirin, RhoGEF kinase	0.496628	0.008288
C2ORF50	chromosome 2 open reading frame 50	0.496825	0.158667
CDH20	cadherin 20, type 2	0.497078	0.254056
WDR86	WD repeat domain 86	0.49759	0.261966
JSRP1	junctional sarcoplasmic reticulum protein 1	0.498405	0.258728
OAS2	2'-5'-oligoadenylate synthetase 2, 69/71kDa	0.499919	0.01178
MICAL1	microtubule associated monooxygenase, calponin and LIM domain containing 1	0.499961	0.034979
OLFML2A	olfactomedin-like 2A	0.500438	0.147682
LINC01266	long intergenic non-protein coding RNA 1266	0.500581	0.550131
IGFBP1	insulin-like growth factor binding protein 1	0.500735	0.00177

Appendix 5: Genes implicated in cell cycle regulation

Differentially expressed genes involved in cell cycle regulation upon PER2 knockdown in decidualizing HESCs. Gene names annotated in bold are implicated in G2/M cell cycle progression

GENE SYMBOL	GENE NAME	FOLD CHANGE
ASNS	**asparagine synthetase (glutamine-hydrolyzing)**	**2.44**
AURKA	**aurora kinase A**	**2.70**
AVPI1	**arginine vasopressin-induced 1**	**2.66**
BEX2	brain expressed X-linked 2	7.05
BMP2	bone morphogenetic protein 2	2.66
BUB1	**BUB1 mitotic checkpoint serine/threonine kinase**	**2.16**
BUB1B	**BUB1 mitotic checkpoint serine/threonine kinase B**	**2.70**
CABLES1	Cdk5 and Abl enzyme substrate 1	5.24
CCNB1	**cyclin B1**	**2.46**
CCNG1	**cyclin G1**	**0.46**
CDC20	**cell division cycle 20**	**2.67**
CDC25A	cell division cycle 25A	2.00
CDC25C	**cell division cycle 25C**	**3.79**
CDCA2	**cell division cycle associated 2**	**2.44**
CDCA8	**cell division cycle associated 8**	**3.08**
CDK1	**cyclin-dependent kinase 1**	**2.64**
CENPA	**centromere protein A**	**2.37**
CENPW	**centromere protein W**	**2.02**
CHTF18	CTF18, chromosome transmission fidelity factor 18 homolog (S. cerevisiae)	2.13
CKS1B	**CDC28 protein kinase regulatory subunit 1B**	**2.29**
CYP26B1	cytochrome P450, family 26, subfamily B, polypeptide 1	2.80
DDIT3	**DNA-damage-inducible transcript 3**	**3.96**
DUSP1	**dual specificity phosphatase 1**	**2.35**
FAM32A	**family with sequence similarity 32, member A**	**0.48**
FAM83D	**family with sequence similarity 83, member D**	**2.81**
FANCD2	Fanconi anemia, complementation group D2	2.18
FIGN	**fidgetin**	**2.46**
GATA3	**GATA binding protein 3**	**4.04**
GEM	GTP binding protein overexpressed in skeletal muscle	7.09
GTSE1	**G-2 and S-phase expressed 1**	**2.51**
HERC5	**HECT and RLD domain containing E3 ubiquitin protein ligase 5**	**3.36**
HGF	hepatocyte growth factor (hepapoietin A; scatter factor)	3.29
HIST1H4E	**histone cluster 1, H4e**	**7.55**
HJURP	**Holliday junction recognition protein**	**2.07**
IQGAP3	IQ motif containing GTPase activating protein 3	2.34
JADE1	jade family PHD finger 1	2.22
JMY	**junction mediating and regulatory protein, p53 cofactor**	**3.12**
JUN	jun proto-oncogene	2.15
KIF15	**kinesin family member 15**	**2.26**
KIF18B	**kinesin family member 18B**	**2.09**
KIF2C	**kinesin family member 2C**	**3.47**
KIFC1	**kinesin family member C1**	**2.07**
KLF11	Kruppel-like factor 11	2.04
L3MBTL1	l(3)mbt-like 1 (Drosophila)	0.48
MAP2K6	mitogen-activated protein kinase kinase 6	0.31
MAPK6	mitogen-activated protein kinase 6	0.44
MYO16	myosin XVI	2.36
NEK2	**NIMA-related kinase 2**	**2.42**
NUF2	**NUF2, NDC80 kinetochore complex component**	**2.66**

PBK	**PDZ binding kinase**	**2.03**
PER2	**period circadian clock 2**	**0.37**
PHGDH	**phosphoglycerate dehydrogenase**	**3.32**
PIWIL4	**piwi-like RNA-mediated gene silencing 4**	**2.55**
PLD6	phospholipase D family, member 6	2.74
PLK1	**polo-like kinase 1**	**3.13**
PPM1D	**protein phosphatase, Mg2+/Mn2+ dependent, 1D**	**2.02**
PPP1R15A	protein phosphatase 1, regulatory subunit 15A	4.03
PRC1	**protein regulator of cytokinesis 1**	**2.34**
PROX1	**prospero homeobox 1**	**2.23**
PTTG1	**pituitary tumor-transforming 1**	**2.24**
RASSF2	**Ras association (RalGDS/AF-6) domain family member 2**	**0.42**
SEPT6	**septin 6**	**0.44**
SIK1	**salt-inducible kinase 1**	**2.38**
SIRT1	**sirtuin 1**	**2.07**
SKA1	spindle and kinetochore associated complex subunit 1	2.74
SPAG5	**sperm associated antigen 5**	**2.27**
TACC3	**transforming, acidic coiled-coil containing protein 3**	**2.29**
TGFB2	transforming growth factor, beta 2	2.50
TOP2A	**topoisomerase (DNA) II alpha 170kDa**	**2.14**
TPX2	**TPX2, microtubule-associated**	**2.07**
UBE2C	**ubiquitin-conjugating enzyme E2C**	**3.34**
USP44	**ubiquitin specific peptidase 44**	**2.64**
WEE1	**WEE1 G2 checkpoint kinase**	**2.34**

Appendix 6: Demographics of participating subjects in correlative analysis.

(n = 70)	***Median***	***S.E.M***
Age (year):	37.0	0.59
Body Mass Index (BMI):	25.0	0.62
First Trimester Loss (n):	4.0	0.23
Live Birth (n):	0	0.07
Day of biopsy relative to LH surge:	+8.0	0.16

Appendix 7: Demographics of participating subjects in PRIP-1 correlative analysis.

(n = 101)	***Median***	***S.E.M***
Age (year):	37.0	0.46
Body Mass Index (BMI):	25.0	0.45
First Trimester Loss (n):	3.0	0.23
Live Birth (n):	0	0.05
Day of biopsy relative to LH surge:	+8.0	0.13

References

Abe, M., Herzog, E. D., Yamazaki, S., Straume, M., Tei, H., Sakaki, Y., Menaker, M. & Block, G. D. (2002) Circadian rhythms in isolated brain regions. *The Journal of Neuroscience*, 22 (1): 350-356.

Abrahamson, E. E., Leak, R. K. & Moore, R. Y. (2001) The suprachiasmatic nucleus projects to posterior hypothalamic arousal systems. *Neuroreport*, 12 (2): 435-440.

Achache, H. & Revel, A. (2006) Endometrial receptivity markers, the journey to successful embryo implantation. *Human Reproduction Update*, 12 (6):

Achache, H., Tsafrir, A., Prus, D., Reich, R. & Revel, A. (2010) Defective endometrial prostaglandin synthesis identified in patients with repeated implantation failure undergoing in vitro fertilization. *Fertility and sterility*, 94 (4): 1271-1278.

Akashi, M. & Nishida, E. (2000) Involvement of the MAP kinase cascade in resetting of the mammalian circadian clock. *Genes & development*, 14 (6): 645-649.

Akiyama, S., Ohta, H., Watanabe, S., Moriya, T., Hariu, A., Nakahata, N., Chisaka, H., Matsuda, T., Kimura, Y., Tsuchiya, S., Tei, H., Okamura, K. & Yaegashi, N. (2010) The Uterus Sustains Stable Biological Clock during Pregnancy (vol 221, 287, 2010). *Tohoku Journal of Experimental Medicine*, 222 (2): 165-165.

Al-Sabbagh, M., Lam, E. W. F. & Brosens, J. J. (2012) Mechanisms of endometrial progesterone resistance. *Molecular and cellular endocrinology*, 358 (2): 208-215.

Albrecht, U., Bordon, A., Schmutz, I. & Ripperger, J. (2007) The multiple facets of Per2. *Cold Spring Harbor Symposia on Quantitative Biology*, 72 95-104.

Alvarez, J. D. & Sehgal, A. (2005) The thymus is similar to the testis in its pattern of circadian clock gene expression. *Journal of biological rhythms*, 20 (2): 111-121.

Amano, T., Tokunaga, K., Kakegawa, R., Yanagisawa, A., Takemoto, A., Tatemizo, A., Watanabe, T., Hatanaka, Y., Matsushita, A. & Kishi, M. (2010) Expression analysis of circadian genes in oocytes and preimplantation embryos of cattle and rabbits. *Animal reproduction science*, 121 (3): 225-235.

Antle, M. C. & Silver, R. (2005) Orchestrating time: arrangements of the brain circadian clock. *Trends in neurosciences*, 28 (3): 145-151.

Aplin, J. D., Hey, N. A. & Li, T. C. (1996) MUC1 as a cell surface and secretory component of endometrial epithelium: reduced levels in recurrent miscarriage. *American Journal of Reproductive Immunology*, 35 (3): 261-266.

Arima, H., House, S. B., Gainer, H. & Aguilera, G. (2002) Neuronal activity is required for the circadian rhythm of vasopressin gene transcription in the suprachiasmatic nucleus in vitro. *Endocrinology*, 143 (11): 4165-4171.

Arnett-Mansfield, R. L., Wain, G. V., Jaworski, R. C., Byth, K., Mote, P. A. & Clarke, C. L. (2001) Relative expression of progesterone receptors A and B in endometrioid cancers of the endometrium. *Cancer Research*, 61 (11): 4576-4582.

Avitabile, D., Genovese, L., Ponti, D., Ranieri, D., Raffa, S., Calogero, A. & Torrisi, M. R. (2014) Nucleolar localization and circadian regulation of Per2S, a novel splicing variant of the Period 2 gene. *Cellular and Molecular Life Sciences*, 71 (13): 2547-2559.

Balsalobre, A., Brown, S. A., Marcacci, L., Tronche, F., Kellendonk, C., Reichardt, H. M., Schütz, G. & Schibler, U. (2000a) Resetting of circadian time in peripheral tissues by glucocorticoid signaling. *Science*, 289 (5488): 2344-2347.

Balsalobre, A., Marcacci, L. & Schibler, U. (2000b) Multiple signaling pathways elicit circadian gene expression in cultured Rat-1 fibroblasts. *Current Biology*, 10 (20): 1291-1294.

Barbacka-Surowiak, G., Surowiak, J. & Stokłosowa, S. (2003) The involvement of suprachiasmatic nuclei in the regulation of estrous cycles in rodents. *Reproductive biology*, 3 (2): 99-129.

Bartsch, O., Bartlick, B. & Ivell, R. (2004) Phosphodiesterase 4 inhibition synergizes with relaxin signaling to promote decidualization of human endometrial stromal cells. *The Journal of Clinical Endocrinology & Metabolism*, 89 (1): 324-334.

Bartscha, O. & Ivell, R. (2004) Relaxin and phosphodiesterases collaborate during decidualization. *Annals of the New York Academy of Sciences*, 1030 (1): 479-492.

Bauer, J., Janecke, A., Gerss, J., Masjosthusmann, K., Werner, C. & Hoffmann, G. (2009) Circadian variation on oxygen consumption in preterm infants. *Journal of perinatal medicine*, 37 (4): 413-417.

Bedaiwy, M. A., Falcone, T., Mohamed, M. S., Aleem, A. A. N., Sharma, R. K., Worley, S. E., Thornton, J. & Agarwal, A. (2004) Differential growth of human embryos in vitro: role of reactive oxygen species. *Fertility and Sterility*, 82 (3):

Bentin-Ley, U., Sjögren, A., Nilsson, L., Hamberger, L., Larsen, J. F. & Horn, T. (1999) Presence of uterine pinopodes at the embryo–endometrial interface during human implantation in vitro. *Human Reproduction*, 14 (2): 515-520.

Bergh, P. A. & Navot, D. (1992) The impact of embryonic development and endometrial maturity on the timing of implantation. *Fertility and sterility*, 58 (3): 537-542.

Bhagwat, S. R., Chandrashekar, D. S., Kakar, R., Davuluri, S., Bajpai, A. K., Nayak, S., Bhutada, S., Acharya, K. & Sachdeva, G. (2013) Endometrial receptivity: a revisit to functional genomics studies on human endometrium and creation of HGEx-ERdb. *PloS one*, 8 (3): e58419.

Bielanska, M., Tan, S. L. & Ao, A. (2002) Chromosomal mosaicism throughout human preimplantation development in vitro: incidence, type, and relevance to embryo outcome. *Human Reproduction*, 17 (2): 413-419.

Bisanti, L., Olsen, J., Basso, O., Thonneau, P., Karmaus, W., Juul, S., Fletcher, T., Bolumar, F., FigaTalamanca, I., Pantelakis, S., Spinelli, A., Schaumburg, I., Wulff, M. & Biczysko, R. (1996) Shift work and subfecundity: A European multicenter study. *Journal of Occupational and Environmental Medicine*, 38 (4): 352-358.

Blockeel, C., Schutyser, V., De Vos, A., Verpoest, W., De Vos, M., Staessen, C., Haentjens, P., Van der Elst, J. & Devroey, P. (2008) Prospectively randomized controlled trial of PGS in IVF/ICSI patients with poor implantation. *Reproductive biomedicine online*, 17 (6): 848-854.

Blockeel, C., Van Vaerenbergh, I., Fatemi, H. M., Van Lommel, L., Devroey, P. & Bourgain, C. (2011) Gene expression profile in the endometrium on the day of oocyte retrieval after ovarian stimulation with low-dose hCG in the follicular phase. *Molecular human reproduction*, 17 (1): 33-41.

Boden, M. J., Varcoe, T. J. & Kennaway, D. J. (2013a) Circadian regulation of reproduction: from gamete to offspring. *Progress in biophysics and molecular biology*, 113 (3): 387-397.

Boden, M. J., Varcoe, T. J. & Kennaway, D. J. (2013b) Circadian regulation of reproduction: From gamete to offspring. *Progress in Biophysics & Molecular Biology*, 113 (3): 387-397.

Bonzini, M., Palmer, K. T., Coggon, D., Carugno, M., Cromi, A. & Ferrario, M. M. (2011) Shift work and pregnancy outcomes: a systematic review with meta-analysis

of currently available epidemiological studies. *BJOG: An International Journal of Obstetrics & Gynaecology*, 118 (12): 1429-1437.

Brar, A. K., Frank, G. R., Kessler, C. A., Cedars, M. I. & Handwerger, S. (1997) Progesterone-dependent decidualization of the human endometrium is mediated by cAMP. *Endocrine*, 6 (2): 301-307.

Brinsden, P. R., Alam, V., de Moustier, B. & Engrand, P. (2009) Recombinant human leukemia inhibitory factor does not improve implantation and pregnancy outcomes after assisted reproductive techniques in women with recurrent unexplained implantation failure. *Fertility and sterility*, 91 (4): 1445-1447.

Brosens, J. J. & Gellersen, B. (2006) Death or survival–progesterone-dependent cell fate decisions in the human endometrial stroma. *Journal of molecular endocrinology*, 36 (3): 389-398.

Brosens, J. J. & Gellersen, B. (2010) Something new about early pregnancy: decidual biosensoring and natural embryo selection. *Ultrasound in Obstetrics & Gynecology*, 36 (1):

Brosens, J. J., Hayashi, N. & White, J. O. (1999) Progesterone receptor regulates decidual prolactin expression in differentiating human endometrial stromal cells. *Endocrinology*, 140 (10): 4809-4820.

Brosens, J. J., Parker, M. G., McIndoe, A., Pijnenborg, R. & Brosens, I. A. (2009) A role for menstruation in preconditioning the uterus for successful pregnancy. *American journal of obstetrics and gynecology*, 200 (6): 615-e611.

Brosens, J. J., Pijnenborg, R. & Brosens, I. A. (2002) The myometrial junctional zone spiral arteries in normal and abnormal pregnancies - A review of the literature. *American Journal of Obstetrics and Gynecology*, 187 (5):

Brosens, J. J., Salker, M. S., Teklenburg, G., Nautiyal, J., Salter, S., Lucas, E. S., Steel, J. H., Christian, M., Chan, Y. W., Boomsma, C. M., Moore, J. D., Hartshorne, G. M., Sucurovic, S., Mulac-Jericevic, B., Heijnen, C. J., Quenby, S., Koerkamp, M. J. G., Holstege, F. C. P., Shmygol, A. & Macklon, N. S. (2014) Uterine Selection of Human Embryos at Implantation. *Scientific Reports*, 4 8.

Brosens, J. J., Tullet, J., Varshochi, R. & Lam, E. W. F. (2004) Steroid receptor action. *Best Practice & Research Clinical Obstetrics & Gynaecology*, 18 (2): 265-283.

Brunet, A., Bonni, A., Zigmond, M. J., Lin, M. Z., Juo, P., Hu, L. S., Anderson, M. J., Arden, K. C., Blenis, J. & Greenberg, M. E. (1999) Akt promotes cell survival by phosphorylating and inhibiting a Forkhead transcription factor. *cell*, 96 (6): 857-868.

Brzezinski, A., Vangel, M. G., Wurtman, R. J., Norrie, G., Zhdanova, I., Ben-Shushan, A. & Ford, I. (2005) Effects of exogenous melatonin on sleep: a meta-analysis. *Sleep medicine reviews*, 9 (1): 41-50.

Cagnacci, A., Maxia, N. & Volpe, A. (1999) Diurnal variation of semen quality in human males. *Human Reproduction*, 14 (1): 106-109.

Can, A., Tekeliioğlu, M. & Baltaci, A. (1995) Expression of desmin and dimentin intermediate filaments in human decidual cells during first trimester pregnancy. *Placenta*, 16 (3): 261-275.

Cardone, L., Hirayama, J., Giordano, F., Tamaru, T., Palvimo, J. J. & Sassone-Corsi, P. (2005) Circadian clock control by SUMOylation of BMAL1. *science*, 309 (5739): 1390-1394.

Chan, R. W. S., Schwab, K. E. & Gargett, C. E. (2004) Clonogenicity of human endometrial epithelial and stromal cells. *Biology of reproduction*, 70 (6): 1738-1750.

Chan, Y. W., Berg, H. A., Moore, J. D., Quenby, S. & Blanks, A. M. (2014) Assessment of myometrial transcriptome changes associated with spontaneous human labour by high-throughput RNA-seq. *Experimental physiology*, 99 (3): 510-524.

Cheng, H.-Y. M., Papp, J. W., Varlamova, O., Dziema, H., Russell, B., Curfman, J. P., Nakazawa, T., Shimizu, K., Okamura, H. & Impey, S. (2007) microRNA modulation of circadian-clock period and entrainment. *Neuron*, 54 (5): 813-829.

Cheng, M. Y., Bullock, C. M., Li, C., Lee, A. G., Bermak, J. C., Belluzzi, J., Weaver, D. R., Leslie, F. M. & Zhou, Q.-Y. (2002) Prokineticin 2 transmits the behavioural circadian rhythm of the suprachiasmatic nucleus. *Nature*, 417 (6887): 405-410.

Cho, N. H., Park, Y. K., Kim, Y. T., Yang, H. & Kim, S. K. (2004) Lifetime expression of stem cell markers in the uterine endometrium. *Fertility and sterility*, 81 (2): 403-407.

Christian, M., Pohnke, Y., Kempf, R., Gellersen, B. & Brosens, J. J. (2002a) Functional association of PR and CCAAT/enhancer-binding proteinβ isoforms: promoter-dependent cooperation between PR-B and liver-enriched inhibitory protein, or liver-enriched activatory protein and PR-A in human endometrial stromal cells. *Molecular Endocrinology*, 16 (1): 141-154.

Christian, M., Zhang, X., Schneider-Merck, T., Unterman, T. G., Gellersen, B., White, J. O. & Brosens, J. J. (2002b) Cyclic AMP-induced forkhead transcription factor, FKHR, cooperates with CCAAT/enhancer-binding protein β in differentiating human endometrial stromal cells. *Journal of Biological Chemistry*, 277 (23): 20825-20832.

Chu, A., Zhu, L., Blum, I. D., Mai, O., Leliavski, A., Fahrenkrug, J., Oster, H., Boehm, U. & Storch, K. F. (2013) Global But Not Gonadotrope-Specific Disruption of Bmal1 Abolishes the Luteinizing Hormone Surge Without Affecting Ovulation. *Endocrinology*, 154 (8): 2924-2935.

Chu, Y., Kalantari, R., Dodd, D. W. & Corey, D. R. (2012) Transcriptional silencing by hairpin RNAs complementary to a gene promoter. *Nucleic acid therapeutics*, 22 (3): 147-151.

Chung, S., Son, G. H. & Kim, K. (2011) Circadian rhythm of adrenal glucocorticoid: its regulation and clinical implications. *Biochimica et Biophysica Acta (BBA)-Molecular Basis of Disease*, 1812 (5): 581-591.

Conneely, O. M., Mulac-Jericevic, B., Lydon, J. P. & De Mayo, F. J. (2001) Reproductive functions of the progesterone receptor isoforms: lessons from knock-out mice. *Molecular and cellular endocrinology*, 179 (1): 97-103.

Czeisler, C. A. & Klerman, E. B. (1998) Circadian and sleep-dependent regulation of hormone release in humans. *Recent Progress in Hormone Research*, 54 97-130.

Dair, E. L., Simoes, R. S., Simões, M. J., Romeu, L. R. G., Oliveira-Filho, R. M., Haidar, M. A., Baracat, E. C. & Soares, J. M. (2008) Effects of melatonin on the endometrial morphology and embryo implantation in rats. *Fertility and sterility*, 89 (5): 1299-1305.

Damiola, F., Le Minh, N., Preitner, N., Kornmann, B., Fleury-Olela, F. & Schibler, U. (2000) Restricted feeding uncouples circadian oscillators in peripheral tissues from the central pacemaker in the suprachiasmatic nucleus. *Genes & development*, 14 (23): 2950-2961.

Delhanty, J. D. A. (2005) Mechanisms of aneuploidy induction in human oogenesis and early embryogenesis. *Cytogenetic and genome research*, 111 (3-4): 237-244.

Delhanty, J. D. A., Harper, J. C., Ao, A., Handyside, A. H. & Winston, R. M. L. (1997) Multicolour FISH detects frequent chromosomal mosaicism and chaotic division in normal preimplantation embryos from fertile patients. *Human genetics*, 99 (6): 755-760.

Deniaud, A., Maillier, E., Poncet, D., Kroemer, G., Lemaire, C. & Brenner, C. (2008) Endoplasmic reticulum stress induces calcium-dependent permeability transition, mitochondrial outer membrane permeabilization and apoptosis. *Oncogene*, 27 (3): 285-299.

Dibner, C., Schibler, U. & Albrecht, U. (2010) The mammalian circadian timing system: organization and coordination of central and peripheral clocks. *Annual review of physiology*, 72 517-549.

Ditisheim, A. J., Dibner, C., Philippe, J. & Pechère-Bertschi, A. (2013) Biological rhythms and preeclampsia. *Frontiers in endocrinology*, 4

Doi, M., Hirayama, J. & Sassone-Corsi, P. (2006) Circadian regulator CLOCK is a histone acetyltransferase. *Cell*, 125 (3): 497-508.

Dolatshad, H., Campbell, E. A., O'hara, L., Maywood, E. S., Hastings, M. H. & Johnson, M. H. (2006) Developmental and reproductive performance in circadian mutant mice. *Human Reproduction*, 21 (1): 68-79.

Dolatshad, H., Davis, F. C. & Johnson, M. H. (2009) Circadian clock genes in reproductive tissues and the developing conceptus. *Reproduction Fertility and Development*, 21 (1): 1-9.

Dubocovich, M. L., Hudson, R. L., Sumaya, I. C., Masana, M. I. & Manna, E. (2005) Effect of MT1 melatonin receptor deletion on melatonin-mediated phase shift of circadian rhythms in the C57BL/6 mouse. *J Pineal Res*, 39 (2): 113-120.

Dvornyk, V., Vinogradova, O. & Nevo, E. (2003) Origin and evolution of circadian clock genes in prokaryotes. *Proceedings of the National Academy of Sciences*, 100 (5): 2495-2500.

Eide, E. J., Vielhaber, E. L., Hinz, W. A. & Virshup, D. M. (2002) The circadian regulatory proteins BMAL1 and cryptochromes are substrates of casein kinase Iε. *Journal of Biological Chemistry*, 277 (19): 17248-17254.

Emera, D., Romero, R. & Wagner, G. (2012) The evolution of menstruation: A new model for genetic assimilation. *Bioessays*, 34 (1): 26-35.

Endo, A. & Watanabe, T. (1989) Effects of non-24-hour days on reproductive efficacy and embryonic development in mice. *Gamete research*, 22 (4): 435-441.

Erzberger, A., Hampp, G., Granada, A. E., Albrecht, U. & Herzel, H. (2013) Genetic redundancy strengthens the circadian clock leading to a narrow entrainment range. *Journal of the Royal Society Interface*, 10 (84): 11.

Farrer-Brown, G., Beilby, J. O. W. & Tarbit, M. H. (1970) The blood supply of the uterus. *BJOG: An International Journal of Obstetrics & Gynaecology*, 77 (8): 673-681.

Feligioni, M., Brambilla, E., Camassa, A., Sclip, A., Arnaboldi, A., Morelli, F., Antoniou, X. & Borsello, T. (2011) Crosstalk between JNK and SUMO signaling pathways: deSUMOylation is protective against H2O2-induced cell injury. *PloS one*, 6 (12): e28185.

Ferretti, C., Bruni, L., Dangles-Marie, V., Pecking, A. P. & Bellet, D. (2007) Molecular circuits shared by placental and cancer cells, and their implications in the proliferative, invasive and migratory capacities of trophoblasts. *Human reproduction update*, 13 (2): 121-141.

Fraser, A. M., Brockert, J. E. & Ward, R. H. (1995) Association of young maternal age with adverse reproductive outcomes. *New England journal of medicine*, 332 (17): 1113-1118.

Fu, L., Pelicano, H., Liu, J., Huang, P. & Lee, C. C. (2002) The circadian gene Period2 plays an important role in tumor suppression and DNA damage response in vivo. *cell*, 111 (1): 41-50.

Fujii, M., Kanematsu, T., Ishibashi, H., Fukami, K., Takenawa, T., Nakayama, K. I., Moss, S. J., Nabekura, J. & Hirata, M. (2010) Phospholipase C-related but catalytically inactive protein is required for insulin-induced cell surface expression of γ-aminobutyric acid type A receptors. *Journal of Biological Chemistry*, 285 (7): 4837-4846.

Fujimoto, Y., Yagita, K. & Okamura, H. (2006) Does mPER2 protein oscillate without its coding mRNA cycling?: post-transcriptional regulation by cell clock. *Genes to Cells*, 11 (5): 525-530.

Fustin, J.-M., Doi, M., Yamaguchi, Y., Hida, H., Nishimura, S., Yoshida, M., Isagawa, T., Morioka, M. S., Kakeya, H. & Manabe, I. (2013) RNA-methylation-dependent RNA processing controls the speed of the circadian clock. *Cell*, 155 (4): 793-806.

Gachon, F., Olela, F. F., Schaad, O., Descombes, P. & Schibler, U. (2006) The circadian PAR-domain basic leucine zipper transcription factors DBP, TEF, and HLF modulate basal and inducible xenobiotic detoxification. *Cell metabolism*, 4 (1): 25-36.

Gargett, C. E. (2007) Uterine stem cells: what is the evidence? *Human reproduction update*, 13 (1): 87-101.

Gargett, C. E. & Masuda, H. (2010) Adult stem cells in the endometrium. *Molecular human reproduction*, 16 (11): 818-834.

Gehring, W. & Rosbash, M. (2003) The coevolution of blue-light photoreception and circadian rhythms. *Journal of Molecular Evolution*, 57 S286-S289.

Gellersen, B. & Brosens, J. (2003) Cyclic AMP and progesterone receptor cross-talk in human endometrium: a decidualizing affair. *Journal of Endocrinology*, 178 (3):

Gellersen, B. & Brosens, J. J. (2014) Cyclic Decidualization of the Human Endometrium in Reproductive Health and Failure. *Endocrinology Review*,

Gellersen, B., Kempf, R. & Telgmann, R. (1997) Human endometrial stromal cells express novel isoforms of the transcriptional modulator CREM and up-regulate ICER in the course of decidualization. *Molecular Endocrinology*, 11 (1): 97-113.

Glass-Marmor, L., Paperna, T., Ben-Yosef, Y. & Miller, A. (2007) Chronotherapy using corticosteroids for multiple sclerosis relapses. *Journal of Neurology, Neurosurgery & Psychiatry*, 78 (8): 886-888.

Glasser, S. R. & Julian, J. (1986) Intermediate filament protein as a marker of uterine stromal cell decidualization. *Biology of reproduction*, 35 (2): 463-474.

Gray, C. A., Bartol, F. F., Tarleton, B. J., Wiley, A. A., Johnson, G. A., Bazer, F. W. & Spencer, T. E. (2001) Developmental biology of uterine glands. *Biology of reproduction*, 65 (5): 1311-1323.

Grewal, S., Carver, J., Ridley, A. J. & Mardon, H. J. (2010) Human endometrial stromal cell rho GTPases have opposing roles in regulating focal adhesion turnover and embryo invasion in vitro. *Biology of reproduction*, 83 (1): 75-82.

Grewal, S., Carver, J. G., Ridley, A. J. & Mardon, H. J. (2008) Implantation of the human embryo requires Rac1-dependent endometrial stromal cell migration. *Proceedings of the National Academy of Sciences*, 105 (42): 16189-16194.

Groothuis, P. G., Dassen, H., Romano, A. & Punyadeera, C. (2007) Estrogen and the endometrium: lessons learned from gene expression profiling in rodents and human. *Human reproduction update*, 13 (4): 405-417.

Guillaumond, F., Dardente, H., Giguère, V. & Cermakian, N. (2005) Differential control of Bmal1 circadian transcription by REV-ERB and ROR nuclear receptors. *Journal of biological rhythms*, 20 (5): 391-403.

Hanna, J., Goldman-Wohl, D., Hamani, Y., Avraham, I., Greenfield, C., Natanson-Yaron, S., Prus, D., Cohen-Daniel, L., Arnon, T. I. & Manaster, I. (2006) Decidual NK cells regulate key developmental processes at the human fetal-maternal interface. *Nature medicine*, 12 (9): 1065-1074.

Harada, K., Takeuchi, H., Oike, M., Matsuda, M., Kanematsu, T., Yagisawa, H., Nakayama, K. i. I., Maeda, K., Erneux, C. & Hirata, M. (2005) Role of PRIP-1, a novel Ins (1, 4, 5) P3 binding protein, in Ins (1, 4, 5) P3-mediated Ca2+ signaling. *Journal of cellular physiology*, 202 (2): 422-433.

Harmar, A. J., Marston, H. M., Shen, S., Spratt, C., West, K. M., Sheward, W. J., Morrison, C. F., Dorin, J. R., Piggins, H. D. & Reubi, J.-C. (2002) The VPAC 2 receptor is essential for circadian function in the mouse suprachiasmatic nuclei. *Cell*, 109 (4): 497-508.

Hermida, R. C., Ayala, D. E., Fernández, J. R. & Calvo, C. (2008) Chronotherapy improves blood pressure control and reverts the nondipper pattern in patients with resistant hypertension. *Hypertension*, 51 (1): 69-76.

Hirota, T. & Fukada, Y. (2004) Resetting mechanism of central and peripheral circadian clocks in mammals. *Zoological science*, 21 (4): 359-368.

Honnebier, M. & Nathanielsz, P. W. (1994) Primate parturition and the role of the maternal circadian system. *European Journal of Obstetrics & Gynecology and Reproductive Biology*, 55 (3): 193-203.

Husse, J., Leliavski, A., Tsang, A. H., Oster, H. & Eichele, G. (2014) The light-dark cycle controls peripheral rhythmicity in mice with a genetically ablated suprachiasmatic nucleus clock. *The FASEB Journal*, 28 (11): 4950-4960.

Ihnatovych, I., Hu, W., Martin, J. L., Fazleabas, A. T., de Lanerolle, P. & Strakova, Z. (2007) Increased phosphorylation of myosin light chain prevents in vitro decidualization. *Endocrinology*, 148 (7): 3176-3184.

Iitaka, C., Miyazaki, K., Akaike, T. & Ishida, N. (2005) A role for glycogen synthase kinase-3β in the mammalian circadian clock. *Journal of Biological Chemistry*, 280 (33): 29397-29402.

Ikeda, M. & Nomura, M. (1997) cDNA cloning and tissue-specific expression of a novel basic helix–loop–helix/PAS protein (BMAL1) and identification of alternatively spliced variants with alternative translation initiation site usage. *Biochemical and biophysical research communications*, 233 (1): 258-264.

Ishikawa, K. & Shimazu, T. (1980) Circadian rhythm of liver glycogen metabolism in rats: effects of hypothalamic lesions. *American Journal of Physiology-Endocrinology and Metabolism*, 238 (1): E21-E25.

Jaworek, J., Brzozowski, T. & Konturek, S. J. (2005) Melatonin as an organoprotector in the stomach and the pancreas. *Journal of pineal research*, 38 (2): 73-83.

Jin, X., Shearman, L. P., Weaver, D. R., Zylka, M. J., De Vries, G. J. & Reppert, S. M. (1999) A molecular mechanism regulating rhythmic output from the suprachiasmatic circadian clock. *Cell*, 96 (1): 57-68.

Jones, M. C., Fusi, L., Higham, J. H., Abdel-Hafiz, H., Horwitz, K. B., Lam, E. W. F. & Brosens, J. J. (2006) Regulation of the SUMO pathway sensitizes differentiating human endometrial stromal cells to progesterone. *Proceedings of the National Academy of Sciences of the United States of America*, 103 (44): 16272-16277.

Jud, C., Chappuis, S., Revell, V. L., Sletten, T. L., Saaltink, D.-J., Cajochen, C., Skene, D. J. & Albrecht, U. (2009) Age-dependent alterations in human PER2 levels after early morning blue light exposure. *Chronobiology international*, 26 (7): 1462-1469.

Kalsbeek, A., Foppen, E., Schalij, I., Van Heijningen, C., van der Vliet, J., Fliers, E. & Buijs, R. M. (2008) Circadian control of the daily plasma glucose rhythm: an interplay of GABA and glutamate. *PLOS one*, 3 (9): e3194.

Kanematsu, T., Mizokami, A., Watanabe, K. & Hirata, M. (2007) Regulation of GABAA-receptor surface expression with special reference to the involvement of GABARAP (GABAA receptor-associated protein) and PRIP (phospholipase C-related, but catalytically inactive protein). *Journal of pharmacological sciences*, 104 (4): 285-292.

Karman, B. N. & Tischkau, S. A. (2006) Circadian clock gene expression in the ovary: Effects of luteinizing hormone. *Biology of Reproduction*, 75 (4): 624-632.

Kastner, P., Krust, A., Turcotte, B., Stropp, U., Tora, L., Gronemeyer, H. & Chambon, P. (1990) Two distinct estrogen-regulated promoters generate transcripts encoding the two functionally different human progesterone receptor forms A and B. *The EMBO journal*, 9 (5): 1603.

Kennaway, D. J. (2005) The role of circadian rhythmicity in reproduction. *Human Reproduction Update*, 11 (1):

Kennaway, D. J., Varcoe, T. J. & Mau, V. J. (2003a) Rhythmic expression of clock and clock-controlled genes in the rat oviduct. *Molecular human reproduction*, 9 (9): 503-507.

Kennaway, D. J., Varcoe, T. J. & Mau, V. J. (2003b) Rhythmic expression of clock and clock-controlled genes in the rat oviduct. *Molecular Human Reproduction*, 9 (9): 503-507.

Khattab, A. F., Mustafa, F. A. & Taylor, P. J. (2005) The use of urine LH detection kits to time intrauterine insemination with donor sperm. *Human Reproduction*, 20 (9): 2542-2545.

Klentzeris, L. D., Bulmer, J. N., Trejdosiewicz, L. K., Morrison, L. & Cooke, I. D. (1993) Infertility: Beta-1 integrin cell adhesion molecules in the endometrium of fertile and infertile women. *Human Reproduction*, 8 (8): 1223-1230.

Knobil, E. (2013) The neuroendocrine control of the menstrual cycle. *Recent progress in hormone research*, 36 53-88.

Ko, C. H. & Takahashi, J. S. (2006) Molecular components of the mammalian circadian clock. *Human Molecular Genetics*, 15 R271-R277.

Kondratov, R. V., Chernov, M. V., Kondratova, A. A., Gorbacheva, V. Y., Gudkov, A. V. & Antoch, M. P. (2003) BMAL1-dependent circadian oscillation of nuclear

CLOCK: posttranslational events induced by dimerization of transcriptional activators of the mammalian clock system. *Genes & development*, 17 (15): 1921-1932.

Koot, Y. E. M., Teklenburg, G., Salker, M. S., Brosens, J. J. & Macklon, N. S. (2012) Molecular aspects of implantation failure. *Biochimica et biophysica acta*, 1822 (12):

Kovanen, L., Saarikoski, S. T., Aromaa, A., Lonnqvist, J. & Partonen, T. (2010) ARNTL (BMAL1) and NPAS2 gene variants contribute to fertility and seasonality. *PLoS One*, 5 (4): e10007.

Koyanagi, S., Hamdan, A. M., Horiguchi, M., Kusunose, N., Okamoto, A., Matsunaga, N. & Ohdo, S. (2011) cAMP-response Element (CRE)-mediated Transcription by Activating Transcription Factor-4 (ATF4) Is Essential for Circadian Expression of the Period2 Gene. *Journal of Biological Chemistry*, 286 (37): 32416-32423.

Kuokkanen, S., Chen, B., Ojalvo, L., Benard, L., Santoro, N. & Pollard, J. W. (2010) Genomic profiling of microRNAs and messenger RNAs reveals hormonal regulation in microRNA expression in human endometrium. *Biology of reproduction*, 82 (4): 791-801.

Kuroda, K., Venkatakrishnan, R., James, S., Sucurovic, S., Mulac-Jericevic, B., Lucas, E. S., Takeda, S., Shmygol, A., Brosens, J. J. & Quenby, S. (2013) Elevated periimplantation uterine natural killer cell density in human endometrium is

associated with impaired corticosteroid signaling in decidualizing stromal cells. *J Clin Endocrinol Metab*, 98 (11): 4429-4437.

Kuroda, K., Venkatakrishnan, R., Salker, M. S., Agrawal, R., Quenby, S. & Brosens, J. J. (2012) The role glucocorticoid receptor and mineralocorticoid receptor signalling in decidualizing endometrium. *Bjog-an International Journal of Obstetrics and Gynaecology*, 119 (6):

Kusama, K., Yoshie, M., Tamura, K., Kodaka, Y., Hirata, A., Sakurai, T., Bai, H., Imakawa, K., Nishi, H. & Isaka, K. (2013) Regulation of decidualization in human endometrial stromal cells through exchange protein directly activated by cyclic AMP (Epac). *Placenta*, 34 (3): 212-221.

L Stewart, C. (1994) Leukaemia inhibitory factor and the regulation of pre-implantation development of the mammalian embryo. *Molecular reproduction and development*, 39 (2): 233-238.

Labied, S., Kajihara, T., Madureira, P. A., Fusi, L., Jones, M. C., Higham, J. M., Varshochi, R., Francis, J. M., Zoumpoulidou, G. & Essafi, A. (2006) Progestins regulate the expression and activity of the forkhead transcription factor FOXO1 in differentiating human endometrium. *Molecular Endocrinology*, 20 (1): 35-44.

Lam, E. W. F., Shah, K. & Brosens, J. J. (2012) The diversity of sex steroid action: the role of micro-RNAs and FOXO transcription factors in cycling endometrium and cancer. *Journal of Endocrinology*, 212 (1): 13-25.

Lee, J., Lee, Y., Lee, M. J., Park, E., Kang, S. H., Chung, C. H., Lee, K. H. & Kim, K. (2008) Dual modification of BMAL1 by SUMO2/3 and ubiquitin promotes circadian activation of the CLOCK/BMAL1 complex. *Molecular and Cellular Biology*, 28 (19): 6056-6065.

Leitao, B., Jones, M. C., Fusi, L., Higham, J., Lee, Y., Takano, M., Goto, T., Christian, M., Lam, E. W. F. & Brosens, J. J. (2010) Silencing of the JNK pathway maintains progesterone receptor activity in decidualizing human endometrial stromal cells exposed to oxidative stress signals. *Faseb Journal*, 24 (5):

Leitao, B. B., Jones, M. C. & Brosens, J. J. (2011) The SUMO E3-ligase PIAS1 couples reactive oxygen species-dependent JNK activation to oxidative cell death. *The FASEB Journal*, 25 (10): 3416-3425.

Lessey, B. A., Castelbaum, A. J., Sawin, S. W. & Sun, J. (1995) Integrins as markers of uterine receptivity in women with primary unexplained infertility. *Fertility and sterility*, 63 (3): 535-542.

Levi, F. (2001) Circadian chronotherapy for human cancers. *The lancet oncology*, 2 (5): 307-315.

Li, Q., Wang, J., Armant, D. R., Bagchi, M. K. & Bagchi, I. C. (2002) Calcitonin down-regulates E-cadherin expression in rodent uterine epithelium during implantation. *Journal of Biological Chemistry*, 277 (48): 46447-46455.

Li, X. & O'Malley, B. W. (2003) Unfolding the action of progesterone receptors. *Journal of Biological Chemistry*, 278 (41): 39261-39264.

Lim, K. J. H., Odukoya, O. A., Ajjan, R. A., Li, T.-C., Weetman, A. P. & Cooke, I. D. (2000) The role of T-helper cytokines in human reproduction. *Fertility and sterility*, 73 (1): 136-142.

Lindow, S. W., Jha, R. R. & Thompson, J. W. (2000) 24 hour rhythm to the onset of preterm labour. *BJOG: An International Journal of Obstetrics & Gynaecology*, 107 (9): 1145-1148.

Lok, I. H. & Neugebauer, R. (2007) Psychological morbidity following miscarriage. *Best Practice & Research Clinical Obstetrics & Gynaecology*, 21 (2): 229-247.

Longo, L. D. & Yellon, S. M. (1988) Biological timekeeping during pregnancy and the role of circadian rhythms in parturition. In: *The endocrine control of the fetus*. Springer: 173-192.

Luciano, A. A., Peluso, J., Koch, E. I., Maier, D., Kuslis, S. & Davison, E. (1990) Temporal relationship and reliability of the clinical, hormonal, and ultrasonographic indices of ovulation in infertile women. *Obstetrics and gynecology*, 75 (3 Pt 1): 412-416.

Luo, W. & Sehgal, A. (2012) Regulation of circadian behavioral output via a MicroRNA-JAK/STAT circuit. *Cell*, 148 (4): 765-779.

Majercak, J., Chen, W.-F. & Edery, I. (2004) Splicing of the period gene 3 ´ -terminal intron is regulated by light, circadian clock factors, and phospholipase C. *Molecular and cellular biology*, 24 (8): 3359-3372.

Mak, I. Y. H., Brosens, J. J., Christian, M., Hills, F. A., Chamley, L., Regan, L. & White, J. O. (2002) Regulated expression of signal transducer and activator of transcription, Stat5, and its enhancement of PRL expression in human endometrial stromal cells in vitro. *The Journal of Clinical Endocrinology & Metabolism*, 87 (6): 2581-2588.

Mangal, R. K., Wiehle, R. D., Poindexter, A. N. & Weigel, N. L. (1997) Differential expression of uterine progesterone receptor forms A and B during the menstrual cycle. *The Journal of steroid biochemistry and molecular biology*, 63 (4): 195-202.

Martin, R. J. & Banks-Schlegel, S. (1998) Chronobiology of asthma. *American journal of respiratory and critical care medicine*, 158 (3): 1002-1007.

Masuda, H., Anwar, S. S., Bühring, H.-J., Rao, J. R. & Gargett, C. E. (2012) A novel marker of human endometrial mesenchymal stem-like cells. *Cell transplantation*, 21 (10): 2201-2214.

Masuda, H., Matsuzaki, Y., Hiratsu, E., Ono, M., Nagashima, T., Kajitani, T., Arase, T., Oda, H., Uchida, H. & Asada, H. (2010) Stem cell-like properties of the endometrial side population: implication in endometrial regeneration. *PloS one*, 5 (4): e10387.

Matsuda, M., Kanematsu, T., Takeuchi, H., Kukita, T. & Hirata, M. (1998) Localization of a novel inositol 1, 4, 5-trisphosphate binding protein, p130 in rat brain. *Neuroscience letters*, 257 (2): 97-100.

Matsuda, M., Tsutsumi, K., Kanematsu, T., Fukami, K., Terada, Y., Takenawa, T., Nakayama, K. I. & Hirata, M. (2009) Involvement of phospholipase C-related inactive protein in the mouse reproductive system through the regulation of gonadotropin levels. *Biology of reproduction*, 81 (4): 681-689.

Meng, X., Ichim, T. E., Zhong, J., Rogers, A., Yin, Z., Jackson, J., Wang, H., Ge, W., Bogin, V. & Chan, K. W. (2007) Endometrial regenerative cells: a novel stem cell population. *Journal of translational medicine*, 5 (1): 57.

Merrow, M. & Roenneberg, T. (2001) Circadian clocks: running on redox. *Cell*, 106 (2): 141-143.

Meseguer, M., Aplin, J. D., Caballero-Campo, P., O'Connor, J. E., Martín, J. C., Remohí, J., Pellicer, A. & Simón, C. (2001) Human endometrial mucin MUC1 is up-regulated by progesterone and down-regulated in vitro by the human blastocyst. *Biology of reproduction*, 64 (2): 590-601.

Millar-Craig, M., Bishop, C. & Raftery, E. B. (1978) Circadian variation of blood-pressure. *The Lancet*, 311 (8068): 795-797.

Miller, B. H., Olson, S. L., Turek, F. W., Levine, J. E., Horton, T. H. & Takahashi, J. S. (2004) Circadian clock mutation disrupts estrous cyclicity and maintenance of pregnancy. *Current Biology*, 14 (15): 1367-1373.

Milne, S. A., Perchick, G. B., Boddy, S. C. & Jabbour, H. N. (2001) Expression, localization, and signaling of PGE2 and EP2/EP4 receptors in human nonpregnant endometrium across the menstrual cycle. *The Journal of Clinical Endocrinology & Metabolism*, 86 (9): 4453-4459.

Miyazaki, K., Maruyama, T., Masuda, H., Yamasaki, A., Uchida, S., Oda, H., Uchida, H. & Yoshimura, Y. (2012) Stem cell-like differentiation potentials of endometrial side population cells as revealed by a newly developed in vivo endometrial stem cell assay.

Miyazaki, K., Wakabayashi, M., Chikahisa, S., Sei, H. & Ishida, N. (2007) PER2 controls circadian periods through nuclear localization in the suprachiasmatic nucleus. *Genes to Cells*, 12 (11): 1225-1234.

Moore, R. Y., Speh, J. C. & Leak, R. K. (2002) Suprachiasmatic nucleus organization. *Cell and tissue research*, 309 (1): 89-98.

Mote, P. A., Balleine, R. L., McGowan, E. M. & Clarke, C. L. (2000) Heterogeneity of progesterone receptors A and B expression in human endometrial glands and stroma. *Human Reproduction*, 15 (suppl 3): 48-56.

Moulton, B. C. & Koenig, B. B. (1983) Progestin increases cathepsin D synthesis in uterine luminal epithelial cells. *American Journal of Physiology-Endocrinology and Metabolism*, 244 (5): E442-E446.

Moulton, B. C. & Koenig, B. B. (1984) Uterine Deoxyribonucleic Acid Synthesis during Preimplantation in Precursors of Stromal Cell Differentiation during Decidualization*. *Endocrinology*, 115 (4): 1302-1307.

Mulac-Jericevic, B. & Conneely, O. M. (2004) Reproductive tissue selective actions of progesterone receptors. *Reproduction*, 128 (2): 139-146.

Murakami, A., Matsuda, M., Nakasima, A. & Hirata, M. (2006) Characterization of the human PRIP-1 gene structure and transcriptional regulation. *Gene*, 382 129-139.

Murakami, K., Lee, Y. H., Lucas, E. S., Chan, Y.-W., Durairaj, R. P., Takeda, S., Moore, J. D., Tan, B. K., Quenby, S. & Chan, J. K. Y. (2014) Decidualization induces a secretome switch in perivascular niche cells of the human endometrium. *Endocrinology*, 155 (11): 4542-4553.

Muter, J., Lucas, E. S., Chan, Y.-W., Brighton, P. J., Moore, J. D., Lacey, L., Quenby, S., Lam, E. W. F. & Brosens, J. J. (2015) The clock protein period 2 synchronizes mitotic expansion and decidual transformation of human endometrial stromal cells. *The FASEB Journal*, 29 (4): 1603-1614.

Nagel, R., Clijsters, L. & Agami, R. (2009) The miRNA-192/194 cluster regulates the Period gene family and the circadian clock. *FEBS journal*, 276 (19): 5447-5455.

Nagoshi, E., Saini, C., Bauer, C., Laroche, T., Naef, F. & Schibler, U. (2004) Circadian gene expression in individual fibroblasts: cell-autonomous and self-sustained oscillators pass time to daughter cells. *Cell*, 119 (5): 693-705.

Naito, Y., Tsujino, T., Kawasaki, D., Okumura, T., Morimoto, S., Masai, M., Sakoda, T., Fujioka, Y., Ohyanagi, M. & Iwasaki, T. (2003) Circadian gene expression of clock genes and plasminogen activator inhibitor-1 in heart and aorta of spontaneously hypertensive and Wistar–Kyoto rats. *Journal of hypertension*, 21 (6): 1107-1115.

Nakamura, T. J., Moriya, T., Inoue, S., Shimazoe, T., Watanabe, S., Ebihara, S. & Shinohara, K. (2005) Estrogen differentially regulates expression of Per1 and Per2 genes between central and peripheral clocks and between reproductive and nonreproductive tissues in female rats. *Journal of Neuroscience Research*, 82 (5): 622-630.

Nakamura, T. J., Nakamura, W., Yamazaki, S., Kudo, T., Cutler, T., Colwell, C. S. & Block, G. D. (2011) Age-related decline in circadian output. *The Journal of neuroscience*, 31 (28): 10201-10205.

Nakamura, T. J., Sellix, M. T., Kudo, T., Nakao, N., Yoshimura, T., Ebihara, S., Colwell, C. S. & Block, G. D. (2010) Influence of the estrous cycle on clock gene expression in reproductive tissues: effects of fluctuating ovarian steroid hormone levels. *Steroids*, 75 (3): 203-212.

Nakamura, T. J., Sellix, M. T., Menaker, M. & Block, G. D. (2008) Estrogen directly modulates circadian rhythms of PER2 expression in the uterus. *American Journal of Physiology-Endocrinology and Metabolism*, 295 (5): E1025-E1031.

Nanba, D., Mammoto, A., Hashimoto, K. & Higashiyama, S. (2003) Proteolytic release of the carboxy-terminal fragment of proHB-EGF causes nuclear export of PLZF. *The Journal of cell biology*, 163 (3): 489-502.

Norman, R. L., Blake, C. A. & Sawyer, C. H. (1973) Estrogen-Dependent Twenty-four-Hour Periodicity in Pituitary LH Release in the Female Hamster 1. *Endocrinology*, 93 (4): 965-970.

Nørgaard, J. P., Pedersen, E. B. & Djurhuus, J. C. (1985) Diurnal anti-diuretic-hormone levels in enuretics. *The Journal of urology*, 134 (5): 1029-1031.

O'Neill, J. S., Maywood, E. S., Chesham, J. E., Takahashi, J. S. & Hastings, M. H. (2008) cAMP-dependent signaling as a core component of the mammalian circadian pacemaker. *Science*, 320 (5878): 949-953.

O'Neill, J. S., Maywood, E. S. & Hastings, M. H. (2013) Cellular mechanisms of circadian pacemaking: beyond transcriptional loops. *Handbook of experimental pharmacology*, (217): 67-103.

Oliver, C., Montes, M. J., Galindo, J. A., Ruiz, C. & Olivares, E. G. (1999) Human decidual stromal cells express α-smooth muscle actin and show ultrastructural similarities with myofibroblasts. *Human Reproduction*, 14 (6): 1599-1605.

Orrenius, S., Zhivotovsky, B. & Nicotera, P. (2003) Regulation of cell death: the calcium–apoptosis link. *Nature reviews Molecular cell biology*, 4 (7): 552-565.

Oster, H., Damerow, S., Kiessling, S., Jakubcakova, V., Abraham, D., Tian, J., Hoffmann, M. W. & Eichele, G. (2006) The circadian rhythm of glucocorticoids is regulated by a gating mechanism residing in the adrenal cortical clock. *Cell metabolism*, 4 (2): 163-173.

Partch, C. L., Shields, K. F., Thompson, C. L., Selby, C. P. & Sancar, A. (2006) Posttranslational regulation of the mammalian circadian clock by cryptochrome and protein phosphatase 5. *Proceedings of the National Academy of Sciences*, 103 (27): 10467-10472.

Patel, A. N., Park, E., Kuzman, M., Benetti, F., Silva, F. J. & Allickson, J. G. (2008) Multipotent menstrual blood stromal stem cells: isolation, characterization, and differentiation. *Cell Transplant*, 17 (3): 303-311.

Pegoraro, M. & Tauber, E. (2011) Animal clocks: a multitude of molecular mechanisms for circadian timekeeping. *Wiley Interdisciplinary Reviews: RNA*, 2 (2): 312-320.

Pilorz, V. & Steinlechner, S. (2008) Low reproductive success in Per1 and Per2 mutant mouse females due to accelerated ageing? *Reproduction*, 135 (4): 559-568.

Pratt, W. B. & Toft, D. O. (1997) Steroid receptor interactions with heat shock protein and immunophilin chaperones 1. *Endocrine reviews*, 18 (3): 306-360.

Quenby, S. & Farquharson, R. (2006) Uterine natural killer cells, implantation failure and recurrent miscarriage. *Reproductive biomedicine online*, 13 (1): 24-28.

Quenby, S., Vince, G., Farquharson, R. & Aplin, J. (2002) Recurrent miscarriage: a defect in nature's quality control? *Human Reproduction*, 17 (8):

Quinn, C., Ryan, E., Claessens, E. A., Greenblatt, E., Hawrylyshyn, P., Cruickshank, B., Hannam, T., Dunk, C. & Casper, R. F. (2007) The presence of pinopodes in the human endometrium does not delineate the implantation window. *Fertility and sterility*, 87 (5): 1015-1021.

Rai, R. & Regan, L. (2006) Recurrent miscarriage. *Lancet*, 368 (9535): 601-611.

Ratajczak, C. K., Asada, M., Allen, G. C., McMahon, D. G., Muglia, L. M., Smith, D., Bhattacharyya, S. & Muglia, L. J. (2012) Generation of myometrium-specific Bmal1 knockout mice for parturition analysis. *Reproduction Fertility and Development*, 24 (5): 759-767.

Ratajczak, C. K., Boehle, K. L. & Muglia, L. J. (2009) Impaired Steroidogenesis and Implantation Failure in Bmal1(-/-) Mice. *Endocrinology*, 150 (4): 1879-1885.

Reppert, S. M., Henshaw, D., Schwartz, W. J. & Weaver, D. R. (1987) The circadian-gated timing of birth in rats: disruption by maternal SCN lesions or by removal of the fetal brain. *Brain research*, 403 (2): 398-402.

Reppert, S. M. & Weaver, D. R. (2002) Coordination of circadian timing in mammals. *Nature*, 418 (6901): 935-941.

Revel, A., Achache, H., Stevens, J., Smith, Y. & Reich, R. (2011) MicroRNAs are associated with human embryo implantation defects. *Human reproduction*, der255.

Richer, J. K., Lange, C. A., Manning, N. G., Owen, G., Powell, R. & Horwitz, K. B. (1998) Convergence of Progesterone with Growth Factor and Cytokine Signaling in Breast Cancer PROGESTERONE RECEPTORS REGULATE SIGNAL TRANSDUCERS AND ACTIVATORS OF TRANSCRIPTION EXPRESSION AND ACTIVITY. *Journal of Biological Chemistry*, 273 (47): 31317-31326.

Ripperger, J. A. & Brown, S. A. (2010) Transcriptional Regulation of Circadian Clocks. In: Albrecht, U., ed. *Circadian Clock*. Springer, 233 Spring St, New York, Ny 10013 USA: 37-78.

Rizzo, P., Raffone, E. & Benedetto, V. (2010) Effect of the treatment with myo-inositol plus folic acid plus melatonin in comparison with a treatment with myo-inositol plus folic acid on oocyte quality and pregnancy outcome in IVF cycles. A prospective, clinical trial. *Eur Rev Med Pharmacol Sci*, 14 (6): 555-561.

Roenneberg, T., Kantermann, T., Juda, M., Vetter, C. & Allebrandt, K. V. (2013) Light and the human circadian clock. *Handbook of experimental pharmacology*, (217): 311-331.

Rogers, P. A. W. (1996) Structure and function of endometrial blood vessels. *Human reproduction update*, 2 (1): 57-62.

Rowan, B. G. & O'Malley, B. W. (2000) Progesterone receptor coactivators. *Steroids*, 65 (10): 545-549.

Rubel, C. A., Lanz, R. B., Kommagani, R., Franco, H. L., Lydon, J. P. & DeMayo, F. J. (2012) Research Resource: Genome-Wide Profiling of Progesterone Receptor Binding in the Mouse Uterus. *Molecular Endocrinology*, 26 (8):

Rutter, J., Reick, M. & McKnight, S. L. (2002) Metabolism and the control of circadian rhythms. *Annual review of biochemistry*, 71 (1): 307-331.

Sakai, N. & Endo, A. (1988) Effects of delayed mating on preimplantation embryos in spontaneously ovulated mice. *Gamete research*, 19 (4): 381-385.

Sakai, T. & Ishida, N. (2001) Circadian rhythms of female mating activity governed by clock genes in Drosophila. *Proceedings of the National Academy of Sciences of the United States of America*, 98 (16): 9221-9225.

Salamonsen, L. A., Zhang, J. & Brasted, M. (2002) Leukocyte networks and human endometrial remodelling. *Journal of reproductive immunology*, 57 (1): 95-108.

Salker, M., Teklenburg, G., Molokhia, M., Lavery, S., Trew, G., Aojanepong, T., Mardon, H. J., Lokugamage, A. U., Rai, R., Landles, C., Roelen, B. A. J., Quenby, S., Kuijk, E. W., Kavelaars, A., Heijnen, C. J., Regan, L., Macklon, N. S. & Brosens, J. J. (2010) Natural Selection of Human Embryos: Impaired Decidualization of Endometrium Disables Embryo-Maternal Interactions and Causes Recurrent Pregnancy Loss. *Plos One*, 5 (4):

Salker, M. S., Christian, M., Steel, J. H., Nautiyal, J., Lavery, S., Trew, G., Webster, Z., Al-Sabbagh, M., Puchchakayala, G., Foeller, M., Landles, C., Sharkey, A. M., Quenby, S., Aplin, J. D., Regan, L., Lang, F. & Brosens, J. J. (2011) Deregulation of the serum- and glucocorticoid-inducible kinase SGK1 in the endometrium causes reproductive failure. *Nature Medicine*, 17 (11):

Salker, M. S., Nautiyal, J., Steel, J. H., Webster, Z., Sucurovic, S., Nicou, M., Singh, Y., Lucas, E. S., Murakami, K., Chan, Y. W., James, S., Abdallah, Y., Christian, M., Croy, B. A., Mulac-Jericevic, B., Quenby, S. & Brosens, J. J. (2012) Disordered IL-33/ST2 Activation in Decidualizing Stromal Cells Prolongs Uterine Receptivity in Women with Recurrent Pregnancy Loss. *Plos One*, 7 (12): 18.

Sanada, K., Okano, T. & Fukada, Y. (2002) Mitogen-activated protein kinase phosphorylates and negatively regulates basic helix-loop-helix-PAS transcription factor BMAL1. *Journal of Biological Chemistry*, 277 (1): 267-271.

Santos, M. A., Teklenburg, G., Macklon, N. S., Van Opstal, D., Schuring-Blom, G. H., Krijtenburg, P.-J., de Vreeden-Elbertse, J., Fauser, B. C. & Baart, E. B. (2010) The fate of the mosaic embryo: chromosomal constitution and development of Day 4, 5 and 8 human embryos. *Human reproduction*, 25 (8): 1916-1926.

Schmutz, I., Ripperger, J. A., Baeriswyl-Aebischer, S. & Albrecht, U. (2010) The mammalian clock component PERIOD2 coordinates circadian output by interaction with nuclear receptors. *Genes & development*, 24 (4): 345-357.

Sellix, M. T. & Menaker, M. (2010) Circadian clocks in the ovary. *Trends in Endocrinology & Metabolism*, 21 (10): 628-636.

Seron-Ferre, M., Valenzuela, G. J. & Torres-Farfan, C. (2007) Circadian clocks during embryonic and fetal development. *Birth Defects Research Part C: Embryo Today: Reviews*, 81 (3): 204-214.

Sharkey, J. T., Puttaramu, R., Word, R. A. & Olcese, J. (2009) Melatonin synergizes with oxytocin to enhance contractility of human myometrial smooth muscle cells. *The Journal of Clinical Endocrinology & Metabolism*, 94 (2): 421-427.

Shibata, H., Spencer, T. E., Oñate, S. A., Jenster, G., Tsai, S. Y., Tsai, M.-J. & O'Malley, B. W. (1996) Role of co-activators and co-repressors in the mechanism of steroid/thyroid receptor action. *Recent Progress in Hormone Research*, 52 141-164.

Shibata, S. & Moore, R. Y. (1988) Development of a fetal circadian rhythm after disruption of the maternal circadian system. *Developmental Brain Research*, 41 (1): 313-317.

Silver, A. C., Arjona, A., Walker, W. E. & Fikrig, E. (2012) The circadian clock controls toll-like receptor 9-mediated innate and adaptive immunity. *Immunity*, 36 (2): 251-261.

Simón, C., Frances, A., Piquette, G., Hendrickson, M., Milki, A. & Polan, M. L. (1994) Interleukin-1 system in the materno-trophoblast unit in human implantation: immunohistochemical evidence for autocrine/paracrine function. *The Journal of Clinical Endocrinology & Metabolism*, 78 (4): 847-854.

Simón, C., Mercader, A., Gimeno, M. J. & Pellicer, A. (1997) The Interleukin-1 System and Human Implantation. *American Journal of Reproductive Immunology*, 37 (1): 64-72.

Smith, E. M., Lin, J.-M., Meissner, R.-A. & Allada, R. (2008) Dominant-negative CK2α induces potent effects on circadian rhythmicity.

So, A. Y. L., Bernal, T. U., Pillsbury, M. L., Yamamoto, K. R. & Feldman, B. J. (2009) Glucocorticoid regulation of the circadian clock modulates glucose homeostasis. *Proceedings of the National Academy of Sciences*, 106 (41): 17582-17587.

So, W. V. & Rosbash, M. (1997) Post-transcriptional regulation contributes to Drosophila clock gene mRNA cycling. *The EMBO Journal*, 16 (23): 7146-7155.

Song, H., Lim, H., Paria, B. C., Matsumoto, H., Swift, L. L., Morrow, J., Bonventre, J. V. & Dey, S. K. (2002) Cytosolic phospholipase A2alpha is crucial [correction of A2alpha deficiency is crucial] for'on-time'embryo implantation that directs subsequent development. *Development (Cambridge, England)*, 129 (12): 2879-2889.

Srinivasan, V., Spence, W. D., Pandi-Perumal, S. R., Zakharia, R., Bhatnagar, K. P. & Brzezinski, A. (2009) Melatonin and human reproduction: shedding light on the darkness hormone. *Gynecological Endocrinology*, 25 (12): 779-785.

Stocker, L. J., Macklon, N. S., Cheong, Y. C. & Bewley, S. J. (2014) Influence of Shift Work on Early Reproductive Outcomes A Systematic Review and Meta-analysis. *Obstetrics and Gynecology*, 124 (1): 99-110.

Stojkovic, K., Wing, S. S. & Cermakian, N. (2014) A central role for ubiquitination within a circadian clock protein modification code. *Frontiers in molecular neuroscience*, 7 69.

Strassmann, B. I. (1996) The evolution of endometrial cycles and menstruation. *Quarterly Review of Biology*, 181-220.

Sugino, N., Shimamura, K., Takiguchi, S., Tamura, H., Ono, M., Nakata, M., Nakamura, Y., Ogino, K., Uda, T. & Kato, H. (1996) Changes in activity of superoxide dismutase in the human endometrium throughout the menstrual cycle and in early pregnancy. *Human Reproduction*, 11 (5): 1073-1078.

Sugiyama, G., Takeuchi, H., Kanematsu, T., Gao, J., Matsuda, M. & Hirata, M. (2013) Phospholipase C-related but catalytically inactive protein, PRIP as a scaffolding protein for phospho-regulation. *Advances in biological regulation*, 53 (3): 331-340.

Summa, K. C., Vitaterna, M. H. & Turek, F. W. (2012) Environmental perturbation of the circadian clock disrupts pregnancy in the mouse.

Sun, C. M., Huang, S. F., Zeng, J. M., Liu, D. B., Xiao, Q., Tian, W. J., Zhu, X. D., Huang, Z. G. & Feng, W. L. (2010) Per2 Inhibits K562 Leukemia Cell Growth In Vitro and In Vivo Through Cell Cycle Arrest and Apoptosis Induction. *Pathology & Oncology Research*, 16 (3): 403-411.

Swanson, W. J. & Vacquier, V. D. (2002) The rapid evolution of reproductive proteins. *Nature Reviews Genetics*, 3 (2): 137-144.

Tabibzadeh, S. (1998) Molecular control of the implantation window. *Human Reproduction Update*, 4 (5): 465-471.

Takano, M., Lu, Z., Goto, T., Fusi, L., Higham, J., Francis, J., Withey, A., Hardt, J., Cloke, B. & Stavropoulou, A. V. (2007) Transcriptional cross talk between the forkhead transcription factor forkhead box O1A and the progesterone receptor coordinates cell cycle regulation and differentiation in human endometrial stromal cells. *Molecular endocrinology*, 21 (10): 2334-2349.

Takayama, H., Nakamura, Y., Tamura, H., Yamagata, Y., Harada, A., Nakata, M., Sugino, N. & Kato, H. (2003) Pineal gland (melatonin) affects the parturition time, but not luteal function and fetal growth, in pregnant rats. *Endocrine journal*, 50 (1): 37-43.

Takeuchi, T., Hinohara, T., Kurosawa, G. & Uchida, K. (2007) A temperature-compensated model for circadian rhythms that can be entrained by temperature cycles. *Journal of theoretical biology*, 246 (1): 195-204.

Tamura, H., Takasaki, A., Miwa, I., Taniguchi, K., Maekawa, R., Asada, H., Taketani, T., Matsuoka, A., Yamagata, Y. & Shimamura, K. (2008) Oxidative stress impairs oocyte quality and melatonin protects oocytes from free radical damage and improves fertilization rate. *Journal of pineal research*, 44 (3): 280-287.

Tanaka, N., Miyazaki, K., Tashiro, H., Mizutani, H. & Okamura, H. (1993) Changes in adenylyl cyclase activity in human endometrium during the menstrual cycle and in human decidua during pregnancy. *Journal of reproduction and fertility*, 98 (1): 33-39.

Tang, A.-W., Alfirevic, Z. & Quenby, S. (2011) Natural killer cells and pregnancy outcomes in women with recurrent miscarriage and infertility: a systematic review. *Human reproduction*, der164.

Teclemariam-Mesbah, R., Ter Horst, G. J., Postema, F., Wortel, J. & Buijs, R. M. (1999) Anatomical demonstration of the suprachiasmatic nucleus-pineal pathway. *The Journal of comparative neurology*, 406 (2): 171-182.

Teklenburg, G., Salker, M., Heijnen, C., Macklon, N. S. & Brosens, J. J. (2010a) The molecular basis of recurrent pregnancy loss: impaired natural embryo selection. *Molecular Human Reproduction*, 16 (12):

Teklenburg, G., Salker, M., Molokhia, M., Lavery, S., Trew, G., Aojanepong, T., Mardon, H. J., Lokugamage, A. U., Rai, R., Landles, C., Roelen, B. A. J., Quenby, S., Kuijk, E. W., Kavelaars, A., Heijnen, C. J., Regan, L., Brosens, J. J. & Macklon, N. S. (2010b) Natural Selection of Human Embryos: Decidualizing Endometrial Stromal Cells Serve as Sensors of Embryo Quality upon Implantation. *Plos One*, 5 (4):

Telgmann, R. & Gellersen, B. (1998) Marker genes of decidualization: activation of the decidual prolactin gene. *Human Reproduction Update*, 4 (5): 472-479.

Telgmann, R., Maronde, E., Taskén, K. & Gellersen, B. (1997) Activated Protein Kinase A Is Required for Differentiation-Dependent Transcription of the Decidual Prolactin Gene in Human Endometrial Stromal Cells 1. *Endocrinology*, 138 (3): 929-937.

Terunuma, M., Jang, I.-S., Ha, S. H., Kittler, J. T., Kanematsu, T., Jovanovic, J. N., Nakayama, K. I., Akaike, N., Ryu, S. H. & Moss, S. J. (2004) GABAA receptor phospho-dependent modulation is regulated by phospholipase C-related inactive protein type 1, a novel protein phosphatase 1 anchoring protein. *The Journal of neuroscience*, 24 (32): 7074-7084.

Thoennissen, N. H., Thoennissen, G. B., Abbassi, S., Nabavi-Nouis, S., Sauer, T., Doan, N. B., Gery, S., Muller-Tidow, C., Said, J. W. & Koeffler, H. P. (2012) Transcription factor CCAAT/enhancer-binding protein alpha and critical circadian clock downstream target gene PER2 are highly deregulated in diffuse large B-cell lymphoma. *Leukemia & Lymphoma*, 53 (8): 1577-1585.

Trowsdale, J. & Betz, A. G. (2006) Mother's little helpers: mechanisms of maternal-fetal tolerance. *Nature immunology*, 7 (3): 241-246.

Tsai, T.-L., Wang, B., Squire, M. W., Guo, L.-W. & Li, W.-J. (2015) Endothelial cells direct human mesenchymal stem cells for osteo-and chondro-lineage differentiation through endothelin-1 and AKT signaling. *Stem cell research & therapy*, 6 (1): 1-14.

Turek, F. W., Joshu, C., Kohsaka, A., Lin, E., Ivanova, G., McDearmon, E., Laposky, A., Losee-Olson, S., Easton, A. & Jensen, D. R. (2005) Obesity and metabolic syndrome in circadian Clock mutant mice. *Science*, 308 (5724): 1043-1045.

Uchikawa, M., Kawamura, M., Yamauchi, N. & Hattori, M.-a. (2011) Down-Regulation of Circadian Clock Gene Period 2 in Uterine Endometrial Stromal Cells of Pregnant Rats During Decidualization. *Chronobiology International*, 28 (1):

Ueyama, T., Krout, K. E., Van Nguyen, X., Karpitskiy, V., Kollert, A., Mettenleiter, T. C. & Loewy, A. D. (1999) Suprachiasmatic nucleus: a central autonomic clock. *Nature neuroscience*, 2 (12): 1051-1053.

Uji, A., Matsuda, M., Kukita, T., Maeda, K., Kanematsu, T. & Hirata, M. (2002) Molecules interacting with PRIP-2, a novel Ins (1, 4, 5) P 3 binding protein type 2: Comparison with PRIP-1. *Life sciences*, 72 (4): 443-453.

Urlep, Z. & Rozman, D. (2013) The interplay between circadian system, cholesterol synthesis, and steroidogenesis affects various aspects of female reproduction. *Frontiers in endocrinology*, 4

Vanneste, E., Voet, T., Le Caignec, C., Ampe, M., Konings, P., Melotte, C., Debrock, S., Amyere, M., Vikkula, M. & Schuit, F. (2009) Chromosome instability is common in human cleavage-stage embryos. *Nature medicine*, 15 (5): 577-583.

Vanselow, K., Vanselow, J. T., Westermark, P. O., Reischl, S., Maier, B., Korte, T., Herrmann, A., Herzel, H., Schlosser, A. & Kramer, A. (2006) Differential effects of PER2 phosphorylation: molecular basis for the human familial advanced sleep phase syndrome (FASPS). *Genes & Development*, 20 (19): 2660-2672.

Wagner, B. L., Norris, J. D., Knotts, T. A., Weigel, N. L. & McDonnell, D. P. (1998) The nuclear corepressors NCoR and SMRT are key regulators of both ligand-and 8-bromo-cyclic AMP-dependent transcriptional activity of the human progesterone receptor. *Molecular and cellular biology*, 18 (3): 1369-1378.

Wang, W., Li, Q. X., Bagchi, I. C. & Bagchi, M. K. (2010a) The CCAAT/Enhancer Binding Protein beta Is a Critical Regulator of Steroid-Induced Mitotic Expansion of Uterine Stromal Cells during Decidualization. *Endocrinology*, 151 (8): 3929-3940.

Wang, Y., Zhao, A.-M. & Lin, Q.-D. (2010b) Role of cyclooxygenase-2 signaling pathway dysfunction in unexplained recurrent spontaneous abortion. *Chinese medical journal*, 123 (12): 1543-1547.

Watanabe, S., Akiyama, S., Hanita, T., Li, H., Nakagawa, M., Kaneshi, Y., Ohta, H. & Japan, R. E. D. f. s. g. (2013) Designing artificial environments for preterm infants based on circadian studies on pregnant uterus. *Frontiers in endocrinology*, 4

Wheeler, M. D. (1991) Physical changes of puberty. *Endocrinology and metabolism clinics of North America*, 20 (1): 1-14.

Wolff, E. F., Wolff, A. B., Du, H. & Taylor, H. S. (2007) Demonstration of multipotent stem cells in the adult human endometrium by in vitro chondrogenesis. *Reproductive sciences*, 14 (6): 524-533.

Woo, K.-C., Ha, D.-C., Lee, K.-H., Kim, D.-Y., Kim, T.-D. & Kim, K.-T. (2010) Circadian amplitude of cryptochrome 1 is modulated by mRNA stability regulation via cytoplasmic hnRNP D oscillation. *Molecular and cellular biology*, 30 (1): 197-205.

Woo, K.-C., Kim, T.-D., Lee, K.-H., Kim, D.-Y., Kim, W., Lee, K.-Y. & Kim, K.-T. (2009) Mouse period 2 mRNA circadian oscillation is modulated by PTB–mediated rhythmic mRNA degradation. *Nucleic acids research*, 37 (1): 26-37.

Wu, J. C., Kelsoe, J. R., Schachat, C., Bunney, B. G., DeModena, A., Golshan, S., Gillin, J. C., Potkin, S. G. & Bunney, W. E. (2009) Rapid and sustained antidepressant response with sleep deprivation and chronotherapy in bipolar disorder. *Biological psychiatry*, 66 (3): 298-301.

Xu, X. B., He, B. & Wang, J. D. (2007) Menstrual-like changes in mice are provoked through the pharmacologic withdrawal of progesterone using mifepristone following induction of decidualization. *Human reproduction*, 22 (12): 3184-3191.

Yamaguchi, S., Isejima, H., Matsuo, T., Okura, R., Yagita, K., Kobayashi, M. & Okamura, H. (2003) Synchronization of cellular clocks in the suprachiasmatic nucleus. *Science*, 302 (5649): 1408-1412.

Yamazaki, S., Numano, R., Abe, M., Hida, A., Takahashi, R.-i., Ueda, M., Block, G. D., Sakaki, Y., Menaker, M. & Tei, H. (2000) Resetting central and peripheral circadian oscillators in transgenic rats. *Science*, 288 (5466): 682-685.

Yoo, S.-H., Yamazaki, S., Lowrey, P. L., Shimomura, K., Ko, C. H., Buhr, E. D., Siepka, S. M., Hong, H.-K., Oh, W. J. & Yoo, O. J. (2004) PERIOD2:: LUCIFERASE real-time reporting of circadian dynamics reveals persistent circadian oscillations in mouse peripheral tissues. *Proceedings of the National Academy of Sciences of the United States of America*, 101 (15): 5339-5346.

Yoo, S. H., Ko, C. H., Lowrey, P. L., Buhr, E. D., Song, E. J., Chang, S. W., Yoo, O. J., Yamazaki, S., Lee, C. & Takahashi, J. S. (2005) A noncanonical E-box enhancer drives mouse Period2 circadian oscillations in vivo. *Proceedings of the National Academy of Sciences of the United States of America*, 102 (7): 2608-2613.

Yoshino, O., Osuga, Y., Hirota, Y., Koga, K., Yano, T., Tsutsumi, O. & Taketani, Y. (2003) Akt as a possible intracellular mediator for decidualization in human endometrial stromal cells. *Molecular human reproduction*, 9 (5): 265-269.

Yu, W., Ikeda, M., Abe, H., Honma, S., Ebisawa, T., Yamauchi, T., Honma, K.-i. & Nomura, M. (1999) Characterization of three splice variants and genomic organization of the mouse BMAL1 gene. *Biochemical and biophysical research communications*, 260 (3): 760-767.

Zhang, Z., Takeuchi, H., Gao, J., Wang, D., James, D. J., Martin, T. F. J. & Hirata, M. (2013) PRIP (phospholipase C-related but catalytically inactive protein) inhibits exocytosis by direct interactions with syntaxin 1 and SNAP-25 through its C2 domain. *Journal of Biological Chemistry*, 288 (11): 7769-7780.

Zhu, J. L., Hjollund, N. H., Boggild, H. & Olsen, J. (2003) Shift work and subfecundity: a causal link or an artefact? *Occupational and environmental medicine*, 60 (9): e12-e12.

Zoumakis, E., Margioris, A. N., Stournaras, C., Dermitzaki, E., Angelakis, E., Makrigiannakis, A., Koumantakis, E. & Gravanis, A. (2000) Corticotrophin-releasing hormone (CRH) interacts with inflammatory prostaglandins and interleukins and affects the decidualization of human endometrial stroma. *Molecular human reproduction*, 6 (4): 344-351.

Publications

The clock protein period 2 synchronizes mitotic expansion and decidual transformation of human endometrial stromal cells

Joanne Muter,* Emma S. Lucas,* Yi-Wah Chan,† Paul J. Brighton,* Jonathan D. Moore,† Lauren Lacey,* Siobhan Quenby,* Eric W.-F. Lam,‡ and Jan J. Brosens*,[1]

*Division of Translational & Systems Medicine, Warwick Medical School, and †Warwick Systems Biology Centre, University of Warwick, Coventry, United Kingdom; and ‡Department of Surgery and Cancer, Imperial College London, Imperial Centre for Translational and Experimental Medicine, London, United Kingdom

ABSTRACT **Implantation requires coordinated interactions between the conceptus and surrounding decidual cells, but the involvement of clock genes in this process is incompletely understood. Circadian oscillations are predicated on transcriptional-translational feedback loops, which balance the activities of the transcriptional activators CLOCK (circadian locomotor output cycles kaput) and brain muscle arnt-like 1 and repressors encoded by *PER* (Period) and *Cryptochrome* genes. We show that loss of PER2 expression silences circadian oscillations in decidualizing human endometrial stromal cells (HESCs). Downregulation occurred between 12 and 24 hours following differentiation and coincided with reduced CLOCK binding to a noncanonical E-box enhancer in the *PER2* promoter. RNA sequencing revealed that premature inhibition of PER2 by small interfering RNA knockdown leads to a grossly disorganized decidual response. Gene ontology analysis highlighted a preponderance of cell cycle regulators among the 1121 genes perturbed upon PER2 knockdown. Congruently, PER2 inhibition abrogated mitotic expansion of differentiating HESCs by inducing cell cycle block at G2/M. Analysis of 70 midluteal endometrial biopsies revealed an inverse correlation between *PER2* transcript levels and the number of miscarriages in women suffering reproductive failure (Spearman rank test, $\rho = -0.3260$; $P = 0.0046$). Thus, PER2 synchronizes endometrial proliferation with initiation of aperiodic decidual gene expression; uncoupling of these events may cause recurrent pregnancy loss.—Muter, J., Lucas, E. S., Chan, Y.-W., Brighton, P. J., Moore, J. D., Lacey, L., Quenby, S., Lam, E. W.-F., Brosens, J. J. The clock protein period 2 synchronizes mitotic expansion and decidual transformation of human endometrial stromal cells. *FASEB J.* 29, 1603–1614 (2015). www.fasebj.org**

Key Words: endometrium · circadian rhythm · cell cycle · miscarriage

MAMMALIAN REPRODUCTION IS dependent on a series of interlocking signals that control the onset of puberty and the timing of ovulation, blastocyst implantation, and parturition (1). The central circadian pacemakers in the suprachiasmatic nucleus (SCN) are responsible for the establishment of daily rhythms entrained by environmental cues (2–4). These SCN pacemakers relay photic information to GnRHs in the hypothalamus, which is cascaded to the ovaries through the release of pituitary gonadotropins and thus control reproductive cyclicity and ovulation (5, 6). In addition, various cell types in the ovary, fallopian tube, and uterus have their own functional molecular clocks that control circadian gene expression (5, 7, 8). At a cellular level, the circadian clockwork is composed of a set of 4 core clock genes and their paralogs that establish robust and stable transcriptional and translational feedback loops (4). BMAL1 [brain muscle arnt-like 1, encoded by aryl hydrocarbon receptor nuclear translocator-like (*ARNTL*)] and CLOCK (circadian locomotor output cycles kaput) form a heterodimer that binds to specific DNA motifs (E-boxes) in the promoter regions of target genes, including the *Period* (*PER*; *1*, *PER2*, and *PER3*) and the *Cryptochrome* (*CRY*; *1* and *2*) genes. PER and CRY proteins then accumulate in the cytoplasm and, after a lag period, return to the nucleus to inhibit their own transcription as well as the expression of other genes activated by the CLOCK-BMAL1 heterodimer (9, 10). In addition, clock

Abbreviations: 8-br-cAMP, 8-bromoadenosine-cAMP; ARNTL, aryl hydrocarbon receptor nuclear translocator-like; BMAL1, brain muscle arnt-like 1; bp, base pair; ChIP, chromatin immunoprecipitation; CLOCK, circadian locomotor output cycles kaput; CRY, cryptochrome; DCC-FBS, dextran-coated charcoal-treated fetal bovine serum; ERα, estrogen receptor-α; (*continued on next page*)

[1] Correspondence: Department of Reproductive Health, Clinical Science Research Institute, Warwick Medical School, University Hospital, Coventry CV2 2DX, United Kingdom. E-mail: j.j.brosens@warwick.ac.uk

doi: 10.1096/fj.14-267195

This article includes supplemental data. Please visit *http://www.fasebj.org* to obtain this information.

proteins are subjected to a wide range of posttranslational modifications, including phosphorylation (11), acetylation (12), ubiquitination (13), and sumoylation (14), that act to fine-tune rhythmic oscillations over an ~24 hour period.

Tissue-specific gene deletions in mice have highlighted the importance of the peripheral clocks in female reproduction. For example, conditional deletion of *Bmal1* in pituitary gonadotropes impacts on estrous cycle length (15), whereas in the ovary and myometrium, it perturbs steroidogenesis and the timing of parturition, respectively (16, 17). A key uterine response indispensable for pregnancy is decidualization, a process characterized by the transformation of endometrial stromal cells into specialist secretory cells that provide a nutritive and immune-privileged matrix for the invading blastocyst and subsequent placental formation (18). Previous studies using transgenic rats expressing a destabilized luciferase reporter under the control of the mouse *Per2* promoter have shown that decidualization is associated with down-regulation of Per2 and loss of circadian luciferase oscillations (19). Moreover, female mice lacking both *Per1* and *Per2* reportedly have more implantation sites but fewer live offspring when compared to wild-type animals (20), indicating that these clock proteins are indispensable for optimal utero-placental interactions.

Unlike the rat and other rodents, decidualization of the human endometrium is not under the control of an implanting blastocyst. Instead, this process is driven by the postovulatory rise in progesterone levels and increasing local cAMP production. Consequently, this process is initiated in each ovulatory cycle and enhanced in response to embryonic signals (18, 21). Decidualization is a dynamic and temporally regulated process that commences with proliferative expansion of the stromal cells during the midluteal phase of the cycle (22). Once initiated, differentiating human endometrial stromal cells (HESCs) mount a transient proinflammatory response that renders the endometrium receptive to implantation. This is followed by an anti-inflammatory response, expansion of cytoplasmic organelles, and acquisition of a secretory phenotype that characterizes decidualizing cells during the late-luteal phase of the cycle (23, 24). Disruption of the temporal organization of the decidual response leads to reproductive failure. For example, endometriosis is associated with uterine progesterone resistance, a blunted decidual response, implantation failure, and conception delay (25). Conversely, a disordered proinflammatory decidual response prolongs the window of endometrial receptivity, which in turn increases the risk for out-of-phase implantation and recurrent pregnancy loss (RPL) (23, 24).

This study investigated the role and regulation of clock proteins during decidual transformation of HESCs. As is the case in rodents, we found that circadian oscillations are lost in differentiating HESCs as a consequence of down-regulation of PER2, which occurs between 12 and 24 hours after exposure of a deciduogenic stimulus. Timing of this event is critical because premature loss of PER2 abolishes mitotic expansion of HESCs and predisposes for a highly disorganized decidual response. The importance of this transitional pathway was underscored by analysis of midluteal endometrial biopsies from recurrent miscarriage patients, showing an inverse correlation between *PER2* mRNA levels and the number of preceding failed pregnancies.

MATERIALS AND METHODS

Patient selection and endometrial sampling

The study was approved by the National Health Service (NHS) National Research Ethics-Hammersmith and Queen Charlotte's & Chelsea Research Ethics Committee (1997/5065). Subjects were recruited from the Implantation Clinic, a dedicated research clinic at University Hospitals Coventry and Warwickshire NHS Trust. Written informed consent was obtained from all participants in accordance with the guidelines in The Declaration of Helsinki 2000. Samples were obtained using a Wallach Endocell sampler (Wallach Surgical Devices, Trumbull, CT, USA), starting from the uterine fundus and moving downward to the internal cervical ostium. A total of 57 fresh endometrial biopsies were processed for primary cultures. The average age (±SD) of the participants was 35.1 ± 4.7 years. For analysis of *PER2* mRNA expression, 70 additional biopsies stored in RNA*later* solution (Sigma-Aldrich, Poole, United Kingdom) were obtained from patients with RPL. Demographic details are summarized in Supplemental Table 1. All endometrial biopsies were timed between 6 and 10 days after the preovulatory LH surge. None of the subjects was on hormonal treatments for at least 3 months before the procedure.

Primary cell culture

HESCs were isolated from endometrial tissues as described previously (26). Purified HESCs were expanded in maintenance medium of DMEM/F-12 containing 10% dextran-coated charcoal-treated fetal bovine serum (DCC-FBS), L-glutamine (1%), and 1% antibiotic-antimycotic solution. Confluent monolayers were decidualized in DMEM/F-12 containing 2% DCC-FBS with 0.5 mM 8-bromoadenosine-cAMP (8-br-cAMP; Sigma-Aldrich) with or without 10^{-6} M medroxyprogesterone acetate (MPA; Sigma-Aldrich) to induce a differentiated phenotype. For synchronization, dexamethasone (Sigma-Aldrich) was used at 100 nM for 30 minutes. Actinomycin D (Sigma-Aldrich) was used at a final concentration of 2 μM in DMSO. All experiments were carried out before the third cell passage.

Real-time quantitative RT-PCR

Total RNA was extracted from HESC cultures using RNA STAT-60 (AMS Biotechnology, Abingdon, United Kingdom). Equal amounts of total RNA (1 μg) were treated with DNase and reverse transcribed using the QuantiTect Reverse Transcription Kit (Qiagen, Manchester, United Kingdom), and the resulting cDNA was used as template in quantitative RT-PCR (qRT-PCR) analysis. Detection of gene expression was performed with Power SYBR Green Master Mix (Life Technologies, Paisley, United Kingdom) and the 7500 Real-Time PCR System (Applied Biosystems, Foster City, CA, USA). The expression levels of the samples were calculated using the ΔCt method, incorporating the efficiencies of each primer pair. The variances of input cDNA

(*continued from previous page*)

GEO, Gene Expression Omnibus; GO, gene ontology; HESC, human endometrial stromal cell; ID, identification; IGFBP1, IGF-binding protein-1; MPA, medroxyprogesterone acetate; NHS, National Health Service; NT, nontargeting; PER1, period 1; PER2, period 2; PPARG, peroxisome proliferator-activated receptor γ; PRL, prolactin; qRT-PCR, quantitative RT-PCR; RPL, recurrent pregnancy loss; RTCA, real-time cell analyzer; SCN, suprachiasmatic nucleus; SDS, sodium dodecyl sulfate; siRNA, small interfering RNA; TPM, transcripts per million

were normalized against the levels of the *L19* housekeeping gene. All measurements were performed in triplicate. Melting curve analysis confirmed amplification specificity. Primer sequences used are as follows: CLOCK, forward 5′-gac aaa gcg aaa aga gta tct ag-3′ and reverse 5′-cat ctt tct agc att acc agg aa-3′; BMAL1, forward 5′-gac att cct tcc agt ggc cta-3′ and reverse 5′-tac cta tgt ggg ggt tct cac-3′; CRY1, forward 5′-cat cct gga ccc ctg gtt-3′ and reverse 5′-cac tga agc aaa aat cgc c-3′; CRY2, forward 5′-ctg ttc aag gaa tgg gga gtg-3′ and reverse 5′-ggt cat aga ggg tat gag aat tc-3′; PER1, forward 5′-atg gtt cca ctg ctc cat ctc-3′ and reverse 5′-ccg gtc agg acc tcc tc-3′; PER2, forward 5′-gtc cga aag ctt cgt tcc aga-3′ and reverse 5′-gtc cac atc ttc ctg cag tg-3′; and prolactin (PRL), forward 5′-aag ctg tag aga ttg agg agc aaa c-3′ and reverse 5′-tca gga tga acc tgg ctg act a-3′. In the actinomycin D experiments, *PER2* mRNA half-life was calculated using $t_{1/2} = 0.693/k$, where k is the slope derived from the linear equation $\ln C = lnC_0 - kt$, and where C is the relative level of *PER* mRNA in HESCs (27).

Western blot analysis

Whole-cell protein extracts were prepared by lysing cells in RIPA buffer containing protease inhibitors (cOmplete, Mini, EDTA-free; Roche, Welwyn Garden City, United Kingdom). Protein yield was quantified using the Bio-Rad Protein Assay Dye Reagent Concentrate (Bio-Rad Laboratories, Hemel Hempstead, United Kingdom). Equal amounts of protein were separated by SDS-PAGE before wet transfer onto PVDF membrane (GE Healthcare, Buckinghamshire, United Kingdom). Nonspecific binding sites were blocked by overnight incubation with 5% nonfat dry milk in Tris-buffered saline with 1% Tween 20 [130 mM NaCl, 20 mM Tris (pH 7.6), and 1% Tween 20]. The following primary antibodies were purchased from Abcam (Cambridge, United Kingdom): anti-CLOCK (catalog number ab3517, diluted 1:3000); anti-BMAL1 (ab3350, 1:375); anti-CRY1 (ab54649, 1:500); anti-CRY2 (ab38872, 1:2000); anti-PER1 (ab3443, 1:300); anti-PER2 (ab179813, 1:300); and anti-β-actin (ab8226, 1:10,000). Protein complexes were visualized with ECL Plus chemiluminescence (GE Healthcare). The Western blots are collated in Supplemental Fig. 1.

Transient transfection

Primary HESCs were transfected with small interfering RNA (siRNA) by jetPRIME Polyplus transfection kit (VWR International, Lutterworth, United Kingdom). For gene silencing, undifferentiated HESCs were transiently transfected with 50 nM PER2-siGENOME SMARTpool or siGENOME Non-Targeting siRNA Pool 1 (Dharmacon, GE Healthcare). Transfection studies were performed in triplicate and repeated on primary cultures from 3 subjects.

Chromatin immunoprecipitation

HESCs in 10 cm culture dishes were fixed with 1% formaldehyde for 10 minutes at 37°C. Fixation was stopped with 125 mM glycine, and nuclei were isolated by incubating at 4°C for 10 minutes in 1 ml Swelling buffer [25 mM 4-(2-hydroxyethyl)-1-piperazineethanesulfonic acid (pH 7.9), 1.5 mM $MgCl_2$, 10 mM KCl, and 0.1% NP40 alternative]. The cells were scraped, homogenized, and centrifuged for 3 minutes at 16,000 × *g* at 4°C. Pelleted nuclei were resuspended in 500 μl sodium dodecyl sulfate (SDS) lysis buffer [1% SDS, 1% Triton X-100, 0.5% deoxycholate, 10 mM EDTA, and 500 mM Tris-HCl (pH 8.1)] and sonicated for 30 minutes at 4°C on high power in a Diagenode Bioruptor sonicator (Diagenode, Liege, Belgium). The resulting suspension was centrifuged for 15 minutes at 16,000 × *g* at 4°C and supernatant diluted in immunoprecipitation buffer [0.01% SDS, 1.1% Triton X-100, 1.2 mM EDTA, 16.7 mM Tris-HCl (pH 8.1), and 167 mM NaCl] and then precleared at 4°C for 3 hours with Protein A Dynabeads (Life Technologies, Carlsbad, CA, USA). The chromatin was then complexed overnight at 4°C with the appropriate antibody bound to Protein A Dynabeads. Post complexing, samples were washed with the following buffers before eluting the chromatin with 250 μl Elution buffer (1% SDS and 100 mM $NaHCO_3$) and incubating at room temperature for 15 minutes: low-salt buffer [0.1% SDS, 1% Triton X-100, 2 mM EDTA, 20 mM Tris-HCl (pH 8.1), and 150 mM NaCl]; high-salt buffer [0.1% SDS, 1% Triton X-100, 2 mM EDTA, 20 mM Tris-HCl (pH 8.1), and 500 mM NaCl]; LiCl buffer [250 mM LiCl, 1% NP40 alternative, 1% deoxycholate, 1 mM EDTA, and 10 mM Tris-HCl (pH 8.1)]; and Tris-EDTA buffer [10 mM Tris-HCl (pH 8) and 1 mM EDTA]. A total of 200 mM NaCl was added to reverse cross-link the proteins and the DNA. After an overnight incubation at 65°C, 10 mM EDTA, 40 mM Tris-HCl (pH 8), and 40 μg/ml protease K (Sigma-Aldrich) were added, and the sample was incubated for a further hour at 55°C before proceeding with the DNA purification using the QIAquick PCR purification kit (Qiagen). Buffers were supplemented with protease and phosphatase inhibitor cocktails (Sigma-Aldrich) and 10 mM sodium butyrate (28). The following antibodies were used in the chromatin immunoprecipitation (ChIP) experiments: CLOCK (Abcam), and as negative control, the rabbit polyclonal anti-mouse IgG (M7023; Sigma-Aldrich). The purified DNA was amplified by qRT-PCR using the following primers: PER2 E-box, forward 5′-cag at gaga cgg agt cgc-3′ and reverse 5′-ccc aca gct gca cgt atc-3′; and PER1 E-box, forward 5′-cac gtg cgc ccg tgt gt-3′ and reverse 5′-ccg att ggc tgg gga tct c-3′.

RNA sequencing and data analysis

Total RNA was extracted using RNA STAT-60 from primary HESC cultures first transfected with either PER2 or nontargeting (NT) siRNA and then decidualized with 8-br-cAMP and MPA for 24 hours. There were 3 biologic repeat experiments performed. RNA quality was analyzed on an Agilent 2100 Bioanalyzer (Agilent Technologies, Wokingham, United Kingdom). RNA integrity number score for all samples was ≥8.9. Transcriptomic maps of single-end reads were generated using Bowtie 2.2.3 (29), SAMtools 0.1.19, and TopHat 2.0.12 (30) against the University of California, Santa Cruz, hg19 reference transcriptome (2014) from the Illumina iGenomes resource using the fr-firststrand setting. Gene counts were estimated using HTSeq 0.6.1 (*www-huber.embl.de/users/anders/HTSeq/*). Transcripts per million (TPM) were calculated as recently described (31). Count data from the TopHat-HTSeq pipeline were analyzed using 2 different methods for differential expression detection, *i.e.*, DESeq and edgeR (32, 33). Expression was considered to be significantly different if the false discovery rate value (edgeR) or adjusted *P* value (DESeq) was <0.01. Differentially expressed genes were retained if they were detected by at least 2 of the methods used. Expression data have been submitted to the Gene Expression Omnibus (GEO) repository (GSE62854).

In vitro colony-forming assay

Transfected HESCs were seeded at a clonal density of 50 cells/cm^2 (to ensure equal loading) onto fibronectin-coated 60 mm culture dishes and cultured in growth medium: DMEM/F-12 containing 10% DCC-FBS, 1% L-glutamine (Invitrogen, Paisley, United Kingdom), 1% antibiotic-antimycotic solution (Invitrogen), insulin (2 μg/ml) (Sigma-Aldrich), estradiol

(1 nM) (Sigma-Aldrich), and basic fibroblast growth factor (10 ng/ml) (Merck Millipore, Watford, United Kingdom). The first medium change was after 7 days. Colonies were monitored microscopically to ensure that they were derived from single cells. Cultures were terminated at 10 days and stained with hematoxylin.

Cell cycle analysis, viability, and proliferation assays

For cell cycle analysis, HESCs in suspension were washed with PBS, fixed with cold 70% ethanol, ribonuclease-A (Qiagen) treated, stained with propidium iodide (Sigma-Aldrich), and subjected to flow cytometry analysis. Cell cycle distribution was assessed using FlowJo software (Ashland, OR, USA).

Real-time adherent cell proliferation was determined by the label-free xCELLigence Real-Time Cell Analyzer (RTCA) DP instrument (Roche Diagnostics Gesellschaft mit beschränkter Haftung, Basel, Switzerland), which utilizes specialized microtiter culture plates containing an interdigitized gold microelectrode on which cells attach and proliferate. Cell contact with the electrode increases the impedance across these gold arrays and reported as an arbitrary "cell index" value as an indication of confluency and adherence (34). HESCs were seeded into 16-well plates (E-plate-16; Roche Diagnostics Gesellschaft mit beschränkter Haftung) at a density of 10,000 cells per well and cultured in 10% DCC-FBS until ~80% confluent. The RTCA DP instrument was placed at 37°C in a humidified environment with 95% air and 5% CO_2, and cells were decidualized following transient transfection as per standard protocols. Individual wells within the E-plate-16 were referenced immediately and monitored first every 15 minutes for 3 hours and then hourly for 4 days. Changes in cell index were captured and analyzed using the RTCA Software v1.2 supplied with the instrument.

Statistical analysis

Data were analyzed with the statistical package GraphPad Prism 6 (GraphPad Software Incorporated, La Jolla, CA, USA). Unpaired Student's *t* test, Mann–Whitney *U* test, Spearman rank correlation, and 1-way ANOVA with *post hoc* Tukey's test were used when appropriate. Statistical significance was assumed when $P < 0.05$.

RESULTS

Loss of circadian oscillations upon decidualization of HESCs

Decidualization of stromal cells in the rat uterus is associated with loss of circadian rhythms (19). We speculated that this phenomenon may aid in synchronizing maternal and embryonic gene expression at implantation and, thus, be conserved. To test this hypothesis, we measured the transcript levels of 6 core clock genes, *i.e.*, *CLOCK*, *BMAL1* (*ARNTL*), *CRY1*, *CRY2*, *PER1*, and *PER2*, in primary undifferentiated HESCs and cells decidualized for 4 days. Following dexamethasone synchronization, all 6 clock genes exhibited circadian regulation in undifferentiated cultures with the amplitude of gene expression varying up to 5-fold over a 26 hour period (**Fig. 1**). By contrast, expression was uniformly aperiodic in decidualizing cultures, confirming that differentiation of HESCs is also associated with loss of rhythmicity.

To investigate the underlying mechanism, we profiled the expression of the same clock genes in undifferentiated HESCs and cells decidualized for 2, 4, or 8 days. Decidualization elicited modest but consistent changes in the

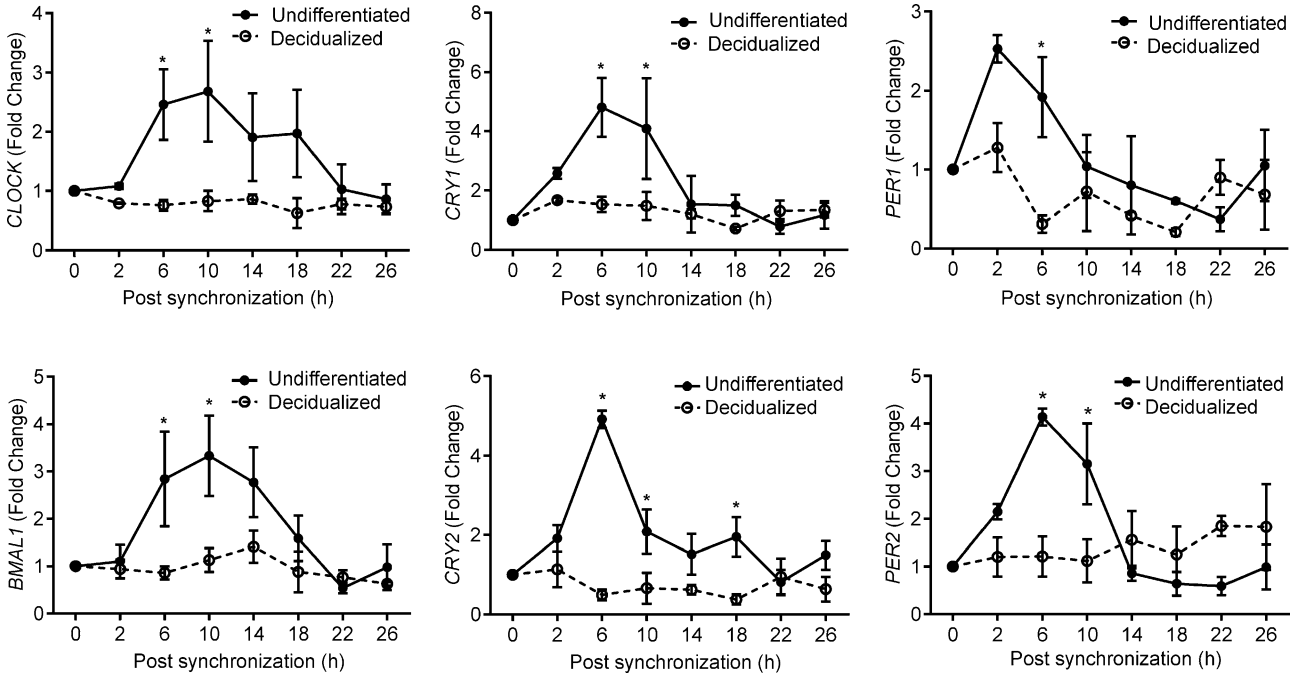

Figure 1. Decidualization silences circadian oscillations in HESCs. Primary undifferentiated HESCs and cultures first decidualized with 8-br-cAMP and MPA for 4 days were treated with dexamethasone for 30 minutes, and transcript levels of 6 core clock genes were measured at the indicated time points. The data show relative change (mean ± SEM) in transcript levels in 3 independent primary cultures. *$P < 0.05$.

expression of several transcripts, including up-regulation of *BMAL1* mRNA levels and down-regulation of *CRY1* and *CRY2* expression (**Fig. 2*A***). The changes at transcript level were also apparent at protein level (Fig. 2*B*). Although up-regulation of *PER1* transcripts did not reach statistical significance, expression of the protein gradually increased as the decidual process unfolded. By contrast, *CLOCK* expression remained constant over the 8 day time course. The most striking observation, however, was the rapid and profound inhibition of *PER2* expression with transcript levels falling by 80% within 2 days of differentiation (Fig. 2*A*). Western blot analysis confirmed the dramatic decline in PER2 levels upon decidualization (Fig. 2*B*). Furthermore, PER2 mobility on SDS-PAGE became more focused and noticeably enhanced, suggesting that decidualization also impacts on the posttranslational modification status of this component of the circadian machinery.

Because circadian oscillations are predicated on autoregulatory feedback loops, we postulated that PER2 knockdown in undifferentiated HESCs would recapitulate the changes in core clock components associated with decidualization. To test this hypothesis, primary undifferentiated HESCs were transfected with either PER2 or NT siRNA and harvested after 4 days. Although PER2 knockdown resulted in a reciprocal up-regulation of PER1, it did not recapitulate the other decidual changes, suggesting that multiple clock regulators are modulated in response to HESC differentiation (Fig. 2*C*, *D*).

Mechanism of PER2 inhibition

To provide insight into the mechanism of *PER2* down-regulation, we first treated primary HESCs with 8-br-cAMP, MPA, or a combination. The decline in *PER2* expression was more pronounced with MPA than 8-br-cAMP (**Fig. 3*A***), although the level of inhibition was not statistically significant with either treatment. By contrast, combined treatment had an additive effect, reducing *PER2* expression by 70% after 48 hours when compared to vehicle-treated control ($P < 0.01$). Mining of available ChIP data sets revealed no changes in the levels of trimethylated lysine

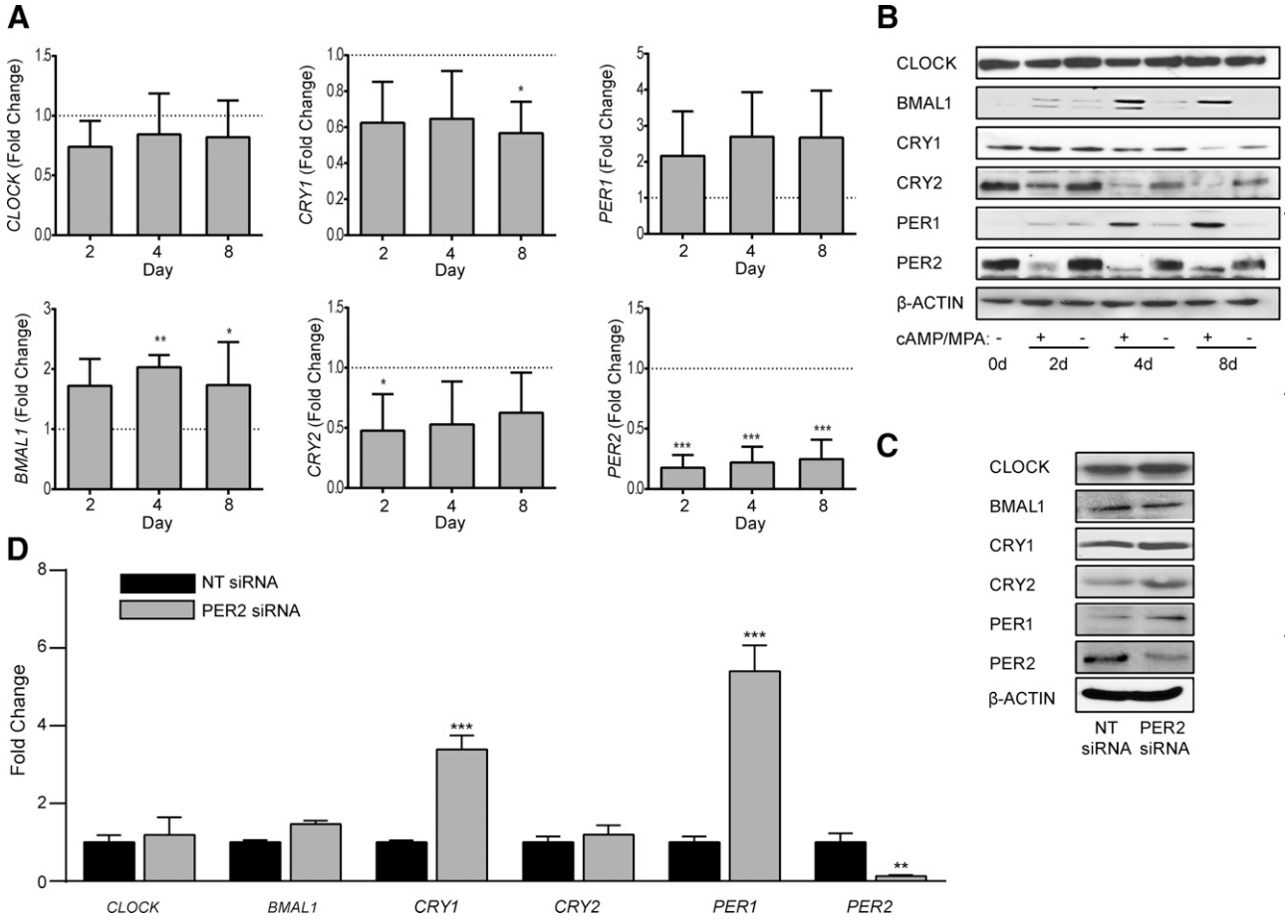

Figure 2. Expression of clock genes in decidualizing HESCs. *A*) The transcripts levels of 6 core clock genes were measured in undifferentiated HESCs and cells decidualized with 8-br-cAMP and MPA for 2, 4, or 8 days. The data show expression (mean ± SEM) relative to that in undifferentiated cells (dotted line) in 3 independent primary cultures. *B*) Total protein lysates from parallel cultures were subjected to Western blotting. β-Actin served as a loading control. *C*) Western blot analysis of total cell lysates obtained 48 hours following transfection of primary cultures with NT or PER2 siRNA. *D*) mRNA levels of core clock genes were also determined 48 hours following transfection of primary cultures with NT or PER2 siRNA. At 2 days after transfection, the efficacy of siRNA-mediated knockdown of PER2 was 87 and 53% at mRNA and protein level, respectively. The data show relative change (mean ± SEM) in transcript levels in 3 independent primary cultures. $^*P < 0.05$; $^{**}P < 0.01$; $^{***}P < 0.001$.

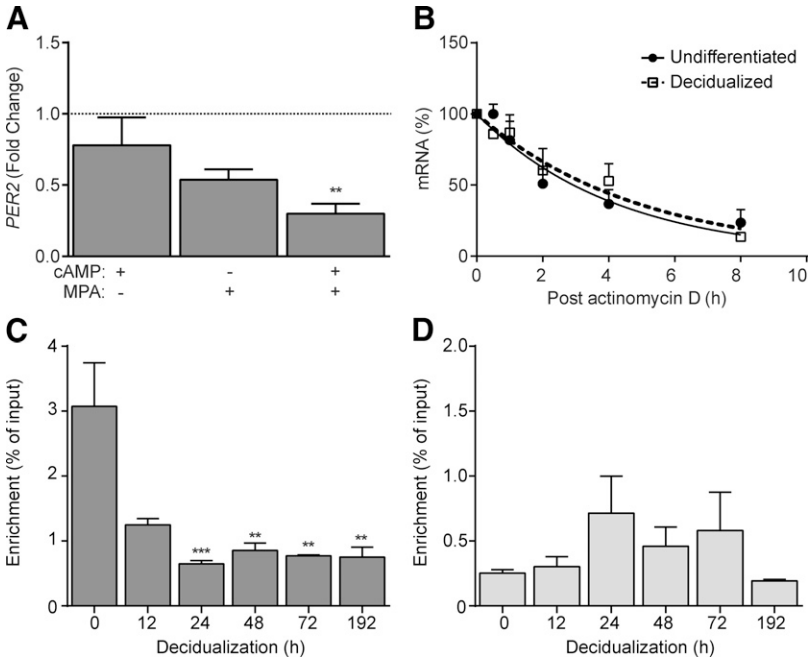

Figure 3. Regulation of *PER2* in decidualizing HESCs. *A*) Primary HESC cultures were treated with 8-br-cAMP, MPA, or a combination for 48 hours and *PER2* transcript levels measured. The data show relative change (mean ± SEM) in mRNA levels compared to vehicle-treated undifferentiated cultures established from 3 different biopsies. *B*) Primary cultures remained undifferentiated or were decidualized for 48 hours prior to treatment with 5 μg/ml actinomycin D. RNA was extracted at the indicated time points and subjected to qRT-PCR analysis. *C*) Binding of CLOCK to E2, a noncanonical E-box enhancer in the *PER2* promoter, was assessed by ChIP in 3 independent primary cultures, either undifferentiated (0 hour) or decidualized for the indicated time points. The data show relative enrichment compared to input. *D*) In parallel, CLOCK binding to a regulatory E-box element (E5) in the *PER1* promoter was determined. The data show the mean ± SEM. $^{**}P < 0.01$; $^{***}P < 0.001$.

27 or lysine 4 of histone 3 (H3K27me3 and H3K4me3, respectively) at the *PER2* promoter upon decidualization (data not shown). In the absence of obvious epigenetic changes, we speculated that PER2 could be regulated at the level of RNA stability. To test this hypothesis, undifferentiated and decidualized HESCs were treated with actinomycin D, a potent transcription inhibitor, for 0.5, 1, 2, 4, or 8 hours. As shown in Fig. 3*B*, the half-life of *PER2* transcripts was comparable in undifferentiated and decidualizing cells (2.93 versus 3.39 hours, respectively; $P > 0.05$).

In the mouse, *Per2* expression is critically dependent on constitutive binding of CLOCK to a noncanonical 5′-CACGTT-3′ E-box enhancer, termed E2, located 20 base pairs (bp) upstream of the transcriptional start site (35). The E2 enhancer and the extended CLOCK:BMAL1 M34 core binding site are highly conserved in humans, raising the possibility that disruption of CLOCK binding disables *PER2* transcription in decidualizing cells. ChIP analysis using a CLOCK antibody showed that decidualization was associated with a rapid and sustained loss of CLOCK binding at this locus (amplicon −301 to −162 bp). In 3 independent time course cultures, treatment with MPA and 8-br-cAMP for 24 hours was sufficient to reduce CLOCK binding to E2 in *PER2* promoter by 59%, and this level of repression was maintained over an 8 day time course (Fig. 3*C*). By contrast, CLOCK binding to the E-box (E5; amplicon −142 to −54 bp) in the *PER1* promoter remained constant throughout the time course (Fig. 3*D*).

PER2 knockdown silences circadian oscillations and disrupts HESC decidualization

Next, we examined whether PER2 knockdown in undifferentiated HESCs would suffice to disrupt circadian rhythm generation. Paired primary cultures transfected with either NT or PER2 siRNA were synchronized with dexamethasone, and total RNA was harvested at 4 hours intervals over a 28 hour period. Cells transfected with NT siRNA demonstrated robust circadian oscillations in the 6 core clock genes. PER2 knockdown resulted in a non-oscillating expression profile in undifferentiated HESCs (**Fig. 4**), indicating that down-regulation of this clock protein accounts for the loss of autonomous circadian oscillations in decidual cells.

We speculated that loss of PER2-dependent circadian oscillations may sensitize undifferentiated HESCs to decidugenic cues. However, this was not the case. Instead, PER2 knockdown severely compromised the induction of *PRL* and *IGFBP1* (IGF-binding protein-1), 2 cardinal decidual marker genes, in response to cAMP and MPA signaling (**Fig. 5**). Thus, whereas PER2 down-regulation is a striking feature of decidual cells, this clock protein seems nevertheless essential for the initial responsiveness of HESCs to differentiation signals.

Based on the kinetics of cAMP-dependent induction of the decidual *PRL* promoter activity, HESC differentiation has been shown to be a biphasic process, characterized by an initial rapid but modest response, which is followed by an accelerated rise in promoter activity after 12 hours of stimulation (36). Hence, we examined the kinetics of *PER2* inhibition and *PRL* induction in a short time course. *PER2* transcript levels transiently increased in response to 8-br-cAMP and MPA, with levels peaking at 12 hours, which was followed by a sharp drop by 24 hours (**Fig. 6*A***). As anticipated, the rise in *PRL* mRNA was modest within the first 12 hours of stimulation but then accelerated in concert with the drop in *PER2* transcript levels (Fig. 6*B*). Intriguingly, PER2 knockdown in HESCs had no significant impact on the expression of *PRL* transcripts in the first 12 hours of stimulation but inhibited the accelerated induction of this decidual marker between 12 and 24 hours (Fig. 6*C*).

To investigate further the consequences of PER2 knockdown on activation of the decidual transcriptome, total RNA harvested from 3 independent unsynchronized HESC cultures, first transfected with either PER2 or NT

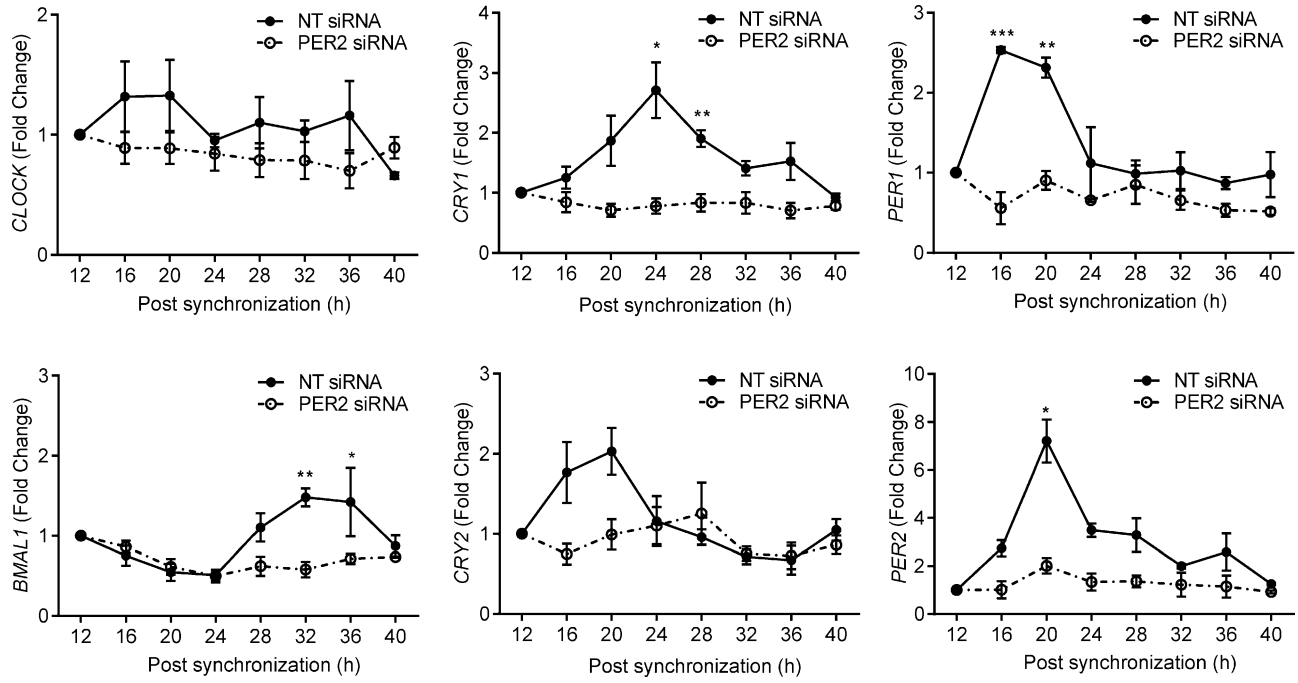

Figure 4. PER2 knockdown in HESCs causes loss of rhythmic expression in core clock genes. Primary HESC cultures were transfected with either NT or PER2 siRNA. After 48 hours, the cultures were synchronized with dexamethasone, and total RNA was harvested at indicated time points. Transcript levels of core clock genes were analyzed by qRT-PCR in 3 independent experiments. The data show the mean ± SEM. $*P < 0.05$; $**P < 0.01$; $***P < 0.001$.

siRNA and then decidualized for 24 hours, was subjected to RNA sequencing. On average, 25 million single-end reads were sequenced per sample. By combining 2 different analysis tools, DESeq and edgeR, we identified 1121 genes that were significantly altered upon PER2 knockdown, 572 (51%) of which were up-regulated and 549 (49%) down-regulated. To assess further the relatedness of the cultures, we calculated *Z* scores of the TPM values for the differentially expressed genes. A heat map of this association is depicted in Fig. 6*D*.

Among the down-regulated genes were *PRL* and *IGFBP1*, confirming the initial qRT-PCR analysis. More puzzling, however, was the observation that PER2 knockdown up-regulated various other genes essential for decidual transformation in HESCs, including genes encoding key transcription factors [*e.g.*, CREM, CEBPβ, CEBPα, and NURR1 (37, 38)], kinases and phosphatases (*e.g.*, SGK1 and MKP1) (39, 40), the cell surface receptor for IL33 (IL1RL1, also known as ST2) (23), and BMP2, a key decidual morphogen (41). Thus, rather than preventing or attenuating differentiation, premature down-regulation of PER2 predisposes for a disordered decidual program. Also striking was the induction of genes coding metabolic regulators, including peroxisome proliferator-activated receptor γ (*PPARG*) and PPARG coactivator 1-α, following siRNA-mediated PER2 inhibition.

PER2 prevents clonal expansion of HESCs by inducing G2/M arrest

Gene ontology (GO) analysis (GO slim) identified "cell cycle" and "proliferation" among the biologic processes prominently affected by PER2 knockdown (Fig. 6*E*). It is well established that stromal cells must undergo mitotic expansion prior to full decidualization (22). Based on the sequencing data, we speculated that premature PER2 inhibition deregulates decidual gene expression by interfering with the proliferative potential of HESCs. In agreement, the ability of HESCs to form colonies when plated at low density was severely compromised upon PER2 knockdown (**Fig. 7*A***, *B*). Flow cytometry analysis of 3 independent primary cultures revealed accumulation of HESCs in G2/M phase of the cycle following transfection with PER2 siRNA when compared to NT siRNA (mean ± SEM, 22.1 ± 1.4% versus 8.8% ± 2.3, respectively; $P = 0.03$), which was accompanied by a reduction of cells in S phase (11.7 ± 1.1% versus 17.6 ± 1.0%, respectively; $P = 0.03$) (Fig. 7*C*). Interestingly, the apoptotic cell fraction (<2 N) tended to be lower upon transfection with PER2 siRNA when compared to NT siRNA. Real-time monitoring of cell proliferation over 100 hours using microelectronic sensor technology (xCELLigence) confirmed that siRNA-mediated PER2 knockdown results in complete growth inhibition of HESC cultures (Fig. 7*D*). These results show that the lack of mitotic expansion observed upon PER2 knockdown is, at least in part, due to imposition of cell cycle block at G2/M. This observation fits well with the RNA-sequencing data, showing that 52 of the 73 cell cycle-related genes perturbed upon PER2 knockdown are involved in G2/M transition (Supplemental Table 2).

Midluteal endometrial PER2 expression in recurrent miscarriage

A search of the GEO database revealed that endometrial *PER2* transcript levels [GEO profiles; identification (ID)

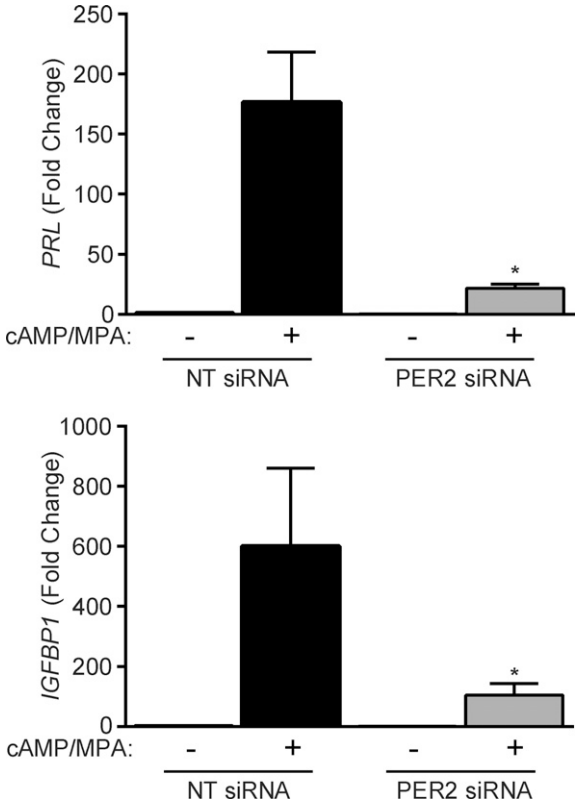

Figure 5. PER2 is required for the induction of decidual marker genes. Primary HESCs were transfected with NT or PER2 siRNA. The cultures remained untreated or were decidualized for 48 hours. The data show relative induction (mean ± SEM) of the decidual marker genes *PRL* and *IGFBP1* in 3 independent primary cultures. $*P < 0.05$.

24460199] increase 4-fold between the proliferative and early-secretory phase of the cycle (**Fig. 8*A***). Elevated levels are maintained during the midluteal phase of the cycle but then fall in concert with a sharp increase in the expression of decidual marker genes, including *IGFBP1* (ID 24460250) (42). Next, we examined *PER2* expression in midluteal endometrial biopsies obtained from 70 women with ovulatory cycles attending a dedicated miscarriage clinic. All patients suffered consecutive miscarriages, ranging between 2 and 11 (median ± SD, 4 ± 2). Most losses occurred in the first trimester of pregnancy. Within this cohort, endometrial *PER2* transcript levels correlated inversely with the number of previous miscarriages (Spearman rank test, $\rho = -0.3260$; $P = 0.0046$) (Fig. 8*B*). By contrast, no association was found between PER2 expression and other demographics relevant to miscarriages such as age ($\rho = 0.01070$; $P = 0.9$) or body mass index ($\rho = -0.1501$; $P = 0.2$) (Fig. 8*C*, *D*).

DISCUSSION

Circadian rhythms permeate a vast array of physiologic processes by maintaining tissue homeostasis in anticipation of environmental change (43). We show that oscillations of the core clock machinery are halted, or potentially "paused," upon decidualization of HESCs. Decidualization is a tightly spatiotemporally controlled process that commences with proliferative expansion of stromal cells in the superficial endometrial layer during the midluteal phase of the cycle. Differentiating cells then transit through defined phenotypic changes that sequentially control endometrial receptivity, embryo selection, and, ultimately, either menstrual shedding or resolution of pregnancy (18). Human preimplantation embryos do not express circadian genes apart from maternal transcripts, but these are degraded prior to the implantation-competent blastocyst stage (1). A parsimonious explanation for the silencing of circadian oscillations in both conceptus and surrounding decidualizing cells is that it synchronizes embryo-maternal interactions. Although PER2 levels drop significantly, all components of the core clock machinery remain expressed in nonoscillatory decidual cells, suggesting that these cells are poised to resume rhythmicity, possibly entrained by embryonic cues.

Down-regulation of *PER2* in the endometrium is precisely timed. In the rat, it marks the transition from oscillatory receptivity to the nonoscillatory decidual (postreceptive) endometrium (19). This pattern of expression is recapitulated in the human uterus with the decline in *PER2* transcript levels heralding the progression from mid-to-late-luteal endometrium. In primary culture, down-regulation of *PER2* mRNA occurred between 12 and 24 hours following exposure to a standard deciduogenic treatment. Again, inhibition of this clock gene marked the onset of an important transitional phase, characterized by increases in reactive oxygen production, altered redox signaling, and accelerated expression of decidual marker genes (26, 44). Previous studies reported that PER2 is acutely responsive to hormonal and other signals that converge onto a cAMP-response element in its promoter region (45–47). This pathway provides a likely explanation for the initial transient rise in *PER2* transcript levels in differentiating HESCs. However, sustained expression and circadian oscillations in peripheral tissues require constitutive binding of a transcriptional complex containing CLOCK to the highly conserved E2 enhancer in the proximal *PER2* promoter. In agreement, we found that loss of *PER2* expression in decidualizing HESCs coincided with attenuated binding of CLOCK to the E2 enhancer. This was not accounted for by a general reduction in the DNA-binding activity of the CLOCK:BMAL1 heterodimer as exemplified by the ChIP analysis of the *PER1* promoter. The precise mechanism of selective silencing of *PER2* in differentiating HESCs remains to be defined. One possibility is that *PER2* repression in decidualizing cells reflects accumulation of p53 (48), which in other cell systems has been shown to disrupt the binding of CLOCK to the E2 enhancer (49).

PER2 differs from other core clock proteins in that it exhibits several structural features of steroid receptor coregulators (50), including 2 conserved nuclear receptor-binding motifs (L*XX*LL). Furthermore, PER2 has been shown to bind estrogen receptor-α (ERα) and antagonize estrogen-dependent proliferation of breast cancer cell lines, at least in part by enhancing receptor degradation (51, 52). It acts as a transcriptional corepressor by recruiting histone deacetylases (*e.g.*, HDAC2) and components of the polycomb repressor complex (*e.g.*, EZH2 and SUZ12) to promoter regions of target genes (53). The kinetics of

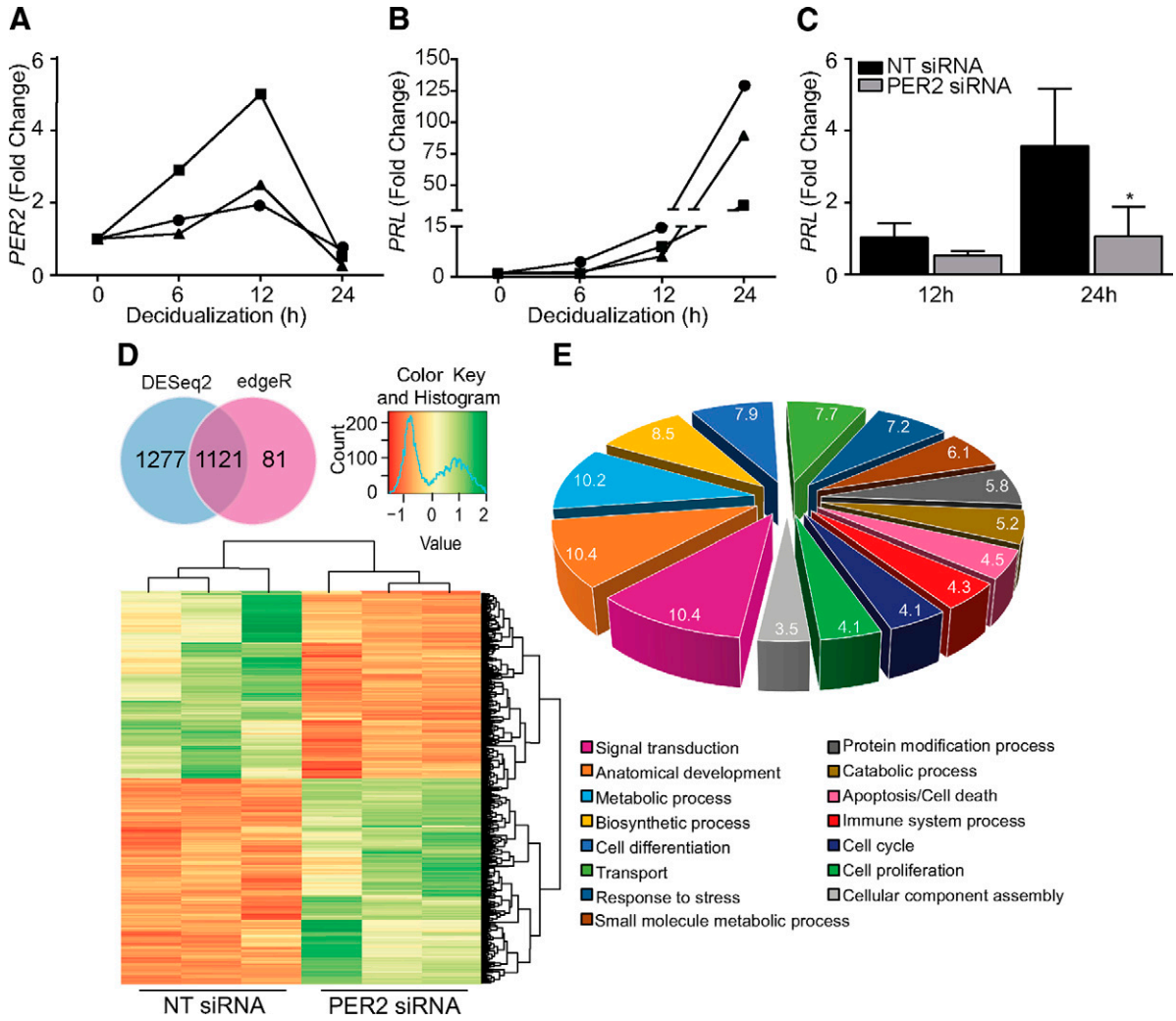

Figure 6. Premature PER2 down-regulation leads to a disorganized decidual response. *A*) The kinetics of *PER2* expression in response to 8-br-cAMP and MPA treatment were monitored in 3 independent cultures at the indicated time points by qRT-PCR. *PER2* transcript levels were normalized to those in undifferentiated cells. *B*) Kinetics of *PRL* induction in the same short time course. *C*) Primary HESCs were transfected with NT or PER2 siRNA. After 48 hours, the cultures were treated with 8-br-cAMP and MPA for 12 or 24 hours. *PRL* mRNA levels were normalized to those in undifferentiated cells. The data show mean fold change (±SEM) in 3 independent cultures. $*P < 0.05$. *D*) Venn diagram comparison of differentially expressed transcripts, identified by DESeq and edgeR, in primary HESCs decidualized for 24 hours following transfection with either NT or PER2 siRNA. Numbers represent differentially expressed transcripts with nonzero counts in 3 independent experiments. Clustered heat map of top-ranked differentially expressed transcripts is also shown. *E*) Graphic representation of the top 15 GO slim annotations of differentially expressed genes.

PER2 down-regulation in differentiating HESCs coupled to the enhanced activation of marker genes, such as *PRL* and *IGFBP1*, suggest that this clock protein is a major repressor of decidual gene expression, either through an epigenetic mechanism, as a putative corepressor of the progesterone receptor, or possibly through a combination of these mechanisms. Yet, PER2 knockdown did not sensitize HESCs to deciduogenic signals but resulted in a grossly disordered differentiation response. These seemingly contradictory findings are explained by the imposition of G2/M block upon PER2 knockdown, which prevented the obligatory mitotic expansion of stromal cells prior to the onset of decidual gene expression. This observation is itself intriguing because PER2 is widely regarded to be a tumor suppressor (54, 55). As mentioned previously, PER2 knockdown accelerates proliferation of ERα-positive breast cancer cells (51). Notably, endometrial *PER2* transcript levels are also low during the proliferative phase of the cycle. In leukemia cell lines, PER2 overexpression induces growth arrest in the G2/M phase of the cell cycle by inhibiting c-MYC and cyclin B1 and up-regulating p53 (54). Thus, the ability of PER2 to promote or inhibit cell cycle progression seems to be dependent on hormonal inputs within a cell-specific context.

Miscarriage is the most common complication of pregnancy. One in 7 recognized pregnancies ends in miscarriage during the first trimester, and 1–2% fail between 13 and 24 weeks gestation (18). The American Society for Reproductive Medicine defines RPL as ≥2 consecutive miscarriages before the fetus reaches viability. Affected couples are routinely screened for various anatomic, endocrine, immunologic, thrombophilic, and genetic risk

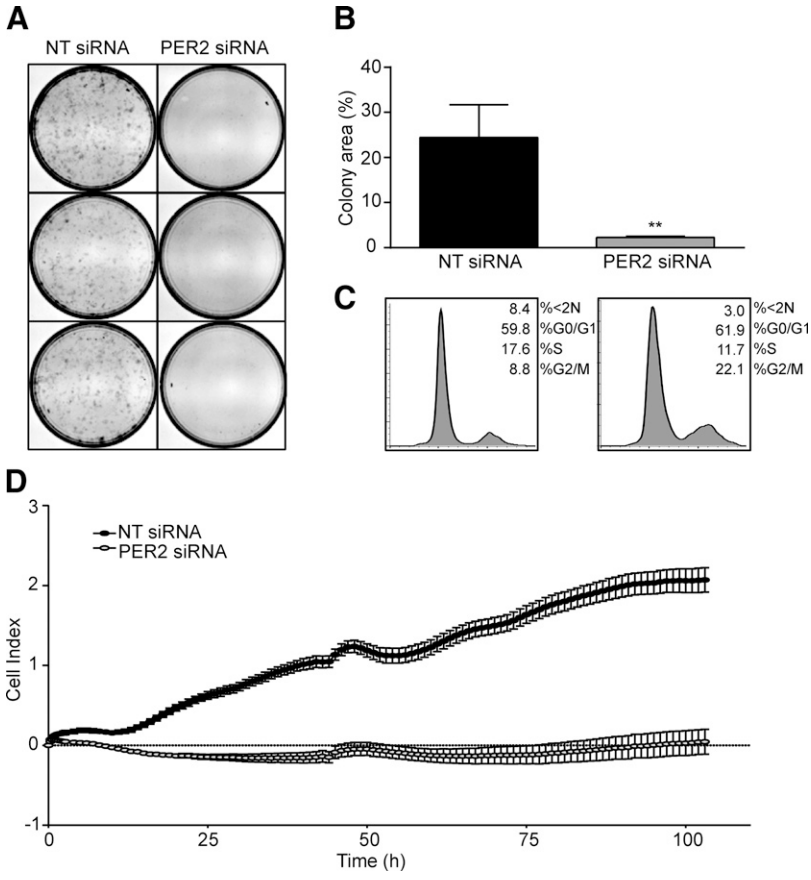

Figure 7. PER2 knockdown blocks mitotic expansion of HESCs. *A*) Colony-forming assays of 3 independent primary cultures first transfected with either NT or PER2 siRNA. *B*) Total colony area as measured by ImageJ analysis (U.S. National Institutes of Health, Bethesda, MD, USA), and the data represent mean colony area (±SEM). *C*) Representative gated cell cycle histograms obtained 48 hours after transfection of primary HESCs with either NT or PER2 siRNA. *D*) Real-time monitoring of cell growth over 100 hours following transfection with NT or PER2 siRNA. $^{**}P < 0.01$.

factors, although the value of these investigations is highly contentious. In a majority of patients, no underlying associations are found, and conversely, many subclinical disorders or risk factors perceived to cause miscarriages are also prevalent in women with uncomplicated pregnancies. Embryonic chromosomal imbalances are estimated to account for approximately 50% of all miscarriages; but importantly, the incidence of euploidic fetal loss increases with each additional miscarriage, whereas the likelihood of a future successful pregnancy decreases (56–58). In other

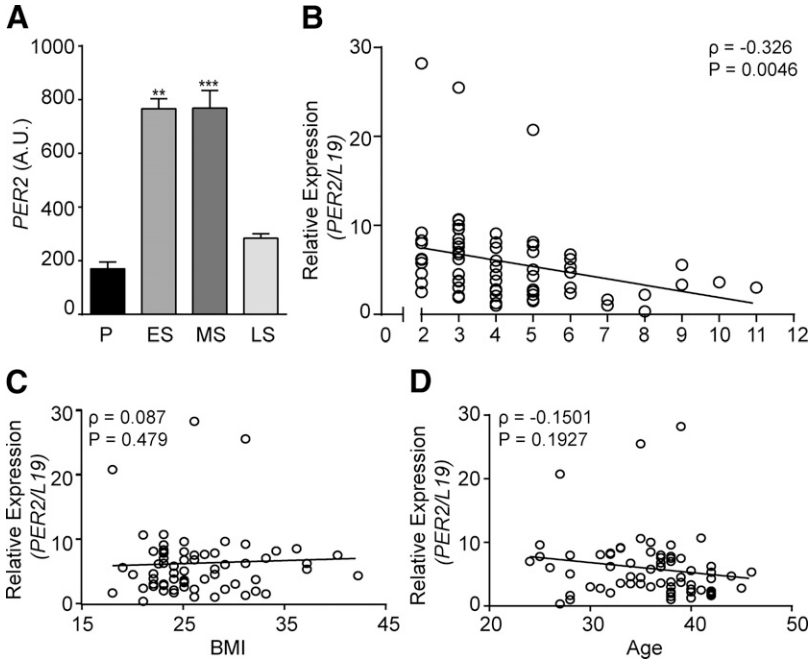

Figure 8. Endometrial *PER2* expression in RPL. *A*) *PER2* transcripts, expressed in arbitrary units (A.U.), in proliferative (P), early-secretory (ES), midsecretory (MS), and late-secretory (LS) human endometrium. Expression levels were derived from *in silico* analysis of publicly available microarray data (GEO profiles; ID 24460199) (42). *B*) Correlation between *PER2* transcript levels in midluteal endometrial biopsies and the number of preceding miscarriages in 70 subjects with RPL. *C*) Correlation between *PER2* transcript levels in midluteal endometrial biopsies and body mass index (BMI) in the RPL cohort. *D*) Correlation between *PER2* transcript levels in midluteal endometrial biopsies and age of cohort subjects. $^{**}P < 0.01$; $^{***}P < 0.001$.

words, the likelihood of a causal maternal factor increases with each additional pregnancy loss.

Several lines of evidence from experimental as well as epidemiologic studies suggest that an aberrant decidual response predisposes for subsequent pregnancy failure (18, 23, 39). The observation of a significant inverse correlation between midluteal PER2 transcript levels and the number of previous miscarriages strongly infers that deregulation of this core clock gene increases the likelihood of persistent miscarriages. Additional studies are warranted to assess the role of PER2 in the endometrial epithelial cells and to examine the tissue distribution of this clock protein in patients with RPL and control subjects. Interestingly, a recent systematic review and meta-analysis reported a significant association between night shifts and miscarriages (adjusted odds ratio, 1.41; 95% confidence interval, 1.22–1.63) (59). Taken together, these observations demonstrate that disruption of both central as well as peripheral circadian outputs predisposes for reproductive failure. FJ

This work was supported by the Biomedical Research Unit in Reproductive Health, a joint initiative between the University Hospitals Coventry and Warwickshire National Health Service Trust and Warwick Medical School. J.M. is the recipient of a Warwick Chancellor's studentship. The authors declare no conflicts of interest.

REFERENCES

1. Boden, M. J., Varcoe, T. J., and Kennaway, D. J. (2013) Circadian regulation of reproduction: from gamete to offspring. *Prog. Biophys. Mol. Biol.* **113**, 387–397
2. Markson, J. S., and O'Shea, E. K. (2009) The molecular clockwork of a protein-based circadian oscillator. *FEBS Lett.* **583**, 3938–3947
3. Morin, L. P. (2013) Neuroanatomy of the extended circadian rhythm system. *Exp. Neurol.* **243**, 4–20
4. Reppert, S. M., and Weaver, D. R. (2002) Coordination of circadian timing in mammals. *Nature* **418**, 935–941
5. Dolatshad, H., Davis, F. C., and Johnson, M. H. (2009) Circadian clock genes in reproductive tissues and the developing conceptus. *Reprod. Fertil. Dev.* **21**, 1–9
6. Chappell, P. E., White, R. S., and Mellon, P. L. (2003) Circadian gene expression regulates pulsatile gonadotropin-releasing hormone (GnRH) secretory patterns in the hypothalamic GnRH-secreting GT1-7 cell line. *J. Neurosci.* **23**, 11202–11213
7. Kennaway, D. J., Varcoe, T. J., and Mau, V. J. (2003) Rhythmic expression of clock and clock-controlled genes in the rat oviduct. *Mol. Hum. Reprod.* **9**, 503–507
8. Karman, B. N., and Tischkau, S. A. (2006) Circadian clock gene expression in the ovary: Effects of luteinizing hormone. *Biol. Reprod.* **75**, 624–632
9. Ko, C. H., and Takahashi, J. S. (2006) Molecular components of the mammalian circadian clock. *Hum. Mol. Genet.* **15**, R271–R277
10. Fu, L., and Lee, C. C. (2003) The circadian clock: pacemaker and tumour suppressor. *Nat. Rev. Cancer* **3**, 350–361
11. O'Neill, J. S., Maywood, E. S., and Hastings, M. H. (2013) Cellular mechanisms of circadian pacemaking: beyond transcriptional loops. *Handb. Exp. Pharmacol.* **217**, 67–103
12. Grimaldi, B., Nakahata, Y., Kaluzova, M., Masubuchi, S., and Sassone-Corsi, P. (2009) Chromatin remodeling, metabolism and circadian clocks: the interplay of CLOCK and SIRT1. *Int. J. Biochem. Cell Biol.* **41**, 81–86
13. Stojkovic, K., Wing, S. S., and Cermakian, N. (2014) A central role for ubiquitination within a circadian clock protein modification code. *Front.* Mol. Neurosci. **7**, 69
14. Lee, J., Lee, Y., Lee, M. J., Park, E., Kang, S. H., Chung, C. H., Lee, K. H., and Kim, K. (2008) Dual modification of BMAL1 by SUMO2/3 and ubiquitin promotes circadian activation of the CLOCK/BMAL1 complex. *Mol. Cell. Biol.* **28**, 6056–6065
15. Chu, A., Zhu, L., Blum, I. D., Mai, O., Leliavski, A., Fahrenkrug, J., Oster, H., Boehm, U., and Storch, K. F. (2013) Global but not gonadotrope-specific disruption of Bmal1 abolishes the luteinizing hormone surge without affecting ovulation. *Endocrinology* **154**, 2924–2935
16. Ratajczak, C. K., Boehle, K. L., and Muglia, L. J. (2009) Impaired steroidogenesis and implantation failure in Bmal1-/- mice. *Endocrinology* **150**, 1879–1885
17. Ratajczak, C. K., Asada, M., Allen, G. C., McMahon, D. G., Muglia, L. M., Smith, D., Bhattacharyya, S., and Muglia, L. J. (2012) Generation of myometrium-specific Bmal1 knockout mice for parturition analysis. *Reprod. Fertil. Dev.* **24**, 759–767
18. Gellersen, B., and Brosens, J. J. (2014) Cyclic decidualization of the human endometrium in reproductive health and failure. *Endocr. Rev.* **35**, 851–905
19. Uchikawa, M., Kawamura, M., Yamauchi, N., and Hattori, M. A. (2011) Down-regulation of circadian clock gene period 2 in uterine endometrial stromal cells of pregnant rats during decidualization. *Chronobiol. Int.* **28**, 1–9
20. Pilorz, V., and Steinlechner, S. (2008) Low reproductive success in Per1 and Per2 mutant mouse females due to accelerated ageing? *Reproduction* **135**, 559–568
21. Jones, M. C., Fusi, L., Higham, J. H., Abdel-Hafiz, H., Horwitz, K. B., Lam, E. W. F., and Brosens, J. J. (2006) Regulation of the SUMO pathway sensitizes differentiating human endometrial stromal cells to progesterone. *Proc. Natl. Acad. Sci. USA* **103**, 16272–16277
22. Wang, W., Li, Q., Bagchi, I. C., and Bagchi, M. K. (2010) The CCAAT/enhancer binding protein beta is a critical regulator of steroid-induced mitotic expansion of uterine stromal cells during decidualization. *Endocrinology* **151**, 3929–3940
23. Salker, M. S., Nautiyal, J., Steel, J. H., Webster, Z., Sućurović, S., Nicou, M., Singh, Y., Lucas, E. S., Murakami, K., Chan, Y. W., James, S., Abdallah, Y., Christian, M., Croy, B. A., Mulac-Jericevic, B., Quenby, S., and Brosens, J. J. (2012) Disordered IL-33/ST2 activation in decidualizing stromal cells prolongs uterine receptivity in women with recurrent pregnancy loss. *PLoS One* **7**, e52252
24. Salker, M., Teklenburg, G., Molokhia, M., Lavery, S., Trew, G., Aojanepong, T., Mardon, H. J., Lokugamage, A. U., Rai, R., Landles, C., Roelen, B. A. J., Quenby, S., Kuijk, E. W., Kavelaars, A., Heijnen, C. J., Regan, L., Macklon, N. S., and Brosens, J. J. (2010) Natural selection of human embryos: impaired decidualization of endometrium disables embryo-maternal interactions and causes recurrent pregnancy loss. *PLoS One* **5**, e10287
25. Al-Sabbagh, M., Lam, E. W. F., and Brosens, J. J. (2012) Mechanisms of endometrial progesterone resistance. *Mol. Cell. Endocrinol.* **358**, 208–215
26. Brosens, J. J., Hayashi, N., and White, J. O. (1999) Progesterone receptor regulates decidual prolactin expression in differentiating human endometrial stromal cells. *Endocrinology* **140**, 4809–4820
27. Ross, J. (1995) mRNA stability in mammalian cells. *Microbiol. Mol. Biol. Rev.* **59**, 423–450
28. Grimaldi, G., Christian, M., Steel, J. H., Henriet, P., Poutanen, M., and Brosens, J. J. (2011) Down-regulation of the histone methyltransferase EZH2 contributes to the epigenetic programming of decidualizing human endometrial stromal cells. *Mol. Endocrinol.* **25**, 1892–1903
29. Langmead, B., Trapnell, C., Pop, M., and Salzberg, S. L. (2009) Ultrafast and memory-efficient alignment of short DNA sequences to the human genome. *Genome Biol.* **10**, R25
30. Trapnell, C., Pachter, L., and Salzberg, S. L. (2009) TopHat: discovering splice junctions with RNA-Seq. *Bioinformatics* **25**, 1105–1111
31. Wagner, G. P., Kin, K., and Lynch, V. J. (2012) Measurement of mRNA abundance using RNA-seq data: RPKM measure is inconsistent among samples. *Theory Biosci.* **131**, 281–285
32. Anders, S., and Huber, W. (2010) Differential expression analysis for sequence count data. *Genome Biol.* **11**, R106
33. Robinson, M. D., McCarthy, D. J., and Smyth, G. K. (2010) edgeR: a Bioconductor package for differential expression analysis of digital gene expression data. *Bioinformatics* **26**, 139–140

34. Lal, S., Allan, A., Markovic, D., Walker, R., Macartney, J., Europe-Finner, N., Tyson-Capper, A., and Grammatopoulos, D. K. (2013) Estrogen alters the splicing of type 1 corticotropin-releasing hormone receptor in breast cancer cells. *Sci. Signal.* **6**, ra53
35. Yoo, S. H., Ko, C. H., Lowrey, P. L., Buhr, E. D., Song, E. J., Chang, S., Yoo, O. J., Yamazaki, S., Lee, C., and Takahashi, J. S. (2005) A noncanonical E-box enhancer drives mouse Period2 circadian oscillations in vivo. *Proc. Natl. Acad. Sci. USA* **102**, 2608–2613
36. Telgmann, R., and Gellersen, B. (1998) Marker genes of decidualization: activation of the decidual prolactin gene. *Hum. Reprod. Update* **4**, 472–479
37. Lamas, M., Monaco, L., Zazopoulos, E., Lalli, E., Tamai, K., Penna, L., Mazzucchelli, C., Nantel, F., Foulkes, N. S., and Sassone-Corsi, P. (1996) CREM: a master-switch in the transcriptional response to cAMP. *Philos. Trans. R. Soc. Lond. B Biol. Sci.* **351**, 561–567
38. Mantena, S. R., Kannan, A., Cheon, Y. P., Li, Q., Johnson, P. F., Bagchi, I. C., and Bagchi, M. K. (2006) C/EBPbeta is a critical mediator of steroid hormone-regulated cell proliferation and differentiation in the uterine epithelium and stroma. *Proc. Natl. Acad. Sci. USA* **103**, 1870–1875
39. Salker, M. S., Christian, M., Steel, J. H., Nautiyal, J., Lavery, S., Trew, G., Webster, Z., Al-Sabbagh, M., Puchchakayala, G., Föller, M., Landles, C., Sharkey, A. M., Quenby, S., Aplin, J. D., Regan, L., Lang, F., and Brosens, J. J. (2011) Deregulation of the serum- and glucocorticoid-inducible kinase SGK1 in the endometrium causes reproductive failure. *Nat. Med.* **17**, 1509–1513
40. Leitao, B., Jones, M. C., Fusi, L., Higham, J., Lee, Y., Takano, M., Goto, T., Christian, M., Lam, E. W. F., and Brosens, J. J. (2010) Silencing of the JNK pathway maintains progesterone receptor activity in decidualizing human endometrial stromal cells exposed to oxidative stress signals. *FASEB J.* **24**, 1541–1551
41. Li, Q., Kannan, A., Wang, W., Demayo, F. J., Taylor, R. N., Bagchi, M. K., and Bagchi, I. C. (2007) Bone morphogenetic protein 2 functions via a conserved signaling pathway involving Wnt4 to regulate uterine decidualization in the mouse and the human. *J. Biol. Chem.* **282**, 31725–31732
42. Talbi, S., Hamilton, A. E., Vo, K. C., Tulac, S., Overgaard, M. T., Dosiou, C., Le Shay, N., Nezhat, C. N., Kempson, R., Lessey, B. A., Nayak, N. R., and Giudice, L. C. (2006) Molecular phenotyping of human endometrium distinguishes menstrual cycle phases and underlying biological processes in normo-ovulatory women. *Endocrinology* **147**, 1097–1121
43. Ripperger, J. A., and Brown, S. A. (2010) Transcriptional regulation of circadian clocks. In *Circadian Clock*, Vol. 12, (Albrecht, U., ed.), pp. 37–78, Springer, New York
44. Al-Sabbagh, M., Fusi, L., Higham, J., Lee, Y., Lei, K., Hanyaloglu, A. C., Lam, E. W. F., Christian, M., and Brosens, J. J. (2011) NADPH oxidase-derived reactive oxygen species mediate decidualization of human endometrial stromal cells in response to cyclic AMP signaling. *Endocrinology* **152**, 730–740
45. Nakamura, T. J., Moriya, T., Inoue, S., Shimazoe, T., Watanabe, S., Ebihara, S., and Shinohara, K. (2005) Estrogen differentially regulates expression of Per1 and Per2 genes between central and peripheral clocks and between reproductive and nonreproductive tissues in female rats. *J. Neurosci. Res.* **82**, 622–630
46. Koyanagi, S., Hamdan, A. M., Horiguchi, M., Kusunose, N., Okamoto, A., Matsunaga, N., and Ohdo, S. (2011) cAMP-response element (CRE)-mediated transcription by activating transcription factor-4 (ATF4) is essential for circadian expression of the Period2 gene. *J. Biol. Chem.* **286**, 32416–32423
47. O'Neill, J. S., Maywood, E. S., Chesham, J. E., Takahashi, J. S., and Hastings, M. H. (2008) cAMP-dependent signaling as a core component of the mammalian circadian pacemaker. *Science* **320**, 949–953
48. Pohnke, Y., Schneider-Merck, T., Fahnenstich, J., Kempf, R., Christian, M., Milde-Langosch, K., Brosens, J. J., and Gellersen, B. (2004) Wild-type p53 protein is up-regulated upon cyclic adenosine monophosphate-induced differentiation of human endometrial stromal cells. *J. Clin. Endocrinol. Metab.* **89**, 5233–5244
49. Miki, T., Matsumoto, T., Zhao, Z., and Lee, C. C. (2013) p53 regulates Period2 expression and the circadian clock. *Nat. Commun.* **4**, 2444
50. Albrecht, U., Bordon, A., Schmutz, I., and Ripperger, J. (2007) The multiple facets of Per2. *Cold Spring Harb. Symp. Quant. Biol.* **72**, 95–104
51. Gery, S., Virk, R. K., Chumakov, K., Yu, A., and Koeffler, H. P. (2007) The clock gene Per2 links the circadian system to the estrogen receptor. *Oncogene* **26**, 7916–7920
52. Nakamura, T. J., Sellix, M. T., Menaker, M., and Block, G. D. (2008) Estrogen directly modulates circadian rhythms of PER2 expression in the uterus. *Am. J. Physiol. Endocrinol. Metab.* **295**, E1025–E1031
53. Hwang-Verslues, W. W., Chang, P. H., Jeng, Y. M., Kuo, W. H., Chiang, P. H., Chang, Y. C., Hsieh, T. H., Su, F. Y., Lin, L. C., Abbondante, S., Yang, C. Y., Hsu, H. M., Yu, J. C., Chang, K. J., Shew, J. Y., Lee, E. Y., and Lee, W. H. (2013) Loss of corepressor PER2 under hypoxia up-regulates OCT1-mediated EMT gene expression and enhances tumor malignancy. *Proc. Natl. Acad. Sci. USA* **110**, 12331–12336
54. Sun, C. M., Huang, S. F., Zeng, J. M., Liu, D. B., Xiao, Q., Tian, W. J., Zhu, X. D., Huang, Z. G., and Feng, W. L. (2010) Per2 inhibits k562 leukemia cell growth in vitro and in vivo through cell cycle arrest and apoptosis induction. *Pathol. Oncol. Res.* **16**, 403–411
55. Thoennissen, N. H., Thoennissen, G. B., Abbassi, S., Nabavi-Nouis, S., Sauer, T., Doan, N. B., Gery, S., Müller-Tidow, C., Said, J. W., and Koeffler, H. P. (2012) Transcription factor CCAAT/enhancer-binding protein alpha and critical circadian clock downstream target gene PER2 are highly deregulated in diffuse large B-cell lymphoma. *Leuk. Lymphoma* **53**, 1577–1585
56. Ogasawara, M., Aoki, K., Okada, S., and Suzumori, K. (2000) Embryonic karyotype of abortuses in relation to the number of previous miscarriages. *Fertil. Steril.* **73**, 300–304
57. Rai, R., and Regan, L. (2006) Recurrent miscarriage. *Lancet* **368**, 601–611
58. Brosens, J. J., Salker, M. S., Teklenburg, G., Nautiyal, J., Salter, S., Lucas, E. S., Steel, J. H., Christian, M., Chan, Y. W., Boomsma, C. M., Moore, J. D., Hartshorne, G. M., Sućurović, S., Mulac-Jericevic, B., Heijnen, C. J., Quenby, S., Koerkamp, M. J. G., Holstege, F. C. P., Shmygol, A., and Macklon, N. S. (2014) Uterine selection of human embryos at implantation. *Sci. Rep.* **4**, 3894
59. Stocker, L. J., Macklon, N. S., Cheong, Y. C., and Bewley, S. J. (2014) Influence of shift work on early reproductive outcomes: a systematic review and meta-analysis. *Obstet. Gynecol.* **124**, 99–110

Received for publication November 6, 2014.
Accepted for publication December 10, 2014.